U.PORTO

DOUTORAMENTO

CIÊNCIAS BIOMEDICAS

Establishment of a three-dimensional *in vitro* model of air-blood barrier to assess the translocation of nanoparticles targeted to the lung

Ana Margarida Costa

D

2018

U.PORTO

Ana Margarida Costa. Establishment of a three-dimensional *in vitro* model of air-blood barrier to assess the translocation of nanoparticles targeted to the lung

Establishment of a three-dimensional *in vitro* model of air-blood barrier to assess the translocation of nanoparticles targeted to the lung

Ana Margarida Costa

D.ICBAS2018

INSTITUTO DE CIÊNCIAS BIOMÉDICAS ABEL SALAZAR

Ana Margarida Martins Maia da Costa

Establishment of a three-dimensional *in vitro* model of air-blood barrier to assess the translocation of nanoparticles targeted to the lung

Tese de Candidatura ao grau de Doutor em Ciências Biomédicas submetida ao Instituto de Ciências Biomédicas Abel Salazar da Universidade do Porto

Orientador
Doutor Vítor Manuel Fernandes Seabra da Silva
Categoria – Professor Associado
Afiliação – IUCS - Instituto Universitário de Ciências da Saúde

Coorientador
Doutor Bruno Filipe Carmelino Cardoso Sarmento
Categoria – Investigador Auxiliar/Professor Auxiliar
Afiliação – i3S - Instituto de Investigação e Inovação em Saúde, INEB - Instituto de Engenharia Biomédica, Universidade do Porto & IUCS - Instituto Universitário de Ciências da Saúde

Tutor
Doutor Pedro Lopes Granja
Categoria – Investigador Principal/Professor Associado
Afiliação – i3S - Instituto de Investigação e Inovação em Saúde, INEB - Instituto de Engenharia Biomédica & Instituto de Ciências Biomédicas Abel Salazar (ICBAS), Universidade do Porto

This work has been performed at:

Nanomedicines & Translational Drug Delivery
i3S – Instituto de Investigação e Inovação em Saúde
INEB – Instituto de Engenharia Biomédica
Universidade do Porto, Porto, Portugal
Rua Alfredo Allen, 208
4200-135 Porto, Portugal

Drug Discovery, Delivery & Toxicology
IINFACTS – Institute of Research and Advanced Training in Health Sciences and Technology
Rua Central de Gandra, 1317
4585-116 Gandra, Paredes, Portugal

DDEL – Department of Drug Delivery
HIPS – Helmholtz-Institut für Pharmazeutische Forschung Saarland
Universitätscampus E8 1
66123 Saarbrücken, Germany

Helmholtz-Institut für Pharmazeutische Forschung Saarland

“A mente que se abre a uma nova ideia nunca mais volta ao seu tamanho original”

“The mind that opens to a new idea never returns to its original size”

Albert Einstein

ACKNOWLEDGMENTS

I could not reach the end of this stage without expressing my gratitude and acknowledgments to all the people and institutions that were involved directly and indirectly in this journey:

To my supervisors Professor Vítor Seabra and Professor Bruno Sarmento, first for the invitation and the opportunity to enroll on a doctoral program; second, for all the scientific discussion, guidance and support during the last four years. It was not an easy path and walking through it required a lot of patience from their side. I am grateful for their trust, freedom, encouragement and for the opportunities that allowed me to grow as a researcher. A special thanks to Professor Bruno Sarmento for the close supervision at Instituto de Investigação e Inovação em Saúde (i3S)/Instituto de Engenharia Biomédica (INEB), always with a good sense of humor that I appreciated;

To Professor Claus-Michael Lehr for the kindness of letting me perform part of my work at Department of Drug Delivery (DDEL) from Helmholtz-Institut für Pharmazeutische Forschung Saarland (HIPS), and for the scientific discussion that allowed me to see my work with a different point of view; also Dr. Cristiane Carvalho-Wodarz for the close supervision, for all ideas and suggestion given, and mostly, for her friendship, trust and the motivation which were important to carry on this work during my stay in Germany;

To Professor Pedro Granja for being my co-supervisor/tutor on this work and for providing me, as well as all INEB members, a constant positive energy;

To all my work colleagues from Nanomedicines & Translational Drug Delivery from i3S/INEB, Universidade of Porto, that supported my work on a daily-basis, and for the funny and good moments that I will not forget. I would like to give my deepest acknowledge to Rute Nunes for the fully support, trust, encouragement and her friendship that started from the beginning. No doubt you were like sister for me during this period of my life. Also, to all members that belonged to this research group on the past, in particular Pedro Fonte who introduced me the interest for research, and

provided me the opportunity to start my research career by working close with him; also, to Cassilda Cunha-Reis, for all the advice, encouragement, and for teaching me how to see life in a different perspective;

To my HIPS foodies, my family when I was far from Portugal. To all I am grateful for the help and the funny moments inside and outside the lab, for the friendship and for making me feel at home. A special thanks to Stephanie Kletting (for the scientific discussions and help with performing my *in vitro* model), Carlos Montefusco and Adriely de Góis (my Brazilian brothers), Remi Hendrix-Jastrzebski (my crazy Zumba partner that shared the same questions and doubts about cells), Sara Menina (for the friendship, joy and the good time spent together) and Hanzey Yasar (for the time together during our coffee talks on Sundays afternoons);

To Andreia Almeida, my fellow citizen (from Gandra) and my sweetest friend from the lab, that always helped me, even on small things. Thanks for the all information regarding the permeability studies. You were always there, ready for everything, even when I was in Germany;

To Francisca Araújo for the assistance during the preparation of histology slices at i3S;

To Vírginia Gonçalves from Instituto de Investigação e Formação Avançada em Ciências e Tecnologias da Saúde (IINFACTS) for all the help with the high-performance liquid chromatography (HPLC) experiments;

To Maria Gomes Lázaro for the assistance at confocal laser scannining microscopy (CLSM) ImageStream®^{X} imaging flow cytometry analyses performed at Bioimaging i3S Scientific Platform;

To Rui Fernandes and Francisco Rosário Figueiredo from the assistance at transmission electron microscopy analyses performed at Histology and Electrom Microscopy i3S Scientific Platform; It was not easy to get the cut, but we got it!!;
To Biointerfaces and Nanotechnology i3S Scientific Platform for the support with particle size and zeta potential analyses;

To the technicians Petra König and Jana Westhues for the support on cell culture and all the help during my stay on Germany;

To Chiara de Rossi for the help, friendship and for the support with scanning electron microscopy experiments;

To Marijas Jurisic for the availability, patience, for teaching me how to work with CLSM and last, for the help during the histology experiments;

To all research institutions involved in this work and their members, namely i3S and INEB from University of Porto, IINFACTS/CESPU and last to HIPS from Saarland University;

To my close friends for the friendship, motivation and encouragement throughout my life, in particularly for the last four years. Thank you for spending times listening to my failures, doubts, concerns, sadness, and always believing that I would be able to give one more step ahead;

To my family for the unconditional support, patient and love throughout my life, and for understanding my absence during the hard times. I always appreciated the trust of my family on me and the freedom in choosing my own career, even knowing I would be far from home. I am grateful for having you remembering me all the time that “knowledge does not occupy space, there is always space for more”, which were essential values for carrying on my studies for four more years.

Obrigada! Thanks! Danke!

FINANCIAL SUPPORT

Ana Costa gratefully acknowledges Fundação para a Ciência e a Tecnologia (FCT), Portugal for the financial support (Grant SFRH/BD/95227/2013).

This thesis was partially supported by the project NORTE-01-0145-FEDER-000012, supported by Norte Portugal Regional Operational Programme (NORTE 2020), under the PORTUGAL 2020 Partnership Agreement, through the European Regional Development Fund (ERDF). This work was financed by FEDER - Fundo Europeu de Desenvolvimento Regional funds through the COMPETE 2020 - Operacional Programme for Competitiveness and Internationalisation (POCI), Portugal 2020, and by Portuguese funds through FCT - Fundação para a Ciência e a Tecnologia/ Ministério da Ciência, Tecnologia e Ensino Superior in the framework of the project "Institute for Research and Innovation in Health Sciences" (POCI-01-0145-FEDER-007274

PUBLICATIONS

Ao abrigo do disposto do nº 2, alínea a) do artigo 31º do Decreto-Lei n.º 115/2013 de 7 de Agosto, fazem parte integrante desta tese de doutoramento os seguintes trabalhos já publicados ou submetidos para publicação:

Costa A, Sarmento B, Seabra V. Targeted Drug Delivery Systems for Lung Macrophages. Current Drug Targets. 2015;16(14):1565-81;

Costa A, Andrade F. Tissue-based *in vitro* and *ex vivo* models for pulmonary permeability studies In: Sarmento B, editor. Concepts and Models for Drug Permeability Studies. Amsterdam: Woodhead Publishing; 2016. p. 255-72;

Costa A, Pinheiro M, Magalhães J, Ribeiro R, Seabra V, Reis S, Sarmento B. The formulation of nanomedicines for treating tuberculosis. Advanced Drug Delivery Reviews.2016;102:102-15;

Costa A, Sarmento B, Seabra V. Mannose-functionalized solid lipid nanoparticles are effective in targeting alveolar macrophages. European Journal of Pharmaceutical Sciences. 2017; 114:103-13;

TABLE OF CONTENTS

CHAPTER III

CHAPTER IV

ABSTRACT

The use of *in vitro* models for drug screening as an alternative to animal experiments is increasing over the last years, in particular, models to assess the permeation through biological membranes. Initially, cell culture models were constituted by one type of cells forming a confluent monolayer, but due to its oversimplicity they are being replaced by three-dimensional (3D) *in vitro* models, that present a higher complexity and reflect more the *in vivo*-like conditions. Being the pulmonary route one of the most studied approaches for drug administration, several *in vitro* models of alveolar epithelium have been used to assess the drug permeability and the translocation of nanocarriers.

This work aims to develop a 3D *in vitro* model of air-blood barrier, comprising alveolar epithelial cells, capillary endothelium and macrophages, to test the translocation of nanocarriers. For that purpose, in this work was developed a solid lipid nanoparticles (SLN) and isoniazid (Isn), an antituberculosis drug, was encapsulated inside of the lipid matrix of this system. The formulation was further functionalized with mannose, in order to target SLN towards the mannose receptors expressed on the surface of alveolar macrophages (AMs), the main cells responsible for the *Mycobacterium tuberculosis* survival during the latent states of infection, and at the same time, the therapeutic target.

Different SLN formulations were developed, varying the type of lipid, the inner phase composition, the surfactant agents, the organic solvent and the stearylamine concentration. The selected formulation presented an average particle size around 500 nm, a polydispersity index between 0.3-0.4, a positive surface charge (around + 37 mV), an Isn association efficiency close to 35%. and a slow drug release kinetics (less than 10%) up to 48 hours. The functionalization of SLN with mannose was confirmed through fourier transform infrared spectroscopy. Uptake studies on differentiated THP-1 cells showed that mannosylated SLN were efficiently internalized through receptor-mediated endocytosis.

The 3D *in vitro* model of air-blood barrier was initiated by establishing the suitable conditions for the co-culture of a single monolayer of epithelial cells (NCI-H441) and a monolayer of endothelial cells (HPMEC-ST1.6R), seeded at the apical side and

basolateral side of the Transwell®, respectively. The Transwell® membrane (with a pore size of 3.0 µm) aims to mimic the basement membrane. Finally, differentiated THP-1 cells were added apically, on the top of NCI-H441 cells, in order to mimic the AMs that are presented at alveolar space.

During the optimization, this of 3D *in vitro* model (being also designed as triple co-culture in this work) was characterized regarding transepithelial electrical resistance, morphology, topography and the analysis of its ultrastructural was also performed. A successful model was established based on 1.0 x 10^5 NCI-H441 cells/Transwell®, 5.0 x 10^4 HPMEC-ST1.6R cells/Transwell® and 1.0 x 10^5 dTHP-1 cells/Transwell®, cultured for 5 days, and translocation of different systems were tested across this new model.

Fluorospheres with an average size of 50 nm could translocate across the 3D *in vitro* model (18%), but fluorospheres with a size of 1.0 µm were retained on the apical side of the Transwell®, and less than 1% of these fluorospheres were found at basolateral compartment of this model. Based on these outcomes, it was concluded that this air-blood barrier model can be used to study the retention of 1.0 µm-sized inhaled particles, that may deposit on the alveoli, but still allows to study the translocation of small nanocarriers.

In this work SLN were produced to enable the local delivery of Isn at alveolar airways, so that this system was also used for validation the retention capacity of the 3D *in vitro* model. The majority SLN (with Isn loaded) did not translocate, while around 35% of free Isn could permeate this *in vitro* model.

Inflammatory response through the release of interleukin (IL)-8 was assessed after lipopolysaccharide (LPS) incubation. 3D *in vitro* model exhibited a higher IL-8 release regarding the NCI-H441 monoculture, which showed to be unresponsive on the presence of LPS. During the inflammatory process the permeability of alveolo-capillary membrane is generally enhanced. Thus, the Isn permeability across each monoculture, bi-cultures (NCI-H441+dTHP-1 and NCI-H441+HPMEC-ST1.6R) and across the 3D model was also assessed after LPS incubation. Overall, the permeability of free Isn through different *in vitro* cell culture model was not influenced by the LPS treatment.

In conclusion, the 3D *in vitro* model presented a better morphology that resembles the air-blood barrier when compared with epithelial cell monolayer, but based on different

translocation studies, no significant differences were observed comparatively to NCI-H441 monocultures and both bi-cultures. However, due to
higher release of IL-8 after incubation of a proinflammatory stimulus, this new 3D model can be a potential *in vitro* tool to assess the inflammatory response of drugs/nanocarriers due to its higher sensibility regarding monocultures of epithelial cells.

Keywords: Nanotechnology; macrophages targeting; pulmonary administration; 3D *in vitro* models; translocation studies.

RESUMO

O uso de modelos *in vitro* como alternativa à experimentação animal tem vindo a aumentar durante a fase de investigação de novos fármacos, em especial, os modelos para avaliar a permeação de membranas biológicas. Inicialmente, os modelos de cultura celular eram constituídos por um único tipo de células que formavam uma monocamada confluente, mas devido à sua simplicidade estes têm sido substituídos por modelos *in vitro* tridimensionais (3D), que apresentam uma maior complexidade e melhor refletem as condições *in vivo*. Sendo a administração pulmonar uma das estratégias mais estudas para a administração de fármacos, vários modelos de epitélio alveolar têm sido utilizados para avaliar a permeabilidade de fármacos e a translocação de nanotransportadores.

Este trabalho pretende desenvolver um modelo *in vitro* 3D de barreira alvéolo-capilar, constituído por células epiteliais alveolares, endotélio capilar e macrófagos, de forma a avaliar a translocação de nanotransportadores. Para esse efeito, neste trabalho foram desenvolvidas nanopartículas lipídicas sólidas (SLN) e a isoniazida (Isn), um fármaco antituberculoso, foi encapsulado dentro da matriz lipídica deste sistema. A formulação foi posteriormente funcionalizada com manose, com o objetivo de direcionar as SLN para os recetores de manose expressos na superfície dos macrófagos alveolares (AMs), que são principais células responsáveis pela sobrevivência da *Mycobacterium tuberculosis* nas fases latentes da infeção, e ao mesmo tempo, o alvo terapêutico.

Diferentes formulações de SLN foram desenvolvidas, variando o tipo de lípido, a composição da fase interna, o surfactante, o solvente orgânico e as concentrações de estearilamina. A formulação selecionada apresentou um tamanho médio aproximado de 500 nm, um índice de polidispersão compreendido entre 0.3-0.4, uma superfície com carga positiva (por volta dos + 37 mV), uma eficiência de associação de Isn próxima dos 35% e uma cinética de liberação do fármaco lenta (menos de 10%) durante 48 horas. A funcionalização das SLN com manose foi confirmado por espectroscopia de infravermelho por transformada de fourier. Os estudos de uptake realizados em células THP-1 diferenciadas demonstraram que as SLN manosiladas foram eficientemente internalizadas através de endocitose mediada por recetor.

O modelo *in vitro* 3D de barreira alvéolo-capilar foi iniciado pelo estabelecimento das condições de co-cultura de uma única monocamada de células epiteliais (NCI-H441) e uma monocamada de células endoteliais (HPMEC-ST1.6R), cultivadas do lado apical e basolateral do Transwell®, respetivamente. A membrana do Transwell® (com um diâmetro de poro de 3.0 µm) pretende mimetizar a membrana basal. Por último, células THP-1 diferenciadas foram adicionados apicalmente, no topo das células NCI-H441, de forma a mimetizar os AMs que estão presentes no espaço alveolar.

Durante a otimização, este modelo *in vitro* 3D (sendo designado também por co-cultura tripla neste trabalho), foi caracterizado relativamente à resistência elétrica transepitelial, morfologia, topografia e a análise da sua ultra-estrutura foi também realizada. O modelo foi estabelecido com sucesso, baseado em 1.0 x 10^5 NCI-H441 células/Transwell®, 5.0 x 10^4 HPMEC-ST1.6R células/Transwell® e 1.0 x 10^5 dTHP-1 células/Transwell® cultivadas por apenas 5 dias, e a translocação de diferentes sistemas foi testado através deste novo modelo.

Fluorosferas com tamanho médio de 50 nm conseguiram translocar através do modelo *in vitro* 3D (18%), mas as fluorosferas com tamanho de 1.0 µm ficaram retidas no lado apical do Transwell®, e menos de 1% destas fluorosferas foram encontradas no lado basolateral deste modelo. Com base nestes resultados, concluiu-se que este modelo de barreira alvéolo-capilar pode ser usado para estudar a retenção de partículas inaladas com de tamanho de 1,0 µm, que podem depositar nos alvéolos, mas ainda permite estudar a translocação de pequenos nanotransportadores.

Neste trabalho foram produzidas SLN para permitir a libertação local de Isn nas vias aéreas alveolares, de modo que este sistema foi também utilizado para validação da capacidade de retenção deste modelo *in vitro* 3D. A maioria das SLN (com Isn encapsulada) não translocaram, enquanto que cerca de 35% de Isn na sua forma livre conseguiu permear este modelo *in vitro*.

A resposta inflamatória através da produção de interleucina (IL)-8 foi avaliada após incubação de lipopolissacarídeo (LPS). O modelo *in vitro* 3D exibiu uma maior libertação de IL-8 em relação à monocultura de NCI-H441, que não apresentou uma resposta na presença de LPS. Durante um processo inflamatório a permeabilidade da membrana alvéolo-capilar está aumentada. Deste modo, a permeabilidade de Isn através de cada monocultura, bi-culturas (NCI-H441+dTHP-1 and NCI-H441+HPMEC-ST1.6R) e através do modelo 3D foi também avaliada após a

incubação de LPS. De um modo geral, a permeabilidade da Isn através dos diferentes modelos celulares *in vitro* não foi influenciada com o tratamento de LPS.

Em conclusão, o modelo *in vitro* 3D apresentou uma morfologia que melhor se assemelha à barreira alvéolo-capilar quando comparada com uma monocamada de células epiteliais, mas baseados nos diferentes estudos de translocação, não foram observadas diferenças significativas em relação à monocultura de NCI-H441 e a ambas bi-culturas. Contudo, devido à maior libertação IL-8 após a incubação de um estímulo pró-inflamatório, este novo modelo 3D poderá ser uma potencial ferramenta *in vitro* para avaliar a resposta inflamatória de fármacos/nanotransportadores, devido à sua maior sensibilidade em relação às monoculturas de células epiteliais.

Palavras-chave: Nanotecnologia; direcionamento para os macrófagos; administração pulmonar; modelos *in vitro* 3D, estudos de translocação.

ABBREVIATIONS AND LIST OF ACRONYMOUS

ACN – Acetonitrile

ALI – Air-liquid interface

AMs – Alveolar macrophages

Anti-TB – Antituberculosis

ASL – Airway surface liquid

ATI – Alveolar type I

ATII – Alveolar type II

ATCC – American Type Culture Collection

BCS – Biopharmaceutical classification system

BM – Basement membrane

Chol – Cholesterol

CLSM – Confocal laser scanning microscopy

CRDs – Carbohydrate-recognition domains

CRs – Complement receptors

DAPI – 4′,6-diamidino-2-phenylindole

DCM – Dichloromethane

Dex – Dexamethasone

DMSO – Dimethyl sulfoxide

dTHP-1 – Differentiated THP-1

ECGS – Endothelial cell growth supplement

EDTA – Ethylenediamine tetraacetic acid

ELISA – Enzyme-linked immunosorbent assay

EMA – Ethyl methacrylate

End:epi – endothelial:epithelial cells

ET – Empty Transwell®

ET (+ Matrigel) – Empty Transwell® with Matrigel™ coating

ET (- Matrigel) – Empty Transwell® without Matrigel™ coating

FBS – Fetal bovine serum

FcRs – Fc receptors

FTIR – Fourier transform infrared

GAM – Galactomannan

GAM-h – Galactomannan hydrolyzed

hAELVi – Human alveolar epithelial lentivirus immortalized

hAEpC – Human alveolar epithelial cells

HBSS – Hank's balanced salt solution

HPLC – High-performance liquid chromatography

ICAM-1 – Intercellular adhesion molecule-1

ICC – Immunocytochemistry

Ig – Immunoglobulin

IL – Interleukin

IFN – Interferon

ITS – Insulin-transferrin-selenium

Isn – Isoniazid

Isn-SLN – Isoniazid-loaded solid lipid nanoparticles

KRB – Krebs-Ringer Buffer

LDH – Lactate dehydrogenase

LLI – Liquid-liquid interface

LPS – Lipopolysaccharide

ManLAM – Lipoarabinomannan

MBSA – Maleylated bovine serum albumin

MDR-TB – Multidrug-resistant tuberculosis

MHC – Major histocompatibility complex

MRs – Mannose receptors

M-SLN – Mannosylated SLN

MTB – *Mycobacterium tuberculosis*

MTT – 3-(4,5-Dimethylthiazol-2-yl)-2,5-Diphenyltetrazolium bromide

MV – Microvillus

NaFlu – Sodium fluorescein

NHBE – Normal human tracheal/bronchial epithelial

NPs – Nanoparticles

OATs – Organic anion transporters

OATPs – Organic anion-transporting polypeptides

OCTs – Organic cation transporters

OPM – *O*-palmitoyl mannan

OPP – *O*-palmitoylated pullulan

O-SAP – *O*-steroyl amylopectin

P_{app} – Apparent permeability

PAM – Aminophenylmannopyranoside

Pen/Strep - Penicillin-Streptomycin

PAMPs – Pathogen-associated molecular patterns

PBS – Phosphate buffered saline

PdI – Polydispersity Index

PFA – Paraformaldehyde

PLGA – Poly(lactide-co-glycolide) acid

PM – Physical mixture

PMA – Phorbol 12-myristate 13-acetate

PMA-dTHP-1 – Phorbol 12-myristate 13-acetate-differentiated THP-1

PVA – Poly(vinyl alcohol*)*

Pza – Pyrazinamide

Rif – Rifampicin

RLDPI –Rifapentine-loaded proliposomal dry powder for inhalation

SA – Stearylamine

SD – Standard deviation

SEM – Scanning electron microscopy

SLC – Solute carrier

SLN – Solid lipid nanoparticle

4-SO4GalNAc – 4-sulfated-N–acetylgalactosamine

SP – Surfactant protein

SV – Secretory vesicles

TB – Tuberculosis

TEER – Transepithelial electrical resistance

TEM – Transmission electron microscopy

TFA – Trifluoroacetic acid

TJ/AJ – Tight junctions/adherent junctions

TLRs – Toll-like receptors

TGF – Transforming growth factor

TNF – Tumor necrosis factor

2D – Two-dimensional

3D – Three-dimensional

WHO – World Health Organization

W/O – Water/oil

W/O/W – Water/oil /water

XDR-TB – Extensively drug-resistant tuberculosis

ZO – Zonula occluden

CHAPTER I

STATE-OF-ART

This chapter was partially published in the following publications:

- Costa A, Sarmento B, Seabra V. Targeted Drug Delivery Systems for Lung Macrophages. Current Drug Targets. 2015;16(14):1565-81;

- Costa A, Andrade F. Tissue-based *in vitro* and *ex vivo* models for pulmonary permeability studies In: Sarmento B, editor. Concepts and Models for Drug Permeability Studies. Amsterdam: Woodhead Publishing; 2016. p. 255-72;

- Costa A, Pinheiro M, Magalhães J, Ribeiro R, Seabra V, Reis S, Sarmento B. The formulation of nanomedicines for treating tuberculosis. Advanced Drug Delivery Reviews.2016;102:102-15;

STATE-OF-ART

1. Morphology and physiology of respiratory tract

1.1. Lung physiology and tissue biology

The respiratory system is the main entrance of exterior air, enabling the body oxygenation through gas exchange between environment and organs. It is a complex system that possesses several airways parts (nose, pharynx, larynx, trachea, bronchi, bronchiole and alveoli) with different characteristics that conduct the inhaled air until it reaches the alveoli. Airways at distal portions become more branched, smaller and thinner, with an increase of the surface area that allows the gas exchange between alveoli and blood capillaries (1).

Inhaled air may contain microorganism and particles that can be dangerous to the organism, but the respiratory system contains defense mechanisms that are able to remove and/or neutralize possible threats. The same defense mechanisms that prevent the development of diseases are also responsible for the clearance of particles or even pharmaceutical systems when administered by pulmonary route, influencing this way, the bioavailability of the inhaled drugs. Cough, mucociliary escalator, macrophages and epithelium are the main defense mechanisms of lungs that maintains its health, and their inefficiency or failure could result in several lung diseases (2, 3). The epithelium throughout airways forms a physical barrier; the presence of ciliated cells and the production of mucus and antimicrobial compounds in the bronchial region constitute important defense mechanisms, that in conjugation with macrophages and surfactant at alveolar region, clear the potential noxious substances and pathogens (3).

Respiratory system is anatomically divided in upper airways (nose, pharynx and larynx), and lower airways, composed by trachea, bronchioles and alveoli. (1). Upper airways are responsible for conducting inhaled air towards lower alveoli where the gas exchange occur, but also presents the function of air filtration, heating and humidification (4)**.** Each part of respiratory system present physiological, morphological and functional specificities, being this way constituted by different types of tissues to

fulfill its functions (1). Special attention is given to epithelium, since it delimits all respiratory tract acting as a barrier against injury and is also responsible for pathogens and particles clearance from inhaled air. According with location, this barrier is composed by different types of epithelium with different cell proportions and morphologies (5, 6).

1.1.1. Nasal cavity

Nasal cavity is the main entrance of air into respiratory systems, and it is characterized by having different types of epithelium, with different morphologies and functionalities: at nasal vestibule there is a squamous epithelium that changes towards a pseudostratified columnar ciliated epithelium at the nasopharynx region; a transitioned epithelium with non-ciliated cuboidal cells and an olfactory epithelium can be also found (7). Basal cells, responsible for renew and differentiation of new populations (8), and goblet cells, which segregate mucus (7, 9), are also presented on the respiratory epithelium of nasal mucosa.

Nasal mucosa promotes the humidification and heating of the air; additionally, nasal cavity shape creates a turbulent flow on the inhaled air that causes the impact and deposition of particles (10). It is covered by mucus layer and through underlying cilia beating, the mucus layer moves distally towards the oropharynx being posteriorly swallowed (7).

Nasal cavity is highly vascularized and permeable, being an interesting route for drug administration. However, the excessive secretion of mucus observed in some occasions compromise the proper drug absorption (11-13).

1.1.2. Tracheobronchial tree

Inhaled air passes through nose or month and reaches the pharynx, where large particles can impact; thereafter it flows towards the trachea, a cylindrical and semiflexible tube of 12-17 mm internal diameter and 10-13 cm in length (10, 14). The pseudostratified columnar epithelium of trachea with 50 µm of thickness is constituted by goblet cells that produce mucus, ciliated and brush cells, which allows the transport

of particles and debris towards upper airways. It is also possible to find a subpopulation of basal cells with the main function of cell renewing and replacing in the events of injury. The wall of trachea is also constituted by a basement membrane (BM) and connective tissue, which is surrounded by incomplete C-shaped rings of hyaline cartilage (14-16).

Trachea has three main functions: warming and humidification of air, clearance of particles and conduct the air between larynx and bronchi (14). At distal portion, trachea divides into two main bronchi, which in turn branch themselves, so that the number of airways increases and became smaller, forming bronchioles (1, 10).

Main bronchi still have cartilage with the function of support, but with branching and decrease of size at distal portions, cartilage becomes scarce until be inexistent in the terminal bronchioles (10). Epithelium at bronchi varies upon the location: at upper bronchial region epithelium is similar with the one of trachea, with large ciliated cells; but at distal portions it changes for a simple ciliated epithelium with cuboid cells and ends with a simple non-ciliated cuboidal epithelium at terminal bronchiole (figure 1.1) (1, 17). Bronchiole's walls present smooth muscle and connective tissue (composed by collagen I/III, elastin and fibroblast, which regulate the diameter of airway and airflow (6)), and are also irrigated by blood from bronchial circulation (1).

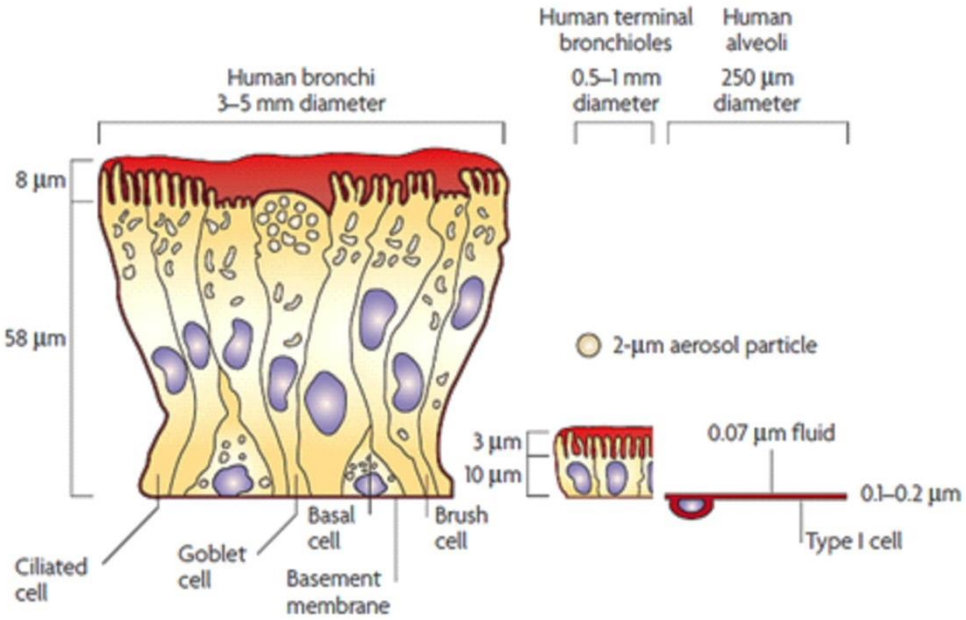

Figure 1.1. Morphology and thickness of epithelium in different lung regions. Reprinted with permission from (18).

At tracheobronchial airways there are goblet cells at epithelial surface, which are characterized by presenting secretory granules that produce mucins (19, 20), the main components of mucus, that form a barrier and maintain the homeostasis between environment and lung epithelium. In a general way, when mucins are overexpressed cause airway obstruction, such in the case of asthma, cystic fibrosis and chronic obstructive pulmonary disease (21).

At submucosal level are present the submucosa glands, which comprises a secretory tubule, a collecting duct and last, a ciliated duct which opens at airway surface. At most distal and acinar portion of secretory tubules there are serous cells, whereas mucus cells are usually located at proximal region of tubules and ducts (figure 1.2) (22, 23). Submucosa glands produce gel forming mucins by mucus cells, especially MUC5B (19), while the antimicrobial components are secreted by serous cells (24).

Submucosa glands are innervated, being regulated by autonomic nervous system (22, 24) through neural and also by humoral mediators, such histamine, tumor necrosis factor (TNF)-α, interleukin (IL)-1β, among others (24). They are mainly located at nasal cavity, trachea and bronchi, decreasing in number at terminal bronchi. Moreover, in this region there are some histological changes, since epithelium becomes simple cuboidal with less ciliated cells and with no goblet cells, being Clara Cells the predominant secretory cells in this region (20, 25, 26).

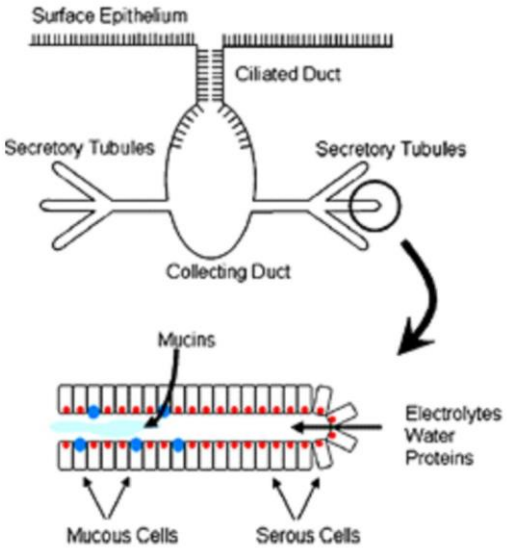

Figure 1.2. Representative image of submucosal gland presented at submucosa. Reprinted with permission from (23).

Clara Cells are non-ciliated secretory cells presented at small airways, with several functions: synthesis and production of Clara cell secretory protein (CC16) and other immunomodulatory substances (such surfactant protein (SP), anti-microbial peptides, cytokines and chemokines, and galectin-3), metabolic activity, and mucus secretion when exposed to some injury (27, 28). In addition, a subset of Clara cells are responsible for the maintenance of epithelium due to its activity as a bronchiolar tissue-specific stem cell (27).

Tracheobronchial epithelium possesses ciliated and mucus producing cells, acting as a mechanism of mucociliary clearance (3). Serous cell and mucus cells continuously secrete mucus that trap inhalable particle (29), and through cilia movements, the mucus and large diameter inhalable particles are transported towards oropharynx where they are swallowed (1, 30, 31). Nonetheless, fine particles can overcome these barriers and reach the lower airways (1, 30).

Mucociliary clearance mechanisms depends not only the action of mucus and ciliary beating, but also on the volume of airway surface liquid (ASL) (32). ASL is constituted by a sol phase, also called periciliary liquid layer which is composed by a non-viscous serous fluid placed adjacently to the epithelial cells. On the top of periciliary fluid there is a mucus layer (designate as gel phase). This is constituted by a viscous and elastic layer with glycosylated macromolecules (mucins) that enable the entrapment of bacteria and airborne particles (33, 34). Periciliary liquid presents the function of mucus lubrication and maintain an optimum distance between mucus and underlying epithelia, allowing the mucus clearance through the cilia beating or even by cough (33, 34).

A disorder on the production and transport of ASL (such imbalance of ASL composition) impairs the ciliary beating and can cause the failure of mucociliary clearance, causing lung diseases (35).

1.1.3. Air-blood barrier tissue

Bronchioles end at alveolar space containing about 480 millions of alveoli where the gas exchange occurs (17). Epithelium in this region is composed by two different types of alveolar epithelial cells (6, 17): alveolar type I cells (ATI) cells and alveolar type II cells (ATII) cells. The first ones are large squamous cells that cover the majority of alveolar surface. ATII cells, on the other hand, are cuboid cells with the ability to

reproduce, representing only 3-5% of alveolar surface. They are also responsible for the surfactant production, a thin liquid layer that covers the epithelial cells, whose functions are the reduction of surface tension inside of alveoli and to help the clearance of inhalable particles (36, 37).

The alveolar epithelium forms part of the air-blood barrier, a physiologic structure with about 140 m^2 and a thickness between 0.2-2 µm (17, 38) that enables the gas exchange between alveoli and blood capillaries. The air-blood barrier also comprises a continuous endothelium, that is separated from the epithelium by the BM, a layer of extracellular matrix and connective tissue. In several zones of air-blood barrier the alveolar epithelium and capillary endothelium are fused (17) (figure 1.3).

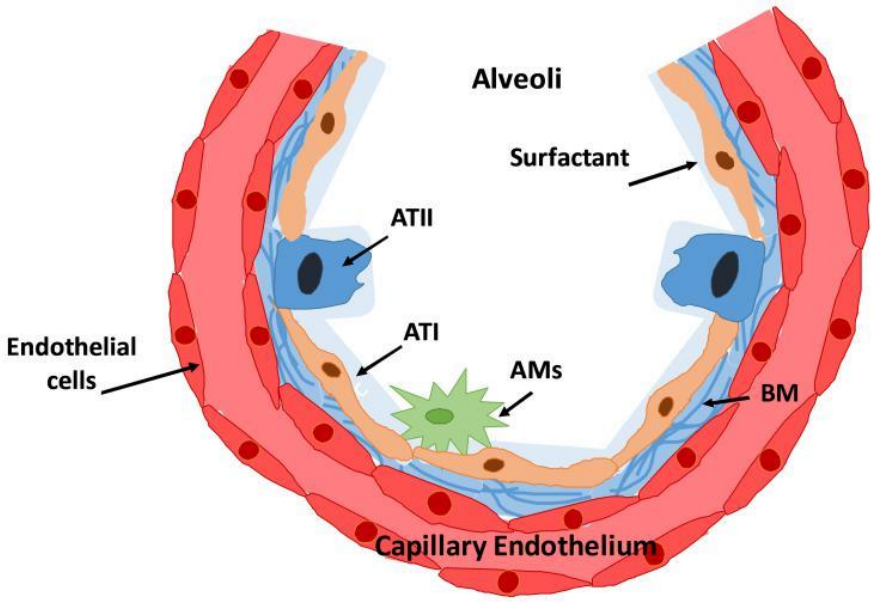

Figure 1.3. Air-blood barrier structure: epithelium at alveoli is mainly covered by ATI cells and a few percentage of ATII cells, that produce the surfactant. Alveolar macrophages (AMs) are presented at alveolar space. The capillary endothelium is in close contact with alveolar epithelium, being only separated by the BM.

1.2. The importance of lung macrophages on host-defense

In the lower respiratory tract, it is possible to find resident lung macrophages. According to its location, there are two types of pulmonary macrophages: AMs are the

main phagocytic cell at the alveolar space, constituting the first line of defense at lower airways (37), and the interstitial macrophages which are located at lung interstitial spaces of lung parenchyma (39, 40). Some species reveal the presence of constitutive pulmonary intravascular macrophages, residing on pulmonary capillaries, but it is believed that they are absent humans (41), Nonetheless, there is a lack of studies regarding these macrophages, due to the difficulty to perform *in vitro* isolation, as they are attached to the endothelium (42).

Besides pulmonary macrophages, there are other mediastinal macrophages which can be found at pleura space and at local lymph nodes (43). Pleura membrane covers the lung surface and constitute a barrier against pathogens agents. Its cavity contains different cells among them, mast cells, lymphocytes, and resident macrophages, also called pleural macrophages, representing 50% of total free cells in the pleural fluid (44, 45). These macrophages revealed functionality and phenotype similar to peritoneal macrophages (46), and are involved in some pathologies associated with lung diseases (43).

AMs and interstitial macrophages are both formed in the bone marrow as monocytes (37), and through competent migration processes are recruited to the lung where they maturate (47). However their source is still controversial, as recent studies demonstrated that monocytes may not be the source of resident macrophages in the steady state (48). Furthermore, it was described that the establishment of resident macrophages occurs before the birth and its maintenance and renewing is not dependent of blood monocytes (49).

Interstitial macrophages are considered the precursor of AMs (50), presenting morphology, function and phenotypic differences from AMs. They present half of diameter of AMs and are more heterogeneous in terms of morphology, but its phagocytic capacity is lower, despite of presenting higher levels of intercellular adhesion molecule-1 (ICAM), complement C3 protein and better antigen presentation properties (47, 50). Nonetheless, information regarding these macrophages are limited, whereas due to easy acquisition through bronchoalveolar lavage, AMs are extensively studied (50).

AMs are in quiescent state through the release of anti-inflammatory IL-10 (51) and transforming growth factor (TGF)-β produced by epithelial cells (52), avoiding the continuous activation of host-defense mechanisms when exposed to harmless airborne antigens, and consequently preventing lung injury. But the presence of

pathogens or particles, triggers an inflammatory response, with the release of inflammatory mediators and phagocytic mechanisms (37). At surface of AMs is possible to found several receptors responsible for phagocytosis, namely immunoglobulin (Ig) receptor, complement receptors (CRs), MRs and also scavenger receptors (53). They also have the potential of producing proinflammatory mediators responsible for local inflammatory response at lungs, such as granulocyte-macrophage colony-stimulating factor, IL-6, IL-1β, IL-8 and TNF-α (54, 55).

Activated macrophages can have two distinct polarized states, M1 and M2, which is influenced by different stimuli. AMs are activated for M1-like classically activated or M1 macrophage, after being exposed at different components, such lipopolysaccharide (LPS) or interferon (IFN)-γ. An immune response is initiated, characterized by the detachment of AMs from alveolar epithelial surface, production of inflammatory substances (TNF-α, IL-1β, IL-12, IL-23), reactive oxygen species, nitrogen radicals and an improvement of phagocytic capacity. In this M1 stage, cells present the ability to kill the harmful agent through phagocytosis and antigen presentation through major histocompatibility complex (MHC) receptors (47, 56, 57).

M2-like alternatively activated macrophages can be divided in different subsets. M2a is a wound-healing phenotype induced by IL-4 and IL-13, being responsible for cell matrix organization. In this phenotype, there is low phagocytic ability and low production of proinflammatory cytokines and reactive oxygen species. Tumor-associated macrophages expressed the M2b phenotype, being responsible for the initiation and development of tumor. M2c phenotype presents regulatory features through downregulation of IL-12 and up-regulation of IL-10, but AMs still present their main functions, such as phagocytosis and antigen presentation in this stage (47, 56, 58). Table 1.1 describes the features of each polarized macrophage.

Phagocytosis occurs after opsonization of an antigen by complement proteins or antibodies followed recognition trough CRs and Fc receptors (FcRs), respectively. Recognition of microorganism or apoptotic cells can be opsonin-independent, through recognition by other surface receptors, namely MR, scavenger receptors, integrins or asialoglycoprotein receptors (59).

Table 1.1. Characteristic and functional properties of different polarized macrophages*

	M1	M2a	M2c	M2b
	Classically activated	Wound-healing	Regulatory	Tumor-associated
Drivers of phenotype	INF-γ + LPS/TNF-α	IL-4 and IL-13	TGF-β and $\alpha_v\beta^6$ integrin	Dependent on tumor microenvironment
Cytokine secretion	Proinflammatory (IL-12, IL-1β, IL-6, IL-23))	Reduced cytokine secretion	Anti-inflammatory (IL-10)	Pro-angiogenic (TNF-α, vascular endothelial growth factor, IL-1), IL-10
Enzyme activity	Inducible nitric oxide synthase, matrix metallopeptidase-9	Arginase, chitinases	_____	Matrix metallopeptidase 9
Phagocytosis	Enhanced	Reduced	Normal	Dependent on tumor microenvironment
Physiological role	Host defense	Tissue repair	Immunological homeostasis	_____
Associated pathologies	Chronic inflammation; tissue damage promoting neoplasia	Fibrosis; asthma; susceptibility to infection	Susceptibility to infection	Neoplasia

* Adapted with from (47)

For the phagocytosis process, size is a critical factor. Phagocytosis is actin-dependent mechanism, where cytoplasmic membrane of AMs engulfs the particle, forming the phagosome. It enables the uptake of particles with a diameter ranging between 0,5 and 6 µm (60), but this process is more efficient when particles have size between 2-3 µm (61, 62). There are other mechanisms that enable the clearance of small particles, microorganisms and macromolecules (63). Among the endocytic mechanisms which enable the internalization of particles with small size, are of importance clathrin-mediated endocytosis, caveolae-mediated endocytosis and clathrin- and caveolae-independent endocytosis (64).

Besides the phagocytic skills, AMs are also responsible for antigen processing and antigen presentation. When the antigen is processed through endocytic route, it will combine with MCH II, to form a MCH II complex in order to be expressed at cell surface of antigen presentation cells, followed by activation of CD4+ T cells (65, 66).
In a technical laboratorial perspective, AMs refer to the macrophages obtained from bronchoalveolar lavage of the lung, and they are not characterized to be an homogenous population, but instead they are a macrophage population with different functions and atypical features (37). Moreover, on a healthy individual, AMs represent more than 80% of total cells acquired from the bronchoalveolar lavage (67).
Therefore, AMs are the first line of defense at lower airways, since they have the capacity to phagocyte inhaled particles or pathogen agents, segregation proinflammatory cytokines and antigen presentation function, being responsible for activation of the innate immunity and adaptive immune response.

1.3. The importance of lung as a route for drug delivery

Lung is the main entrance of air, pollutants, allergens and microorganism through the inhaled air. Due to its unique features, inhalation is for long time considered one of the most important non-invasive routes for drug delivery. The high surface area and vascularization at bronchioles and alveoli, the thin epithelium, low metabolism and enzymatic activity makes the respiratory system a target of growing interest as a non-invasive route for drug administration with both local and systemic action (68).
To achieve a successful delivery of drugs through the pulmonary route, several aspects must be taken into consideration during the design of drug delivery systems. The first aspect is to overcome the defense mechanisms presented throughout the respiratory tract. Cough is a protective mechanism to clear the upper respiratory tract from particles and to help the mucus removal. The cilia beating and the presence of mucus on upper airways at bronchioles also allow the removal of entrapped particles through mucociliary escalator (69). At lower airways the epithelial surface is covered by SP, that helps to regulate the tension inside of the lungs, and also the entrapment of particles that could not be removed by the defense mechanisms on upper airways. Moreover, the presence of resident macrophages (AMs) enable the phagocytosis of particles and the pathogen clearance (37). Throughout respiratory system, the different

types of epithelium also constitute a barrier to the entrance of particles and pathogens, as well as to the drug permeability into the bloodstream (69, 70).

The physical-chemical properties of drugs (aerodynamic size, density, hygroscopicity), as well the pattern of inhalation/exhalation have a great influence on drug deposition and absorption at different parts of respiratory airways (71, 72). The aerodynamic size distribution of particles is one of the main characteristic that will influence the drug deposition. Large particles, with an aerodynamic size higher than 5 µm, can impact at oropharynx and mouth and be posteriorly swallowed, while particles with an aerodynamic size between 1-3 µm can have a deep lung deposition through inertial impaction and sedimentation mechanisms (68, 73). Particles with an aerodynamic size below 1 µm can reach the alveoli through diffusion mechanism but can be exhaled (74, 75), nevertheless, particles with a size lower than 100 nm can translocate through the alveolar epithelium and be distributed through extra-pulmonary organs, such as brain, liver, kidney or heart (76, 77). By other hand AMs can efficiently phagocyte particles with an average size of 500 nm (60, 78).

For the pulmonary administrations an inhaler must be used. Pressurized metered-dose inhalers, dry powder inhalers and nebulizers are the most well-known inhalers. The device can influence the deposition pattern after aerosolization, so that its selection must be done in order to achieve the highest efficacy for a specific formulation (68).

2. Nanotechnology for pulmonary drug delivery against *Mycobacterium tuberculosis*

2.1. Physiopathology of *Mycobacterium tuberculosis* infection

Tuberculosis (TB) is the second most prevalent human infectious disease caused by the etiologic agent *Mycobacterium tuberculosis* (MTB) (79). According to World Health Organization (WHO), the number of deaths is globally falling, but in 2015 were estimated 10.4 million new cases of TB (80).

The infection starts by inhalation of aerosol droplets containing the bacteria. Once the bacillus reaches the alveolar space, it can be phagocyted by the AMs (81), and resides inside the phagosome, through the preventing of phagosome-lysosome fusion (82).

Infected macrophages induce the release of inflammatory cytokines leading to the attraction of new phagocytic cells, despite their inability to remove the previous phagocyted mycobacteria, forming focal lesions called granulomas (83). Early granulomas are composed by a core of infected macrophages surrounding by other cells, such foamy macrophages, (granuloma-specific cell population with high lipid content) (84), lymphocytes and other mononuclear cells (85). With the maturation of granuloma, a fibrous capsule is formed containing infected macrophages, lymphocytes, fibroblasts, endothelial cells and foamy macrophages (85).

At latent stage of this disease, TB infection is asymptomatic and non-transmissible, granuloma can heal forming small fibrous and calcified lesions at immunocompetent patients. Granuloma is useful to limit the spreading of bacteria, but during an immunosuppressive state, granuloma can liquefy, enabling the activation and replication of bacteria, so that TB can spread to other organs (liver, kidney, genitalia, central nervous system) through lymphatic and blood circulation, giving rise to extrapulmonary TB (83).

AMs are crucial for TB infection and resolution, since are the main target of TB, their long-standing reservoir, and they can promote an immune response which might lead to the infection resolution.

2.2. Tuberculosis therapy and limitations

Current therapy for TB starts by daily oral administration of first-line antituberculosis (anti-TB) drugs (isoniazid (Isn), pyrazinamide (Pza), rifampicin (Rif) and ethambutol) for a period of 2 months, followed the administration of Isn and Rif for more 4 months (86). Second-line anti-TB drugs, which includes aminoglycosides, fluoroquinolones and oral agents (prothionamide, ethionamide, terizidone, D-cycloserine, and para-amino salicylic acid), can be used in association with first-line anti-TB drugs (87), especially in the case of drug-resistant TB.

Resistant to TB strains is one of the main drawbacks of current TB therapy. It is defined as multidrug-resistant tuberculosis (MDR-TB) when TB presents *in vitro* resistance to Isn and Rif, or as extensively drug-resistant tuberculosis (XDR-TB) when *in vitro* resistance is observed to four drugs, at least one injectable second-line anti-TB drug and fluoroquinolone, in addition to Isn and Rif (88, 89). To overcome the TB resistant,

two new drugs, delamanid and bedaquiline, have been approved by the European Medicine Agency in 2014 (90, 91), for treatment of MDR-TB and XDR-TB in adults, for a maximum period of 6 months (88). Delamanid was also approved to be used on children with more than 6 years of age (92).

TB treatment is associated with several toxic effects, which associated with long-term therapy, can cause low patient compliance. Hepatotoxicity is the main secondary effect caused by the first-line anti-TB drugs, but the second-line anti-TB drugs are recognized for being more toxic (93): aminoglycosides may cause nephrotoxicity and ototoxicity (94), fluoroquinolones can cause cardiotoxicity and D-cycloserine may originate central nervous system toxicity (95)

Anti-TB drugs are mainly administered through oral route (some drugs are administered through parenteral route), requiring high dosages to reach an effective drug accumulation at lung for the bacteria killing (71, 96). The first-pass metabolism by the liver is also responsible for the side-effects and low drug bioavailability. Therefore, several approaches are under investigation for pulmonary delivery of anti-TB drugs, with the main goal of reduce the side effects, improve the lung bioavailability, reducing the time of therapy and lastly, the anti-TB drug resistance. The use of nanotechnology to design anti-TB drugs-loaded nanocarriers can be a suitable approach for the local treatment of pulmonary TB (71, 96).

2.3. Nanocarriers for the pulmonary delivery of antituberculosis drugs

Nanotechnology is an area of science regarding the design and study of structures, called nanoparticles (NPs), in which at least one of the dimensions is measured at the nanoscale range (1 to 1000 nm). NPs can be used for medical purposes, namely as nanocarriers for therapeutic and diagnostic agents by means of encapsulation, covalent attachment, or surface adsorption of these agents (97). The use of NPs as a strategy for pulmonary drug delivery is a promising area of research for several reasons. First, the size of these particles can be fine-tuned to reach different areas of the lung, allowing for successful passive targeting strategies. Second, their surface can be modified and ligands attached to actively target bodies of interest, such as AMs (98). Third, studies have demonstrated that pulmonary delivery of nanosuspensions

favor higher lung tissue concentrations and markedly raise the lung to serum ratio of drugs, compared with other routes of administration (99, 100). This could improve bioavailability and consequently dosing frequency, which ultimately leads to the improvement of patient compliance and better efficacy of treatment (100).

Inhalable nanocarriers offers a potential value in local and passive delivery of anti-TB therapy (68, 71). The most common carriers to achieve pulmonary delivery are liposomes, lipid-based (Solid lipid nanoparticles (SLN) and nanostructured lipid carriers(NLC) and polymer-based NPs (figure 1.4).

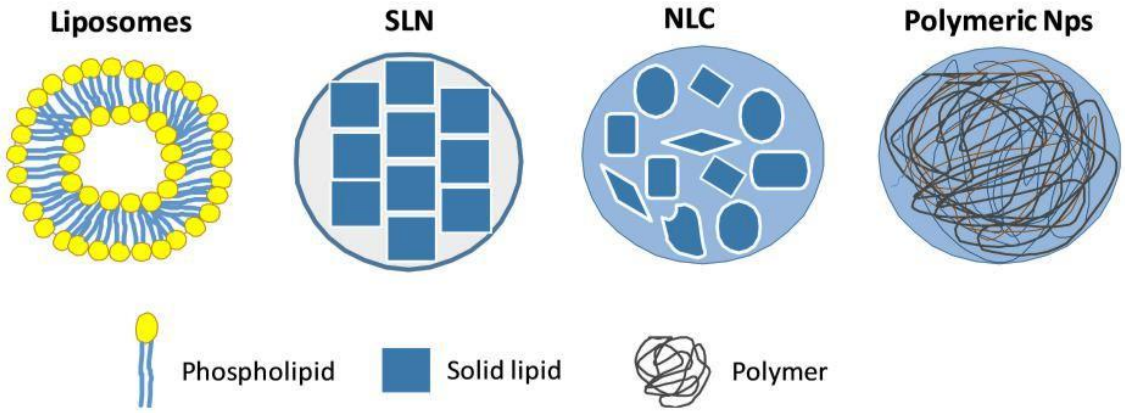

Figure 1.4. Different types of nanocarriers for anti-TB drug delivery.

2.3.1. Liposomes

Liposomes are vesicular structures, constituted by phospholipid bilayers enclosing an aqueous medium (101, 102). They were discovered in 1965 and possess a unique and versatile structure, with a lipid and aqueous regions, which can be altered to make them better suited to carry hydrophilic, lipophilic or amphiphilic particles (103, 104). Their size can be fine-tuned to achieve different regions of the lung by passive targeting, and their structure and composition can be changed to achieve active targeting to specific cells, namely AMs (105-108). Liposomes seem particularly appropriate for pulmonary delivery, since they can be formulated with endogenous compounds, such as the components of pulmonary surfactant (109). However, many aerosolization techniques can compromise liposome structure and integrity. In most

aerosolized liposome formulations for pulmonary delivery, liposomes are formed before packaging. This usually results in rupturing of vesicle structure during administration, thereby losing the ability of promoting a sustained release. However, it had already been demonstrated that PEGylated and plain tuftsin-conjugated liposomes are stable enough to undergo nebulization in the course of an inhalational therapy (110). For all the above-mentioned reasons, it is therefore not uncommon to find a vast number of studies involving pulmonary delivery of drugs with liposomal formulations, many of them focusing on antibiotics and particularly anti-TB drugs. Recently, Chattopadhyay *et al*. (2012) showed that changing their composition, by incorporation of charged lipids into the bilayer, such as cholesterol (Chol) molecules, prevented the particle aggregation and preserved bilayer integrity after air-jet nebulization (111). Another approach is based on the fact that a drug–lipid mixture solubilized in chlorofluorocarbon will form liposomes upon hydration in small airways. Gaur *et al*. (2012) explored the hypothesis of forming liposomes *in situ*, since the lung has a wet surface, which could provide an aqueous phase for spontaneous formation (112). The formulation encapsulating Rif with a loading efficiency of 29-38% was formed by egg phosphatidylcholines, Chol and dicetylphosphate. They have reported that no vesicle rupture was observed with *in situ* formed liposomes and a prolonged drug release was achieved.

Other anti-TB drugs have already been encapsulated in liposomes. Liposomes made of dipalmitoylphosphatidylcholine for the delivery of Isn (loading efficiency of approximately 37%) were developed and evaluated *in vitro* by Chimote *et al*. (2009) (113). They observed a sustained release of Isn encapsulated into liposomes, held over 24 hours after a burst release in the first 5 hours of 50% of the drug. They have also conducted biocompatibility and stability studies, and found the formulations to be haemocompatible, cytocompatible, and stable for the duration of at least one month. Justo *et al*. (2003) studied the possibility of co-encapsulation of several anti-TB drugs (*i.e.,* Isn, Pza, Rif, ethionamide, and streptomycin) in liposomes made of distearoylphosphatidylcholine and Chol (109). However, under the tested conditions, Rif and ethionamide were not successfully encapsulated. Low encapsulation efficiency was achieved to both Isn and Pza, with loading efficiency respectively of 3 and 2%, being the encapsulation of streptomycin the highest (42%). Gaur *et al*. (2010) published a feasibility study where they used Rif as the model drug (112). In this study, *in situ* formed liposomes made of phosphatidylcholine and Chol showed a better

sustained release profile than the preformed liposomes, but both aerosolized liposomes showed an improved delivery of Rif over plain drug aerosols, with an encapsulation efficiency around 30%. Recently, Patil *et al*. (2015) developed Rif-loaded freeze-dried liposomes and their results confirmed that as the concentration of Chol increased, the drug release decreased (114). The optimized formulation had 79.25% of drug entrapment efficiency and showed a slow and sustained release of drug. Aerodynamic characterization data suggested that the developed NPs were within respirable size range. *In vitro* results revealed an enhanced solubility of drug and higher anti-TB activity, when compared to pure drug alone (114). Patil-Gadhe *et al*. (2014) successfully applied the principles of quality by design to develop rifapentine-loaded proliposomes for inhalation by spray drying in a single step. Their results demonstrated a sustained drug release with a longer retention of drug in lungs (115). One year later, Patil-Gadhe *et al*. (2015) evaluated the anti-TB activity, *in vitro* cytotoxicity and *in vivo* toxicity of rifapentine-loaded proliposomal dry powder for inhalation (RLDPI) (114). The results confirmed anti-TB potential of rifapentine in spray-dried RLDPI. Moreover, the direct delivery of rifapentine in the form of RLDPI to the lungs, achieved higher drug concentration in the lungs than free drug (114). These studies clearly indicate that anti-TB-encapsulated liposomes have remarkable potential as direct drug delivery system to the lungs.

2.3.2. Lipid Nanoparticles

Lipid NPs show higher drug loading capacity, higher stability, and may not require the use of organic solvents during production in contrast to liposomes and polymeric NPs (79). On the other hand, like liposomes and most polymeric NPs, these nanocarriers are biocompatible, can be produced with appropriate size and morphology for lung targeting and deposition (116), being studied as a viable pulmonary drug delivery strategy (117). SLN and NLC are the most common lipid NPs used, and their surface can be modified to achieve active targeting of AMs.

Several studies have showed that SLN are suitable systems for pulmonary drug anti-TB delivery. Jain *et al*. (2008), who compared four different nanocarriers for the incorporation of ciprofloxacin, showed that SLN are capable of prolonged drug release

(118). Pandey and Kuller (2005) have prepared SLN constituted by stearic acid for pulmonary delivery through nebulization (117). They incorporated Isn, Rif and Pza with loading efficiencies of roughly 50% for each drug. All the formulations promoted a sustained drug release with a burst drug release less than 20% in the first 6 hours, and 11-15% during 6-72 hours, in the case of Isn and Pza; for Rif, 9% of release was observed in the first 6 hours, while 11% occurred during 6-72 hours. The nebulized SLN were successfully deposited in the lungs and were detected in other organs up to 7 days after administration. Administrated free drug was cleared within 24-48 hours. Chuan *et al*. (2013) developed Rif-loaded SLN as an AMs-target drug delivery system. Their Rif -loaded SLNs had an average size of around 800 nm and showed relatively low cytotoxicity when their concentration was higher than 20 µg/mL. Moreover, their results demonstrated that Rif-loaded SLN were internalized more selectively in AMs than in ATII cells (119).

NLC are a novel type of lipid NPs, composed by a mixture of solid and liquid lipids which creates an imperfect crystal matrix, enhancing the drug loading and minimizing the drug expulsion during storage (120). Studies already explored the encapsulation of Rif (121) and rifabutin (122) into NLC, as a strategy for pulmonary TB treatment. Both systems presented a good encapsulation efficiency (above 80%), a minimum toxicity and they could be mannosylated with the aim to target AMs. Due to their characteristics, lipid NPs offer an economical approach for pulmonary administration of anti-TB drugs.

2.3.3. Polymeric NPs

Natural and synthetic polymers are used for the purpose of producing polymeric NPs as nanocarriers for drug delivery (97). Common examples of natural polymers suitable for pulmonary delivery are alginate, chitosan and gelatin. Synthetic polymers include poly(lactide-co-glycolide) acid (PLGA), poly lactic acid, poly anhydride and poly acrylate (123).

Polymeric NPs are among the most widely researched systems for drug delivery in general, and many reports focus on pulmonary delivery in particular. These delivery systems fulfill the requirements for pulmonary delivery, such as: sufficient association

of the therapeutic agent with the carrier particles, targeting towards specific sites or cell populations in the lung, protection the therapeutic agent against degradation, promotion of drug release at a therapeutically optimal rate, low toxicity, and stability against forces generated during aerosolization (124).

Drug delivery formulations containing anti-TB drugs have already been used with these nanocarriers. Jain *et al.* (2008) compared four different NPs formulations for ciprofloxacin delivery, three of them being polymeric NPs. The authors incorporated the drug into albumin, gelatin and chitosan NPs and studied their drug release profiles. Of the three polymers, albumin and chitosan NPs proved to be more capable of drug incorporation (48% and 35% loading efficiency, respectively) and sustained release (up to 120 and 96 hours, respectively) (118).

Alginate NPs have been studied by Ahmad *et al.* (2005) for the incorporation of Rif, Isn and Pza. The mentioned particles had aerodynamic diameters in the respirable range and presented high drug encapsulation efficiencies for both drugs (between 70-90%). *In vivo* studies showed that inhalation of alginate NPs had a higher accumulation at lung and other tissues and also enable to reduce the number of administration when compared with to oral administration (125).

Abdulla *et al*. (2010) used two different molecular weights of poly-(ethylene oxide)-block-distearoyl phosphatidyl-ethanolamine polymers to produce nanocarriers for pulmonary delivery of Rif (126). It was reported a high drug loading and entrapment efficiency (84-104%) and noticed that these values were influenced by drug:polymer ratio, but not by the molecular weight. Particle size and aerodynamic characterization showed that the prepared formulations were suitable for lung deposition through inhalation.

Chitosan presents important properties to act as an inert carrier, such as mucoadhesive properties, biocompatibility, biodegradability, low toxicity and ability to promote the macromolecules permeation through a well-organized epithelium (127). Moreover, it has recently been shown that cross-linked chitosan NPs can be used with pressurized metered-dose devices (128). This study also showed that this approach could be used for local therapy of lung diseases, such as TB. Pourshahab *et al*. (2011) produced chitosan/tri-poly phosphate NPs for Isn delivery, with a size around 449 nm and a loading efficiency of 17%. The formulation exhibited a release profile with an initial drug release burst, followed by slow and sustained release in the following 6 days (129). Garg *et al*. (2015) prepared and characterized spray dried inhalable

chitosan NPs for sustained delivery of Isn and Rif (130). Their results include NPs with an average size of 230 nm and a drug encapsulation efficiency of 69% for Isn and 71% for Rif. Additionally, their formulations showed lower cytotoxicity and significant reduction in the number of bacilli in the lungs comparatively to free drug (130).

PLGA NPs are extremely common in nanosystems and have been used to encapsulate some anti-TB drugs. Sung *et al*. (2009) demonstrated that PLGA NPs loaded with Rif could be formulated, resulting in "porous NPs-aggregate particle", particles with aerosol properties suitable for lung delivery (131). *In vitro* and *in vivo* studies showed a delayed release of the drug up to 8 hours. Moreover, the presence of Rif in the lung of guinea pigs was detected up to 8 hours after the delivery. Jain *et al*. (2010) reported enhanced results when using PLGA NPs conjugated with lactose and encapsulated with Rif (loading efficiency between 38-42%) (132). The conjugated particles resulted in greater average size and drug payload, slower drug release, and enhanced uptake in lung tissue over uncoupled NPs and drug solution.

Incorporation of hydrophilic drugs into polymeric nanosystems proved to be challenging. Cheow *et al.* (2010) modified PLGA preparation methods to achieve higher encapsulation efficiencies of water-soluble antibiotics, using levofloxacin as a model drug (133). The formulation exhibited a loading efficiency between 4-23%. In addition, the obtained formulation showed antibacterial activity even after spray drying. In other instance, lipid-polymer hybrid NPs (with a polymeric core and a lipid coat) were developed to incorporate levofloxacin, ciprofloxacin and ofloxacin (134). The authors showed that lipophilicity of drug influenced the drug loading and the release profile: more lipophilic drugs (namely levofloxacin) can have a higher drug loading and due to interaction with the lipid coat, lipophilic drugs showed a sustained release profile. These studies support the idea that polymeric NPs-based drug delivery systems are suitable for targeting the cellular reservoirs of TB.

3. Functionalized nanosystems for alveolar macrophages targeting

3.1. The relevance of surface receptors of alveolar macrophages for drug delivery

AMs express different receptors on its surface with the ability to recognize different foreign compounds, and to promote its internalization. Of special relevance are MRs, belonging to the subgroup of C-type lectin-like superfamily. This glycoprotein has the ability to bind several polyanionic molecules as well pathogen-associated molecular patterns (PAMPs), playing an important role on the development of an immune response (135, 136). Mannose residues are not found at terminal ending of mammalian glycoproteins, but are present at surface of many microorganisms, enabling the recognition between self and non-self (137). Through MRs, AMs can recognize several mannose residues, enabling the receptor-mediated cellular uptake. Therefore, mannose-functionalized nanosystems can be a suitable approach for AMs targeting. The MRs also recognize some sulfated carbohydrates whose recognition motif is 4-sulfated-N–acetylgalactosamine (4-SO4GalNAc). Usually these sugars are presented at some pituitary hormones (lutropin, thyroid-stimulating hormones), so that MRs participate on its clearance (136, 138). C-type lectin-like receptors of AMs not only respond in presence of mannose, but also in presence of galactose residues which are also expressed on the surface of several microorganism such, *Yersinia pestis*, *Streptococcus pneumonia*, MTB and influenza viruses (67). MRs present a good strategy for targeting drugs towards AMs (139). Although they are not a specific receptor of these cells and are expressed on other types of cells, namely dendritic cells, kidney mesangial, hepatic endothelial, tracheal smooth muscle, and retinal pigment epithelial cells (138).

On the surface of AMs are present several receptors besides MRs, like toll-like receptors (TLRs), scavenger receptors, integrin receptors and FcRs.

AMs express sialoadhesion, a receptor of Siglec (sialic acid binding Ig-like lectin) family (140, 141), with the ability to internalize virus through endocytosis (142, 143). This receptor is not only expressed at lung macrophages, but also in macrophages located in the spleen, lymph nodes and at stroma of bone marrow (144). In humans, it was demonstrated that alveolar and interstitial macrophages have sialoadhesion, but this

receptor is also present in other resident macrophages at liver, bone marrow, spleen, colon and lymph nodes (145).

TLRs recognizes microbial compounds, which initiates signal transduction pathways, leading the expression of genes-related to immune response (146). The pattern of TLRs expression is different according with the organs (TLR3 and TLR5 are expressed at gut epithelial cells (147) whereas TLR1, TLR2, TLR3, TLR4 and TLR5 are presented at blood monocytes, lung and colon macrophages (148)), and each type of TLRs presents specificity for a ligand. Cellular components or degradation products from cellular matrix, namely polysaccharides and proteoglycan, proteins and peptides, nucleic acids and phospholipids can be recognized through TLRs (149). TLRs do not present a direct relationship with microorganism uptake (150). They can recognize PAMPs, having an impact on innate and acquired immunity through the regulation of phagocytosis and antigen presentation (151). Unlike C-type lectin receptors, whose functions are antigens uptake, processing and presentation, TLRs combine the function of non-self-antigens recognition, and also enable the initiation of intracellular signaling cascades that promote the proinflammatory cytokines release, and the expression of co-stimulatory molecules for T cells activation (151, 152).

Integrins are also receptors expressed at surface of AMs responsible for extracellular matrix adhesion (153). These receptors play a role on the interaction of cells with the extracellular matrix (such as laminin, fibronectin or collagen), having influence on cell and tissue organization, cell-cell interaction and differentiation (154). They are in contact with cytoskeletal proteins of the actin contractile system, and can produce intracellular signals, enabling the control of cell surveillance and proliferation (154).

AMs also express at surface scavenger receptors, which usually are able to recognize polyanionic molecules (155), as acetylated or oxidized *l*ow-density lipoprotein, phosphatidylserine, dextran sulfate, polyinosinic acid and bacterial components (156).

Additionally, receptors for the Fc portion of antibodies are expressed in different types of immune cells, namely polymorphonuclear leukocytes, monocytes, macrophages, lymphocytes and natural killer cells (157, 158). Phagocytosis is an innate immune mechanism responsible for the engulfment of particles, usually higher than 500 nm (159). This process is activated by interactions between opsonins and receptors expressed by the macrophage surface, namely CRs and FcRs. When Ig binds to FcR of leukocytes, an immune response is triggered, being involved mechanism of

phagocytosis, antibody-dependent cell-mediated cytotoxicity, production of cytokines and the release of proinflammatory mediators (158).

3.2. Lipid-based nanoparticles for mannose receptors targeting

Different approaches of mannosylated drug delivery systems, such liposomes or SLN, have already been addressed with the aim to target MRs, enabling its internalization through receptor-mediated endocytosis (figure 1.5) (108, 139, 160, 161).

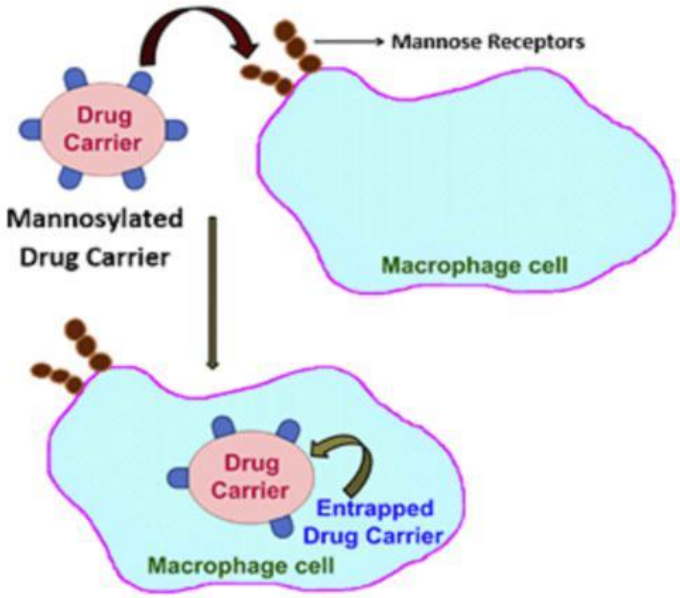

Figure 1.5. Macrophages targeting through lectin receptors. Adapted from (162).

Usually mannosylated systems present a high uptake by AMs (108, 139, 160). Systems with high ligand density can be more effectively internalized by macrophages (163), but the internalization of mannosylated nanocarriers can be inhibited by the presence of specific ligands for MRs, such mannan (108, 164).

Liposomes are biocompatible nanocarriers, with the ability to improve the drug bioavailability and efficacy, allowing at same time, the reduction of side effects. Moreover, they improve drug stability and can promote a drug sustained release (165). According with the type of lipids, composition and proportion of each component used during the formulation, these systems can have different physical-chemical

properties, namely size, charge, fluidity, and can be sensitive to different pHs or temperatures (166), being this way considered a good approach for an efficient target towards AMs (165).

Some strategies to improve the AMs targeting were performed through the coating of liposomes with specific ligands that present affinity for the MRs.

Liposomes based on soya phosphatidylcholine and Chol were produced, for amphotericin B incorporation. These liposomes were followed coated with *O*-palmitoyl mannan (OPM). On the same study, amphotericin B-loaded liposomes, constituted by soya phosphatidylcholine, Chol and phosphatidylethanolamine, were coated with *p*-aminophenylmannopyranoside (PAM) through covalent linking (167). Biodistribution assay showed that both formulations were able to accumulate at liver and spleen when compared with plain liposomes. However, the accumulation of PAM-coated liposomes was higher at liver and spleen, whereas OPM-coated liposomes were more effective on lung targeting, suggesting that OPM when anchored at liposomes is more effective on delivery amphotericin B or other drugs at lungs (167).

Similarly, after administration of *O*-palmitoylated pullulan (OPP)-coated liposomes and OPM-coated liposomes through aerosol, there was a higher drug accumulation at lung tissue for both system comparatively to the respective plain liposomes or free drug, providing this way, another approaches for a specific lung macrophages targeting (168).

Other study published by Vyas *et al*. (2004) analyzed two different approaches for AMs targeting. Through the incorporation of dicetylphosphate that conferred a negative charge, the liposomes were further coated with alveolar macrophage-specific ligands. In this case, maleylated bovine serum albumin (MBSA) and *O*-steroyl amylopectin (O-SAP) were conjugated with phospholipid tails (169). Both ligand-mediated liposomes presented a higher drug accumulation at lungs than neutral or negative charged liposomes (169), because MBSA is an anionic ligand with affinity to scavenger receptors (169, 170), while O-SAP-coated liposomes were internalized by AMs, since these cells have affinity for amylopectin-coated liposomes (169).

Beside liposomes, SLN have been studied as an alternative to liposomes since they present a good physical stability with high drug payload, and the ability to improve drug stability. As they are constituted by biocompatible lipids, they are well tolerated and have low toxicity. Moreover, SLN present feasibility of scaling-up and can be manufactured without organic solvent (165, 171, 172).

SLN can be functionalized with mannose residues through ring opening of mannose followed reaction with aldehyde group of mannoses with free amines of lipids, presented on the surface of the particle (161, 173). *In vivo* studies performed by Sahu *et al.* (2014) showed that mannosylated SLN (M-SLN) had a higher accumulation at lung tissues than bare SLN. Moreover, the percentage of paclitaxel recovery at lungs was higher at M-SLN (26%) over bare SLN (18%) and plain drugs (4%) after 24-hour of intravenous administration, indicating that M-SLN are a good approach for lung diseases targeting (173). The functionalization of SLN with mannose or other related compounds, such mannan also showed ability to target AMs with a favorable *in vitro* cell uptake over bare SLN (139, 174).

3.3. Polymeric nanoparticles for alveolar macrophages targeting

As mentioned before, mammalian AMs express MRs on their surface, able to recognize glycoprotein residues, whose terminal ending are constituted by mannose, glucose, L-fucose residues, and N-acetyl-D-glucosamine (175).

In this regard, Song *et al.* (2012), synthesized a glycopolymer through the use of functionalized carbohydrates as precursors. Each sugar monomer (mannose and N-acetylglucosamine and galactose) was functionalized with ethyl methacrylate (EMA), followed polymerization and conjugation with maleimide-containing fluorophore. The glycopolymer containing mannose-EMA and N-acetylglucosamine-EMA were internalized by AMs after administration in mice, but glycopolymer containing galactose-EMA showed less internalization. Through flow cytometric analysis, the uptake of mannose-EMA was up 6-fold higher than galactose-EMA, demonstrating its specificity for intracellular drug delivery on macrophages (176).

Chitosan is a biodegradable, biocompatible, non-toxic copolymer constituted by monomers of β-linked D-glucosamine and N-acetyl-D-glucosamine (177). Besides its mucoadhesive properties, chitosan is able to interact with MRs of macrophages, enabling chitosan-vesicles phagocytosis and its degradation at phagolysosome (178). *In vitro* study published by Park *et al.* (2013) demonstrated that ofloxacin-loaded glutaraldehyde-cross linked chitosan microspheres were internalized by AMs, and the uptake was 3.6-fold higher than free drug powder. It was suggested that positive charge of chitosan can have electrostatic interaction with negative cell membrane due

to N-acetylglucosamine residues of chitosan, that allows the macrophages recognition and phagocytosis of this polymer (178). However, Sarmento *et al.* (2011) demonstrated that chitosan provided stealth properties to NPs, and the uptake of chitosan-coated particles by macrophages decreased over uncoated particles (179). As an alternative to chitosan, mannosylated chitosan systems have been widely used for different purpose such gene therapy (180, 181), intranasal immunization (182) or for Rif delivery against visceral leishmaniasis (183).

Galactomannan (GalM) is a polysaccharide constituted by galactose and mannose monomers, both recognized by lectin-like receptors. Moretton *et al.* (2013) developed two systems, one constituted by chitosan NPs modified with galactomannan hydrolyzed (GalM-h) and a second one formed by polymeric micelles, coated with GalM-h/chitosan. Through fluorescence studies and by the measurement of intracellular Rif concentration was verified that both GalM-h-modified systems presented a higher uptake by RAW 264.7 macrophages over the controls. In parallel, interaction between mannose residues and soluble lectins occurred, and due to mannose residues presented at GalM, these systems were recognized by lectin-like receptors and further internalized by macrophages (184).

The use of polymers for microspheres production have also been used to target drugs against AMs. Polymeric particles produced by double emulsion solvent evaporation method or spray-drying showed a higher stability when compared to liposomes and can be formulated as a dry powder for pulmonary delivery (185).

Hyaluronan is a biodegradable polymer with mucoadhesive properties (186). It is endogenously secreted in the lung (187), and have the ability to avoid pleura thickening in TB-infected patients (188). Study with hyaluronan microspheres containing ofloxacin prepared by spray-drying, showed that macrophage cells were able to internalize higher amounts of this system when compared with free drug solution (2.1-fold) and ofloxacin microspheres (1.7-fold) (187).

PLGA microspheres demonstrated to have the ability of being phagocyted by AMs (189-191). This synthetic polymer presents several advantageous properties such non-toxicity, biodegradability and biocompatibility. For an efficient drug delivery into AMs, it is important that the system can be phagocyted as many as possible, and the phagocytic activity must be the highest. The surface of microsphere is important for macrophage clearance. It was demonstrated that microspheres with primary amine groups presented an effective internalization by AMs, when compared with different

functional groups (sulfate, hydroxyl and carboxyl groups). Microparticles with carboxyl group on their surface were also effectively internalized, but with a slight lesser extension than primary amine groups (60).

The particle size is another issue which must not be neglected during development of formulations for lung delivery. PLGA microspheres can be used to develop aerosolized formulations, since its aerodynamic diameter is nearby of 3 µm with a narrow size distribution, being suitable for pulmonary administration (192). PLGA microparticles ranged from 1 up to 6 µm can be considerably more phagocyted than 10-µm particles. Moreover, a large population of macrophages were able to phagocyte 3-µm particle size (190). These outcomes, in the other hand are in agreement with the study performed by Hasegawa *et al.* (2003), where drug-loaded PLGA were more efficiently uptake when they present a 3-µm diameter (60).

PLGA has been widely used to produce large porous particles because it presents a large surface contact area and good flow characteristics required for lung delivery. But this polymer presents low mucoadhesiveness, due to limited ability to produce hydrogen bonding with mucous glycoproteins (192), allowing a rapid clearance of particles from lungs, a reduction of drug absorption and consequently a reduction of drug efficacy. According with monomer ratio lactide/glycolide and molecular weight, different drug release profiles can be also achieved. It was already demonstrated that PLGA with 20000-molecular weight presented a 7-day lag phase and a constant drug release almost during 20 days, whereas almost 90% of drug was released from the system after 10 days when PLGA with lower molecular weight (5000 or 10000) was used (189).

Table 1.2 summarizes the different nanocarriers systems for AMs targeting.

Table 1.2. Overview of systems used for AMs targeting.

	Ligand/polymer	Cell line used/Type of study	Outcomes/Advantages and disadvantages	Reference
SLN	Mannose	Uptake studies on J774 cell line	Mannose coating SLN presented 6 times higher internalization than uncoated SLN;	(139)
	Mannan	RAW 264.7 to study *in vitro* transfection efficiency	Functionalized SLN had a higher transfection efficiency than uncoated SLN, trough ligand-receptor-mediated active targeting mechanism;	(174)
NLC	Mannose	No uptake studies	High encapsulation efficiency of rifabutin (higher than 80%): Mannose coating confirmed by fourier transform infrared (FTIR) spectroscopy; Faster release at pH acid;	(122)
	Mannose	Uptake studies on NR8383 cells and AMs	Mannosylated NLC were more efficiently internalized than unmodified NLC;	(121)
Dendrimers	Mannose	Uptake studies on AMs isolated from rats	Slower release rate of drug at pH 7.4, which is enhanced at pH 5.0. Mannosylated dendrimers were internalized by AMs;	(160)
	Sialic acid conjugated and mannosylated poly(propyleneimine) (PPI)	Uptake studies on AMs	Internalization of zidovudine by AMs was significant higher in the system containing both ligands over free zidovudine;	(193)

Liposomes	Cholesten-5-yloxy-*N*-(4-((1-imino-2-d-thiomannosylethyl)amino)alkyl) formamide	Uptake studies on AMs isolated from Wistar rats	Mannosylated liposomes with a high content of mannose exhibit high affinity for MRs, leading to a higher internalization by AMs;	(108)
	4-aminophenyl-a-D-mannopyranoside	Uptake studies on NR8383 cells	Mannose ciprofloxacin-liposomes had an efficient target against AMs over free drug or bare liposomes;	(194)
	Palmitoyl mannose and 4-SO4GalNAc	Uptake studies on J774A.1 and RAW 267.4 cell lines	4-SO4GalNAc-functionalized Amphotericin B - liposomes presented a higher internalization over mannosylated liposomes (almost 2-fold in J774 cell lines and almost 2.5-fold in RAW 267.4 cells;	(136)
	OPM	*In vivo* biodistribution study	After 24 hours, OPM-coated liposomes presented a higher lung accumulation, when compared with PAM-coated liposomes (the percentage of drug recovered was 4.6 ± 0.02% and 1.8 ± 0.1%, respectively);	(167)
	OPM and OPP	*In vivo* pharmacokinetics studies	After 24-hour administration through aerosol, the percentage of drug recovered at lung was higher for OPM-liposome (11.23 ± 0.9%) and OPP-liposome (9.86 ± 1.6%), when compared with plain liposomes (1.01± 0.03%) and amphotericin B solution (not detectable);	(168)

Liposomes	MBSA and *O*-SAP	*In vivo* biodistribution studies	After 24 hours, it was observed an accumulation of Rif in lungs when *O*-SAP- and MBSA- coated liposomes were used (% of drug recovered was 10.75 ±1.8 and 8.12 ± 1.6, respectively), whereas Rif were not detectable when aerosolized as a solution or entrapped into bare liposomes;	(169)
Polymeric NPs	Glycopolymers (Mannose-EMA and galactose-EMA)	*In vivo* uptake studies by AM derived from C57BL6 mice	AMs had 6-fold higher internalization of mannose-EMA, when compared with galactose-EMA after intratracheal administration in mice;	(176)
	Glutaraldehyde-crosslinked chitosan	Uptake studies on NR8383 cells	Ofloxacin uptake was up to 3.6-fold higher from the chitosan microspheres when compared with free drug powder;	(178)
	Hyaluronan	Uptake studies on RAW 264.7	Uptake of ofloxacin from hyaluronan microspheres was 1.7-fold and 2.1-fold higher than ofloxacin microspheres and aqueous solution, respectively;	(187)
	Mannosylated gelatin	Cell uptake studies performed on AMs	Mannosylated formulation showed 2.7 and 18.0 times higher internalization by AMs than uncoated formulation and free drug, respectively;	(195)
	Mannosylated gelatin	*In vivo* biodistribution and antitubercular activity	Mannosylated particles showed a high Isn delivery at alveolar tissues and a reduction of bacterial counts after administration on TB-infected mice;	(196)

Polymeric NPs	Albumin	Tissue distribution in albino mice	After I.V. administration, ofloxacin concentration at lungs was higher (432 µg/g), regarding control group treated with free drug (1.32 µg/g). Furthermore, drug concentration at lungs was higher than other tissues and blood, suggesting that the microspheres could deliver ofloxacin mainly at lung tissue;	(197)
	GalM-h and GalM-h/chitosan	Uptake studies on RAW 264.7	Both GalM-h-modified systems presented a higher internalization by AMs over the controls;	(184)
	PLGA/ polylactic acid -*b*-poly (ethylene glycol)-mannose, associated with SP-A	Uptake studies on THP-1 and AMs macrophages from BALB/c mice	Internalization by THP-1 macrophages was higher when SP-A was associated; SP-A coated mannosylated NPs showed a higher uptake by AMs comparatively to SP-A coated non-mannosylated NPs;	(198)
	Mannose-modified chitosan	*In vivo* studies on C57BL/6 mice	Mannose-modified chitosan were accumulated on AMs when observed on lung cryosection from mice;	(199)

4. *In vitro* cell culture models as a tool to assess the lung permeability

4.1. General considerations

High-throughput techniques are in high demand, especially during the discovery of new chemical-entities or even during the early stage of drug development. These techniques can be a valuate tool to predict pharmacokinetic parameters, such as drug absorption and metabolism, efficacy and the toxicity of compounds (200).

In vitro cell models offer a good approach to predict drug absorptions and its bioavailability, and until now, different models to assess permeability across intestinal mucosa (201), blood-brain barrier (202) and pulmonary epithelium (203) have been established.

The cells used for building these models can be derived directly from tissue (primary cells) or can be immortalized. Primary cells present relevant markers and transporters similar to *in vivo* tissue, but they required a laborious isolation process, and the cost of maintenance is quite high comparatively to immortalized cell lines. They also present a high-donor variability, being usually replaced by the immortalized cell lines (204, 205). Cell lines present advantages over primary cells, due to its easy handling and low cost of maintenance, and usually can provide more reproducible results due to constant phenotype and genotype; nevertheless, during the cell immortalization process, cell lines can lose important features and functions that are present on primary cell cultures (204, 206, 207).

Animal models can give valuable biological and medical information (208), but not always reproduce the human outcomes (209). The use of cell models fulfils the 3Rs requirements, and does not present such overwhelming ethical issues comparatively to animal models; its use has been considered simple, economic, conferring an alternative path to the study of transport/metabolism mechanisms of drugs (210).

4.2. Mechanisms involved on drug absorption at lung tissue

Lung is the major route to the entrance of compounds, pollutants, microorganism from inhaled air, but also confer an important gateway for drug delivery. The drug absorption is dependent on its main physical-chemical features, like size, lipophilicity, pH, charge,

but intrinsic factors related with pulmonary route also have an impact on drug bioavailability (airway geometry, absorption area, presence of disease, mucociliary clearance or the macrophage clearance) (210, 211).

The alveolar epithelium is the most lung region where drug absorption may occur, nevertheless the absorption through bronchial epithelium is also important specially when new pharmaceutical systems are designed for asthma or chronic obstructive pulmonary disease (212). Absorption of drug across lung epithelium can occur through different mechanisms, namely paracellular route or transcellular route.

Paracellular route is mediated by the tight junctions, and the transport occurs between adjacent cells. This route is important for the absorption of small hydrophilic drugs, ions (213) and proteins with low molecular weight (214, 215), although the mechanism for the transport proteins is not clear, and transcytosis mechanisms can have a role on its absorptions (216). The loss of tight junction structure can increase the leakage of water and proteins into airways, originating an alveolar edema (217).

Small drugs that do not permeate through paracellular route, can cross the lung epithelium through transcellular transport, which comprises the mechanisms of passive diffusion, vesicle-mediated transcytosis and last, through transporters (figure 1.6) (215, 216).

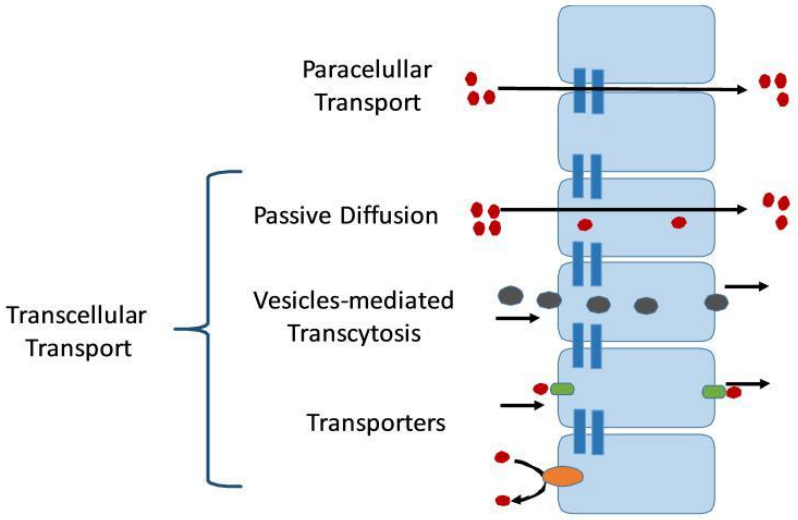

Figure 1.6. Mechanisms of absorption that occurs in lung epithelium.

Passive diffusion is the movement of a substance from a high concentration compartment towards a low concentration compartment, and it can be influence by the physical-chemical properties of the drug, blood perfusion rate and by the thickness of air-blood barrier (216). The drug absorption showed to be dependent of hydrophobicity: small water-soluble molecules can be absorbed rapidly (within 65 minutes), while small lipophilic molecules presented a fast absorption (1-2 mins); by other hand, highly positive charge and highly insoluble molecules remained for longer periods (days or even hours) (218).

Macromolecules can be transported across a polarized epithelium through vesicle-mediated transcytosis, and the transport may occur between apical-to-basolateral side, or basolateral-to-apical side (219, 220). Study performed by Bur *et al.* (2006) demonstrated that proteins, like transferrin, IgG or albumin can be transported though transcytosis mechanisms (221). The transcytosis may occur through clathrin-coated pits presented on both alveolar epithelial cells, and through caveolae presented at ATI cells and at endothelial cells (219).

Epithelial cells from alveolar tissue and bronchial tissue express several receptors that mediate the transport of drugs as well as endogenous substances. The solute carrier (SLC) transporters include the members of organic anion transporters (OATs) and organic cation transporters (OCTs), which can interact with small hydrophilic organic anions and organic cations, respectively (222). The organic anion-transporting polypeptides (OATPs) are responsible for the transport of large hydrophobic anions (222). Some of the transporters, like OCTs and OATPs present the ability of provide a bidirectional transport (222, 223). On lung epithelium were also identified transporters which trough ATP-dependent mechanism, enable the efflux of compounds out of the cells. P-glycoprotein, breast cancer resistance protein and multidrug resistance-associated protein-1, that belongs to the ATP-binding cassette (ABC) transporters family, are identified either at bronchial and alveolar tissue, being responsible for the drug efflux to the extracellular space, and consequently the resistance of anti-cancer drugs (224, 225).

Transporters play an important role on drug absorption at pulmonary tissue, but its expression differs according to the lung region, and each cell line presents a unique expression pattern, and differently from primary cell cultures (226).

4.3. *In vitro* cell based models to assess the pulmonary permeability

In vitro cell models are high-demand for the replacement of animal models. Cell cultures with one type of cells have been performed for many years, but these models were usually cultured only as a single flat monolayer (two-dimensional (2D) *in vitro* models), and in that situation, models were very simplistic and did not represent the realistic tissue-like conditions. Therefore, the combination of different types of cells and the inclusion of a scaffold/cell matrix allows the formation of a complex systems (three-dimensional (3D) *in vitro* models) that would better represent the specific features of each tissue (204, 227).

In this section the bronchial and alveolar *in vitro* cell models used for permeability studies will be briefly discussed.

4.3.1. *In vitro* models of bronchial epithelium

Calu-3 and 16HBE14o- cells are the main cell lines used to mimic the bronchial epithelium. These cells form a polarized epithelium with the expression of tight junctions when cultured under Transwell® membrane (228). The cultures conditions, either at air-liquid interface (ALI) or liquid-liquid interface (LLI), confer different characteristics to each cell line. Calu-3 presented a high transepithelial electrical resistance (TEER) and the expression of tight junction when cultured at LLI conditions (229). However, ALI conditions enable a change on the cell morphology, the production of mucus (229, 230), and allowed a different expression of membrane transporters (231) that consequently influenced the drug transport (232). Overall, ALI conditions formed a Calu-3 monolayer whose features better resemble the *in vivo*-like condition. The culture conditions also influenced the characteristic of 16HBE14o- cell line, since this cell line did not produce mucus under ALI, and the tight junction markers were only expressed when cultured at LLI (233, 234).

Other cell lines have been used as an *in vitro* model of bronchial epithelium. Primary normal human tracheal/bronchial epithelial (NHBE) are cell derived from the distal parts of trachea and carina. They were able to form a pseudostratified epithelium with a tight junction collar, with goblet cells at apical side and last, with cilia, although with less density per each cell (235). The infection of NHBE with an adenovirus SV40 (236)

originated an immortalized normal human bronchial epithelial cell, BEAS-2B, and both cells were able to express the same magnitude and pattern of genes after exposure to crystalline silica (237). But unlike Calu-3, BEAS-2B cell line did not express tight junctions (238).

NCI-H441 cell line is another human bronchiolar epithelial cell line isolated from patients with papillary adenocarcinoma, and presents morphological characteristics of Clara-like cells, and the expression of different markers associated to ATII cells (239). Salomon *et at* (2014) demonstrated that this cell was able to form a relevant barrier with high TEER (nearby 1000 $\Omega.cm^2$) with the production of tight junctions when cultured at LLI and presented relevant membrane transporters that are usually expressed on the primary cultures of human alveolar epithelial cells (hAEpC), being considered as a suitable model for mimic the ATI cells (240).

Several *in vitro* co-cultures models have been established by the combination of bronchial epithelial cells with immune cells (241-244) or even with fibroblasts (245, 246), whose main goals were to assess the barrier properties, nanocarriers interaction or even the inflammatory response. Moreover, there is on the market fully differentiated organotypic 3D airway tissue models of epithelia, called MucilAir™ (from Epithelix) or EpiAirway™ (from MatTek Corporation). Cells are from different tissues (either from nasal, tracheal and bronchial in the case of MucilAir™ or from NHBE cells in the case of EpiAirway™). Both organotypic models are from donors in a healthy or disease state and showed similar morphological and metabolic feature to the mucociliary epithelium (247-249).

4.3.2. *In vitro* models of alveolar epithelium

The alveolar epithelium has an extensive surface area where the drug absorption occurs. *In vitro* models of alveolar epithelium have been purposed to study the drug permeability. Primary ATII cells can be obtained after the isolation and purifications from lung biopsies, and when placed under appropriated culture conditions they can differentiate into hAEpC cells (250, 251). These cells form a tight barrier (TEER reached 1000 $\Omega.cm^2$) with a similar morphology to alveolar tissue (251, 252) as well type-I cell markers (low levels of SP and high level of caveolin-1 (250). Nevertheless, due to time-consuming process of isolation/purification the use of immortalized cell

lines still present advantages, and several *in vitro* models with a single epithelial monolayer or in co-culture with a different cell types (macrophages, dendritic cells or endothelial cells) have been established.

A549 is a human lung adenocarcinoma cell line, mostly used to mimic the alveolar epithelium. This cell line presents similarities with ATII cells, with a cuboidal morphology and the presence of lamellar bodies (253). It does not form a tight polarized barrier due to its inability to express functional tight junctions (254, 255), so that the use of A549 for evaluation of drug transport must be carefully interpreted. Co-culture of A549 culture with blood monocyte–derived macrophages and dendritic cells has been used to study the particle translocation and inflammatory response after exposure to different types of particles (256, 257). Polystyrene particles with a size of 1.0 µm were found inside of three cell lines used, even when dendritic cells were seeded on the basolateral side of filter inserts, being in this way, not directly exposed to the particles (256). Alfaro Moreno *et al.* (2008) also established co-culture models of alveolar epithelium to assess the inflammatory response after exposure to particulate matter (258). This study showed that the levels of cytokines were higher when either macrophages or endothelial cells were presented, being these models a tool to study the cell-cell interaction or cellular mechanisms (like inflammatory response or endothelial dysfunction), that can be involved after exposure to foreign particles.

The presence of endothelium also plays a role on the drug transport as well on the inflammatory response, but most of time, its presence is neglected. Hermanns *et al.* (2004) performed a co-culture model where human primary cells from pulmonary microvascular tissue were cultured at basolateral side of Transwell®, while two different human pulmonary adenocarcinoma cells (A549 and NCI-H441) were seeded on the apical side. The results showed the formation of a tight polarized membrane when NCI-H441 cells were incubated with dexamethasone (Dex): TEER was 218 ± 93 $\Omega.cm^2$ and 565 ± 48 $\Omega.cm^2$ for NCI-H441 monoculture or in co-culture with endothelial cells, respectively (239). This *in vitro* co-culture model demonstrated to be a step forward to the use of conventional alveolar epithelial monolayer, by the presence of endothelial cells and also by its responsiveness when incubated with proinflammatory stimuli. The use of primary cells in this *in vitro* model constituted a limitation regarding the cost of cell culture maintenance, donor-donor variations and limited number of passages. The absence of immune cells also represents a drawback, once they are

essential for the development of an *in vitro* inflammatory response. Recently, Kasper *et al.* (2017) developed a triple co-culture containing macrophage-like cells with different states of polarization, seeded on the top of a co-culture constituted by epithelial cells (A549 or NCI-H441) and microvascular endothelial cells ISO-HAS-1. The results showed that these models presented the ability to perform an inflammatory response after LPS exposure, even when the macrophages were in an alternative activated stated (M2 phenotype) (259).

As an alternative to primary human epithelial cell and A549, a human alveolar epithelial lentivirus immortalized (hAELVi) cell line was recently established, with type I-like features, namely the presence of caveolin-1, caveolae and the absence of SP-C. This cell line formed a tight barrier (TEER higher than 1000 $\Omega.cm^2$) and produced tight intercellular junctions (zonula occluden (ZO) -1 and occludin) (260). The integrity of this cellular barrier was kept when hAELVi cells were co-cultured with differentiated THP-1 (dTHP-1) cells under ALI, indicating that this new *in vitro* model could be used to assess the transport of inhaled drugs or nanocarriers (261).

4.4. Microengineering for lung-on-a-chip

The development of *in vitro* cell culture models is having a great contribution on the high throughput screening of drugs. 3D *in vitro* co-culture models offer an advantage through the use of different cell types and extracellular matrix, enabling the study of interaction between cells or even cell-extracellular matrix. These complex *in vitro* models allow to study cell differentiation, migration, transport, gene and protein expression, inflammatory response and to evaluate pharmacokinetic parameters.

The majority of these cell culture models are established on Transwell® system, and consequently cells are mainly cultured under static conditions. Moreover, pharmacokinetic parameters of drugs/nanocarriers are usually assessed without consideration the fluid flow or mechanical forces, causing a misinterpretation of the outcomes (262). Therefore, the development of 3D cell culture models on organ-on-a-chip is being explored with the aim to form an *in vitro* model that morphologically and physiologically resemble a specific organ. Through microfabrication and microfluidics techniques, organ-on-a-chip comprises the use of microfabricated channels and the manipulation of small volumes (10^{-9} to 10^{-18} liters) to form a organotypic 3D model.

With these devices, cells may be continuously perfused, and a tissue can be formed with an architecture and organization similar to the *in vivo*-like conditions (262-264). The environment of a specific tissue can be mimic through the manipulation of system geometry, flow rate or mechanical force (262, 265).

Polydimethylsiloxane is the most material used for the microfabrication of chips for cell culture purpose. It is a flexible, economic, biocompatible material, ease of prototyping, and with the ability to sustain the cells under perfusion conditions. It also presents good optical transparency and gas permeability that allows the cell oxygenation (265-267), however, this material can adsorb small hydrophobic molecules (268).

Organ-on-a-chip platforms have been employed to create different types of tissues, namely Intestine (269), lung (270), blood-brain barrier (271), liver and skin (272). Huh *et al.* (2010) developed a new microfluidic system through microfabrication, being constituted by two channels separated by a membrane coated with extracellular matrix. On each side of this membrane, epithelial and endothelial cells were seeded, and when confluence was reached, epithelial cells were exposed to the air. Stretching forces through the use of vacuum was applied to this microfluidic device in order to mimic the breathing movements, and those mechanical forces showed an impact on the NPs transport across this model, being more similar with the *in vivo* outcomes (273). The use of microfabrication devices was also employed to study fluid mechanical stress that may occur upon lung injury (270, 274).

Lastly, the connection of multi organs-on-a-chip allow the formation of a human-on-a-chip, a more physiologic relevant model that would better allow to study interactions between different organs as well the drug pharmacokinetics during pre-clinical trials (262, 275).

3D printing technique can be a valuable approach for the fabrication of organ-on-a-chip (276). 3D bioprinting allows the construction of tissues with a precise anatomy and physiology, where spatial distribution of cells can be controlled, as well the microenvironment essential for the organ function (like stiffness or tissue perfusion) (276). This technique can be an added value for the development of *in vitro* models with high throughput screening purposes. Tissue can be fabricated through cell seeding onto an acellular scaffold or through directly deposition of cells (being called bioprinting) (277). Two-different approaches can be used to integrate 3D printing techniques with microfluidic technology: one-step of fabrication, which includes the printing of the entire chip (276, 278), including the microfluidic device and cells, or

through two-step of fabrication, where cell can be printed into a pre-formed device (276, 279).

Tissues like liver (279, 280), skin (281) or kidney (282) have been engineered through 3D printed organ-on a-chip approach. Horváth *et al.* (2014) used the 3D bioprinting technique for the fabrication of an 3D model of air-blood barrier on a Transwell® system. The use of this technique allowed the formation of thinner cell layers comparatively to the manual seeding. Besides that, epithelial and endothelial cells formed a tighter layers with a better homogenous distribution, while the manually seeding originated the formation of clusters and consequently a non-uniform distribution of cell (283). Nevertheless, the fabrication of 3D printed lung-on-a-chip has not been reported.

CHAPTER II

OVERVIEW AND AIMS OF THE WORK

OVERVIEW AND AIMS OF THE WORK

1. Overview

The use of nanocarriers for drug delivery into the lung is the focus of study for many research groups and pharmaceutical companies. When compared to classical dosage forms, nanocarriers have the ability to increase the transport, the cellular uptake and drug stability, protecting them from degradation, promoting an overall increase of drug bioavailability and the reduction of side effects.

To predict the pharmacokinetic and toxicity of drugs and nanocarriers on the early stage of development, the use of *in vitro* models has been widely explored as a high throughput screening platform. *In vitro* models composed by different types of cells, mounted on different scaffolds allow to create a model system that mimic the anatomy and physiology of a specific tissue, like gut, air-blood barrier, blood-brain barrier.

Pulmonary route is one of most well-known non-invasive routes for drug administration. The alveolar epithelium is a thin and vascularized epithelium, with low enzymatic and metabolic capacity, and for that reasons, this epithelium has gained relevance as a portal for drug delivery, either for locally delivery or even for the systemic drug absorption. *In vitro* models that mimic the alveolar epithelium are common based on primary cultures isolated from lung biopsies, facing problems with the isolation/purification as well with the cost of maintenance. A549 cell line, an immortalized cell line with features of ATII-like cells, is widely used as a model of alveolar epithelium, but still lacks the formation of a relevant barrier. Most of *in vitro* models are culture as a unique epithelial monoculture under LLI conditions, being considered as simple model that not resembles the alveolar environment. Moreover, the air-blood barrier is also constituted by macrophages and endothelial cells that can have an important role on the translocation of nanoparticles, although these cells are still neglected during the establishment of *in vitro* models.

2. Aims of the work

The main aim of this work was to establish a 3D *in vitro* model of air-blood barrier to evaluate the translocation of nanocarriers. Eventually, as a proof of concept, the suitability of this model as a platform of safety/toxicity screening, through the release of proinflammatory cytokines, was also assessed.

The specific objectives of this thesis were:

- To develop a nanocarrier system based on SLN for pulmonary delivery of anti-TB drugs, with the potential of circumventing the limitations of current dosage forms for the TB therapy (high toxicity, long-term therapy, resistance); Isn was selected as a model drug and encapsulated inside of lipid matrix of this nanocarrier;
- To decorate the surface of isoniazid-loaded solid lipid nanoparticles (Isn-SLN) with mannose residues, to target this system towards the MRs expressed on the AMs cells, the main reservoir of MTB;
- To establish and characterize the culture conditions essentials for built a 3D *in vitro* model of air-blood barrier, composed by a single monolayer of epithelial cells and endothelial cells on the apical and basolateral side of a Transwell® membrane, respectively, with macrophage-like cells on the top of epithelial layer;
- To explore the functional/barrier properties conferred by this *in vitro* model, in particularly the paracellular transport of small hydrophilic substances and the translocation of fluorospheres with different sizes;
- To validate the 3D *in vitro* model by assessing the translocation of Isn-SLN and M-SLN, which were deliberated designed for delivering drug at lung tissue instead of being translocated;
- To assess the release of proinflammatory cytokines after induction of an immune response with LPS.

CHAPTER III

DEVELOPMENT AND CHARACTERIZATION OF MANNOSE-FUNCTIONALIZED SOLID LIPID NANOPARTICLES FOR ISONIAZID DELIVERY

This work was published in the following publication:

- Costa A, Sarmento B, Seabra V. Mannose-functionalized solid lipid nanoparticles are effective in targeting alveolar macrophages. European Journal of Pharmaceutical Sciences. 2017; 114:103-13;

DEVELOPMENT AND CHARACTERIZATION OF MANNOSE-FUNCTIONALIZED SOLID LIPID NANOPARTICLES FOR ISONIAZID DELIVERY

1. Introduction

The surface of alveolar epithelium is a crescent relevant gateway for drug delivery, being mainly covered by squamous ATI cells and by a few percentage of ATII cells, responsible for the surfactant production and epithelium regeneration upon injury (284). On the surface of this physiologic barrier there are important resident cells, namely AMs that present the ability to phagocyte airborne particles and pathogenic agents at alveolar space (53, 285). Those cells also have an impact on lung homeostasis, since they present the ability to produce anti-inflammatory cytokines (IL-10) that avoids the inflammatory response when exposed to harmless antigens (286), or can mediate an opposite reaction by promoting the release of inflammatory mediators and reactive oxygen species, as well as ensuring neutrophils recruitment towards alveolar space. Moreover, during the inflammatory process, phagocytic capacity is enhanced as well as the ability to process and present antigens on its surface (47).

The presence of AMs at alveolar space represents a duality regarding the pulmonary administration of nanocarriers. Due to its phagocytic ability, they are able to clear the nanocarriers from alveolar surface, originating a reduction of local and systemic drug bioavailability (287). Different surface modifications on nanocarriers have been devised to promote stealth properties, namely by coating with polyethylene glycol (287), peptides (288) or chitosan (289). However, the phagocytic properties of these cells can be advantageous when a delivery system is aimed to target AMs, especially for treatment intracellular bacterial infections, such as TB. MTB, the agent responsible for this lethal disease, infects the AMs and survive inside macrophages on a latent state (290). Due to toxic effects and inefficacy of the conventional anti-TB drug on the market, different nanocarriers are being developed for the treatment of MTB (160, 291-293).

In order to enhance the internalization of nanocarrier by AMs and consequently to improve the drug accumulation on lung tissue, surface modification of nanocarriers with different ligands can also be performed (294). Mannose is one of the most common ligands used to functionally decorate the surface of these nanosystems, and they can be recognized by the MRs expressed on the surface of AMs. This receptor has eight C-type carbohydrate-recognition domains (CRDs) with the ability to recognize D-mannose, N-acetylglucosamine and L-fucose residues presented on the surface of pathogens and also endogenous ligands, namely lutropin and thyrotropin (295). Mannose receptor is involved on recognition of pathogens, on antigen processing and presentation (296, 297). Lastly, it presents an important role on clearance of MTB (298): the CDRs of mannose receptor is able to recognize the mannose-capped lipoarabinomannan (ManLAM), a component of bacteria wall that causes the phagocytosis of bacilli, and the inhibition phagosome-lysosome fusion, enabling the bacteria survival inside of macrophage (299). Therefore, the preparation of a mannosylated formulation may be a good approach for targeting drugs towards AMs. Besides the ligand-anchored to nanocarrier, the mean particle size, surface, morphology or even the inherent composition of nanosystem may influence the internalization of the nanocarriers by macrophages (60, 178, 190).

In this study different SLN were optimized by screening the lipid matrix, the inner phase composition, the surfactant phase, and last, the amount of stearylamine (SA). The final formulation with best physical-chemical properties that might promote its internalization by macrophages was further functionalized with mannose according to the methodology described at (160, 161). As a model drug it was selected Isn, a hydrophilic drug used for MTB treatment.

2. Materials and Methods

2.1. Materials

Witepsol® E85 (hydrogenated coco-glycerides, m.p.42–44◦C) and Compritol® 888 ATO(glyceryl behenate, m.p. 70 ◦C) were kindly supplied by Sasol (Witten, Germany) and Gattefossé (Saint Priest,France), respectively; Stearic acid (Edenor ST1 GW) come from Oleo Solutions (York, United Kingdom); Isn, paraformaldehyde (PFA), ethyl acetate and sodium acetate were bought from Merck (Darmstadt, Germany); Tween® 80, poly(vinyl alcohol) (PVA) (87-90% hydrolyzed, average molecular weight 30,000-70,000), coumarin-6, stearylamine SA 97%, phosphate buffered saline (PBS), D-(+)-mannose, phorbol 12-myristate 13-acetate (PMA), triethylamine High-performance liquid chromatography (HPLC) gradient grade and dichloromethane (DCM) (99.9% purity), Manucol LD and Keltone LV were purchased from Sigma-Aldrich (St. Louis, USA) ; Methanol and acetonitrile (ACN) HPLC gradient grade were from Fisher Scientific (Leicestershire, UK); Trifluoroacetic acid (TFA) was purchased from Acros Organic (New Jersey, USA); 3-(4,5-Dimethylthiazol-2-yl)-2,5-Diphenyltetrazolium Bromide (MTT), 4',6-Diamidino-2-Phenylindole, Dihydrochloride (DAPI), dimethyl sulfoxide (DMSO), sodium pyruvate and trypsin solution were bought from Sigma (St. Louis, USA); RPMI-1640, hank's balanced salt solution (HBSS), versene were purchased from Gibco (Waltham, USA); Fetal bovine serum (FBS) was from Biochrom (Cambridge, UK); Penicillin-Streptomycin (Pen/Strep) solution 100x was from Biowest (Nuaillé, France); Lactate dehydrogenase (LDH) kit was purchased from Takara Bio Inc. (Shiga, Japan); Triton X-100 was purchased from Spi-Chem (Atlanta, USA); CellMask™ Deep Red Plasma membrane Stain was purchase from Life technologies (Carlsbad, USA); IL-4 was purchase from ImmunoTools (Friesoythe, Germany). Milli-Q® water and PBS for cell culture were produced in-house.

2.2. Preparation and characterization of SLN

2.2.1. Preparation of Isn-SLN

To produce Isn-SLN, three different solid lipids commonly used for pulmonary drug delivery were selected and tested, namely Witepsol® E85, stearic acid and Compritol® 888 ATO (300). SLN were produced through a modified solvent emulsification-evaporation method based on a water/oil/water (W/O/W) double emulsion technique (172, 301). Briefly, the organic phase was composed by 200 mg of lipid and 2 mg of SA dissolved in 2 mL of DCM, while the inner phase was constituted by 200 µL of Isn aqueous solution containing 5, 10 or 20 mg of Isn. After adding the aqueous solution to the organic solution, the mixture was sonicated through a sonication probe (Vibra-Cell™ ultrasonic processor, Sonics & Materials, Inc., Newtown, USA), during 30 seconds with an amplitude of 70%; the formed water/oil (W/O) primary emulsion was dispersed in 8 mL of surfactant solution (PVA 1% (w/v)) and sonicated for another 30 seconds. The W/O/W double emulsion formed was poured into 15 mL of PVA solution and left under magnetic stirring during 3 hours for organic solvent evaporation.

Based on physical-chemical properties of SLN of formulation, Witepsol® E85 was selected as the main component of the lipid matrix, further modification on Isn-SLN were performed, through the modification of inner phase, organic solvent and the surfactant solution. The lipid matrix (constituted by 200 mg of Witepsol® E85 and 2 mg of SA) and the amount of drug (10 mg of Isn) at inner phase were kept constant in all formulations. The parameters changed are described on the following table 3.1, and all formulations were prepared according to the methodology described above in this section. The z-average, polydispersity index (PdI), zeta potential and association efficiency of these formulation were compared with control, namely the Witepsol® E85-based SLN previous selected, whose physical-chemical characteristics are showed at figure 3.1 and at the first row of table 3.1. All formulations were produced in triplicate.

2.2.2. Preparation of SLN with different amounts of SA

To improve the functionalization with mannose, the formulation selected on the previous section was prepared with different amounts of SA (either with 5, 10 and 20 mg of SA), using the same procedure already mentioned on section 2.2.1, with a slight modification: Witepsol® E 85 and SA were both weight and dissolved in 2 mL of DCM with the help of moderate heating (up to 50-60°). To avoid the DCM evaporation, all tubes were covered with parafilm during the heating. These formulations were characterized regarding the Z-Average, PdI, zeta potential and association efficiency, and the results are presented on the table 3.2.

To perform *in vitro* uptake studies, fluorescent SLN were first prepared. Briefly, 4 mg of coumarin-6 was added to the organic phase, and the preparation of this formulation was carried out according to the methodology described in this section. The physical-chemical characterization of fluorescent SLN was performed as described on the Appendix I and the results are described on the table A1 from Appendix I. Fluorescent M-SLN were further prepared using the same procedure described on section 2.6.

2.3. Physical-chemical characterization of Isn-SLN

All samples were diluted in Milli-Q® water for further characterization of z-average and PdI by dynamic light scattering; zeta potential was characterized by Electrophoretic Light Scattering. These parameters were analyzed through a Malvern Zetasizer Nano ZS instrument (Malvern Instruments Ltd, Malvern, UK). All analyses were performed in triplicate.

Association efficiency was determined by indirect method. Briefly, 1 mL of each formulation was ultracentrifuged (Beckman Coulter, Brea, USA) twice, at 50000 rpm (TLS-55-Rotor), 1 hour, 4 °C and the supernatant was collected and filtered by polyethersulfone syringe filters with 0.2 µm pore size (Merck Millipore, Billerica, USA) to remove SLN in suspension that did not sediment. The amount of Isn was quantified on the filtered supernatant by HPLC, using a Shimadzu UFLC Prominence System (Shimadzu Corporations Kyoto, Japan) coupled with an autosampler SIL-20AC, a degasser DGU-20A5, and SPD-20A detector, to

detect Isn at 260 nm. A HPLC column Licrospher® 100 RP-C18 with 5 µm particle size (LiCroCART®) and 250 mm length x 4.0 mm internal diameter was used together with a guard column (5 µm particle size); both columns were from Merck (Darmstadt, Germany).

All samples were analyzed under isocratic conditions with a mobile phase 93:7 (v/v) of triethylamine 0.1% (v/v) (pH 5.0 adjusted with concentrated TFA) and methanol, respectively, and using a running time of 10 min. Analysis was performed at 30 °C through the use of a column oven CTO-20AC (Shimadzu Corporations), with a flow rate of 1 mL/minute and a feed volume of 10 µL.

Association efficiency and loading capacity were calculated according to the equation 3.1 and 3.2, respectively, and both results were expressed in percentage.

Equation 3.1.

$$\text{Association efficiency } (\%) = \frac{\text{Total mass of Isn } - \text{Mass of free Isn on supernatant}}{\text{Total mass of Isn}} \times 100$$

Equation 3.2.

$$\text{Loading capacity } (\%) = \frac{\text{Total mass of Isn } - \text{Mass of free Isn on supernatant}}{\text{Mass of formulation}} \times 100$$

2.4. Morphological characterization of SLN

The Isn-SLN and the respective M-SLN with different amounts of SA (5, 10 and 20 mg of SA) were characterized regarding the morphology by transmission electron microscopy (TEM) (figure 3.2 and figure A1 from Appendix I). All samples were diluted 500 times in Milli-Q® water, placed on a grid for treatment with uranyl

acetate and then observed through a JEOL JEM-1400 electron microscope (JEOL Ltd., Tokyo, Japan).

2.5. *In vitro* release studies

In vitro release studies were performed at pH 7.4 (physiologic pH) and at pH 4.8 to mimic the lysosomal conditions (302, 303).

Each formulation with a mass of 1.2 mg of Isn (concentration of 1.25 mM) was placed inside of a membrane dialysis SnakeSkin® Dialysis Tubing, 10000 MWCO from Thermo Scientific (Meridian Rd, Rockfort, USA) and the ends were tied with a cord. The dialysis bag was merged into 25 mL of pre-warmed PBS (pH 7.4 and 4.8) and samples were incubated on an Ecotron Incubation Shaker (Inforts HT, Basel, Switzerland) at 37 °C with 100 rpm, assuring the sink conditions. At different time points (0.5, 1, 2, 4, 8, 24 and 48 hours) 600 µL of medium was collected and replaced with pre-warmed fresh medium. The amount of Isn in each supernatant was quantified through HPLC method described on section 2.4.

2.6. Mannose functionalization

To prepare M-SLN, mannose was dissolved in acetate buffer (pH 4, adjusted with HCl 1M) with a concentration of 50 mM and heated up to 60 °C; consequently, a specific amount of heated mannose solution was added dropwise to unloaded SLN, in order to obtain different molar ratios of SA:mannose (1:5, 1:10, 1:15 and 1:30). The mixture was maintained under magnetic stirring during 72 hours at room temperature, in order to allow the attachment of mannose to primary amine groups of SA, incorporated on lipid matrix. Then, the formulations were placed inside of membrane dialysis (MWCO 12-14000 Da from Medicell Membranes (Greenwich, UK) and dialyzed against Milli-Q® water during 1 hour to remove the free mannose and other impurities.

The M-SLN were lyophilized without cryoprotectant in order to assess the attachment of mannose to the surface of unloaded SLN by FTIR spectroscopy.

M-SLN was characterized through the detection the Schiff base band that is formed during the reaction. All characterization was performed at unloaded SLN with different amounts of SA (5, 10 and 20 mg), in order to avoid the interference of Isn on the spectra analysis.

FTIR analysis were performed using an ABB MB3000 FTIR spectrometer from ABB (Zurich, Switzerland) equipped with a MIRacle single reflection attenuated total reflectance (ATR) accessory from PIKE Technologies (Madison, USA.). All spectra were collected with 100 scans and a 4 cm^{-1} resolution in the region of 4000−600 cm^{-1}. The spectra collected were analyzed between 1800-900 cm^{-1} region, submitted to a baseline correction and area-normalized for further comparison. All spectra were treated through the Horizon MB FTIR software from ABB (Zurich, Switzerland), and plotted on Origin Pro software version 8.0 (Origin Lab Coorporations, Northampton, USA).

Physical mixture (PM) with the components of SLN formulation, namely Witepsol E85®, SA and mannose (with the same molar ratios of SA:mannose used) were prepared and also analyzed through FTIR. PM of Witepsol E85® with SA, but without mannose, was also performed (figure A2 from Appendix I).

2.7. Cell culture maintenance

NCI-H441 cell line was kindly offered by Dr. Carsten Ehrhardt from School of Pharmacy and Pharmaceutical Sciences, Trinity College Dublin, Ireland. THP-1 cell line was purchase from American Type Culture Collection (ATCC) (Manassas, USA).

NCI-H441 cells were routinely maintained into T75 cell culture flask with RPMI1640 culture medium supplemented with 10% (v/v) FBS, 1% (v/v) Pen/Strep and 1% (v/v) sodium pyruvate. When cells reached 70-80% of confluence, cells were washed with PBS and detached through the use of trypsin. Trypsin was inactivated by adding two times the volume of culture medium containing serum and after centrifugation, the pellet was resuspended and NCI-H441 cells were seeded into new culture flask.

THP-1 cells were maintained in suspension into T75 flask with RPMI1640 containing 10% (v/v) FBS and 1% (v/v) Pen/Strep. When cells reached the state of confluence, they were centrifuged and splitted into new cell culture flasks.

2.8. Metabolic activity and cytotoxicity

The influence of free Isn, Isn-SLN and M-SLN on the metabolic activity of NCI-H441 and dTHP-1 cell lines and the cytotoxicity were assessed by MTT and LDH assay, respectively, as described before (304). Briefly, NCI-H441 cells were seeded into a 96-well (4.0×10^4 cells/well) during 24 hours with RPMI1640 medium supplemented 1% (v/v) Pen/Strep, 10% (v/v) FBS and 1% (v/v) sodium pyruvate. Cells were then washed once with PBS and the samples were diluted in free-serum medium culture and incubated for 24 hours. Free Isn was added in a concentration range between 0.1-100 µM, and the Isn-SLN (with 10 mg of SA) and the respective M-SLN (with a molar ratio of SA:mannose (1:15)) were incubated with the same correspondent concentration as free Isn; the concentration of Isn in each formulation was based regarding the association efficiency of Isn-SLN. The amount of unloaded-SLN tested corresponded to the same amount of Isn-SLN. Moreover, in both assays two controls were also performed: cell treated with culture medium and cells treated with Triton X-100 1% (v/v).

After 24 hours of incubation, cells were washed twice with PBS and incubated with 0.5 mg/mL of MTT reagent for 4 hours. The medium was discharged and 200 µL/well of DMSO was added to solubilize the formazan crystals, with the help of shaking for 30 minutes. Lastly, the absorbance was measured at 570 nm through a microplate reader Synergy Mx (BioTek, Winooski, USA).

For LDH assay, after 24 hours incubation of the compounds, the 96-well plate was centrifuged (250 *g*, 10 minutes, at room temperature) and 100 µL of each supernatant was collected and transferred for another 96-well; 100 µL of LDH kit reaction mixture was added into each well, and after 5 minutes of incubation at room temperature and protected from the light, the absorbance was read at 490 nm using the same microplate reader.

2.9. *In vitro* uptake studies

2.9.1. *In vitro* uptake studies using dTHP-1 cells

Phorbol 12-myristate 13-acetate-differentiated THP-1 (PMA-dTHP-1) cells can achieve a polarized M2 phenotype, with the ability to express the mannose receptor (305-307). Therefore, before performing uptake studies on THP-1, cells were first differentiated into macrophage-like cells (dTHP-1) with PMA, and then the M2 phenotype was stimulated according to the methodology described by Chanput *et al*. (2013) (306). Briefly, THP-1 cells were seeded in 24-well plate (5.0 x 10^5 cells/well) with new culture medium supplemented with 100 ng/mL of PMA for 48 hours to allow the cell differentiation. Afterwards, cells were washed with PBS to remove the PMA and incubated with fresh medium for another 24 hours to achieve the M0 phenotype. Finally, cells were incubated with 20 ng/mL of IL-4 for another 24 hours, to allow the M2 polarization and consequently the mannose receptor expression.

For performing the *in vitro* uptake studies, dTHP-1 cells were first incubated with a 50 mM solution of mannose dissolved in HBSS (containing calcium and magnesium) during 1 hour, with the purpose to promote a competitive inhibition of the receptor between formulation and its agonist (308). In parallel, some wells were only incubated with HBSS for the same period of time. The HBSS solution was then carefully removed from each well and the fluorescent SLN and M-SLN suspension were added to each well with a concentration of coumarin-6 of 5 µg/mL, following the incubation for 2 hours. When dTHP-1 cells were pre-treated with mannose solution, the same concentration of mannose was also incubated together with the formulations during the time of experience. After incubation, the supernatant was discharged and cells were washed three times with PBS. Cells were detached from the well through the use of versene (309). The cell suspension was centrifuged, and the cells were resuspended in PFA 2%, following 20 minutes of incubation at room temperature. After a new centrifugation step to remove PFA, cells were washed with 200 µL of PBS, followed a new centrifugation step. The supernatant was discharged again, and cells were resuspended in 80 µL of fresh PBS for further analysis by confocal laser scanning microscopy (CLSM) and ImageStream®^{X} imaging flow cytometry.

2.9.2. CLSM analysis

Uptake studies were conducted as described on section 2.9.1. After fixation with PFA and washing, cells were stained with CellMask™ Deep Red Plasma membrane stain (dilution 1:20000 in PBS) for 10 minutes at room temperature. Cells were centrifuged and the pellet was resuspended in PBS to remove the staining. After two consecutive washing steps, cell nuclei were counterstained with DAPI (100 ng/mL) during 15 minutes at room temperature. Cells were centrifuged again and resuspended in PBS to remove the excess of DAPI. Lastly, after centrifugation, the supernatant was discharged and the pellet was resuspended in PBS before analysis at CLSM. Only cells without pre-treatment with mannose were observed by CLSM.

Cells were analyzed through a Spectral Confocal Microscope Leica TCS-SP5 AOBS, Leica Microsystems (Wetzlar, Germany) using a 63x HCX PL APO CS oil objective and a zoom of 2.0. Images were acquired by set the pinhole at 95.5 µm, the image size of 1024 x 1024 pixels, 16-bits of resolution and a bidirectional scanning speed at 700 Hz. DAPI, coumarin-6-loaded SLN and the CellMask™ Deep Red Plasma membrane staining was excited through a 405 Diode UV, an argon and a DPSS 561 laser, respectively. Untreated cells were used as a control to adjust the gain of each detector and to remove the green autofluorescence of the cells. Using the same adjusted settings, a Z-stacks of all treated samples was performed with a step size of 2.99-3.99 µm (4-6 slices per each image). The brightness and the contrast of each image was adjusted through ImajeJ 1.48 vs Software.

2.9.3. ImageStream®^{X} imaging flow cytometry analysis

After filtration through a nylon mesh, all samples were analyzed through the ImageStream®^{X} imaging flow cytometer equipped with INSPIRE® software (Amnis Corporation, Seattle, USA). Intensity adjusted brightfield images of the cells were collected and the fluorescent SLN or M-SLN were analyzed through an excitation laser at 488 nm with intensity of 10 mW. Untreated cells (untreated control) was also analyzed to evaluate the autofluorescence of the cells, and for

each sample 500-1000 cells were analyzed. All experiments were performed in triplicate. The fluorescence intensity of each cell was analyzed through the use of internalization wizard provided by the IDEAS® v6.2 software (Amnis Corporation). The internalization score was achieved after the generation of an erode mask with 4 pixel on the whole cell (brightfield channel), which allowed the elimination of fluorescence signal caused by adsorbed SLN on the cell surface, and consequently only the fluorescence intensity provided by internalized SLN will be quantified (310). Cells with internalization score higher than 1 were gated and the fluorescence intensity of each cell were acquired. T

2.10. Statistical analysis

Statistical analysis was done through the GraphPad Prism Software vs. 6.01 (GraphPad Software Inc., La Jolla, USA), and differences were compared using One-way ANOVA or Two-way ANOVA according to the experiment. Differences were considered to be significant at a level of $p < 0.05$ (*), very significant at level of $p < 0.01$ (**) and highly significant at a level of $P < 0.001$ (***).

3. Results and discussion

SLN are safe and biodegradable colloidal systems composed by physiologic solid lipids, and they have been used as an approach for drug encapsulation, with the aim of protect it from degradation, improve its bioavailability or even to promote its sustain release. (311). Due to its lipid matrix, this nanocarrier has been widely used for administration of hydrophobic drugs, but SLN can be also used for the delivery of hydrophilic drugs, like Isn, when produced by a modified solvent emulsification-evaporation method based on a W/O/W double emulsion technique (172, 301).

3.1. Preparation and physical-chemical characterization of SLN

3.1.1. Evaluation of SLN composed by Compritol® 888 ATO, Witepsol® E85 and stearic acid

Compritol® 888 ATO-based system originated SLN with the highest z-average (around 1 µm) when compared with SLN constituted by Witepsol® E85 or stearic acid (figure 3.1). Compritol® 888 ATO is a fatty acid constituted by glyceryl dibehenate (a mixture of mono-, di- tri- behenate of glycerol) and although being widely used to produce SLN (312), this solid lipid has influence on forming large particles, once glycerides present fatty acids with different lengths, and due to the increased distances between alkyl chain, it originates SLN with a wider space on the lipid matrix (313, 314).

Compritol® 888 ATO-based formulations also presented the highest PdI (between 0.4-0.6), which indicates the lack of stability of these formulation, as it was observed after 2-3 weeks of storage at 4 °C. In some of the batches there was a formation of a viscous semi-solid system when the W/O/W secondary emulsion was being prepared; this phenomenon called as gelatinization was described by Rui Yang *et al.* (315), when the same lipid and organic solvent were used.

Polymorphisms of Compritol 888® ATO have been studied and according to the transition state, they can influence the drug encapsulation and release, as well the stability of SLN over the time. (316). Drugs loaded into lipid matrices are able to accelerate the polymorphic transition of Compritol 888® ATO towards more stable forms (317), although surfactants agents are usually added during the SLN production in order to avoid the phase transition of Compritol 888® ATO from a less-organized state to high-organized state (312). In this case, the PVA at concentration of 1% (w/v) was not able to reduce polymorphic transition of this lipid and consequently to stabilize the Isn-SLN.

The zeta potential of formulations constituted either by Witepsol® E85 and Compritol® 888 ATO was positive, which was conferred by the presence of SA on lipid matrix, while the same formulations without SA presented a negative zeta potential, which ranged from -13 mV to -16 mV (data not shown). The inclusion of SA on SLN made of stearic acid did not change the zeta potential towards

more positive values (zeta potential of stearic acid-based SLN without SA was -18 ± 0.2 mV, data not shown). SA is a cationic lipid and it has been reported that its presence change the zeta potential of microemulsions towards more positive values (318), but when it was incorporated together with stearic acid, SA may be able to interact with carboxyl groups of this lipid, and therefore, the amine group of SA may not reach the outer interface of formulation to provide the positive surface (319).

Regarding the Isn association efficiency, Witepsol® E85-based formulations presented the lower association efficiency when the lowest amount of Isn was used (5 mg of Isn). The association efficiency increased two-fold when the amount of Isn duplicated (10 mg), but when 20 mg of the same drugs was used, no improvement was observed, mainly because this pharmaceutical system has probably reached the saturation and was not able to incorporate more drug inside of its inner aqueous phase.

During this first preliminary study, Witepsol® E 85-based SLN originated particles with the highest association efficiency, low PdI and positive surface, characteristics suitable for further functionalization with mannose. The best size for nanoparticle engineering with the aim of target macrophages is not well defined. Small particles (lower than 100 µm) can be internalized through endocytose-mediated receptors (like caveolae and clathrin (78, 159), while microparticle with size between 1-3 µm provided the highest phagocytic activity by macrophages (61, 190). The particle size's cutoff for phagocytosis is not well defined and was already suggested that particles with size higher than 500 nm can be phagocyted through actin-dependent mechanisms (60, 78, 320). In this study Compritol® 888 ATO-based SLN were not selected for the following studies due to low stability of the system, while stearic acid-based SLN might not present SA on its surface, compromising the further functionalization step. Therefore Witepsol® E 85 was selected to form the lipid matrix of SLN, once originated a nanocarrier with a size nearby of 500-600 nm, a positive surface and a good stability.

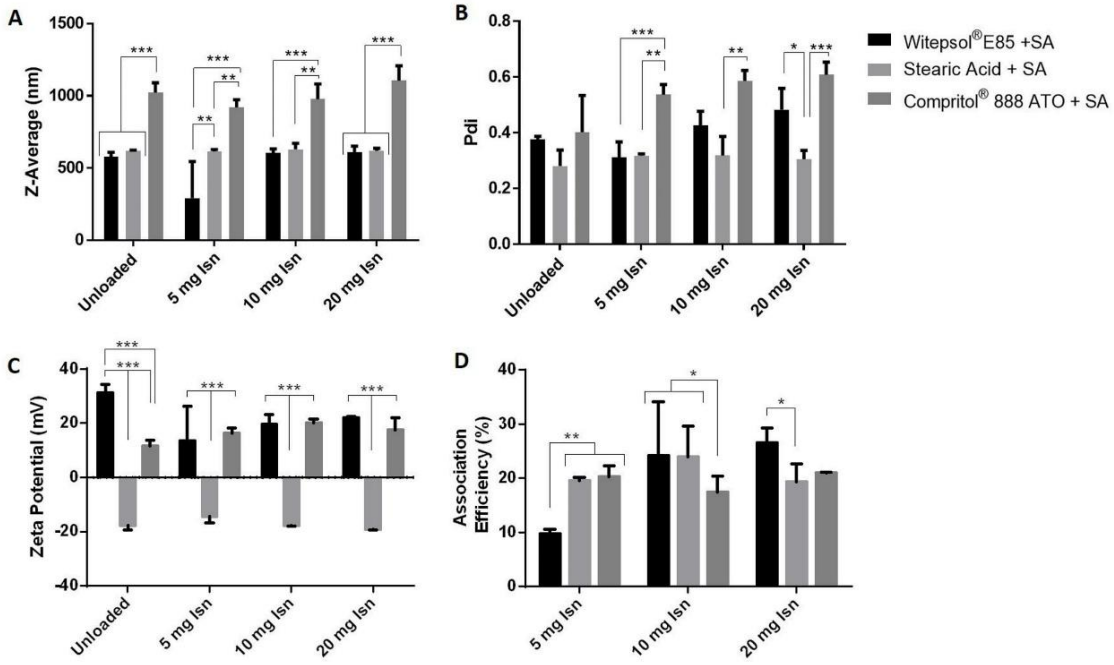

Figure 3.1. Z-average (A), PdI (B), zeta potential (C) and association efficiency (D) of Isn-SLN constituted by different solid lipid; mean ± standard deviation (SD); n=3; All formulations presented 2 mg SA on lipid matrix. Statistical analysis Two-way ANOVA with Tukey's multiple comparisons test.

3.1.2. Evaluation of physical-chemical properties of modified Witepsol® E85-based SLN

Based on the previous study, Witepsol® E85-based SLN were selected and this formulation was further optimized with the aim to increase the association efficiency of Isn. Changes on the inner phase, organic solvent and on the surfactant agent were performed. The physical-chemical analysis of the modified formulations was performed and compared with the control (Witepsol® E 85-based SLN previously selected, see first row of table 3.1).

The increase amount of PVA did not affect the physical-chemical properties of SLN. But the replacement of PVA by Tween® 80 originated SLN with a significant increased drug association efficiency (around 42%), nevertheless the PdI was higher than 0.5, and these formulations destabilized after 1 month of storage at 4 °C.

Ethyl acetate is a partially water-miscible solvent organic solvent used for SLN production, and it presents less interfacial tension than DCM, forming more stable primary emulsions (321). Therefore, when this organic solvent was used, the SLN had a lower z-average (192 ± 6.7 nm) and a narrow PdI (0.12 ± 0.1). Due to its low z-average, this formulation presented a higher surface and consequently more amine groups of SA were exposed at surface of SLN, forming a SLN with higher positive zeta potential. However, it was the formulation with the lower association efficiency (lower than 8%). SLN with a size around 200 nm can be internalized through clathrin-mediated endocytosis (322), although this mechanism is not restrictive to macrophages and can also be performed by epithelial cells (323), which could compromise the targeting of this nanocarrier. For these reason, the ethyl acetate was not selected to form the organic phase of SLN.

The changes at inner phase also influenced the characteristics of SLN. When Isn was dissolved in PBS (pH 7.4) it was produced the formulation with a size nearby of 500 nm, a positive zeta potential, and last, originated the SLN with the highest association efficiency (50.2 ± 0.5 %). This higher association efficiency may be due to influence of ionic strength of PBS that allowed the stabilization of the primary emulsion, keeping the drug inside of SLN.

In order to increase the amount of drug inside of SLN, the viscosity of inner phase was increased through the use of PVA 1% and alginates with lower (Manucol LD) and medium (Keltone LV) molecular weight. When PVA 1% was used to dissolve Isn, the z-average, PdI and the zeta potential did not change, but only 15% of drug was associated to the SLN. In the other hand, formulations containing alginates (F7 and F8) originated solid lipid microparticles, which were unstable (PdI close to 1.0) and presented a low zeta potential, so that the association efficiency of these microsystems were not assessed.

This pre-formulation study demonstrated that the modification of Milli-Q® water by PBS (pH 7.4) at inner phase of Witepsol® E85-based SLN originated a formulation with a higher association efficiency of Isn, keeping at the same time the desirable mean particle size suitable for macrophages uptake and the positive surface for further functionalization with mannose.

Table 3.1. Different modifications of Witepsol® E85-based SLN and respective physical-chemical characterization.

Inner aqueous Phase	Organic Phase	Surfactant, (w/v)	Z-Average (nm)	PdI	Zeta Potential (mV)	Association efficiency (%)
Milli-Q® water	DCM	PVA 1%	604.3 ± 29.4	0.43 ± 0.05	19.6 ± 3.5	24.2 ± 9.8
Milli-Q® water	DCM	PVA 2%	488.2 ± 6.2	0.36 ± 0.04	23.1 ± 2.2	13.6 ± 1.7
Milli-Q® water	DCM	Tween® 80 1%	511.8 ± 51.0	0.54 ± 0.03	15.8 ± 0.5	41.6 ± 1.8 **
Milli-Q® water	Ethyl Acetate	PVA 1%	192.1 ± 6.7 *	0.12 ± 0.10 **	31.8 ± 1.5***	7.7 ± 2.8*
PBS (pH 7.4)	DCM	PVA 1%	489.8 ± 7.8	0.41± 0.02	26.9 ± 2.2	50.2 ± 0.5 **
PVA 1% (w/v)	DCM	PVA 1%	915.2 ± 74.7	0.48 ± 0.07	12.7 ± 2.3	15.3 ± 2.23
Manucol LD 1% (w/v)	DCM	PVA 1%	1398.7 ± 169.8 ***	0.94 ± 0.10 ***	9.8 ± 5.4**	NA
Keltone LV 1% (w/v)	DCM	PVA 1%	1509.0 ± 372.3 ***	0.91 ± 0.16 ***	7.6 ± 3.4***	NA

The lipid matrix of each SLN contained 200 mg of Witepsol® E85 and 2 mg SA, while the inner aqueous phase had 10 mg of Isn. Z-Average, PdI, zeta potential and association efficiency of each modified SLN were compared with the characteristics of control (first row). Statistical analysis was performed through One-way ANOVA, with Dunnett's multiple comparison test; Mean ± SD; n=3; NA: not assessed.

3.2. Preparation of SLN with different amounts of stearylamine

The amount of SA presented on the lipid matrix of SLN was increased in order to improve the mannose functionalization. Formulations with 5 mg, 10 mg and 20 mg of SA were produced and its physical-chemical properties were compared with SLN only containing 2 mg of SA. The increased amount of SA at Isn-SLN did not have a statistical influence on z-average, PdI and association efficiency (table 3.2). Zeta potential increased significantly due to amount of positive charges conferred by SA. The loading capacity of SLN with 10 mg of SA decreased when compared with the SLN containing 2 mg of SA, which could be explained by the reduced amount of drug associated to the SLN with 10 mg of SA, and although not statistically significant, it conferred a significant reduction on the loading capacity.

The morphology of SLN with 5 mg, 10 mg and 20 mg of SA were assessed through TEM, and independently of the amount of SA, Isn-SLN presented a spherical shape (figure 3.2). These formulations were functionalized afterwards with mannose (139, 161, 173, 324), forming M-SLN, that were further analyzed by FTIR spectroscopy.

Table 3.2. Physical-chemical properties of Isn-SLN with different amounts of SA.

SA (mg)	Z-Average (nm)	PdI	Zeta Potential (mV)	Association efficiency (%)	Loading capacity (%)
2	489.8 ± 7.8	0.41 ± 0.02	26.9 ± 2.2	50.2 ± 0.5	2.27 ± 0.04
5	487.3 ± 16.4	0.44 ± 0.04	35.9 ± 1.5 ***	38.2 ± 8.1	1.73 ± 0.38
10	452.0 ± 16.1	0.38 ± 0.01	37.1 ± 1.1 ***	34.0 ± 7.8	1.51 ± 0.38*
20	530.5 ± 27.1	0.41 ± 0.02	38.6 ± 1.5 ***	37.2 ± 10.0	1.57 ± 0.42

Witepsol E85® was selected as a lipid matrix. Statistical analysis through One-way ANOVA, with Dunnett's multiple comparison test; all formulations were compared with SLN containing 2 mg of SA (control); Mean ± SD; n=3.

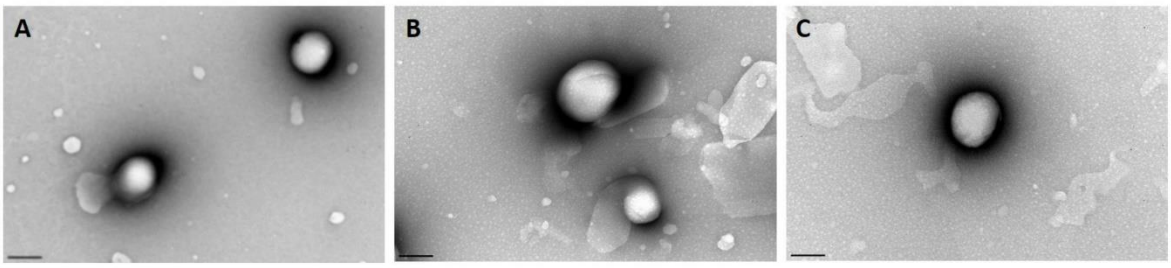

Figure 3.2. TEM microphotographs of Isn-SLN with 5 mg of SA (A), 10 mg of SA (B), and 20 mg of SA(C); Scale bar: 200 nm.

3.3. *In vitro* release studies

In vitro release studies showed that all formulations with different amounts of SA presented the same release pattern, and the release profile of Isn was similar for both physiologic and acid pH (figure 3.3). Only 10-15% of Isn was released during the first 2 hours, which may correspond to the amount of Isn that was adsorbed onto the surface of SLN. Overall, SLN presented a slow drug release during 48 hours, which can be attributed to the solid lipid core that did not allow the Isn diffusion through lipid matrix and eventually to the presence of surfactant associated at surface of SLN, that prevented the drug diffusion (325-327).

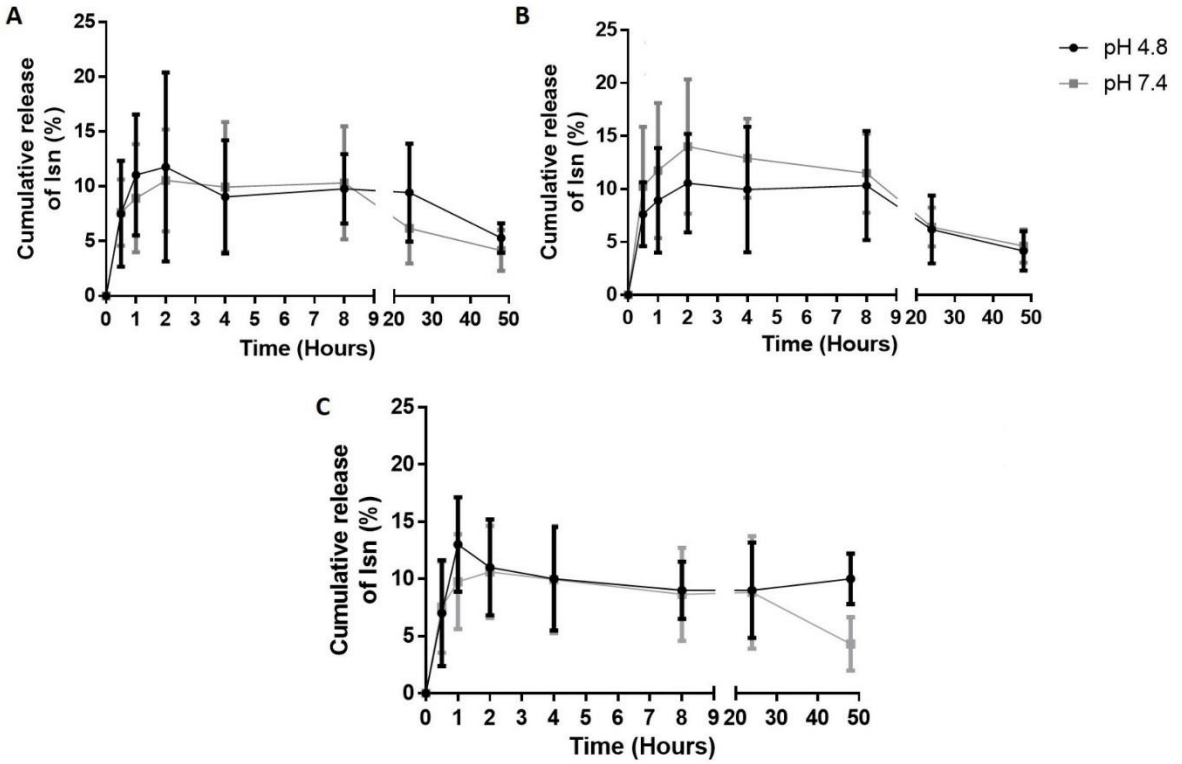

Figure 3.3. *In vitro* release study at pH 4.8 and 7.4 of Isn -loaded SLN with 5 mg of SA (A), 10 mg of SA (B) and 20 mg of SA(C); Results expressed as mean ± SD from 3 independent studies.

3.4. Fourier transform infrared characterization of M-SLN

M-SLN with 5 mg of SA did not present changes comparatively to SLN, even when higher amounts of mannose were used (figure 3.4A). PM of Witepsol, SA and mannose (PM Witepsol E85® + SA:mannose) presented bands with higher intensity between 1100-1000 cm^{-1} (figure A2a from Appendix I), that are related with the presence C-O streatch of mannose (139, 173), and the absence of these bands on M-SLN spectrum with 5 mg of SA suggested the absence of mannose on its surface.

On spectra of figure 3.4B and C, M-SLN with 10 mg and 20 mg of SA, respectively, showed bands between 1600-1540 cm^{-1} when compared with SLN without modification, and their intensity increased with the ratio of SA:mannose; however the spectra of PM (figure A2B and A3.2C from Appendix I) did not present any band on

the same wavenumber. The presence of these bands on M-SLN'spectra can be attributed to the the stretching vibration of C=N caused by the formation of Schiff base achieved during the mannose functionalization of SLN (161, 328, 329), and not due to the PM of SLN with mannose. Also, both M-SLN presented the same bands as the respective PM Witepsol E85® + SA:mannose spectra between 1100-1000 cm^{-1} (figure A2b and A3.2c from Appendix I), specially when a molar ratio SA:mannose of 1:15 and 1:30 were used, indicting the presence of mannose on the surface of SLN.

M-SLN with 20 mg of SA (figure 3.4C) presented higher intensity between 1600-1550 cm^{-1} over M-SLN with 10 mg of SA (Fig 4B), however SA has been described to originate cytotoxicity effects (139, 330, 331), which could compromise the amount of Isn delivery during the following experiments.

TEM experiments of M-SLN showed that the spherical morphology of formulations was kept after functionalization, with exception of M-SLN containing 10 mg SA with a SA:mannose ratio of 1:30 and M-SLN with 20 mg SA (figure A1 from Appendix I). They presented alterations on its morphology, and in some cases M-SLN seemed to be partially melted, probably because it was used an higher amount of hot acetate buffer during functionalization.

Therefore, for the following studies, the surface of Isn-SLN with 10 mg SA was decorated, using a molar ratio SA:mannose of 1:15. This formulation after functionalization did not suffer significant differences on the Z-Average and PdI, but the zeta potential reduced 20%, which also indicate the presence of mannose on the surface of SLN.

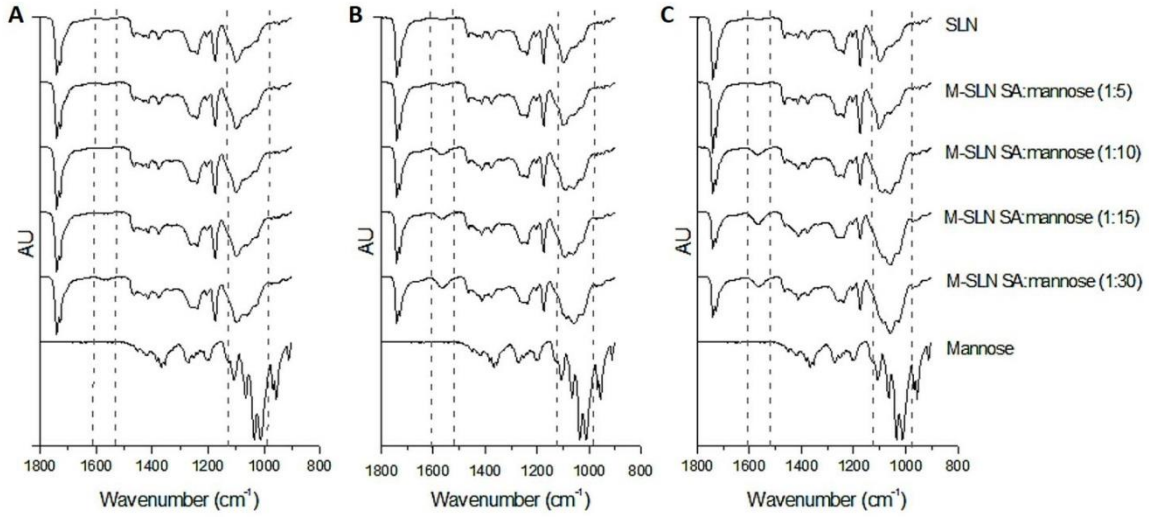

Figure 3.4. Normalized-FTIR spectra of M-SLN: lipid matrix of SLN was constituted by 5 mg (A), 10 mg (B) and 20 mg (C) of SA, and then, the different systems were modified with different molar ratios of SA:mannose.

3.5. Metabolic activity and cytotoxicity

The reduction of MTT to formazan (MTT assay) and cell cytotoxicity (LDH assay) after incubation of free Isn, Isn-SLN and the mannose derivative (M-SLN), were tested using NCI-H441 cell line (figure 3.5A and 3.5B), a Clara-like cell which expresses some membrane receptors similar to human primary ATI cells (240), and assessed on dTHP-1 cells (figure 3.5C and 3.5D) for a period of 24 hours.

Concentrations of Isn below 10 µM did not show any effect on MTT reduction and cytotoxicity for free Isn as well for the formulations tested after 24 hours of incubation at NCI-H441 and dTHP-1 cells. At concentration of 100 µM, free Isn decreased the ability of cells in convert MTT and conferred a significant cytotoxicity on both cell lines. But SLN (either functionalized or not) with 100 µM of Isn associated presented a statistically significant improvement of metabolic activity, and a marked reduced of cytotoxicity when compared with free Isn. The same patterns were also observed for unloaded-SLN, suggesting that the nanocarrier itself is safe. These outcomes suggest the ability of this nanocarrier to reduce the *in vitro* toxicity of Isn on lung epithelial cells and macrophage-like cells at high concentrations.

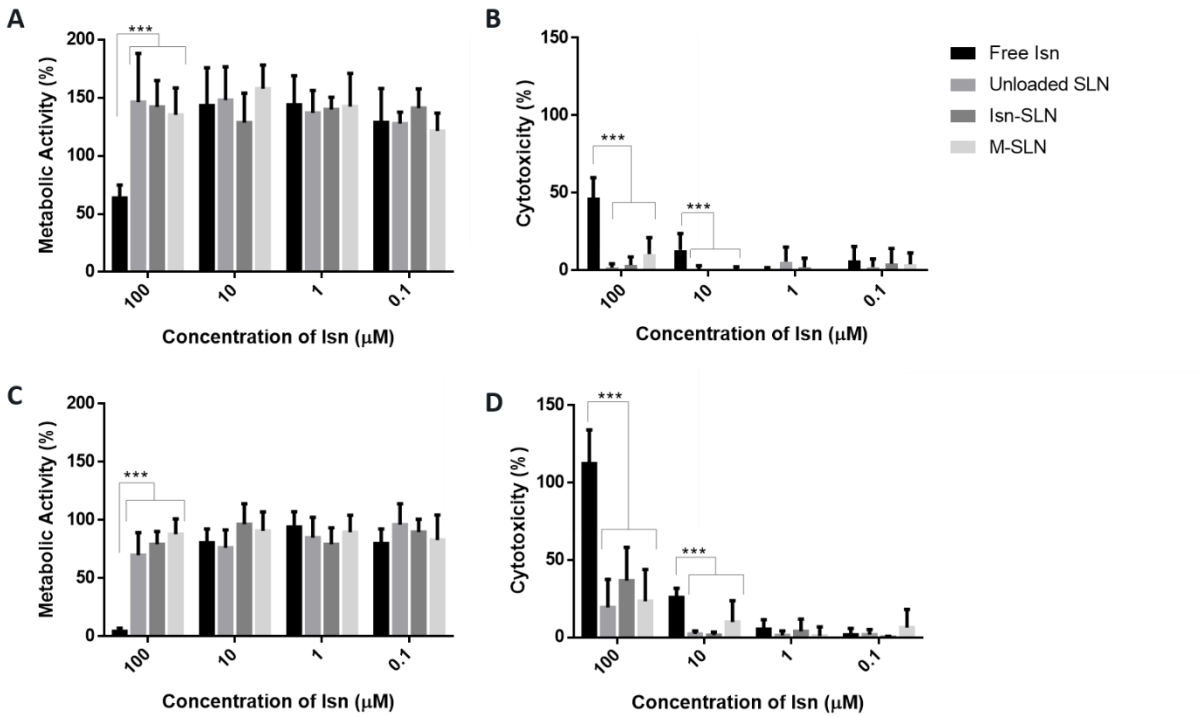

Figure 3.5. Metabolic activity and cytotoxicity assay at NCI-H441 cell line (A and B) and at dTHP-1 cell line (C and D) after 24 hours of incubation of free Isn and different formulations; Results of unloaded, Isn-SLN and M-SLN were compared with free Isn (control group) and statistical differences were analyzed through a One-way ANOVA with Dunnett's multiple comparisons test; Mean ± SD, from 2 independent experiments, with 5-6 replicates in each experiment.

3.6. *In vitro* uptake studies

In vitro uptake studies were performed by incubation of dTHP-1 with fluorescent SLN or M-SLN. CLSM analyze showed that dTHP-1 cells were able to internalize both formulations (figure 3.6A). These outcomes are in agreement with images captured by ImageStream®^{X} flow cytometer (figure A3A from Appendix I), where cells presented green fluorescence when incubated either with SLN and M-SLN.

For quantification of the fluorescence intensity, it was first obtained the internalization score, a ratio between the fluorescence intensity detected inside the cells (which was quantified by the use of an eroded mask with 4.0 pixels) and the total fluorescence intensity provided by the whole cell (310). Positive scores suggest the internalization

of system by the cells, while negative scores indicate that the nanocarrier is adsorbed on the cell surface; internalization score of 0 means that there is an equal amount of system adsorbed and internalized on the cell surface. In this study the internalization score ranged between 2 and 3 (figure A3B from Appendix I), suggesting that dTHP-1 cells were able to internalize SLN and M-SLN, and the pre-treatment with mannose did not change the internalization score. After gating cells with an internalization score higher than 1 (to exclude cells that may have adsorbed SLN and M-SLN), the fluorescence intensity internalized of each cell was quantified through IDEAS® software, and the results are showed on figure 3.6B. In this *in vitro* uptake study, the fluorescence intensity quantified reflects the amount of SLN or M-SLN internalized by each dTHP1.

After recognition and antigen capture, the mannose receptor is able to deliver the antigen on the early endosomes for posterior lysosomal degradation, while the receptor is recycled on the cell surface (298). For this reason, cells were treated with mannose, the agonist of MRs, 30 minutes before and also during the incubation of formulations, to allow the competitive binding by the receptor. Consequently, a statistical increase of uptake of M-SLN over SLN was observed, and when the receptor was incubated with its agonist, M-SLN had a lower internalization.

The presence of mannose promoted the uptake of SLN, even without any functionalization. This result may be caused by the presence of mannose that physically adsorb to SLN and binds to the cells receptor, enabling its internalization and consequently the internalization of SLN at same time. Moreover, the internalization of M-SLN was reduced when cells were incubated with mannose comparatively with same formulation without the mannose treatment, which demonstrate the ability of mannose to compete with formulation by the binding sites of the receptor and to reduce its phagocytosis.

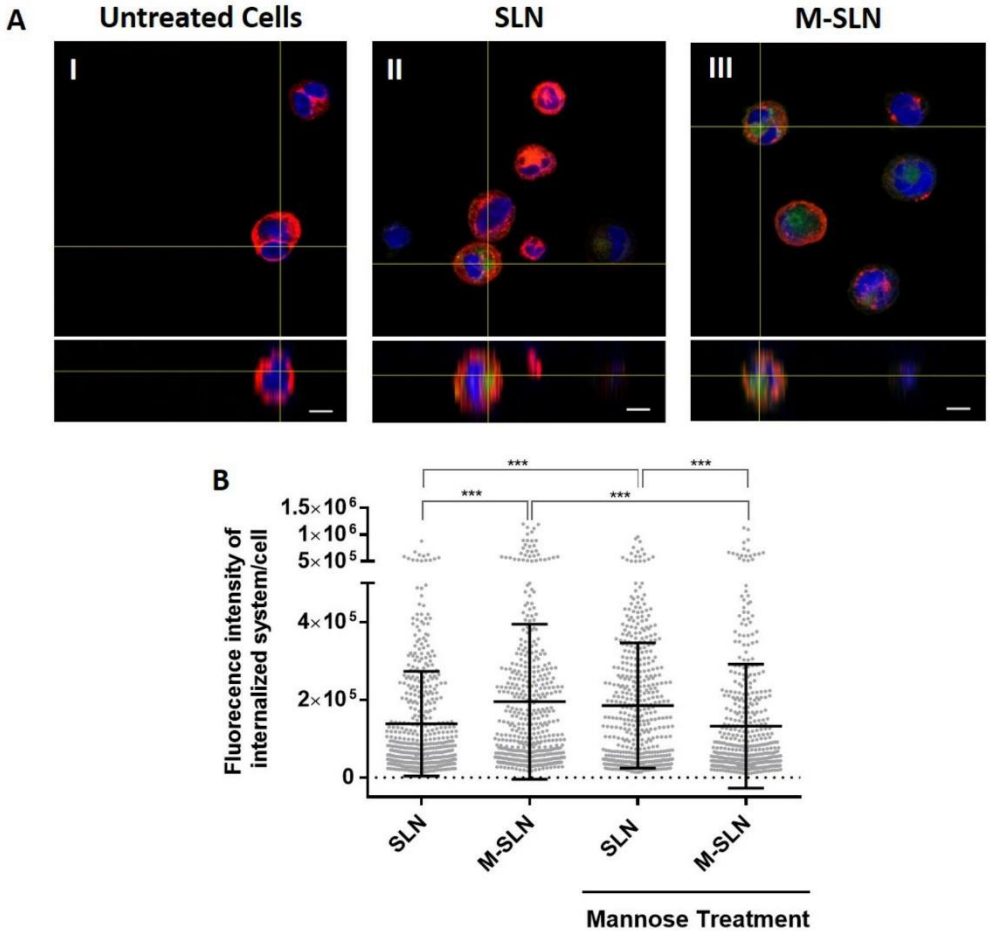

Figure 3.6. CLSM images of uptake studies performed in dTHP-1 cells after 2 hours of incubation; Scale barr: 10 µm. Fluorescence intensity internalized of SLN and M-SLN by dTHP-1 cells after 2 hours of incubation (B) assessed by ImageStream®^{X} imaging flow cytometry; 460 ± 10 dTHP-1 cells from 3 independent studies were analyzed and results were expressed as mean ± SD; Statistical analysis performed through One-way ANOVA with Bonferroni's multiple comparisons test.

4. Conclusions

In this work Isn-SLN were initially prepared with different solid lipids and based on physical-chemical properties of SLN produced, Witepsol® E85 was selected to form the lipid matrix of SLN. SA was also incorporated onto the lipid matrix in order to provide the amine groups that allowed the mannose attachment. Further modifications in the formulation were performed in order to achieve a stable SLN, with a higher Isn

association efficiency and last, a mannose-anchoring on the surface of SLN that enhanced the macrophage uptake. The functionalization of mannose was confirmed by FTIR and biologically through *in vitro* uptake studies on dTHP-1 cells. M-SLN presented a higher uptake over SLN; when cells were treated with mannose to compete with the formulations for the receptor biding sites, there was a significant reduction of internalization of M-SLN, suggesting that M-SLN were phagocyted through mannose receptor-mediated endocytosis.

CHAPTER IV

ESTABLISHMENT AND CHARACTERIZATION OF A THREE-DIMENSIONAL *IN VITRO* MODEL OF AIR-BLOOD BARRIER

ESTABLISHMENT AND CHARACTERIZATION OF A THREE-DIMENSIONAL *IN VITRO* MODEL OF AIR-BLOOD BARRIER

1. Introduction

The air-blood barrier is a complex structure involved on gas exchange between the respiratory tract and blood circulation. This barrier is composed by a thin layer of epithelial and endothelial cells, both separated by the BM. Epithelium is mainly constituted by ATI cells, flat cells that cover around 90-93% of the epithelial surface, and ATII cells that are spread among ATI cells. ATII cells present a cuboidal morphology and its main functions are the production of surfactant as well as type-I cells renewal. At the alveolar space there are AMs with the ability to phagocyte air particulate matter or pathogenic agents, and last, they can promote the release of inflammatory cytokines and trigger an immune response. Separated by a BM, this physiologic barrier has a continuous non-fenestrated microvascular endothelium cell layer that forms the capillary walls, which are in contact with the bloodstream (332, 333).

Due to a high surface area, high vascularization and low enzymatic and metabolic activity, pulmonary administration has been considered as a relevant route for either local and systemic drug delivery. The delivery of drugs through this route faces challenges: pharmaceutical systems must overcome the clearance mechanisms throughout the tracheobronchial tree, namely the entrapment caused by cilia beating and mucus at upper airways, while at distal part of airways the systems can be retained by the surfactant layer or internalized by AMs (294, 334). In the alveolar space, epithelial cells are exposed to the air – a condition so called ALI. Inhaled material or microorganisms and compounds that reach the alveolar region are therefore exposed to the ALI condition. This feature has gained relevance when *in vitro* models are being established, once the properties of the cellular barrier, cell morphology and gene expression are influenced when cells are cultured at ALI (335, 336). Moreover, cells cultured at LLI culture condition do not represent *in vivo*-like conditions, and the

pharmacokinetic parameters of nanocarriers can be influenced by the presence of medium, due to interaction between compounds and the cell culture medium (namely with supplements and serum proteins) leading to its agglomeration; nanoparticle deposition on the top on cells occurs by diffusion and not by direct sedimentation, so that partial amount of compounds can remain in suspension on the medium, influencing the dose that interacts with cells (337-339).

In this work a 3D *in vitro* cell culture model of the air-blood barrier cultured under ALI conditions was established, by the combination of three different cells lines: NCI-H441 cell line, a human lung adenocarcinoma cell line with features of ATI-like cells (240); HPMEC-ST1.6R, a human pulmonary microvascular endothelial cell line and last, human macrophage-like cells (dTHP-1 cells), with the aim of mimicking AMs. NCI-H441 cells were cultured at the apical side of Transwell® membrane, while HPMEC-ST1.6R cells were seeded on the basolateral side; dTHP-1 cells were seeded on top of epithelial cells (scheme 4.1). Characterization of this 3D model (that will be mentioned as triple co-culture throughout the text) was performed and compared with the respective monocultures and bi-cultures (NCI-H441 cells either seeded with HPMEC-ST1.6R or dTHP-1 cell lines).

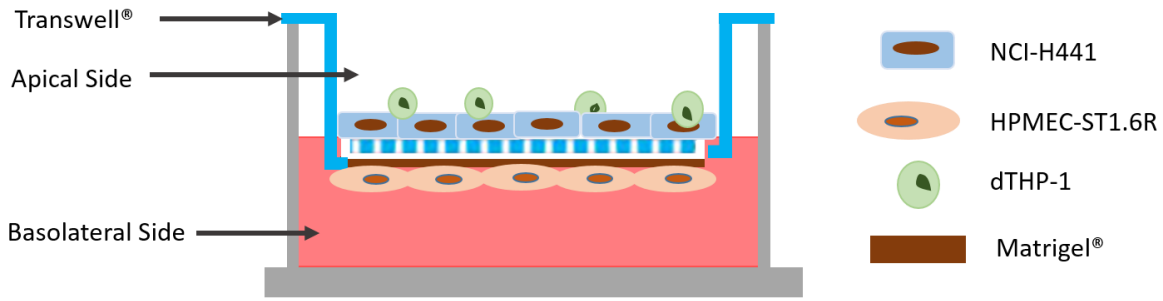

Scheme 4.1. Scheme of the *in vitro* triple co-culture model.

2. Materials and Methods

2.1. Materials

RPMI-1640, trypsin-EDTA and Pen/Strep solution 10.000 U/mL were acquired from Gibco (Waltham, USA); FBS was purchase from Biochrom (Cambridge, UK);

Endothelial cell growth supplement (ECGS), medium M-199 with Earle's salts, stable glutamine (100 mg/L), 2.2 g/l NaHCO3 and glucose (1000 mg/L) were purchased from Merck (Darmstadt, Germany); Heparin sodium salt from porcine intestinal mucosa was acquired from Alfa-Aesor (Haverhill, USA); Dex, gelatin from porcine skin, PMA and PBS were purchase from Sigma-Aldrich (St. Louis, USA); Matrigel™ BM Matrix was obtained from Corning® (New York, USA); Insulin-transferrin-selenium (ITS) was purchased from Life Technologies (Carlsbad, USA); Anti-human E-cadherin - Alexa Fluor® 488 (reference 324110) was from Grupo Taper (Madrid, Spain); Rabbit occludin antibody (H-279) (reference sc-5562), rabbit polyclonal IgG ZO-1 antibody (H-300) (reference sc-10804) were acquired from Santa Cruz Biotechnology (Dallas, USA); Goat anti-rabbit IgG (H+L), Alexa Fluor® 488 (reference A11008) and 4′,6-diamidino-2-phenylindole (DAPI), Vybrant® CFDA SE Cell Tracer were purchase from Invitrogen (Carlsbad, USA); CellTrace™ Far Red Cell Proliferation Kit and CellTrace™ Yellow Cell Proliferation Kit were acquired from Thermo-Fisher Scientific (Waltham, USA); Glutaraldehyde was purchase from Electron Microscopy Sciences (Hatfield, USA); PFA was bought from Merck (Darmstadt, Germany); Epon resin was purchased from TAAB (Berks, England); Dako® mouting medium was purchased from Palex Medical (Barcelona, Spain); Histowax® Embedding Medium was obtained from Leica Biosystems (Wetzlar, Germany).

2.2. Cell culture maintenance

NCI-H441 cell line was purchased from ATCC (Manassas, USA). Cells were cultivated in T75 cell culture flasks with RPMI1640 culture medium supplemented with 10% (v/v) FBS, 1% (v/v) Pen/Strep and 1% (v/v) sodium pyruvate. HPMEC-ST1.6R was kindly provided by Professor C. James Kirkpatrick from the Institute of Pathology, Johannes Gutenberg University of Mainz, Germany. Before HPMEC-ST1.6R seeding, the T75 cell culture flasks were coated with a 0.2% (w/v) gelatin solution for 20-30 minutes at 37 °C. Them, HPMEC-ST1.6R cells (passages between 20-56) were seeded in the culture flask and cultured in medium M-199 (with Earle's salts, stable glutamine (100 mg/L), 2.2 g/L NaHCO3, and glucose (1000 mg/L)) supplemented with 20% (v/v) FBS, 1% (v/v) Pen/Strep, 25 µg/mL of ECGS and 25 µg/mL of heparin sodium salt.

The medium from epithelial and endothelial cell lines was changed every 2-3 days; when cells reached confluence (70-80%), they were washed with PBS and treated with trypsin-EDTA (for 5 minutes at 37 °C). After inactivation of trypsin-EDTA with complete medium, cells were centrifuged and split into new cell culture flaks.
THP-1 cells were also acquired from ATCC and cultivated inT75 cell culture flaks as a suspension. When confluence was reached, cells were centrifuged and divided into new cell culture flasks.
All cell lines were grown inside an incubator at 37 °C and with an atmosphere of 5% of CO_2.

2.3. Evaluation of growth pattern in different culture conditions

NCI-H441 and HPMEC-ST1.6R cells were routinely cultured in different conditions and the growth pattern of each cell line was assessed in different culture media, with the aim of establishing a single culture condition that allowed the growth of both cell lines. Epithelial and endothelial cells were seeded into a 24-well plate (2.0×10^4 cells/cm^2 and 2.5×10^4 cells/cm^2 for NCI-H441 and HPMEC-ST1.6R, respectively), and grown inside an incubator at 37 °C with an atmosphere of 5% of CO_2. Different medium compositions were tested, and the growth of each cell line was compared with the control (cells grown with the medium used for cell culture maintenance, see Table 4.1). Culture medium was changed every 2 days. At different time points (4, 8 and 12 days of growth), cells were washed with PBS. After incubation of 200 µL of trypsin-EDTA, following 5 minutes of incubation at 37 °C, cells were detached from the wells and resuspended on 800 µL of culture medium and counted. Three replicates were performed for each culture condition.
Cell images at different times were collected through a Zeiss light microscope (Zeiss Imager M1m, Zeiss, Germany), using a 4x objective.
After selection of the suitable culture medium for the growth of both cell lines, the growth rate and doubling time at each 4 days (96 hours) were calculated based on equation 4.1 and 4.2, respectively. The results are expressed on the table A1 from Appendix II.

Equation 4.1. $Growth\ rate = \ln(N(t+96)/N(t)\ )/t$

Equation 4.2. $Doubling\ time = ln\ 2/Growth\ rate$

N (t + 96) and N (t) is the number of cells as function of time (t), and t is the time of culture expressed in hours.

Table 4.1. Culture conditions to assess NCI-H441 and HPMEC-ST1.6R growth.

		Medium	FBS (% (v/v))	Pen/Strep (% (v/v))	Sodium Pyruvate (% (v/v))	ECGS (µg/mL)	Sodium Heparin (µg/mL)
NCI-H441	Control	RPMI1640	10	1	1	———	———
	Medium A	RPMI1640	10	1	1	25	25
	Medium B	RPMI1640/M-199 (50:50)	10	1	1	25	25
	Medium C	M-199	10	1	1	25	25
HPMEC-ST1.6R	Control	M-199	20	1	———	25	25
	Medium A	RPMI1640	10	1	1	25	25
	Medium B	RPMI1640/M-199 (50:50)	10	1	1	25	25
	Medium C	M-199	10	1	1	25	25

2.4. Establishment of the number of NCI-H441 and HPMEC-ST1.6R cells

2.4.1. Assessing the integrity and confluence of NCI-H441 cells

NCI-H441 cells were seeded on the apical side of a 12-well Transwell® (12 mm diameter), with the aim of selecting the number of cells and the time of culture that provided the tightest confluent epithelial monoculture. Different numbers of epithelial cells (5.0 x 10^4, 1.0 x 10^5, 1.75 x 10^5, 2.5 x 10^5 and 5.0 x 10^5 cells/ Transwell®) were seeded on the apical side of a 12-well Transwell® (pore size 3.0 µm). Cells were grown at LLI conditions, by placing 0.5 mL and 1.5 mL of complete medium (Medium A) at apical and basolateral compartment, respectively. After 2 days of growth, the culture conditions were changed for ALI, and cells were only fed with 0.5 mL of Medium A (supplemented with 200 nM of Dex) at basolateral compartment. The medium was changed at each 2 days, and the integrity of cell monoculture was assessed by TEER measurement.

2.4.2. Optimization the number of HPMEC-ST1.6R cells

After establishing the number of NCI-H441 cells that provided the highest TEER (2.5 x 10^5 cells/ Transwell®), different amounts of HPMEC-ST1.6R cells were co-cultured with NCI-H441 cells.

The Transwell® was upside down and placed on a petri dish for coating with 50 µL/cm^2 of Matrigel™ BM matrix (concentration of protein used 4.0 mg/mL). After 1 hour of incubation at 37 °C, HPMEC-ST1.6R cells were seeded with different ratios of endothelial:epithelial cells (end:epi), namely (2:2, 1:1, 1:2, 1:4, 1:6) at the basolateral compartment of the Transwell®. After 2 hours of incubation at 37 °C to allow endothelial cell adhesion, the Transwell® was inverted again and placed on the well, following the seeding of NCI-H441 cells at the apical compartment (2.5 x 10^5 cells/ Transwell®). Cells were kept under LLI conditions during 2 days; thereafter, the culture conditions were changed to ALI (with 0.5 mL of Medium A supplemented with 200 nM of Dex). Medium at basolateral compartment was replaced every day.

2.5. Triple co-culture model of air blood barrier with 8 days of culture

2.5.1. Seeding HPMEC-ST1.6R and NCI-H441 cells

The basolateral side of a Transwell® membrane was firstly coated with Matrigel™ (50 µL/cm^2, with 4.0 mg/mL of protein concentration). After incubation of the Transwell® for 1 hour at 37 °C to allow Matrigel™ polymerization, 1.25 x 10^5 cells/ Transwell® of HPMEC-ST1.6R were seeded on basolateral side of the inverted coated Transwell®. Cells were incubated for 2 hours at 37 °C to allow the cell adhesion to the Matrigel™. Transwell® was inverted again and placed on a 12-well plate. 2.5 × 10^5/ Transwell® of NCI-H441 were seeded at the apical compartment of Transwell® and both cells were incubated at LLI conditions during 2 days (0.5 mL and 1.5 mL of Medium A at apical and basolateral side, respectively). 48 hours post-seeding, the culture conditions were changed to ALI by incubating cells with 0.5 mL Medium A. On the lower compartment medium was supplemented with 200 nM of Dex to allow epithelial cells polarization. Medium was replaced every days and cells were kept inside of an incubator at 37 °C with 5% of CO_2, until day 8 of culture. TEER was evaluated over the time to assess the integrity of different *in vitro* cell culture models, following the methodology described on section 2.6 of chapter IV.

2.5.2. THP-1 differentiation and seeding

For differentiation of THP-1 cells into macrophage-like cells, 3.0 x 10^6 of THP-1 cells were seeded on a T75 culture flasks containing culture medium supplemented with 10 ng/mL of PMA for 48 hours.

Before macrophage seeding on the apical side of the Transwell® at day 7 of culture, NCI-H441+HPMEC-ST1.6R bi-culture was washed twice with PBS to remove the Dex. Cells were re-incubated with 0.5 mL of fresh Medium A at basolateral compartment, without Dex.

Meanwhile, dTHP-1 cells were washed two times with PBS and then detached from the flasks after 5 minutes of incubation with trypsin-EDTA. Cells were resuspended in complete medium (for trypsin-EDTA inactivation). After centrifugation and counting, 1.0 × 10^5 of dTHP-1 cells were resuspended in 30 µL of medium (RPMI1640

supplemented with 10% (v/v) FBS + 1% (v/v) Pen/Strep) and incubated on the apical side of the formed bi-culture for 24 hours (until day 8 of culture). The scheme A1 from Appendix II presents the set-up used to perform the triple co-culture. The conditions used to establish the triple co-culture with 8 days of culture are presented on scheme 4.2.

Epithelial barrier integrity of NCI-H441 monoculture and triple co-culture was evaluate through the measurement of TEER. To assess the influence of each cell type on the TEER of triple co-culture, bi-cultures of NCI-H441+dTHP-1 and NCI-H441+HPMEC-ST1.6R were also performed, following the same methodology described on this section 2.5. The morphology and ultrastructure of the triple co-culture after 8 days of culture was also assessed through CLSM, SEM, TEM and histology.

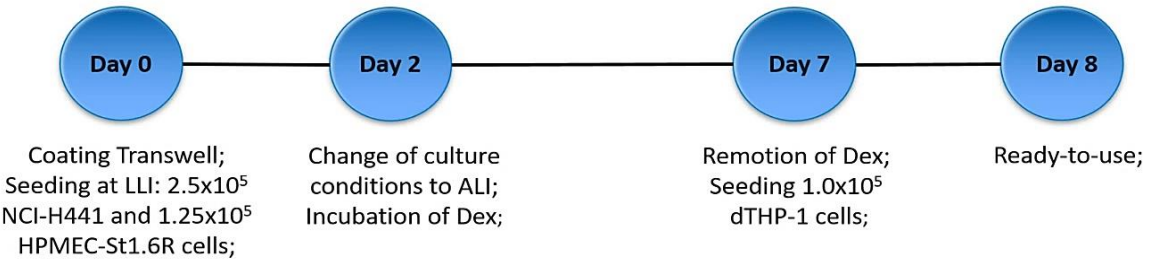

Scheme 4.2. Culture conditions of triple co-culture with 8 days of growth: cells were kept with RPMI 1640 + 10% (v/v) FBS + 1% (v/v) Pen/Strep + 1% (v/v) sodium pyruvate + 25 µg/mL ECGS + 25 µg/mL sodium heparin during 48 hours after seeding; then, the complete medium was further supplemented with 200 nM of Dex; Dex was removed before the dTHP-1 seeding.

2.6. Transepithelial electrical resistance of *in vitro* cell culture models

TEER was measured at different time points of culture. When cells were cultured at LLI conditions, TEER was measured by placing the electrode, connected to an EVOM Voltohmmeter, (both from World Precision Instrument, Sarasota, USA), on the lateral side of the Transwell®. But when cells were cultured at ALI conditions, culture medium was first added to each well (0.5 mL and 1 mL of culture medium at apical and basolateral side of Transwell®, respectively). After 1 hour of incubation at 37 °C with an atmosphere of 5% of CO_2, TEER was measured by placing the electrode on the

Transwell® system. TEER of the blank (Transwell® without cells) was also performed, and this parameter was calculated based on equation 4.3.

Equation 4.3. $TEER = (TEER_{sample} - TEER_{blank}) \times area$

2.7. Morphological and ultrastructural analysis of *in vitro* cell culture models

2.7.1. CLSM analysis

Morphology of cells was evaluated by staining each cell line with different cell tracking dyes, following the manufacturer's instructions. Before dTHP-1 seeding, NCI-H441 cells were labeled with CellTrace™ Yellow Cell Proliferation Kit. The dye was diluted in PBS, and 250 µL of this solution with a concentration of 10 µM was added to the apical side of the Transwell® and incubated for 20 minutes at 37 °C, protected from the light. Cells were washed with complete medium for 5 minutes to remove any free dye and were further incubated with fresh complete medium, for 10 minutes to allow the acetate hydrolysis of the dye. For staining the endothelial cells at the basolateral side of the Transwell®, Vybrant® CFDA SE Cell Tracer was diluted in PBS (concentration of 10 µM) and 800 µL of this solution was placed on the basolateral compartment, following an incubation step of 15 minutes at 37 °C. Thereafter, cells were washed with complete medium and incubated with fresh complete medium for another 30 minutes, to enable the acetate hydrolysis of the probe. Medium was removed again and 500 µL of fresh complete medium was added to the basolateral compartment.

dTHP-1 cells were stained using the CellTrace™ Far Red Cell Proliferation Kit. After trypsinization and centrifugation, cells were resuspended in PBS (containing 3 µM of the dye) and incubated for another 20 minutes at 37 °C. Complete medium was added to the cell suspension, which was centrifuged again to remove the excess of dye. The pellet formed was resuspended in complete medium and incubated for another 10 minutes. Then, dTHP-1 cells (30 µL of cell suspension with 1.0×10^5 cells) were seeded on the top of epithelial cells, following incubation for more 24 hours, at 37 °C with an atmosphere of 5% of CO_2 and protected from the light.

On the following day, the culture medium was removed and cells at the basolateral compartment were washed with 700 µL of PBS. The apical side was not washed to avoid the loss of macrophage-like cells. Then, cells were fixed with PFA 3% overnight at 4 °C (only 700 µL at the basolateral compartment). On the following day, cells were washed with PBS and counterstained with DAPI (concentration 500 ng/mL) during 30 minutes. After one washing step with PBS to remove the excess of DAPI, the membrane of the Transwell® was cut and mounted between two coverslips with the help of DAKO® mounting medium, for later observation at CLSM.
Samples were analyzed through a Leica TCS SP5 II, Leica Microsystems (Wetzlar, Germany), with a 63x oil objective and a zoom of 1. Images were acquired with a size of 1024 × 1024 pixel, 8-bits of resolution and a bidirectional scanning speed at 400 Hz; Z-stacks were performed using a step size between 4-5 µm. The brightness and the contrast of each image was adjusted through ImajeJ 1.48 vs Software.

2.7.2. Immunocytochemistry of epithelial membrane markers

Epithelial cell membrane markers (ZO-1, occludin and E-cadherin) were used to stain intercellular junction structures by immunocytochemistry (ICC). For ZO-1 and occludin staining, epithelial monoculture and triple co-culture were fixed with PFA 3% during 30 minutes. After three washing steps, all samples were permeabilized with PBS-Triton X-100 0.2% (v/v) following three more washing steps to remove the permeabilization solution. Samples were further incubated with a blocking solution (PBS with 0.05% (v/v) of Tween®-20 and 10% (v/v) FBS during 30 minutes. Without washing, the samples were incubated with anti-human rabbit primary antibodies (dilution of 1:200 and 1:50 for ZO-1 and occludin staining, respectively) for 2 hours at room temperature. After this period, samples were washed three times to remove the excess of antibody and were further incubated with a secondary antibody goat anti-rabbit IgG conjugated with Alexa Fluor® 488 during 1 hour at room temperature (dilution of 1:400). Samples were washed three times with PBS and then incubated with DAPI solution (500 ng/mL) for 30 minutes. After a new washing step with PBS, the Transwell® membrane was cut and mounted between 2 coverslips with the help of Dako® mounting medium for CLSM observation.

For E-cadherin staining, samples were first fixed with PFA 3% during 30 min and washed with PBS. After permeabilization and blocking steps as already mentioned, samples were incubated with a direct conjugated antibody (anti-human E-cadherin-Alexa Fluor® 488, dilution 1:200) for 2 hours at room temperature. Samples were washed three times with PBS, incubated with DAPI and then mounted between two coverslips.

Images were collected using a Leica TCS SP5 II, Leica Microsystems (Wetzlar, Germany), with a 63x oil objective and a zoom of 1.7. Images were acquired with a size of 1024 × 1024 pixel, 16-bits of resolution and a bidirectional scanning speed at 700 Hz. ImageJ 1.48 vs Software was used for adjust the brightness and the contrast.

2.7.3. Scanning Electron Microscopy

At day 8 of culture, samples were washed with PBS and fixed with PFA 3% overnight at 4°C. On the following day, samples were dehydrated by a graded series of alcohol (30%, 50%, 70%, 80%, 90%, 96%, 100% and 100%) during 10 minutes each. The washing, fixation and dehydration was performed by placing only 700 µL of each solution on the basolateral compartment, to avoid the loss of dTHP-1 from apical side. Samples were let drying overnight at room temperature. On the day of analysis, the membrane of the Transwell® was cut and placed on carbon discs of a pin stub. Samples were sputtered with an Au/Pd thin film during 50 seconds, using the SPI Module Sputter Coater equipment (SPI® Supplies, West Chester, USA). Images were acquired through a scanning electron microscopy (SEM) on a FEI Quanta 400 FEG SEM from FEI (Hillsboro, USA).

2.7.4. Ultrastructural characterization

The triple co-culture was washed with PBS (only 700 µL) at basolateral compartment, followed fixation with 2.5% glutaraldehyde and 2% PFA in cacodylate buffer 0.1M (pH 7.4). Samples were dehydrated and embedded in Epon resin. Through a RMC Ultramicrotome (PowerTome, USA) and diamond knives (DDK, Wilmington, DE, USA), ultrathin sections with a thickness between 40–60 nm were performed. Samples were

mounted on 200 mesh copper or nickel grids, and stained with uranyl acetate, followed with lead citrate, both for 15 minutes. Examination was performed through a JEOL JEM 1400 TEM (Tokyo, Japan), and images were digitally recorded using a CCD digital camera Orious 1100W (Tokyo, Japan).

2.7.5. Histological sections

After fixation with PFA 3% at 4 °C overnight, samples were dehydrated in a solution of crescent ethanol concentrations (35%, 50%, 70%, 95%, 100%, 100%) for 10 minutes at each concentration. Samples were further incubated two times with Histo-clear II (Histological Clearing Agent; National diagnostics, USA), 10 minutes each incubation, and then embedded in paraffin during 1 hour, two times. After inclusion in paraffin, samples were stored at 4 °C overnight. The paraffin block was cut through a Microtome-Reichert Jung 2040 Autocut (Boston Laboratory Equipment, USA), with a thickness of 7.0 µm. The histological sections were placed at 37 °C overnight to let them drying. On the following day, samples were stained with hematoxylin and eosin, and mounted with the help of Roti®-Histokitt.
Histological sections were observed through a Light microscope Olympus DP25 (using a 40x objective) coupled with a camera; Images were acquired through Software Cell B (Olympus Corporations, Shinjuku, Japan).

2.8. Influence of insulin-transferrin-selenium and time of culture on the multi-layers formation

2.8.1. Influence of insulin-transferrin-selenium on the NCI-H441 growth

NCI-H441 cells were seeded on Matrigel™-coated Transwell® (pore size of 3.0 µm and 0.4 µm) according to the procedure described on section 2.5. However, the number of seeded cells was reduced (1.0×10^5 cells/ Transwell®). Cells were kept with Medium A (containing with 10% (v/v) of serum) for 8 days. The same number of NCI-H441 cells were also cultured in medium containing 5% (v/v) FBS and 1% (v/v) ITS for

8 days. The culture conditions of each group are represented the schemes 4.3A and B.

TEER was measured at day 5, 7 and 8 of culture, following the procedure described on section 2.6. At day 8, cells were fixed with PFA 3% during 30 minutes at room temperature. Then, cells were washed with PBS and counterstained with DAPI (30 minutes with a concentration of 500 ng/mL). Samples were washed again to remove the DAPI, the membrane was cut and placed between two coverslips with the help of DAKO® mounting medium for CLSM examination.

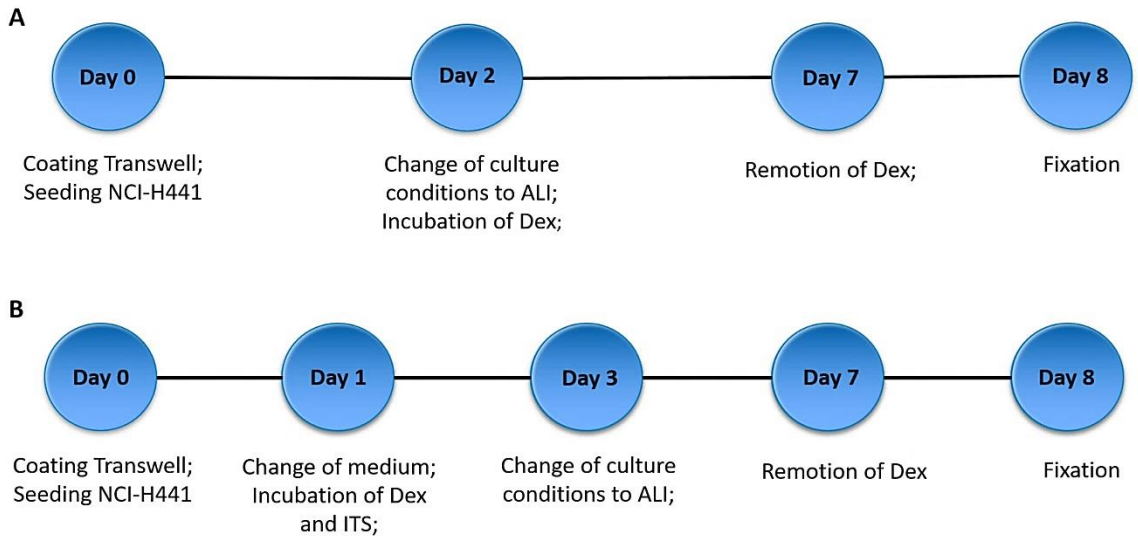

Scheme 4.3. Culture conditions of NCI-H441 with 8 days of growth in different culture conditions: A) Cells were kept in RPMI 1640 + 10% (v/v) FBS + 1% (v/v) Pen/Strep + 1% (v/v) sodium pyruvate + 25 µg/mL ECGS + 25 µg/mL sodium heparin; at day 2 cells were incubated with 200 nM of Dex until day 7; B) Cells were kept in RPMI 1640 + 5% (v/v) FBS + 1% (v/v) Pen/Strep + 1% (v/v) sodium pyruvate + 25 µg/mL ECGS + 25 µg/mL sodium heparin; after 24 hours 200 nM of Dex was incubated between day 1 and 7; 1% (v/v) ITS was also incubated after 24 hours post-seeding and incubated until day 8; Number of cells/Transwell®: 1.0 x 10^5 NCI-H441 cells.

2.8.2. Influence of time of culture on the multi-layer formation

Epithelial and endothelial monocultures as well as triple co-cultures were performed by initially seeding 5.0 x 10^4 HPMEC-ST1.6R and 1.0 x 10^5 NCI-H441 cells on

Matrigel™-coated Transwell®, using the procedure described on section 2.5. All cell culture models were kept with RPMI 1640 containing 5% (v/v) FBS, 1% (v/v) Pen/Strep,1% (v/v) sodium pyruvate, 25 µg/mL of ECGS and 25 µg/mL of sodium heparin. For the triple co-culture, dTHP-1 cells (1.0 x 10^5 cells/ Transwell®) were also seeded either at day 4 or 7 and incubated for more 24 hours. ITS was also included on the culture medium and cells were kept in culture either for 8 or 5 days (scheme 4.4A and B).

At day 5 or day 8 of culture, samples were fixed with PFA during 30 minutes at room temperature. After washing the cells with PBS, they were stained with DAPI (500 ng/mL during 30 minutes). Samples were washed again, the membrane was cut and placed between two coverslips with the help of DAKO® mounting medium.

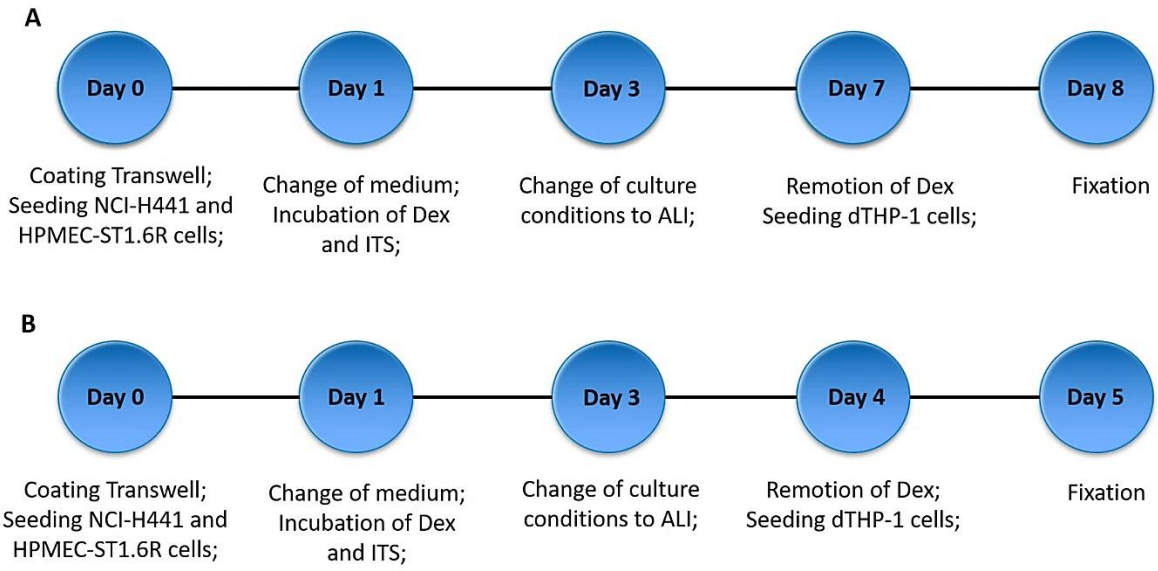

Scheme 4.4. Culture conditions of NCI-H441 monoculture, HPMEC-ST1.6R monoculture and triple co-culture with 8 days (A) and 5 days (B) of growth. Cells were kept in RPMI 1640 + 10% (v/v) FBS + 1% (v/v) Pen/Strep + 1% (v/v) sodium pyruvate + 25 µg/mL ECGS + 25 µg/mL sodium heparin; at day 2 of growth, cells were incubated with 200 nM of Dex until day 7 (A) or day 4 (B); 1% (v/v) ITS was incubated one day after cell seeding (day 1) and was always incubated during the cell culture; In the case of triple co-culture, dTHP-1 cells were incubated on the top of epithelial cells, either at day 7 (A) or day 4 (B) and incubated for more 24 hours; Number of cells/Transwell®: 1.0 x 10^5 NCI-H441 cells and 5.0 x 10^4 HPMEC-ST1.6R and 1.0 x 10^5 dTHP-1 cells.

2.8.3. Cross section examination through CLSM

Samples were observed though CLSM Zeiss LSM 710, Axio Observer (Oberkochen, Germany), using an 40x water immersion. Images were acquired with a size of 1024 x 1024 pixel, a zoom of 0.6, a bit depth of 8, using the frame mode. Z-stacks images from both side of the Transwell® were acquired, and each focal plane presented a thickness of 0.48-0.5 µm. Trough ImageJ 1.48 vs Software cross sections of each sample were recorded using the orthogonal view tool. The brightness and the contrast of each image was adjusted with the same software.

2.9. Statistical analysis

Statistical analyses were performed using GraphPad Prism Software vs. 7 (GraphPad Software Inc., La Jolla, USA). One-way ANOVA tests were used, and different significance levels were considered: significant at a level of $p < 0.05$ (*), very significant at level of $p < 0.01$ (**) and highly significant at a level of $P < 0.001$ (***).

3. Results and discussion

3.1. Evaluation of growth rate for each cell line in different culture medium

An *in vitro* model of air-blood barrier constituted by epithelial cells (NCI-H441), endothelial cells (HPMEC-ST1.6R) and macrophage-like cells (PMA-dTHP-1 cells) has been developed. To achieve an *in vitro* model that closely mimics physiologic conditions, epithelial cells and macrophage-like cells were cultured under ALI conditions on the apical side, being only fed by the medium from the basolateral compartment of the Transwell®. This medium was also responsible for the maintenance of endothelial cells when in co-culture with the epithelial cells and macrophage-like cells. To set-up a bi-culture of epithelium and endothelium, it was required to establish a common culture medium, that could efficiently sustain the growth of both cell lines. NCI-H441 and HPMEC-ST1.6R cells were routinely maintained in different culture conditions, with different amounts of serum and

supplements, as described in the section 2.2. To evaluate the growth rate of each cell line, different media and supplements were used, the number of viable cells was counted at different time points and compared with control groups (cells growth with the same culture medium used for the cell maintenance in cell culture flasks, see table 4.1).

As shown on the figure 4.1A, the number of viable NCI-H441 cells did not change at days 4 and 8 when culture conditions were modified. At day 12 of culture, changes on the NCI-H441 growth were observed: epithelial cell presented the same number of viable cells as the control, when incubated with Media A and B, and the growth pattern was not affected when endothelial supplements (ECGS and sodium heparin) were introduced on the culture medium; when Medium C was used, there was a significant reduction on the number of viable cells, indicating that medium M-199 could influence the growth of epithelial cells.

Endothelial cells are fastidious cells and usually require 20% (v/v) of FBS to grow, and according to Krump-Konvalinkova *et al.* (2001), the number of viable HPMEC-ST1.6R cells slightly reduced when 10% (v/v) of serum was used (340). There were no changes on the number of viable cells over time when endothelial cells were kept in medium M-199 with 10% (v/v) of FBS (Medium C), even if the medium was supplemented with sodium pyruvate. However, endothelial cells presented a higher number of cells over 12 days when cultured only or partially with supplemented RPMI1640 medium (Medium A and B, respectively, figure 4.1B). Despite the reduction of serum over the control, RPMI1640 medium has the double amount of D-glucose than medium M-199 (2000 and 1000 mg/mL respectively), the first source of energy for cell metabolism, providing this way a possible explanation for the observed higher growth rate of HPMEC-ST1.6R. The presence of sodium pyruvate on Media A and B, a second energy source alternative to glucose, can be also a possible explanation for these outcomes. ECGS and heparin were included on Media A, B and C, once they are important factors for the growth of HPMEC-ST1.6R: ECGS is a mitogenic supplement for the optimal growth of endothelial cells and sodium heparin improves the ECGS's affinity towards its receptor (341).

Independendtly of culture medium used, no morphological changes were observed on both cell lines during 12 days (figure A1A and B from Appendix II).

Based on this study, the establishment of an *in vitro* triple co-culture was carried out using Medium A (RPMI1640 with 10% (v/v) FBS, 1% (v/v) Pen/Strep, 1% (v/v) sodium

pyruvate, 25 µg/mL of ECGS and 25 µg/mL of sodium heparin), a medium that allows the combined growth of NCI-H441 and HPMEC-ST1.6R. The growth of THP-1 cells in different culture conditions was not assessed, since these cells must be first differentiated into macrophage-like cells, and only afterwards resuspended in a small volume of medium (30 µL) in order to keep the ALI conditions as described by (261). The medium and the amount of serum used for the maintenance of THP-1 cells is the same as NCI-H441 cell line. For this reason, during the establishment of triple co-culture, the macrophage-like cells were resuspended in the same culture medium used for the THP-1 maintenance (RPMI1640 with 10% (v/v) FBS and 1% (v/v) Pen/Strep). Due to the small amount of medium, short period of incubation (only for 24 hours) and given the similarity of medium used for the regular epithelium growth, it is not expected that the small amount of medium used for the dTHP-1 seeding interfere with the growth of epithelial cells.

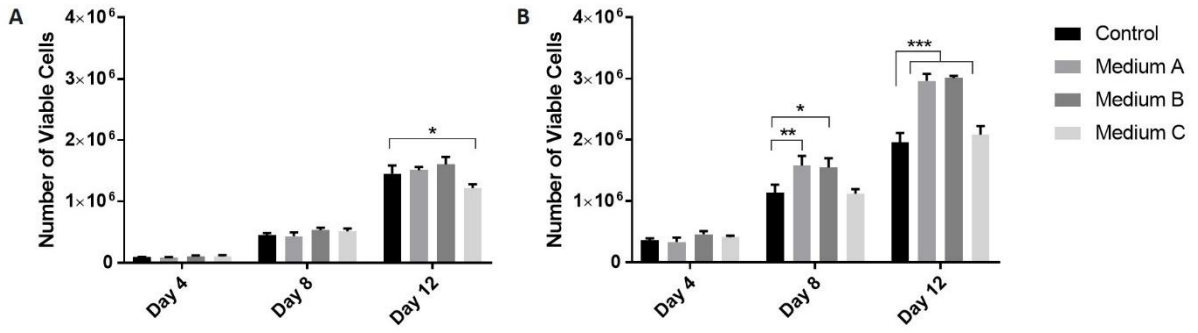

Figure 4.1. Number of viable NCI-H441 (A) and HPMEC-ST1.6R (B) cells maintained in different culture media during 12 days; Results expressed as mean ± SD; Statistical analysis performed through One-way ANOVA with Dunnett's multiple comparison test; * represents the significant differences when compared with the respective control.

3.2. Optimization of the cell number of NCI-H441 and HPMEC-ST1.6R

TEER measurement is an easy non-destructive assay performed on live experiments to evaluate the tight of the intercellular junctional complex, measuring the integrity of a cell layer, and last, its ability to form a selective permeable barrier between the apical and basolateral compartments. When cells present a low TEER, it is an indicator that

the cell layer has a low tightness and the transport of molecules can occur through adjacent cells (paracellular route) (342, 343).

The TEER after seeding different amounts of NCI-H441 cells on the apical side of the Transwell® is depicted on the figure 4.2A. Overall, TEER progressively increased between days 2 and 11, regardless of the initial number of cells seeded, although it was more pronounced when higher number of cells/ Transwell® were seeded. In all cases, between days 11-15, the TEER reached a plateau, probably because the epithelial cells reach confluence. When 5.0 x 10^4 cells/ Transwell® were seeded, a plateau was reached at day 9 of culture, but the TEER was only comprised between 65-85 Ω·cm^2. The maximum TEER (210 ± 46 Ω.cm^2) was reached at day 11 with 2.5 x 10^5 cells/ Transwell®. According to Salomon *et al.* (2014), 2.5 x 10^5 NCI-H441 cells/ Transwell® (12 mm diameter, pore size of 0.4 µm) cultivated at LLI conditions were able to reach TEER around 1000 Ω.cm^2 (240), but when cultured at ALI, the outcomes were similar with the one achieved in this study: TEER reached a plateau between 280 to 315 Ω·cm^2 after 9 days of culture, even when a Transwell® with a different pore size (0.4 µm) and different culture media and cell passage number were used.

The influence of endothelial cells on the integrity of NCI-H441 monoculture was also assessed. Endothelial cells play an essential role on the formation of the air-blood barrier. Morphologically, these cells form a continuous layer without pores between cells (17) but still have a lack of tight junctions (344). However, the high levels of caveolae on these cells can have implications on the caveolae-mediated transcytosis of macromolecules (345, 346).

In this work, NCI-H441 cells (2.5 x 10^5 cells/ Transwell®) were seeded on the Transwell® in combination with different ratios of HPMEC-ST1.6R: ratio end:epi of 2:1, 1:1; 1:2, 1.4 and 1:6, and as shown on figure 4.2B (statistical analysis displayed on figure A2 from Appendix II), the TEER of this bi-culture was significantly higher than in the epithelial monoculture during the first 9 days of culture. After this period of culture, the TEER was the same or even lower, regarding the control.

The increase of TEER on co-cultures of alveolar epithelial cells with endothelial cells has been explored, and different trends were observed. Co-cultures of NCI-H441 cells with HPMEC endothelial cells showed higher TEER (2-fold higher TEER) when compared with single epithelial monoculture (239); Neuhaus *et al.* (2012) also demonstrated that the integrity of NCI-H441 monoculture was enhanced when they were cultured with conditioned medium from HPMEC-ST1.6R, but the epithelial barrier

was weakened when cultured with conditioned medium of a human brain endothelial cell line, indication that the integrity of alveolar epithelium was influenced by tissue-specific endothelial cells, and the soluble factors from lung endothelium could strengthen the epithelial barrier (347). On the other hand, bi-culture of Calu-3 with HPMEC-ST1.6R presented the same TEER comparatively to Calu-3 monoculture (332). The sodium fluorescein (NaFlu) leakage assessed on a tetraculture model of air-blood barrier (A549 cells + EA.hy 926 + THP-1 + HMC-1), cultured at ALI, showed a higher permeability comparatively to the respective epithelial and endothelial monocultures as well as in a bi-culture (epithelial and endothelial cells), demonstrating that endothelial cells in this case did not improve the integrity of co-cultures and tetracultures (348). Based on these studies, the improvement of epithelial integrity by the presence of endothelial cells is not straightforward, and several factors like the culture conditions (ALI and LLI), the cell types and passage number, the porosity of Transwell® and the composition of medium can influence the tightness of epithelial cells.

For building this *in vitro* model, a cell number of 2.5×10^5 NCI-H441 cells/Transwell® was selected, since it was the one that yielded the highest TEER when cultivated on Medium A for 11 days. HPMEC-ST1.R cells grown almost two times faster than the NCI-H441 cells during the first 4 days after seeding (table A1 from Appendix II). The growth rate/doubling time for the NCI-H441 cell line between the first 4 days of culture and between day 4 and day 8 was the same (around 40-48 hours), and after 8 days of culture these cells did not reached the confluence (figure A1A from Appendix II). The growth rate /doubling time between day 4 and day 8 increased for HPMEC-ST1.6R cells, once cells reached the confluence, as observed on figure A1B from Appendix II. Based on these results thereby, less endothelial cells were seeded. A ratio of end:epi (1:2) was selected based on the studies published by Dekali *et al*. (2014) (332), and therefore, the following experiments were carried out using 1.25×10^5 HPMEC-ST1.6R cells/ Transwell®. Regardless of the endothelial cell number used, the TEER reached a plateau between days 6 and 11. Therefore to set-up the triple co-culture, dTHP-1 cells were incubated at day 7, and on the following day (day 8) this model was morphologically characterized.

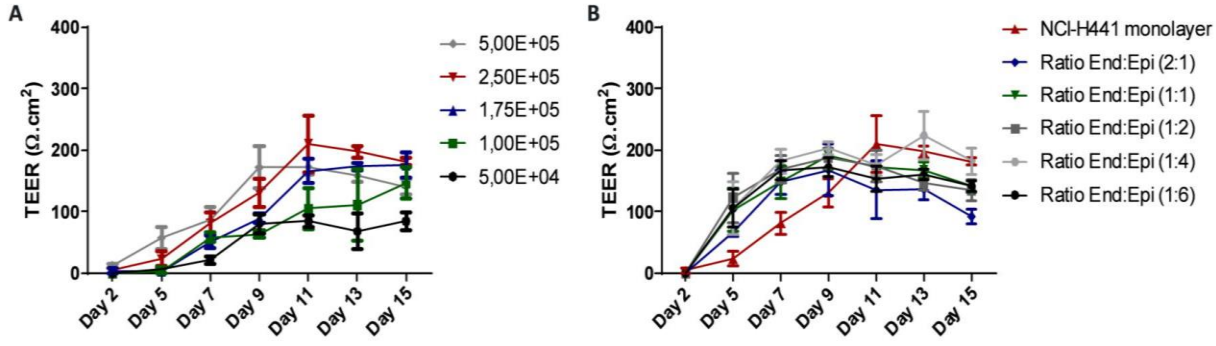

Figure 4.2. TEER measurements of NCI-H441 monoculture with different cell numbers (A). Bi-culture of NCI-H441 cells (2.5 x 10^5 cells/ Transwell®) with different ratios of HPMEC-ST1.6R cells (B). After 2 days of seeding 200 nM of Dex was added to induce the polarization of epithelium; mean ± SD, n=3 from 1 experiment.

3.3. Transepithelial electrical resistance and morphology of *in vitro* models with 8 days of culture

A triple co-culture was obtained by seeding epithelial cells (2.5 x 10^5 cells/ Transwell®) and endothelial cells (1.25 x 10^5 cells/Transwell®) during 7 days, using Medium A (composition described on table 4.1). On day 7, PMA-dTHP-1 cells were seeded on the top of NCI-H441 cells, and the triple co-culture was incubated for more 24 hours (until day 8).

During the first 7 days of culture, there were no statistical differences on the TEER when epithelial cells were cultured alone or in combination with endothelial cells. All co-cultures were incubated from day 2 with Dex, to improve the polarization of epithelial cells. Since Dex may interact with several receptors responsible for inflammatory response, it was removed before the seeding of macrophage-like cells. (349, 350).

At day 8 of culture, the presence of an endothelial layer enhanced the integrity of epithelium (TEER of 166 ± 37 Ω.cm^2 for NCI-H441+HPMEC-ST1.6R bi-culture) when compared with NCI-H441 monoculture (85 ± 31 Ω.cm^2). The seeding of dTHP-1 cells at day 7 of culture also improved the TEER of triple co-culture and bi-culture of NCI-H441+dTHP-1 (227 ± 88 and 176 ± 41 Ω.cm^2, respectively) when compared with epithelial monoculture. TEER achieved by the triple co-culture was lower comparatively to primary cells derived from lung tissue (TEER around 1,000–2,000

Ω.cm^2) (250, 252), but was more similar to the values reported for an A549 monoculture, (between 50-200 Ω.cm^2 (351-353), one of the most commonly used cell lines to mimic the alveolar epithelium region (215).

Epithelial cells are the main responsible for the integrity of co-culture models, and it is known that NCI-H441 cells cultured at ALI presented a low TEER comparatively to LLI conditions (240, 354), being one of the possible reasons for the low integrity of the triple co-culture model. The pore size of Transwell® membrane is another factor that may influence the integrity of epithelial cells, once a large pore size (3.0 µm) decreases the capacity of cells to form a tight barrier (355). The passage number of cells and the presence of some supplements on culture medium may also influence the barrier formation. ITS is a cell culture supplement with the essential components to promote the cell growing in a serum-free culture conditions, having been used by Salomon *et al*. (2014) and Ren *et al*. (2014) (240, 354) for the NCI-H441 culture over the Transwell®. More recently, it was demonstrated that the combination of ITS with Dex had an impact on the TEER, even when NCI-H441 cells were cultured at ALI (356).

In this triple co-culture model, 1.0 x 10^5 dTHP-1 cells/ Transwell® were seeded at day 7 of culture. According to Stone *et al.* (1992) (357), the number of cells at alveolar region is 5990 ± 1900 × 10^6 of macrophages and 19600 ± 9000 × 10^6 of ATI cells per lung (results expressed as mean ± standard deviations of the mean), which results in a proportion of 1 macrophage for each 3 epithelial cells. This ratio 1:3 was used to establish *in vitro* co-cultures of alveolar epithelium (251, 261), although the number of epithelial cells and macrophages proposed by Stone *et al*. (1992) presented a high variation regarding the mean number of epithelial cells and macrophages. The ideal number of macrophages is still not well established and was not often described when co-cultures were established (256, 259, 332). Some studies already used a macrophage:epithelial cell ratio of 1:5 (258), 1:20 (358) or even 2:1 (348). Most of the time the ratio is based on the initial epithelial cell number seeded, not on the number of epithelial cells that are presented on the day of macrophage seeding. This way, factors that may influence the growth of each cell line are not taken into consideration, like the initial amount of cell seeding, the culture conditions (culture medium, the material where cells grow), the presence of other cell types, as well the doubling time of each cell line. Due to difficulty of recovering NCI-H441 cells from the Transwell® membrane after seeding, the number of epithelial cells at day 7 of culture were not counted, and the accurate ratio of dTHP-1/NCI-H441 cells were not performed in this

work. A ratio of 1 macrophage-like cell for 2.5 epithelial cells were used based on the initial number of epithelial cells seeded, but it is expected that this ratio changes due to NCI-H441 cell growth over the time.

The morphology and the confluence of the single epithelial and endothelial monocultures, as well as the triple co-culture was assessed through CLSM by staining each cell line with different cell tracking dyes. It was verified that the epithelium was confluent throughout the Transwell® membrane for NCI-H441 monoculture and triple co-culture (figure 4.3C I and III) and dTHP-1 cells were found on the top of triple co-culture (figure 4.3C III). On the other hand, the basolateral side of the Transwell® membrane presented endothelial cells with an elongated shape (for endothelial monoculture and triple co-culture, figure 4.3C II and IV, respectively), however, some spots of the Transwell® membrane remained empty, eventually due to non-uniform coating of the Transwell® with Matrigel™.

The expression of tight junction markers, namely ZO-1 and occludin was also investigated by ICC. The ZO-1 and occludin expressed by NCI-H441 monoculture and triple co-culture presented a blurred staining, as it is shown on figures A3A, B, D and E from Appendix II. Epithelial cells were able to express E-cadherin, through all epithelial monoculture (figure A3C and F from Appendix II). Tight junctions and adherent junction are intercellular junctions that form the apical junctional complex located apically and laterally on a polarized epithelial membrane. Tight junctions are located at the most apical side of polarized membranes, and form a tight barrier between intercellular spaces, regulating the paracellular transport of compounds based on size and charge (359, 360). Below the tight junctions, are the adherent junctions, namely E-cadherin, that in corporation with a dense network of actin-filaments, are responsible for adhesion between adjacent cells (361, 362). TEER is widely used to evaluate the barrier properties of cells on a porous membrane, in particular the barrier formed by the tight junctions (363-365). The low expression of tight junctions observed can be correlated with the low TEER achieved for NCI-H441 monoculture and triple co-culture. Based on these outcomes, the use of this new *in vitro* triple co-culture model to study the paracellular transport of small substances and ions must be carefully assessed, since the formation of a selective barrier could not occur.

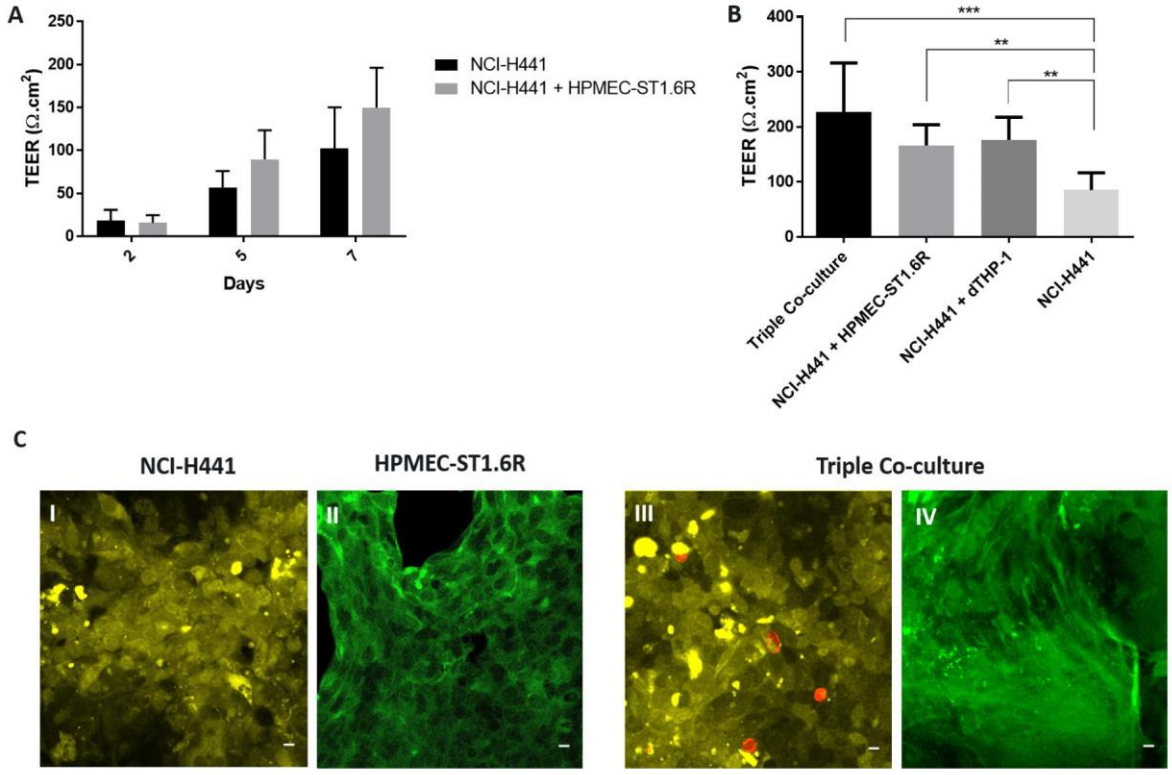

Figure 4.3. TEER of NCI-H441 monoculture, bi-culture and triple co-culture (A and B). A) TEER of NCI-H441 cells as a monoculture or combined with HPMEC-ST1.6R cells during 7 days; Data from 3 independent experiments, with 6 replicates in each experiment. B) At day 7, dTHP-1 cells were seeded on the top of epithelial cells of triple co-culture and TEER was measured at day 8; Data from 3 independent experiments, with 3 replicates in each experiment. For both figures (A and B), the results were expressed as mean ± SD and statistical differences (*) were determined by One-way ANOVA with Tukey's multiple comparison test. C) CLSM images NCI-H441 monoculture, HPMEC-ST1.6R monoculture and triple coculture after 8 days of culture: I and III are images collected from the apical side, while II and IV are from the basolateral side of 12-well Transwell®; NCI-H441 and HPMEC-ST1.6R cells were stained with yellow and green color, respectively, while dTHP-1 cells were stained with red color; Scale bar: 10 µm. Number of cells/ Transwell®: 2.5 x 10^5 NCI-H441 cells, 1.25 x 10^5 HPMEC-ST1.6R cells and 1.0 x 10^5 dTHP-1 cells.

3.4. Surface of *in vitro* cell culture models with 8 days of culture

The epithelial and endothelial surfaces of each monoculture and triple co-culture were characterized by SEM. Images showed that NCI-H441 monoculture presented a rough surface with some protuberances while the surface of endothelial layer was smooth. However, endothelial cells did not cover the whole Transwell® surface, most likely due to non-homogeneous coating with Matrigel™. No dTHP-1 cells were found on the apical side of triple co-culture, probably because they were washed out during the sample preparation, although their presence was observed through SEM on the bi-culture of NCI-H441+dTHP-1 (figure 4.4C). The presence of dTHP-1 cells on the triple co-culture was also confirmed through CLSM and histology.

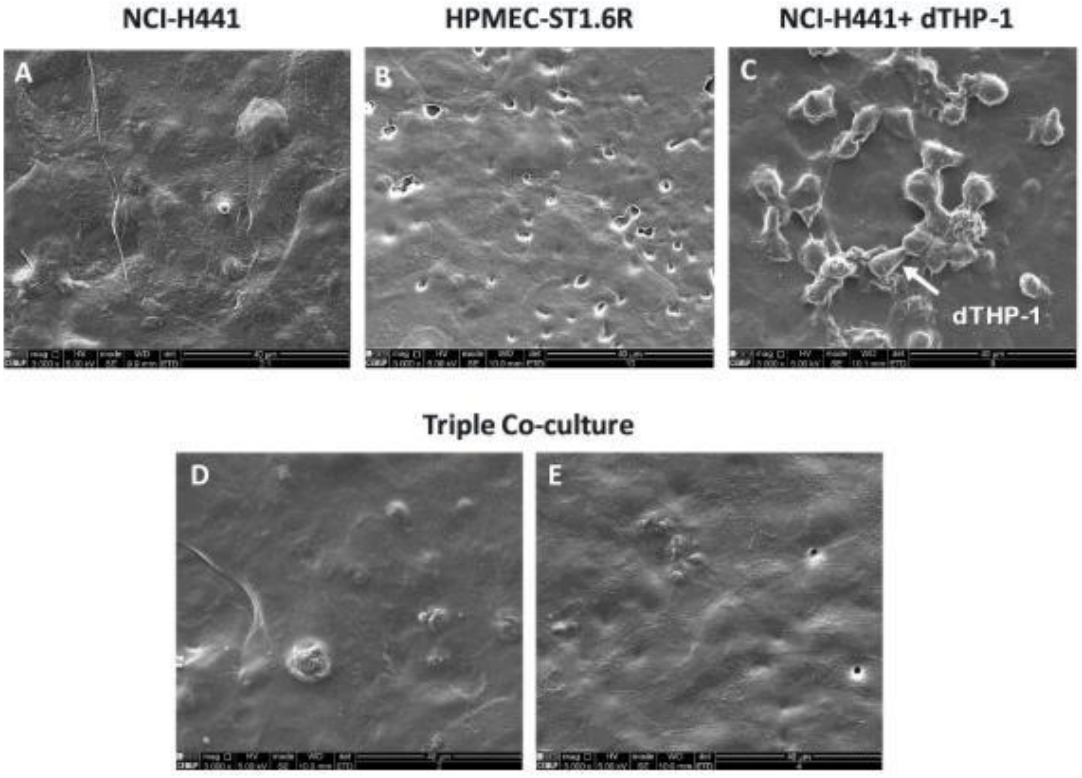

Figure 4.4. SEM images of NCI-H411 monoculture (A), HPMEC-ST1.6R monoculture (B), bi-culture of NCI-H441+dTHP-1 (C) and triple co-culture at apical side (D) and basolateral side (E) of 12-well Transwell®, after 8 days of culture. Scale bar: 40 µm.

3.5. Cross section and ultrastructural characterization

Cross sections of triple co-culture were prepared after 8 days of culture and analyzed by TEM (figure 4.5) and histology (figure 4.6). TEM micrographs showed that the epithelial layer of the triple co-culture presented a cuboidal shape and the presence of tight junctions/adherent junctions (TJ/AJ) was observed, confirming that the triple co-culture still can form a cellular barrier despite the low TEER.

NCI-H441 cells presents an ultrastructure similar to ATII cells and Clara cells (366), an epithelial cell at distal bronchiole with secretory functions, in particular SP (366, 367). In this work, the epithelial layer of the triple co-culture model showed microvillus (MV) (figure 4.5E), and the presence of secretory vesicles (SV) (figure 4.5F and G), that may be related to SP produced by these cells (SP-A, SP-B and SP-C), as already described (239). The endothelial layer showed a lung cytoplasmic extension (Figure 4.5C and 4.6C), which can be correlated with the elongated shape observed through CLSM.

Besides these features, the existence of cell multi-layers, either on the apical and basolateral side, was observed, which were later confirmed by histology (figure 4.6C). Cell multi-layers on single epithelial and endothelial monoculture were also observed (figure 4.6A and B). Ren *et al*. (2016) (356) demonstrated that NCI-H441 cells formed multi-layers when the same cell number of epithelial cells (2.5×10^5 cells/ Transwell®) was cultured at ALI. Regarding the endothelial layer, either cultured as a monoculture or in combination with epithelial cells and macrophage-like cells, they formed multi-layers, even when the Transwell® showed some spots without any cells. In this case, it was assumed that the non-confluence of endothelial monoculture is not due to the reduced number of cells seeded, but probably due to non-homogenous coating of the Transwell®. Furthermore, HPMEC-ST1.6R cells were concentrated in a small volume (1.25×10^5 cells dispersed in 90 µL of medium) that may be the origin of cell aggregation. Instead of being homogenously distributed onto the surface of the Transwell® membrane, endothelial cells formed aggregates and were grown as multi-layered clusters, a pattern that was already observed when cells were manually seeded (283).

The epithelium and endothelium of this new triple co-culture model could interact with each other through the pore of the Transwell® (figure 4.5G and H). The cross-talking between epithelium and endothelium can improve the barrier, probably due to endothelium-derived factors (347, 368, 369), and can be also important to regulate the

inflammatory response (258). This epithelial-endothelial contact may be also responsible for the improvement of TEER as observed for the triple co-culture model.

The aim of this study consisted in establishing a 3D *in vitro* model that mimics the physiological and morphological conditions of alveolo-capillary membrane to study the translocation of nanocarriers. The air-blood barrier is constituted by a flat layer of epithelial cells and by a thin single monolayer of endothelial cells, both separated by the BM. The presence of cell multi-layers at both sides of the Transwell® constitutes a limitation by not resembling morphologically the *in vivo* conditions, and the high thickness of this *in vitro* model could also influence the translocation of nanosystems.

To overcome this drawback, the same number of NCI-H441 and HPMEC-ST1.6R cells were seeded, but the time of culture was reduced in order to avoid the formation of multi-layers. Histological sections of epithelial and endothelial monocultures were performed at different days of culture (figure A4 from Appendix II). At day 4, the NCI-H441 monoculture already formed multi-layers. So, that further optimization was needed to originate a single epithelial monolayer of cells. The number of epithelial cells was reduced from 2.5 x 10^5 cells/ Transwell® to 1.0 x 10^5 cells/ Transwell®. This cell number was based on experiments published by Ren *et al.* (2016) (356), where was demonstrated that this cell line formed multi-layers when 2.5 x 10^5 cells/ Transwell® were cultured.

Histological sections of HPMEC-ST1.6R monoculture were also performed, but the endothelium can easily detach from the Transwell® during sample preparation, and due to non-uniform growth over its surface, the analysis of multi-layers became more difficult to assess. In order to allow a more homogenous distribution of endothelial cells and to keep the ratio of end: epi (1:2), 5.0 x 10^4 HPMEC-ST1.6R cells/Transwell® were seeded, while the number of dTHP-1 cells (1.0 x 10^5 cells/ Transwell®) was kept. The characterization of this new triple co-culture model is described on the Chapter V.

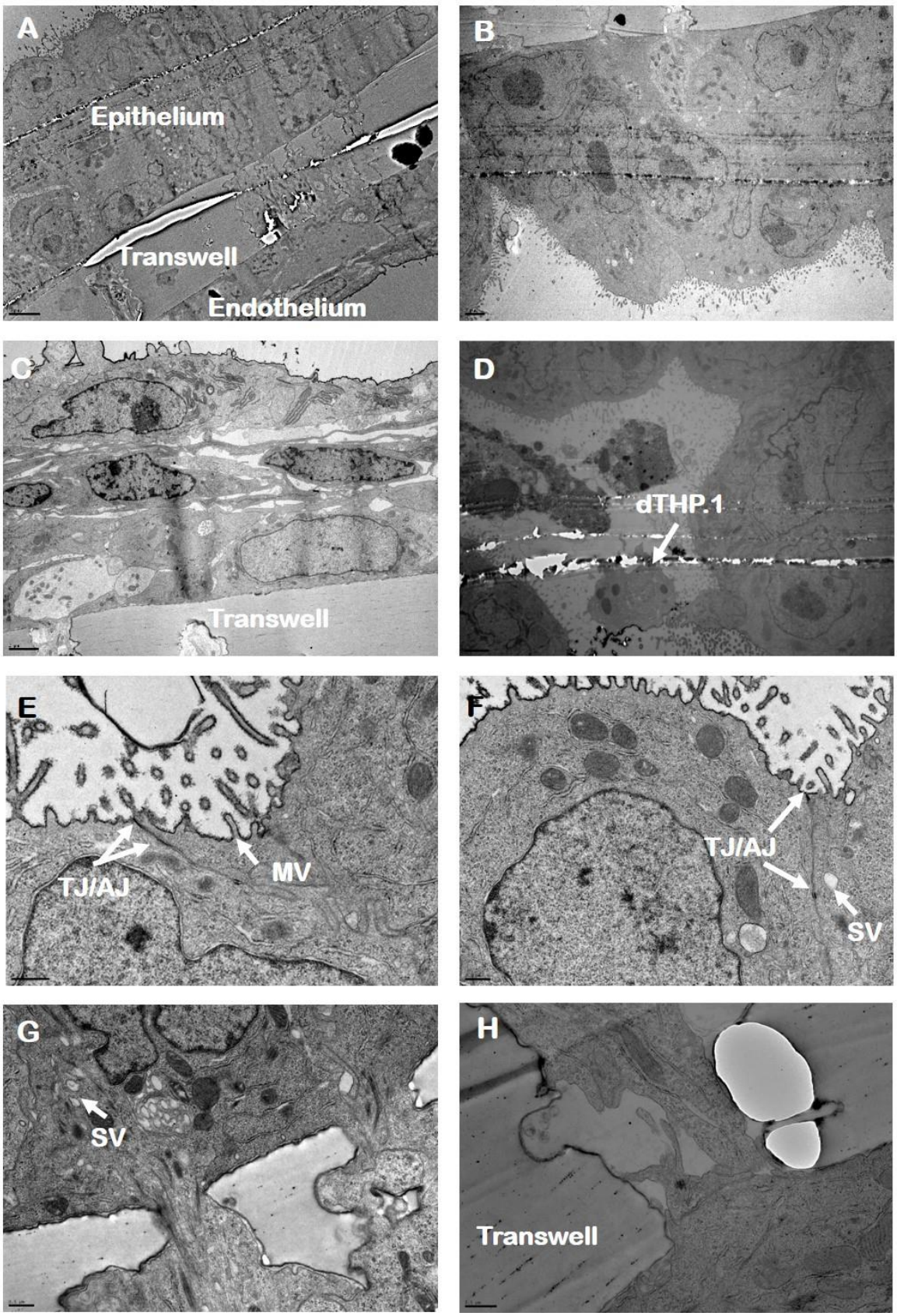

Figure 4.5. TEM micrographs of triple co-culture: overview of cross section of the triple co-culture model (A), epithelial layer (B) and endothelial layer (C); dTHP-1 cells are presented on

the top of epithelial layer (D). Presence of TJ/AJ (E and F), MV (E) on its surface (E) and SV (F and G); G and H showed the contact between epithelial and endothelial cells through the pore of the Transwell® (pore size 3.0 µm); Scale bar: A is 5 µm; B, C and D is 2 µm; E, F, G and H is 0.5 µm.

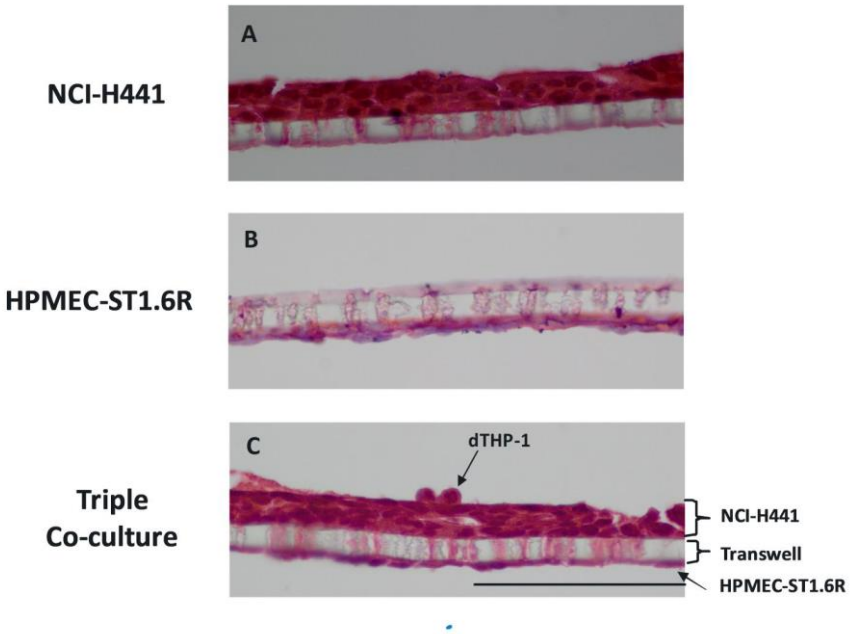

Figure 4.6. Histological section of NCI-H441 monoculture (A), HPMEC-ST1.6R monoculture (B) and triple co-culture model (C) with 8 days of culture on a 12-well Transwell®; Scale bar: 100 µm; Number of cells/ Transwell®: 2.5 x 10^5 NCI-H441 cells, 1.25 x 10^5 HPMEC-ST1.6R cells and 1.0 x 10^5 dTHP-1 cells.

3.6. Influence of insulin-transferrin-selenium and time of culture on the formation of multi-layers

To avoid the formation of multi-layers, the number of NCI-H441 cells seeded per each Transwell® was reduced from 2.5 x 10^5 cells to 1.0 x 10^5 cells. Transwell® with two different pore sizes were tested, 0.4 and 3.0 µm, and a preliminary study was performed to evaluate the presence of multi-layers on this cell line. TEER was also evaluated, once this parameter is dependent on the number of cells as well the pore size of the Transwell®. Cells were cultured during 8 days, and two different culture conditions were tested (scheme 4.3A and B): the culture medium was supplemented either with 10% (v/v) FBS or 5% (v/v) FBS and 1% (v/v) ITS. Instead of performing

histological sections, which is time consuming and may easily lead to sample damage during the preparation, cross sections of each sample were visualized through confocal analysis, by staining the cell nuclei with DAPI; Z-stacks from the top of cell layer until the Transwell® were performed and each focal plane presented a thickness of 1.0 µm. This preliminary study demonstrated that epithelial cells grown with 10% (v/v) FBS presented much more multi-layers formation than the cells grown with 5% (v/v) FBS and 1% (v/v) ITS, and this pattern was observed when cells were grown on Transwell® with different pore sizes (figure 4.7). Interestingly, cells cultured on Transwell® with a small pore size showed less multi-layers formation. TEER of NCI-441 monoculture was much higher when cells were grown on Transwell® with pore size of 0.4 µm (see figure A5 from Appendix II). Although being a preliminary experiment, this outcome allows to support the information achieved on section 3.2 and 3.3, that the use of a Transwell® with a large pore size can be the explanation for the low TEER measured on NCI-H441 monoculture, bi-cultures and triple co-culture. Epithelial cells grown with 10% (v/v) FBS showed a lower TEER over cells grown with 5% (v/v) FBS and 1% (v/v) ITS. The outcomes achieved on this preliminary study supported the information published by Ren *et al.* (2016), that the combination of ITS and Dex had a significant impact on the TEER and on protein expression (namely claudin-3) (356). For the following experiments the medium used to establish the triple co-culture was changed: cells were seeding with RPMI1640 supplemented with 5% (v/v) FBS, 1% (v/v) Pen/Strep, 1% (v/v) sodium pyruvate, 25 µg/mL of ECGS and 25 µg/mL of sodium heparin. After 24 hours, the medium was removed from the wells and new fresh complete medium was added, also containing 1% (v/v) ITS and 200 nM of Dex. These conditions were kept during cell culture, but Dex was removed before seeding dTHP-1 cells.

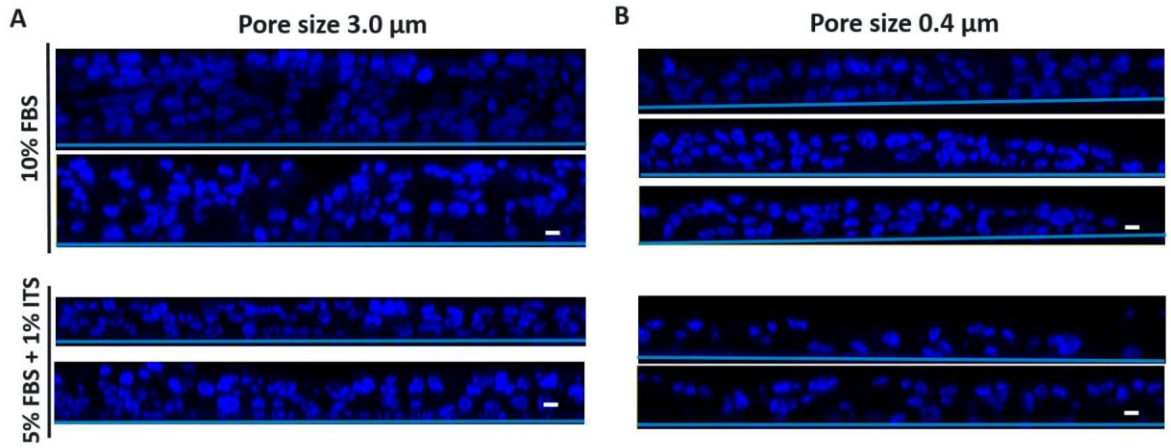

Figure 4.7. Cross section of NCI-H441 culture on 12-well Transwell® with pore size of 3.0 µm (A) and 0.4 µm (B), during 8 days. The influence of 10% (v/v) FBS and 5% (v/v) FBS + 1% (v/v) ITS on the multi-layer formation was assessed. 1.0 x 10^5 NCI-H441 cells/Transwell®; Scale bar 10 µm.

NCI-H441 cells cultured for 8 days with 5% (v/v) FBS and 1% (v/v) ITS still presented multi-layers. Epithelial and endothelial monocultures as well as triple co-culture were performed and fixed at different time points (day 8 and day 5 of culture, following schemes 4.4A and B, respectively), with the aim to evaluate the confluence and the presence of multi-layers. Z-stack images were also acquired to allow the examination of orthogonal view/cross section of each sample (figure 4.8). NCI-H441 cells, either as a monoculture or as a triple co-culture presented confluence at days 5 and 8. Cross sections of each sample showed that epithelial cells mainly formed a single monolayer at day 5 (some areas of the Transwell® still present more than one cell layer), but at day 8 of culture the majority of epithelial cells already formed multi-layers. Endothelial cells (from monoculture and triple co-culture) did not form a confluent layer either at day 5 and day 8. Concerning the multi-layers formation, the same pattern between epithelial and endothelial cells was observed, but endothelial cells still formed multi-layers, even when they were not confluent. These outcomes once again, support that the seeding at the basolateral side of the Matrigel™-coated Transwell® presents limitations regarding the homogenous distribution of endothelial cells. Based on these preliminary studies, the triple co-culture was established using 1.0 x 10^5 NCI-H441

cells, 5.0 x 10^4 HPMEC-ST1.6R cells and 1.0 x 10^5 dTHP-1 cells, following the culture conditions depicted on scheme 4.4B.

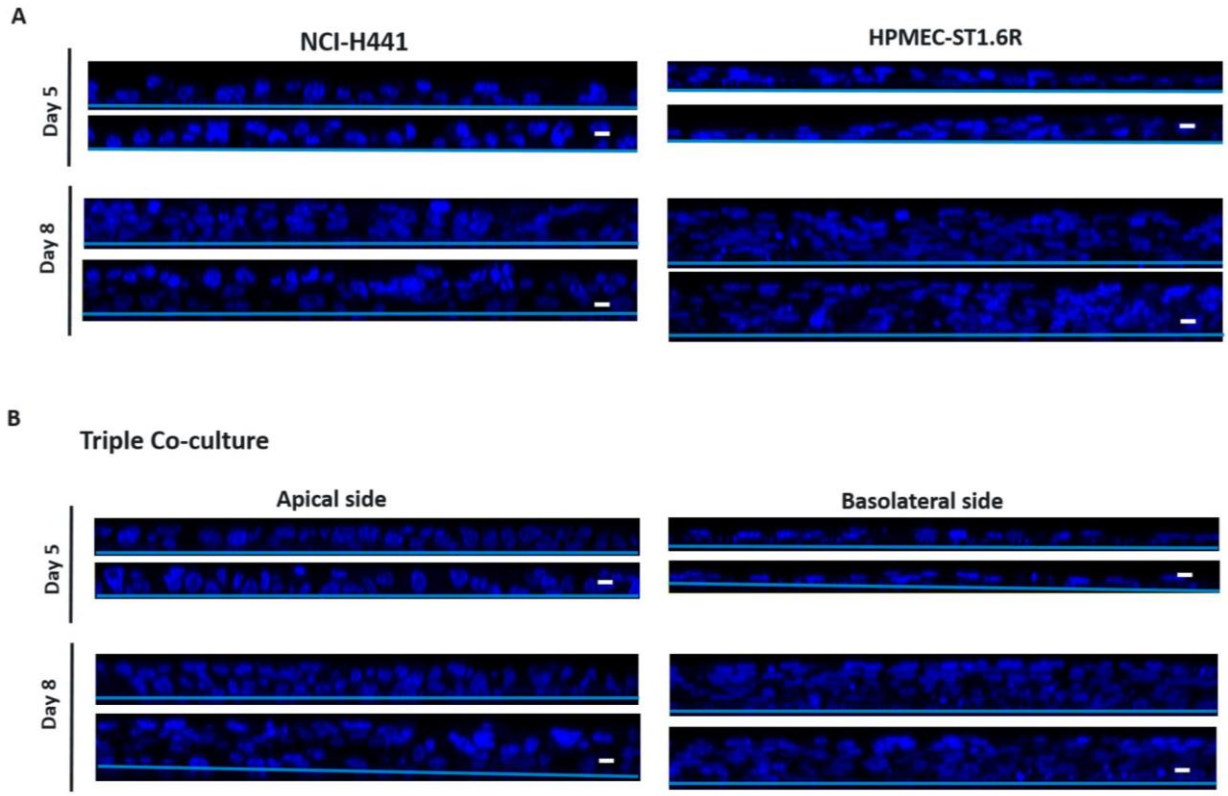

Figure 4.8. Cross section of NCI-H441 and HPMEC-ST1.6R cells (A) and triple co-culture (B) at days 5 and day 8 of culture. Complete medium was supplemented with 5% (v/v) FBS + 1% (v/v) ITS. Scale bar 10 µm; Number of cells/ Transwell®: 1.0 x 10^5 NCI-H441 cells, 5.0 x 10^4 HPMEC-ST1.6R cells and 1.0 x 10^5 dTHP-1 cells.

4. Conclusion

In this work an *in vitro* model of air blood barrier was established, with the aim of studying the translocation of nanocarriers. Cell culture conditions, number of cells seeded and time of culture were analyzed in order to achieve an 3D cell culture model constituted by a thin layer of epithelial and endothelial cells, both separated by the Matrigel™-coated Transwell®, and last, with macrophage-like cells seeded on the top of epithelial cells for mimicking the AMs.

Different culture conditions were initially tested and Medium A was selected as a common medium that allowed the both growth of epithelial and endothelial cells. Based on TEER measurements of epithelial monoculture, 2.5 x 10^5 NCI-H441 cells was selected to initiate the construction of this *in vitro* model. Since endothelial cells had a faster growth over epithelial cells, especially during the first 4 days of culture, it was selected a ratio end:epi (1:2) (1.25 x 10^5 HPMEC-ST1.6R cells/Transwell®). dTHP-1 cells were seeded on the apical side at day 7 (1.0 x 10^5 cells/ Transwell®) and incubated for more 24 hours (day 8). The combination of endothelial and dTHP-1 cells improved the TEER of triple co-culture, although the TEER of this new model was lower than the values reported for primary alveolar epithelial cells from lung tissue. Epithelial cells formed a confluent monolayer over the surface of the Transwell®, unlike the endothelial cells, that did not cover the Transwell® uniformly. Through TEM analysis, the epithelial cells from the triple co-culture showed the presence of MV, the production of SV and TJ/AJ, features already described for NCI-H441 monoculture (239, 240). A physical contact between epithelial and endothelial cells through the pores of the Transwell® was observed, which can be important for the integrity of the triple co-culture observed in this work, or even for the development of an inflammatory response.

On both sides of the Transwell®, NCI-H441 and HPMEC-ST1.6R cells were able to form cell multi-layers, probably due to higher number of cells seeded, the presence of higher amounts of serum and due to culture time, enforcing to a better optimization of the triple co-culture. The reduction of number of cells (either epithelial and endothelial) and the amount of serum (from 10% to 5% (v/v) FBS), alongside with the introduction of 1% (v/v) ITS, significantly reduced the formation of multi-layers on the NCI-H44 monoculture. The reduction of culture time from 8 days to 5 days also enabled the formation of an epithelial monolayer on NCI-H441 monoculture and triple co-culture, although the endothelial surface was still not confluent over the surface of Transwell®. Therefore, a new *in vitro* triple co-culture constituted by 1.0 x 10^5 NCI-H441 cells, 5.0 x 10^4 HPMEC-ST1.6R cells and 1.0 x 10^5 dTHP-1 cells, cultured at ALI conditions, was be established and characterized (see Chapter V). The establishment of this new triple co-culture takes 5 days, which is considerably faster when compared with other *in vitro* alveolar epithelial models, that usually are in culture between 8 up to 14 days (239, 240, 261). Permeability studies with NaFlu and translocation studies with different nanocarriers will be performed across monocultures, bi-cultures and triple co-culture,

with the aim of assessing the barrier properties of this *in vitro* airway model. The release of proinflammatory cytokines will be also evaluated after incubation with an inflammatory stimulus (namely LPS).

CHAPTER V

THREE-DIMENSIONAL *IN VITRO* AIR-BLOOD MODEL AS A TOOL TO EVALUATE THE LUNG TRANSLOCATION OF NANOCARRIERS

THREE-DIMENSIONAL *IN VITRO* AIR-BLOOD MODEL AS A TOOL TO EVALUATE THE LUNG TRANSLOCATION OF NANOCARRIERS

1. Introduction

The use of 3D *in vitro* models has been a valuable tool to study several biologic effects, like bacterial infection, disease mechanisms or even to study the pharmacokinetic parameters of drugs or pharmaceutical systems (370-373). These models are easy of handling, more economic, do not present complex ethical issues comparatively to animal models, and still can better resemble the *in vivo*-like condition over 2D *in vitro* models, constituted by a single flat monolayer of cells (204).

Pulmonary *in vitro* models with a single epithelial monolayer have been used for studying drug permeability, such as Calu-3 (374) or 16HBE14o- (375) being the most relevant models, due to ability to form a selective barrier with functional tight junctions, but both cell lines were derived from bronchial tissue. Primary cell isolated from lung tissue also form a monolayer with relevant properties (251), but the use of primary cells presents many disadvantages, namely a short life-spam, a high cost of maintenance, a limited number of passages and a low reproducibility (204, 376). To overcome these limitations, immortalized cell lines are preferred over primary cells. A549 monoculture was the common model used to mimic the alveolar epithelium, despite the inability to form a functional tight polarized barrier (254, 255). As alternative to A549 cell model, a new cell line (hAELVi) with type-I properties has been recently developed (260) and is now commercially available. Still for permeability studies, the NCI-H441 cells - a Clara-like pulmonary adenocarcinoma cell (377), has been considered as a relevant models to perform permeability studies, since it presents the formation of a cellular barrier and the expression of type-I markers similar to primary alveolar epithelial cells, which are important for the drug transport (240).

An effort has been made to increase the complexity of these *in vitro* epithelial models, in order to produce a physiological and morphological relevant model that allow a better study and understanding of cell-cell interactions or even cell-matrix interactions. Thus,

co-cultures with a different cell types have been established to study the drug/nanocarriers interaction, permeability or even the inflammatory response. Of note, a 3D *in vitro* model constituted by A549 co-cultured with blood monocyte–derived macrophages and dendritic cells has been established to study the particle translocation and inflammatory response (256, 257). The combination of epithelial cells (either NCI-H441 or A549) with endothelium was also performed with aim to study the effect of endothelial cells on the inflammatory response (239). Triple co-cultures constituted by epithelium, endothelium an macrophage-like cells with different states of polarization were also established, with the main goal of assessing inflammatory response after LPS challenge (259).

In this chapter, the already described 3D *in vitro* model of the airway (whose cell culture conditions and cell number were established on the chapter IV) was morphologically characterized. This *in vitro* model was used to assess permeability and translocation of small water-soluble molecules and nanocarriers, respectively, and also used to evaluate the release of proinflammatory cytokines after LPS stimulation.

2. Materials and Methods

2.1. Materials

RPMI-1640, RPMI-1640 without phenol red, trypsin-EDTA and Pen/Strep solution 10.000 U/mL were purchased from Gibco (Waltham, USA); FBS was from Biochrom (Cambridge, UK); Medium M-199 with Earle's salts, with stable glutamine (100 mg/L) with 2.2 g/l NaHCO3, and glucose (1000 mg/L), ECGS and PFA were was from Merck (Darmstadt, Germany); Heparin sodium salt from porcine intestinal mucosa from Alfa-Aesor (Haverhill, USA); Gelatin from porcine skin, PBS, PMA and Dex were purchase from Sigma-Aldrich (St. Louis, USA); Matrigel™ BM Matrix was purchase from Corning® (New York, USA); DAPI, Vybrant® CFDA SE Cell Tracer were purchase from Invitrogen (Carlsbad, USA); Triton X-100 was purchased from Spi-Chem (Atlanta, USA); CellTrace™ Yellow Cell Proliferation Kit, CellTrace™ Far Red Cell Proliferation Kit and ITS were bought from Thermo-Fisher Scientific (Waltham, USA); Glutaraldehyde was acquired from Electron Microscopy Sciences (Hatfield, USA) and Epon resin was bought to TAAB (Berks, England); Methanol and ACN HPLC gradient

grade were from Fisher Scientific (Leicestershire, UK); TFA was purchased from Acros Organic (New Jersey, USA); Entellan® new was acquired from Merck (Darmstadt, Germany); Clear-Rite™ 3 was from Richard-Allan Scientific™ (San Diego, USA). MTT, Isn, NaFlu, ethylenediamine tetraacetic acid (EDTA) dihydrate, K_2HPO_4, $MgCl_2$ x $6H_2O$, Tween®-20 and Pluronic® F-127 were purchase from Sigma (St. Louis, USA); Fluorospheres with a size of 50 nm (reference 17149) and 1.0 µm (reference 17154) were from Polysciences, Inc. (Warrington, EUA); NaCl, KCl and $CaCl_2$ were from VWR® (Leuven, Belgium). Lipopolysaccharides (LPS) from *Escherichia coli* O55:B5 purified by gel-filtration chromatography was purchase from Sigma (St. Louis, USA); Dako® mouting medium was from Palex Medical (Barcelona, Spain).

2.2. Cell culture maintenance

NCI-H441 and THP-1 cells were bought from ATCC (Manassas, USA) while HPMEC-ST1.6R cell line was kindly provided by Professor C. James Kirkpatrick from the Institute of Pathology, Johannes Gutenberg University of Mainz, Germany.

NCI-H441 cells were routinely cultured in T75 cell culture flask with RPMI1640 culture medium, supplemented with 10% (v/v) FBS, 1% (v/v) Pen/Strep and 1% (v/v) sodium pyruvate. HPMEC-ST1.6R cells were also maintained in T75 cell culture flaks, however prior to culture, the cell culture flasks were first coated with gelatin solution 0.2% (w/v) during 20-30 minutes at 37 °C. HPMEC-ST1.6R cells were cultivated with medium M-199 (with Earle's salts, stable glutamine (100 mg/L), 2.2 g/L NaHCO3, and glucose (1000 mg/L)), further supplemented with 20% (v/v) FBS, 1% (v/v) Pen/Strep, 25 µg/mL of ECGS and 25 µg/mL of heparin sodium salt.

For both cell lines, the medium was replaced each 2-3 day, and when cells reached 70-80% of confluence, they were washed with 5 mL of PBS and detached from the flask, after incubation of trypsin-EDTA for 5 minutes. Complete medium was added for Trypsin-EDTA inactivation, and cells were centrifuged, resuspended in fresh medium and seeded into new T75 cell culture flasks.

THP-1 cells were maintained in suspension into cell culture flask with RPMI1640 supplemented with 10% (v/v) FBS and 1% (v/v) Pen/Strep. When they reached 70-80% of confluence, cells were centrifuged and splitted into new cell culture flasks.

2.3. Triple co-culture model of air-blood barrier

Transwell® was inverted on a petri dish and the basolateral side was coated with 50 µL/cm^2 of Matrigel™ (protein concentration of 4.0 mg/mL), following the incubation for 1 hour at 37 °C. Then, HPMEC-ST1.6R cells were seeded on basolateral side of the Transwell® (5.0 x10^4 cells/ Transwell®) and further incubated for more 2 hours to allow the cell adhesion. Transwell® membrane was inverted again and placed on the well. Thereafter, 1.0 x 10^5 NCI-H441 cells were seeded on apical side of each Transwell®. The bi-culture of NCI-H441+HPMEC-ST1.6R was incubated for 24 hours with 0.5 mL and 1.5 mL of complete medium at apical and basolateral compartment, respectively. The medium selected for the culture was selected based on experiments performed by Ren *et al.* (2016) (356), but with slight modifications: both cells were cultured with RPMI 1640 medium, supplemented with 5% (v/v) FBS, 1% (v/v) Pen/Strep, 1% (v/v) sodium pyruvate, 25 µg/mL ECGS and 25 µg/mL sodium heparin for 24 hours; on the following day, the medium was aspirated and fresh complete medium, further supplemented with 200 nM of Dex and 1% (v/v) ITS, was added to each Transwell®. Cells were kept under LLI during 48 h until day 3 of culture; then, the medium was removed and replaced with 0.5 mL of complete medium (also including Dex and ITS) on the basolateral side; cells were kept under ALI for more 24 hours.

At day 4, the medium was removed and cells were washed with PBS to remove the Dex. dTHP-1 cells were differentiated and seeded on the apical side of the Transwell® following the methodology described on section 2.5.2 from chapter IV. Briefly The macrophage-like cells were obtained after differentiation of THP-1 cells with 10 ng/mL of PMA for 48 hours; thereafter 1.0 x 10^5 dTHP-1 cells were resuspended in 30 µL of medium (RPMI1640 with 10% (v/v) FBS and 1% (v/v) Pen/Strep) and placed on the top of epithelial layer. The triple co-culture was incubated for more 24 hours (day 5 of culture). Scheme 5.1 showed the culture conditions used to set-up the triple co-culture with 5 days of culture.

This triple co-culture model was morphologically characterized and different transport studies were performed using different nanocarriers. Translocation studies were also performed across each monoculture and bi-cultures (NCI-H441+dTHP-1 and NCI-H441+HPMEC-ST1.6R), with the goal of evaluate differences between each *in vitro* cell culture model.

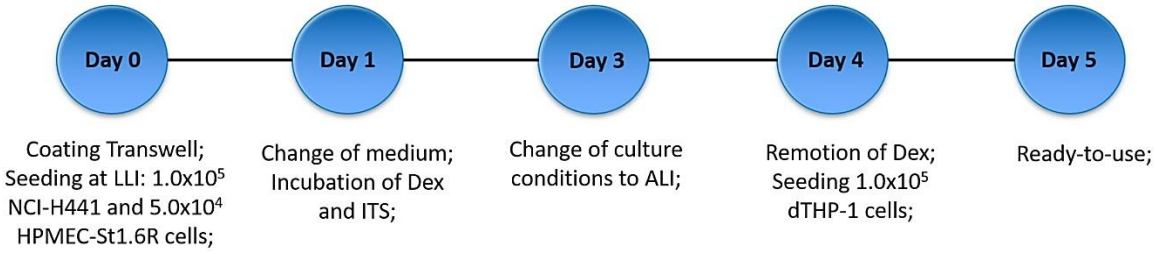

Scheme 5.1. Culture conditions of triple co-culture with 5 days of growth: cells were kept with RPMI 1640 + 5% (v/v) FBS + 1% (v/v) Pen/Strep + 1% (v/v) sodium pyruvate + 25 µg/mL ECGS + 25 µg/mL sodium heparin during 24 hours after seeding; then, the complete medium was further supplemented with 1% (v/v) of ITS and 200 nM of Dex; Dex was removed at day 4, before the seeding of dTHP-1 cells.

2.4. Transepithelial electrical resistance assessment of *in vitro* cell culture models

For TEER measurement was used an electrode connected to an EVOM Voltohmmeter, both from World Precision Instrument, Sarasota, USA). The chopsticks of electrode were directly placed on the lateral side of the Transwell® for TEER measurement when cells were cultured at LLI. When cultured at ALI, 0.5 mL of complete culture medium was first added to apical side while 1 mL of the same medium was placed on the basolateral side of Transwell®. Cells were incubated for 1 hour in an incubator at 37°C with 5% of CO_2, to allow the equilibration before the measurement. TEER of a blank (Transwell® without cells) was measured, to remove the interference of the Transwell® and the medium, and this parameter was calculated according with equation 4.3 from chapter IV.

2.5. Morphological and ultrastructural analysis of *in vitro* cell culture models

2.5.1. CLSM of NCI-H441 monoculture, HPMEC-ST1.6R monoculture and triple co-culture

Morphology of NCI-H441 monoculture, HPMEC-ST1.6R monoculture and triple co-culture was assessed through CLSM, following the methodology described on section 2.7.1 from chapter IV. Briefly at day 4, the epithelial and endothelial cells were stained with CellTrace™ Yellow Cell Proliferation Kit (concentration of 10 µM) and Vybrant® CFDA SE Cell Tracer (concentration of 10 µM), respectively. Cells were stained following the manufacturer's instructions. After trypsinization of PMA-dTHP-1 cells, they were centrifuged and stained with CellTrace™ Far Red Cell Proliferation Kit (concentration of 3 µM), also following the procedure described by the manufacturer. The plate containing the cells were incubated for more 24 hours inside of an incubator at 37 °C, with an atmosphere of 5% CO_2. At day 5 of culture, cells were fixed with PFA 3% overnight at 4 °C. After washing and DAPI staining, cells were mounted between 2 coverslips. All samples were analyzed through a Leica TCS SP5 II, Leica Microsystems (Wetzlar, Germany), using the same settings described on the section 2.7.1 from chapter IV.

2.5.2. Scanning electron microscopy analysis

After 24 hours of dTHP-1 cell seeding, samples were washed with PBS, followed fixation with PFA 3%, overnight at 4 °C. Thereafter, samples were dehydrated through a graded series of alcohol for 10 minutes each*:* 30%, 50%, 70%, 80%, 90%, 96%, 100% and 100%. All steps were performed by placing 700 µL of liquid at basolateral compartment, to avoid the washing out of dTHP-1 cells from apical side. Samples were let drying overnight at 37 °C. The Transwell® membrane was cut and placed on carbon discs of the SEM's pin stub. Samples were sputtered with gold (thickness 10 nm) and images were collected through a SEM, Zeiss SEM EVO® HD15 (Oberkochen, Germany).

2.5.3. Ultrastructural characterization

At day 5 of culture, cells were washed with PBS (only 0.7 mL) at basolateral compartment, fixed with 2.5% of glutaraldehyde and 2% of PFA in cacodylate buffer 0.1M (pH 7.4), following dehydration and embedding in Epon resin. Ultrathin sections (40–60 nm thickness) were performed onto a RMC Ultramicrotome (PowerTome, USA) using diamond knives (DDK, Wilmington, DE, USA) and mounted on 200 mesh copper or nickel grids. Samples were stained with uranyl acetate during 15 min and lead citrate for another 15 minutes, followed examination under a JEOL JEM 1400 TEM (Tokyo, Japan). Images were digitally recorded using a CCD digital camera Orious 1100W (Tokyo, Japan).

2.5.4. Histological section

Samples were fixed with PFA 3% overnight at 4 °C. On the following day, they were dehydrated through a graded series *of* alcohol for 10 minutes each concentration: 35%, 50%, 70%, 95%, 100% and 100%. Samples were further incubated two times with Clear-Rite™ 3, 10 minutes each incubation, and then embedded two times in paraffin (1 hour each embedding). Samples were included in paraffin and stored at 4 °C overnight. The paraffin block containing the samples was cut through a Microtome Leica RM2255 (Leica Bioystems, Nuchloss, Germany), and the histological sections with a thickness of 7.0 µm were let drying overnight at 37 °C. On the following day, samples were stained with hematoxylin and eosin and mounted with Entellan® new (Merck, Darmstadt, Germany). Finally, the histological sections were examined through a Light microscope Olympus DP25 (40x objective) coupled with a camera. Images were acquired through Software Cell B (Olympus Corporations, Shinjuku, Japan).

2.6. Apparent permeability of sodium fluorescein

Cells were washed once with PBS during 5 minutes. After washing, cells were incubated with Krebs-Ringer Buffer (KRB): 114.2 mM of NaCl, 3 mM of KCl, 1.5 mM

of K_2HPO_4, 10 mM of HEPES, 4 mM of D-Glucose, 1.4 mM of $CaCl_2$ and $MgCl_2$ x $6H_2O$; pH 7.4) alone or in combination with EDTA at apical side (0.52 mL), while only KRB was placed at basolateral side (1.7 mL). Cells were incubated during 45 minutes at 37 °C, following the measurement of TEER to assess the integrity of different *in vitro* models (monocultures, bi-cultures and triple co-culture), in the presence or absence of EDTA (± EDTA 16 mM).

Content from apical side was collected and centrifuge to recovery the dTHP-1 cells. The pellet was resuspended in 0.52 mL of KRB, with 10 µg/mL of NaFlu ± 16 mM of EDTA dissolved and placed on the apical side (donor compartment), while 1.7 mL of KRB was incubated on the basolateral side (acceptor compartment). The 12-well plates were placed on an orbital shaker oven (IKA, Germany) at 100 rpm and incubated during 3 hours at 37 °C. At each time point (0, 0.5, 1, 1.5, 2, 2.5 and 3 hours), 200 µL of the content from acceptor compartment was collected and replaced with fresh pre-warmed medium. 20 µL of the supernatant from donor compartment was also collected at the begin and end of experiment. The fluorescence of each supernatant was analyzed through a plate reader, with an excitation/emission wavelength of 460/515 nm. Three replicates of this experiment were performed. The results were expressed as apparent permeability (P_{app}), following the equation:

Equation 5.1. $P_{app} = (dQ/dt)/(C0\ x\ A)$

dQ/dt is the amount of NaFlu that permeated from the donor to the acceptor compartment as a function of the time, C_0 is the initial concentration of NaFlu on the donor compartment and A is the area of the Transwell® membrane.

2.7. Translocation of fluorospheres

At day 4 of culture and after washing the cells to remove Dex, epithelial and endothelial cells from monocultures, bi-cultures and triple co-culture were stained with 7 µM of CellTrace™ Yellow Cell Proliferation Kit according with manufacturer's instructions. The dTHP-1 cells, previously differentiated with 10 ng/mL of PMA, were washed with PBS and trypsinized. dTHP-1 cells in suspension were stained with 3 µM of CellTrace™ Far Red Cell Proliferation Kit, following the procedure described by

the manufacturer. Then, dTHP-1 cells were counted and incubated on the top of epithelial or seeded on an empty Transwell® (ET), previously coated with Matrigel™.

At day 5 of culture, the basolateral side was washed once with PBS during 5 minutes. The 50 nm-fluorosphere and 1.0 µm-fluorospheres were dispersed in 0.52 mL of RPMI1640 medium without phenol red, supplemented with 5% (v/v) of FBS, and added at the donor compartment, while the acceptor compartment was just re-filled with the same medium (1.7 mL). The experiment was conducted at 150 rpm through an orbital shaker (IKA, Germany), inside of an incubator at 37 °C with an atmosphere of 5% of CO_2. At different time points (0, 0.5, 1, 1.5, 2, 2.5 and 3 hours), 200 µL of the content from acceptor compartment was collected and replaced with fresh pre-warmed medium, while 20 µL of donor compartment were also collected at the beguin and end of each experiment. The collected supernatant was transferred to a 96-well plate for further fluorescence analysis through a Tecan® plate reader (Tecan Deutschland GmbH, Germany), using an excitation/emission wavelength of 441/486 nm. Three replicates of each experiment were performed, and results were expressed as cumulative percentage of fluorospheres at basolateral side.

After supernatant collection, the content of apical and basolateral side was removed. To avoid the loss of macrophage-like cells from apical side, only the basolateral side of individual samples was washed with 0.7 mL of PBS. Cells were fixed with PFA 3% for 30 minutes at room temperature, followed a washing step, to remove the PFA. Cells were counterstained with DAPI (500 ng/mL) for 30 minutes, washed with PBS and mounted between two coverslips.

Translocation studies with 50 nm-fluorosphere and 1.0 µm-fluorospheres were also performed across empty Transwell® with Matrigel™ coating (ET (+ Matrigel)) and empty Transwell® without Matrigel™ coating (ET (- Matrigel)). ET was washed and also mounted between two coverslips for CLSM examination.

All samples were observed through a Spectral Confocal Microscope Leica TCS-SP5 AOBS, Leica Microsystems (Wetzlar, Germany), with a HCX PL APO CS 40.0 x 1.30 Oil UV objective, and a zoom of 1.7. The images were acquired with a minimal resolution of 8-bits, an image size of 1024 x 1024 pixel, a bidirectional scanning speed of 700 Hz, a frame-average and line-average of 1. The intensity of gain and the offset on the green channel was adjusted through an ET filter without any treatment, in order to remove the green autofluorescence of the Transwell®. Z-stacks images from both

sides of the Transwell® were acquired with a thickness of 1.01 µm and treated with Leica Application Suite X software (Leica Microsystems, Wetzlar, Germany).

2.8. Translocation of Isn-SLN and Isn permeability

The translocation of Isn-SLN and the permeability of free Isn was assessed through the different monocultures, bi-cultures (NCI-H441+dTHP-1 and NCI-H441+HPMEC-ST1.6R) and triple co-culture; translocation and permeability across ET (+ Matrigel) and ET (- Matrigel) were also assessed, in order to evaluate the retention of nanosystems/free drug by the Transwell® membrane.

Isn-SLN were produced and characterized as described by (378). This formulation with a drug concentration of 50 µM was dispersed in KRB with 0.1% (m/v) of Pluronic® F-127 (to avoids the aggregation of SLN during the experiments). Free Isn with same concentration was dissolved in the same medium as Isn-SLN. Before the incubation of the compounds, the basolateral side of each cell culture model was washed with PBS, to avoid the loss of macrophage-like cells from the apical side. 0.6 mL of Isn-SLN suspension was placed at the apical compartment, while 1.7 mL of KRB was added at basolateral compartment. The plates were placed inside of an orbital shaker oven (IKA, Germany) at 100 rpm and incubated for 3 hours at 37°C. At different time points (0, 1, 2 and 3 hours) 200 µL of medium from acceptor compartment was collected and replaced with pre-warmed fresh KRB. At the beguin and end of experiment, 100 µL of medium was collected from the acceptor compartment. The samples collected were further analyzed through HPLC. For each *in vitro* cell culture model (monocultures, bi-cultures and triple co-cultures), the experiments were performed in three replicates, and the results expressed as percentage of cumulative mass at basolateral compartment.

2.9. Influence of lipopolysaccharide on the Isn permeability

To evaluate the influence of a proinflammation state on the permeability of free Isn, LPS was incubated on different cell culture models. After 4 hours of dTHP-1 seeding, 50 µL of LPS (concentration of 10 µg/mL) or PBS (for the untreated controls) were

placed on the apical side of each cell culture model, followed incubation for more 24 h. The apical side of each Transwell® was washed two times with PBS and the supernatant was centrifuged for the recovery of dTHP-1 cells. These cells were resuspended and re-incubated on the top of epithelial cells.

Free Isn was dissolved in KRB with 0.1% (m/v) of Pluronic® F-127 and 0.6 mL of this solution was incubated on apical side of the Transwell®. Permeability studies were conducted as described on the section 2.8. At different time points, samples from basolateral side were collected for being posteriorly analyzed by HPLC. TEER was assessed at the end of experiment.

2.10. Quantification of Isn

Isn was quantified through HPLC Shimadzu UFLC Prominence System (Shimadzu Corporations Kyoto, Japan) connected to a degasser DGU-20A5, a SPD-20A detector (to detect Isn at 260 nm) and an autosampler SIL-20AC. To quantify the Isn, a mobile phase constituted by triethylamine 0.1% (v/v) (pH 5.0 adjusted with concentrated TFA) and methanol with a proportion of 85:15 (v/v) was selected. Analysis was carry out through a HPLC column Licrospher® 100 RP-C18, with 5 µm of particle size (LiCroCART®) and 250 mm length x 4.0 mm internal diameter, coupled with a guard column with 5 µm particle size, Merck (Darmstadt, Germany). Each analysis had a running time of 8 minutes and was performed at 30 °C (through a column oven CTO-20AC, Shimadzu Corporations), with a feed volume of 10 µL and a flow rate of 1 mL/minute.

2.11. Interleukin measurement

After incubation of PBS or LPS for 24 hours, the apical side of each monoculture, bi-cultures and triple co-culture was washed twice with PBS (total volume of 0.5 mL). The supernatant was collected to quantify the amount of IL released by the cells from each *in vitro* model; the content from basolateral side (0.5 mL) was also collected and mixed with the content from apical side. The supernatant of each sample was centrifuged at 10000 rpm during 10 minutes at 4 °C, and aliquoted for storage at -80 °C until be

analyzed. IL-8 was assessed through a Human IL-8 (CXCL8) Standard TMB enzyme-linked immunosorbent assay (ELISA) development Kit (PeproTech, Rocky Hill, USA), following the manufacturer's instructions.

2.12. Statistical analysis

GraphPad Prism Software vs. 7 (GraphPad Software Inc., La Jolla, USA) was used to perform the statistical analysis. One-way ANOVA and t-test were used, and different significance levels were considered: significant at a level of $p < 0.05$ (*), very significant at level of $p < 0.01$ (**) and highly significant at a level of $P < 0.001$ (***).

3. Results and discussion

3.1. Transepithelial electrical resistance and morphology of *in vitro* models with 5 days of culture

TEER was assessed on each monoculture, both bi-cultures and triple co-culture during the 5 days of culture (see figure 5.1A and B). When 1.0×10^5 NCI-H441 cells/ Transwell® were seeded, the TEER was close to 20 $\Omega.cm^2$. Triple co-culture presented a significant higher TEER over NCI-H441 monoculture and both bi-cultures at day 5. The TEER achieved was lower when compared with the triple co-culture established with higher number of cells and for a longer culture time (8 days, see figure 4.3 from chapter IV). The low TEER achieved for this triple co-culture could be explained by the low number of cells seeded and the short period of time in culture, that reduced significantly the formation of multi-layers and consequently the integrity of the barrier, even when ITS and Dex were incubated with the aim to improve the tightness of this cellular barrier (356). Thus, the permeability of NaFlu, alone or in the presence of EDTA, must be performed to assess if the triple co-culture behaves as a selective permeable barrier for small hydrophilic substances.

CLSM images were acquired to assess the confluence of epithelial and endothelial monocultures and triple co-culture after 5 days of culture. The presence of endothelial cells did not change the structure and morphology of NCI-H441 cells at the triple co-

culture. Epithelial cells, either as a monoculture or as a triple co-culture presented confluence, unlike endothelium that did not cover all the surface of the Transwell®. Histological sections demonstrated that dTHP-1 cells were observed on the apical side of the Transwell® (see figure 5.2C), corroborating with the data obtained from CLSM analysis (figure 5.1C-III). By other hand, NCI-H441 and HPMEC-ST1.6R monocultures, as well as triple co-culture mainly formed a single epithelial and endothelial monolayer of the cells (see figure 5.2A and B).

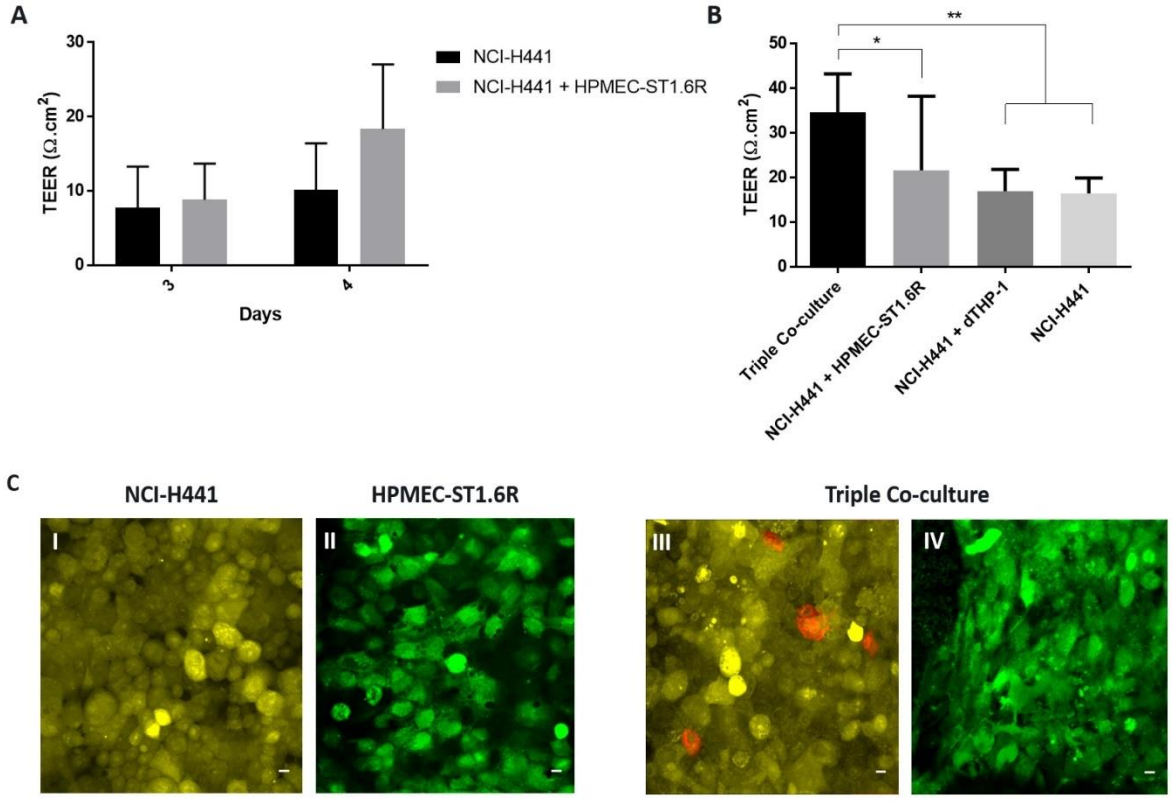

Figure 5.1. TEER of NCI-H441 monoculture, bi-culture and triple co-culture (A and B). A) TEER of NCI-H441 cells as a monoculture or combined with HPMEC-ST1.6R cells during 5 days; Data from 3 independent experiments, with 6 replicates in each experiment. B) At day 4, dTHP-1 cells were seeded on the top of epithelial cells of triple co-culture and TEER was measured at day 5; Data from 3 independent experiments, with 3 replicates in each experiment. For both figures (A and B), the results were expressed as mean ± SD and statistical differences (*) were determined by One-way ANOVA with Tukey's multiple comparison test. C) CLSM images of NCI-H441 monoculture, HPMEC-ST1.6R monoculture and triple coculture with 5 days of culture: I and III are images collected from apical side, while II and IV are from basolateral side of the 12-well Transwell®; NCI-H441 and HPMEC-ST1.6R

cells were stained with yellow and green color, respectively, while dTHP-1 cells were stained with red color; Scale bar: 10 µm. Number of cells/ Transwell®: 1.0 x 10^5 NCI-H441 cells, 5.0 x 10^4 HPMEC-ST1.6R cells and 1.0 x 10^5 dTHP-1 cells.

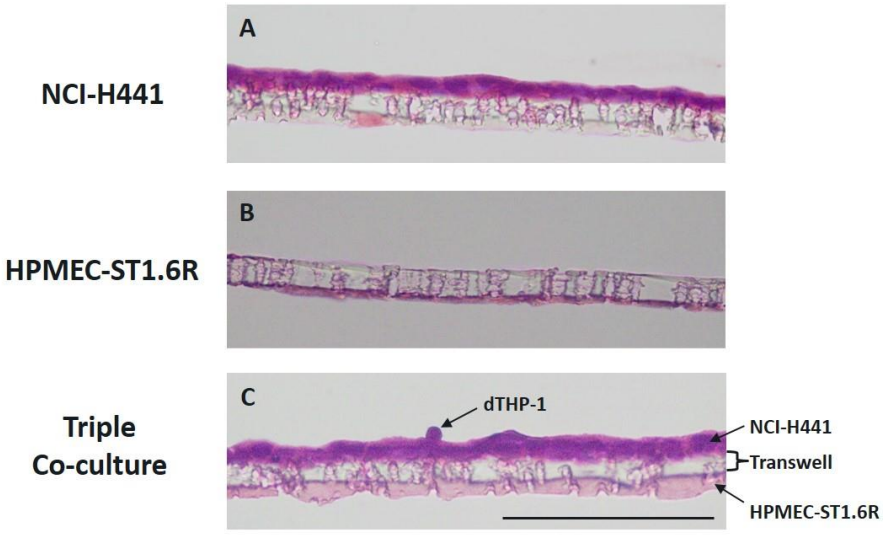

Figure 5.2. Histological section of NCI-H441 monoculture (A), HPMEC-ST1.6R monoculture (B) and triple co-culture model (C) with 5 days of culture on a 12-well Transwell®; Scale bar: 100 µm; Number of cells/Transwell®: 1.0 x 10^5 NCI-H441 cells, 5.0 x 10^4 HPMEC-ST1.6R cells and 1.0 x 10^5 dTHP-1 cells.

3.2. Surface and ultrastructural characterization

The surface of epithelial and endothelial monocultures and triple co-culture was assessed by SEM (see figure A1 from Appendix III). Both monocultures presented a smooth surface. dTHP-1 cells were found on the top of epithelial cells, but the endothelial cells seeded on the basolateral side of triple co-culture were not able to be observed through SEM.

Ultrastructure analyses of NCI-H441 monoculture, HPMEC-ST1.6R monoculture and triple co-culture were performed (figure 5.3). NCI-H441 cells, either as a monoculture or as a triple co-culture presented MV (figure 5.3A and G), expressed TJ/AJ (figure 5.3B and H) and were able to produce SV (figure 5.3C and I), characteristics already described for the NCI-H441 cells co-cultured with endothelial cells (239). All these

features were kept despite the reduction of culture time, from 8 days to 5 days (see section 3.5 from chapter IV).

Acknowleging the difficulty in preparing ultrathin sections, due to the fragility of samples and non-homogeneous distribution of endothelial cells over the Transwell® surface, HPMEC-ST1.6R cells were only found when cultured as a monoculture. TEM micrograph of HPMEC-ST1.6R monoculture showed that cells presented an elongated and flatted morphology (figure 5.3D and E), but a large paracellular space between the adjacent cells were observed, suggesting that contact between cell-to-cell is not strong.

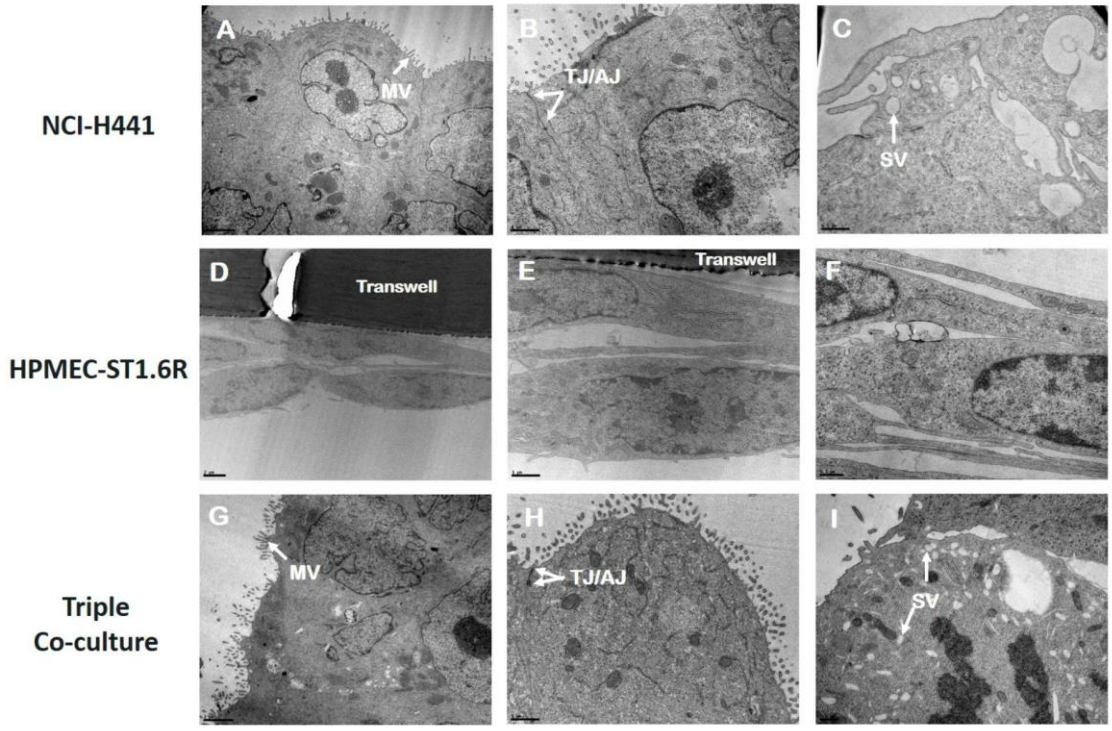

Figure 5.3. TEM images of NCI-H441 monoculture (A-C), HPMEC-ST1.6R monoculture (D-F) and triple co-culture (G-I) with 5 days of culture; Scale bar: A, D and G is 2 µm; B, E and H is 1 µm; C, F and I is 0.5 µm.

3.3. Permanent permeability of sodium fluorescein

The paracellular transport of NaFlu was assessed at day 5 of culture in the presence or absence of EDTA, a chelating agent of calcium ions (343). Extracellular calcium is important for the maintenance of tight junctions' structure (379). When cells are incubated with EDTA, there is a depletion of extracellular calcium ions, and the contact cell-to-cell is disrupted, originating the opening of tight junctions and the increase of NaFlu permeability (343, 380). TEER is another methodology used to assess the tightness of a cellular barrier, being usually measured during the transport studies (342).

Before the incubation of NaFlu on the apical side, TEER was assessed (figure 5.4A), and the P_{app} of NaFlu across each monoculture, bi-cultures (NCI-H441+dTHP-1 and NCI-H441+HPMEC-ST1.6R) and triple co-culture was calculated (figure 5.4B). It is known that pulmonary endothelial cells do not produce tight junctions (344), and therefore, HPMEC-ST1.6R monoculture does not form a strong barrier comparatively to NCI-H441 cells. In this study endothelial cells displayed a TEER of 14.2 ± 7.4 $\Omega.cm^2$, and as expected, TEER and P_{app} of NaFlu was the same regardless the EDTA incubation. The same pattern was observed for dTHP-1 monoculture once these cells do not form a cell layer.

The TEER significantly dropped when NCI-H441 monoculture, bi-cultures and triple co-culture were previously treated with EDTA. Parallelly, a significant increase of P_{app} of NaFlu was observed. This study suggests that NCI-H441 monoculture, bi-cultures and triple co-culture formed a cellular barrier that allowed the mediation of paracellular transport of NaFlu, and the barrier formed can be influenced by the presence of EDTA. However, the P_{app} of NaFlu achieved for the triple co-culture in this work (17.7 ± 4.3 x 10^{-6} cm/s) was still 4- to 10-fold times higher when compared with others *in vitro* studies performed with the same epithelial cell line (see table 5.1). These differences can be caused by several factors that influence the integrity of the cellular barriers, namely the different number of cells seeded/cm^2, the longer period of times in culture, the cell culture medium, the cell passage number or even due to the small pore size of the Transwell® used (namely 0.4 µm).

Primary cultures of hAEpC, either in monoculture or co-cultured with macrophages showed a P_{app} one order of magnitude lower and a higher TEER (more than 400 $\Omega \cdot cm^2$) (241) when compared with triple co-culture. A549 is another cell model widely

used to mimic the alveolar epithelium for cytotoxicity studies (381, 382) and these cells have been used to explore the translocation of macromolecules or microsystems (255, 256, 382). Due to the lack of expression of functional tight junctions, A549 model is not usually selected to study paracellular transport of small substances. Table 5.1 showed the TEER and P_{app} of NaFlu across different *in vitro* alveolar epithelial cell models, in particularly, NCI-H441 and hAEpC (monocultures or co-cultures) as well as across A549 monolayer. It was also observed that the P_{app} of NaFlu across A549 cells was still lower comparatively to the $P_{app.}$´of triple co-culture in this work (356).

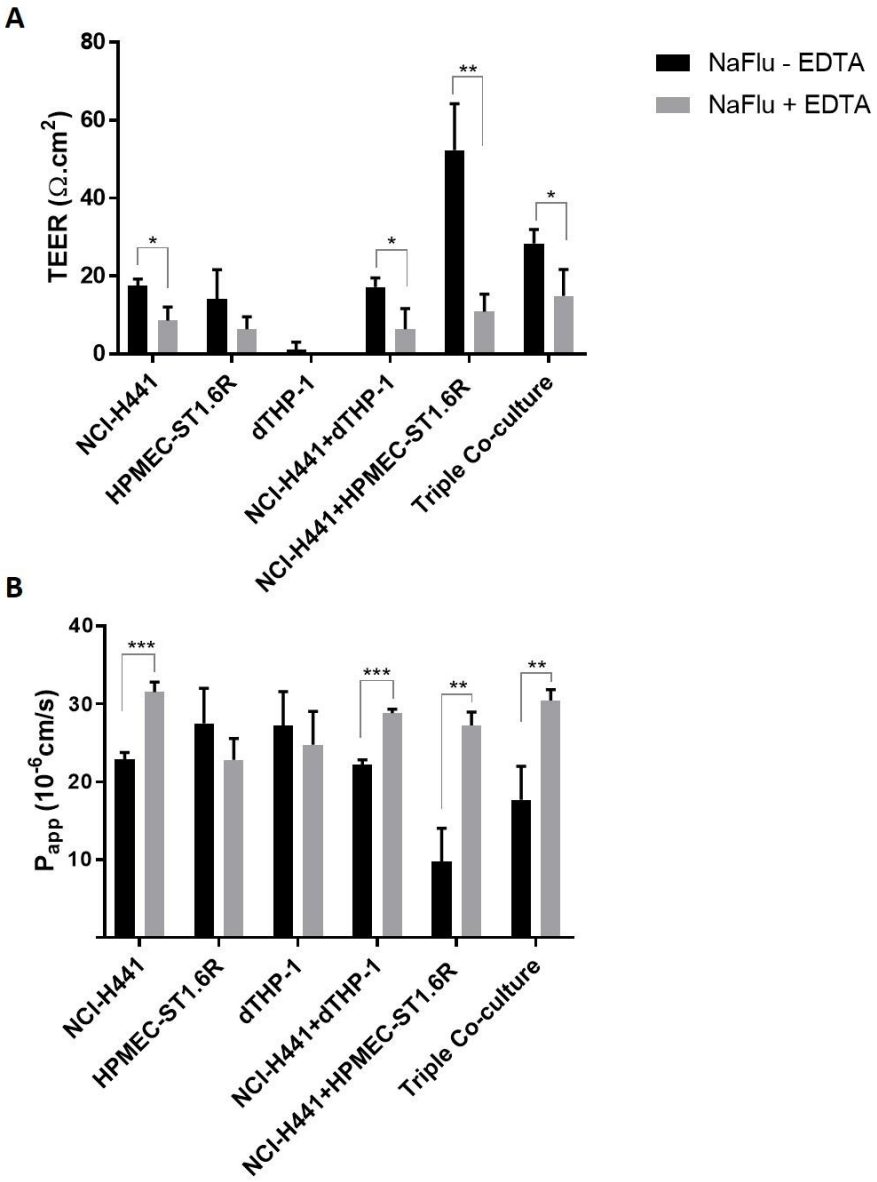

Figure 5.4. Permeability of NaFlu through each monoculture, bi-cultures and triple co-culture, in the presence or absence of EDTA (± EDTA): TEER was measured before the incubation of NaFlu ± EDTA (A) and P_{app} of NaFlu (B) was determined after 3 hours of incubation; Statistical analysis performed through unpaired t-test; Data expressed as mean ± SD from 3 replicates.

Table 5.1. TEER and P_{app} of NaFlu across different *in vitro* alveolar epithelial cells.

	Cell number/cm²	Culture conditions	TEER (Ω/cm²)	P_{app} (10^{-6} cm/s)	Ref.
NCI-H441	8.9 x 10^4	9 days/ALI	529 ± 178	1.76 ± 0.042	(356)
	2.5 x 10^5	12 days/LLI	1010 ± 105	0,48 ± 0.033	(240)
	8.9 x 10^4	7 days/ALI	257.6 ± 27.53	3.71 ± 0.079	(354)
	8.9 x 10^4	7 days/ HBSS-medium culture	182.3 ± 5.63	1.67 ± 0.028	
	2.23 x 10^4	7 days/LLI	1009 ± 14.87	1.57 ± 0.011	
	2.0 x 10^4 *	10-11 days/LLI	218 ± 93	1.11 ± 0.23	(239)
	2.0 x 10^4 (co-cultured with HPMEC-ST1.6R cells) *	11 days/LLI	565 ± 48	0.81 ± 0.05	
hAEpC	6 x 10^5 *	8 days/LLI	2493 ± 876	0,12 ± 0.019	(383)
	3.0 x 10^5*	5 days/ALI	431 ± 30	2.7 ± 0.6	(241)
	3.0 x 10^5 co-cultured with AM*	5 days/ALI	417 ± 22	4.1 ± 1.0	
A549	8.9 x 10^4	9 days/ALI	28 ± 4	7.38 ± 1.90	(356)

Data from this tables is based on studies where cells were seeded on a 12-well Transwell® (12 mm), with a pore size 0.4 µm. Cells culture were performed on 24-well Transwell® (6.5 mm) with a pore size of 0.4 µm are marked with a *.

3.4. Translocation of fluorospheres

The translocation of fluorospheres with different sizes (50 nm and 1.0 µm) was analyzed on different *in vitro* model (monocultures, bi-cultures and triple co-culture).

In order to assess the retention capacity of Transwell® without cells, the translocation of fluorospheres was tested across ET (non-coated and coated with Matrigel™ BM). Around 60% of both fluorospheres were able to pass through the ET (- Matrigel), indicating that the Transwell® retained partially the fluorospheres. By other hand, the ET (+ Matrigel) constituted a hindrance to the translocations of both fluorospheres: only 33.6 ± 6.0% of 50 nm-fluorospheres crossed the coated membrane, significantly lesser than the ET (- Matrigel), while the translocation of 1.0 µm-fluorospheres was approximately 20 times less comparatively to ET (- Matrigel). CLSM images demonstrated that the Transwell® previously coated with Matrigel™ was able to retain the 1.0 µm-fluorospheres (figure A2C and D from Appendix III). Although the Matrigel™ coating can be degraded by the cells (384-386), it can constitute a barrier in some spots of Transwell® without cells, in particularly in the case of HPMEC-ST1.6R and dTHP-1 monocultures which did not form a confluent cell layer. Regarding the 50 nm-fluorospheres, the coating of Transwell® with Matrigel™ also decreased the amount of fluorosphere that translocated, but through CLSM analysis was not possible to conclude that the Matrigel™ coating increased the retention of 50nm-fluorospheres (figure A2 A and B from Appendix III).

Monocultures, bi-cultures and the triple co-culture presented a significantly lower translocation of 50 nm-fluorospheres when compared with ET (+ Matrigel) and ET (- Matrigel), but no differences were observed among the different *in vitro* cell culture models (figure 5.5A).

It is expected that ultrafine particles (less than 100 nm) can cross the air-blood barrier after pulmonary administration and be distributed through several organs (brain, liver, heart and spleen) (76, 387). *In vitro* studies conducted on human pulmonary alveolar epithelium cells showed that the amount of translocated particles with sizes under 100 nm is quite low: around 8% and 3% of 50 nm-carboxy and unmodified polystyrene NPs, respectively, were able to cross human ATI cells (388), while between 0.5 %-5.2% of 15 nm-gold particles translocated over a triple co-culture model of human epithelial airway (389). In this study a higher amount of 50 nm-fluorospheres translocated the different *in vitro* models: around 15 % for each monoculture, between 15-30% for the

bi-cultures and 18% for the triple co-culture. CLSM images of monocultures, bi-cultures and triple co-culture demonstrated that in all cases, 50 nm-fluorospheres were still entrapped on the Transwell® membrane (figure A3 from Appendix III), and partial amount of these systems remained at the apical side (figure A4A from Appendix III). Regarding the 1.0 µm-fluorospheres, the ET (+ Matrigel) formed a barrier that hindered its translocation. With exception of dTHP-1 monoculture, all *in vitro* cell culture models retained the majority of these fluorospheres at apical side (figure A4B from Appendix III), and less than 5% of fluorospheres were found at basolateral side (figure 5.5B). Internalization of 1.0 µm-fluorospheres by dTHP-1 cells, as well retention by the Transwell® in some areas without cells were observed through CLSM (figure A5C from Appendix III), which explain the low amount of 1.0 µm-fluorospheres at apical side (only 62.2 ± 5.8% remained on the apical compartment).

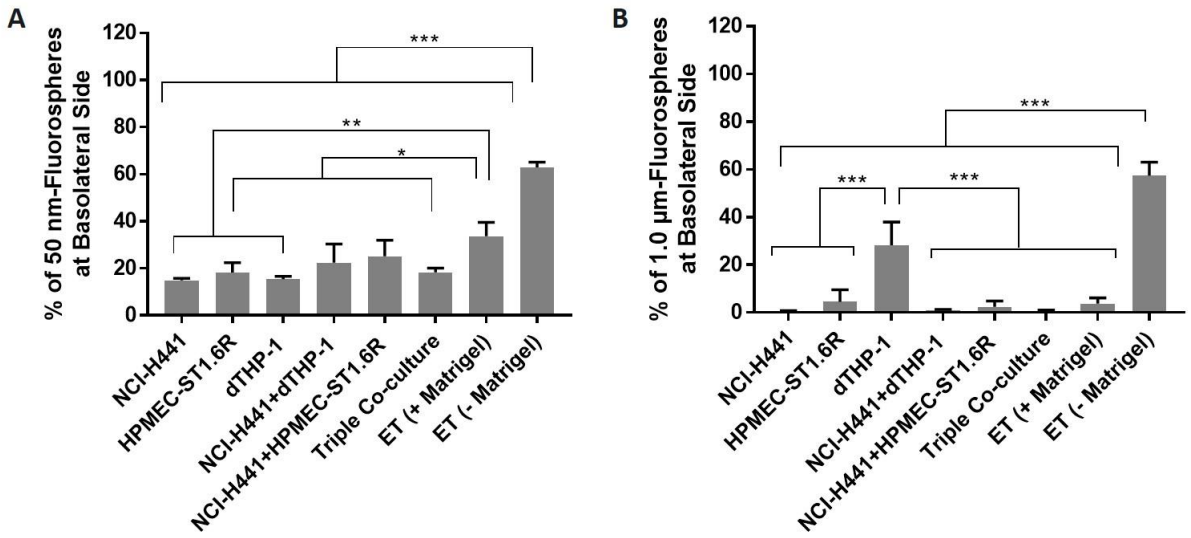

Figure 5.5. Translocation of fluorospheres with a size of 50 nm (A) and 1.0 µm (B) across different *in vitro* models (monocultures, bi-cultures and triple co-culture) and through ET; Statistical analysis performed through One-way ANOVA with Tukey's multiple comparison test; Data expressed as mean ± SD from 3 replicates.

For bi-cultures and triple co-culture, almost 100% of 1.0 µm-fluorospheres remained on the apical side after 3 hours of incubation. Furthermore, internalization of fluorospheres by the dTHP-1 cells were also observed on bi-culture of NCI-H441+dTHP-1 and triple co-culture. CLSM images demonstrated that some

fluorospheres still remained on the top of epithelial cells (figure A5A, D, E and G from Appendix III), but not entrapped on the Transwell® membrane. Overall, 1.0 µm-fluorospheres were not found at endothelial layer of bi-culture NCI-H441+HPMEC-ST1.6R and at triple co-culture (figure A5F and H from Appendix III), but 1.0 µm-fluorospheres were located on the apical side of the Transwell® membrane containing HPMEC-ST1.6R monoculture (figure A5B from Appendix III), another indication for the particle retention by the coated Transwell®, even when it devoid of cells.

The low amount of 1.0 µm-fluorospheres translocated is mainly due to the ability of cells to retain large particle, as observed on CLSM images. The particle deposition on deep lung is dependent of size, density, shape, breathing pattern or even influenced by the presence of pulmonary disease. Large particles (with an aerodynamic diameter higher than 5.0 µm) can be impacted on throat or month, while particles with a size between 0.5-3.0 µm are able to deposited at terminal bronchioles and alveolar space (68, 73). These particles stay confined on the alveolar space due to the presence of surfactant and the tight alveolar epithelium. The low amount (around 5%) of 1.0 µm-fluorospheres translocation can be correlated with the *in vivo* study performed by Sarlo *et al.* (2009). This study demonstrated a recovery of more than 95% of latex fluorospheres with a size of 1.0 µm from the lung tissue, while only 89-95% and 70-80% of the particles with a size of 100 nm and 20 nm, respectively, remained on the lung tissue after 90-120 days post-final repeated and acute lung exposure (390). Other study also showed that microspheres with a size of 2.1 µm were not fond at extrapulmonary organs after tracheal instillation, indicating the absence of translocation (391). The same trend was observed on a *in vivo* study performed by Snipes *et al.* (1984), where only 1.7% of microspheres with a size of 3 µm translocated to the tracheobronchial lymph nodes after lung instillation (392).

There are few *in vitro* data related with the translocation of 1.0 µm-sized particles across *in vitro* models of alveolar epithelium, being usually Calu-3 and 16HBE14o- (both derived from bronchial tissue) the common cell lines used assess the translocation of particles (355, 375, 393) and the permeability of drugs (203, 374, 394). A549 is an adenocarcinomic human alveolar epithelial cell line that has been mainly used to study the uptake of particles rather than to access the drug permeability (395, 396). Despite the inability to form a functional barrier, this cell line was already used to assess the translocation of polystyrene particles with size of 1.0 µm (256, 257).

Given the small amount of 1.0 µm-fluorospheres translocated and the capability to retain microparticles on the apical side, this new *in vitro* model could be a suitable approach to study the deposition and the translocation of particles with a size of 1.0 µm after pulmonary administration.

3.5. Translocation of Isn-SLN and Isn permeability

For the TB treatment through pulmonary route, the pharmaceutical system should be able to deposit at alveolar epithelium and be later phagocyted by AMs, being these cells the main target for anti-TB drug delivery (290). In order to improve the drug accumulation at lung tissue, it is not desirable that the translocation occur through the air-blood barrier and consequently into the blood stream.

In chapter III it was reported the development of a drug delivery system based on SLN for Isn delivery. Isn-SLN presented an average size of 500 nm, a suitable size for deposition at alveolar space and for the internalization by AMs (60). It also showed a low drug release during 48 hours (less than 15%), meaning that once at the alveolar space, this system could slowly release the drug, enabling the reduction in the number of administrations (378).

In this work, translocation of Isn-SLN was assessed across different *in vitro* cell culture model (monocultures, bi-cultures and triple co-cultures) to evaluate the ability of Isn-SLN remain on apical side of the Transwell® and at same time, to validate the capacity of the triple co-culture to retain the nanocarrier. Therefore, a dose of Isn was selected (50 µM) since there was no influence on the metabolic activity of NCI-H441 and dTHP-1 cells (figure A6 from Appendix III).

As mentioned before, ET can have an impact on the translocation, even when the size of Transwell®'s pore is higher than the nanocarrier tested (355, 393). In this study around 42% of Isn-SLN was able to cross the ET (- Matrigel), while only 8.3 ± 5.9% crossed the ET (+ Matrigel) (figure 5.6).

In general, Isn-SLN presented a lower translocation throughout all *in vitro* cell culture model after 3 hours of incubation (less than 15%). The presence of Matrigel™ constituted a hindrance to the translocation of Isn-SLN and although is expected to be degraded by the cells, its presence on areas of Transwell® without cells (in particularly on HPMEC-ST1.6R monoculture and dTHP-1 monoculture), could be a possible

justification for the low amount of Isn-SLN translocated (10 ± 6 and 5 ± 4 %, respectively). Statistical analysis was performed to compare the translocation/permeability of each monoculture and bi-culture with the control group, namely the triple co-culture. Significative amounts of Isn-SLN translocated through ET (- Matrigel) (42 ± 6%), suggesting that triple co-culture formed a barrier that mainly retained the Isn-SLN on the apical side of the Transwell®, nevertheless, no differences were observed when compared to the NCI-H441 monoculture and both bi-cultures.

Regarding the permeability of free Isn, around 85-95% of the drug was able to cross the ET, regardless the presence of Matrigel™, indicating that the coating did not influence the Isn permeability. This data can be correlated with high permeability of free Isn across HPMEC-ST1.6R and dTHP-1 monocultures once they do not form a confluent cell monolayer, and consequently do not retain the drug. Also, no differences on the Isn permeability across NCI-H441 monoculture and bi-cultures were observed when compared with the triple co-culture.

According with Biopharmaceutical Classification System (BCS), Isn belongs to class III, a drug with high aqueous solubility but low permeability (79, 397), but it was already suggested to be on the borderline of BCS Class I (high aqueous solubility and high permeability) and BCS Class III (398), which explains the high drug permeability across NCI-H441 epithelial model, bi-cultures and triple co-culture (between 30-45%). Given the evidence that Isn permeates in higher extension the different *in vitro* models, and due to low *in vitro* release from the formulation, the amount of Isn quantified on the basolateral compartment could be related with the mount of Isn that is associated on the surface of Isn-SLN.

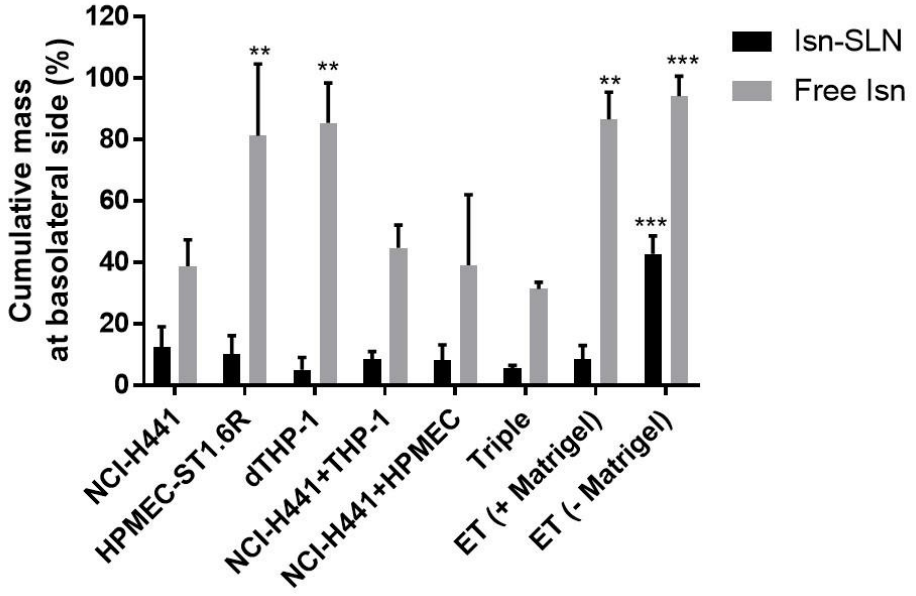

Figure 5.6. Translocation of Isn-SLN and permeability of free Isn across different *in vitro* cell culture models (monocultures, bi-cultures and triple co-cultures) and through ET. Study was performed during 3 hours; The permeability of Isn-SLN and free Isn across the different *in vitro* models was compared with the control group (triple co-culture), and statistical analysis was performed through One-way ANOVA with Dunnett's multiple comparisons;

3.6. Influence of lipopolysaccharide on the release of interleukin-8

The air blood is a physiologic barrier responsible for gas-exchange and for the retention and clearance of inhaled compounds or bacteria. Once at alveolar space, they can initiate an inflammatory response, which is characterized by an increase of vascular permeability and loss of integrity of alveolar–capillary membrane, infiltrations of inflammatory cells, as well the release of several inflammatory mediators (399, 400).
During an inflammatory process, the AMs can phagocyte pathogens and also release proinflammatory cytokines. Epithelial cells produce substances with antimicrobial properties (like lysozyme, lactoferrin), inflammatory cytokines (401) and mediators that allow the recruitment of other immune cells (402). Macrophages and endothelial cells also produce proinflammatory cytokines, namely IL-8 that presents chemoattractant properties and stimulates the recruitment of neutrophils (403-405). During an inflammatory process the endothelium expresses adhesion molecules that allow the adhesion of leukocytes and its migration towards the infection local (399, 406).

The release of IL-8 by each monoculture, bi-cultures and triple co-culture was assessed after LPS-challenge. Figure 5.7 depicts the relative fold increase of IL-8 comparatively with non-LPS-treated *in vitro* model, while the concentration of IL-8 on the supernatant collected from each *in vitro* model is displayed on figure A7 from Appendix III.

Epithelial cells in monocuture were unresponsive to LPS, given the similar release of IL-8 comparatively to untreated control. According with Kasper *et al*. (2017), bi-cultures of epithelial cells (either A549 or NCI-H441) with endothelial cells (ISO-HAS-1) had a different response after apical exposure of LPS: A549/ ISO-HAS-1 presented an overall 3-fold increase of IL-8 release at both sides of the Transwell®, but no differences on IL-8 release was observed after LPS stimulation of NCI-H441/ISO-HAS-1 co-culture (259). The authors suggested that the absence of response by NCI-H441 cells upon LPS stimulus could be explained by the lack of TLR-4 expression, a receptor involved on the LPS recognition (407).

The LPS treatment promoted a 28- and 35-fold increase of IL-8 release on HPMEC-ST1.6R monoculture and dTHP-1 monoculture, respectively. Endothelial cells have an important role on the IL-8 expression upon an inflammatory stimuli (408), and it was already demonstrated that HPMEC-ST1.6R cell line (409) and PMA-dTHP-1 cells (410, 411) are able to produce proinflammatory cytokines.

In this experiment, triple co-culture had a higher fold increase of IL-8 release regarding the NCI-H441 monoculture, but still showed a reduction when compared to individual endothelial and macrophage monocultures. Similar results were achieved for both bi-cultures (NCI-H441+dTHP-1 and NCI-H441+HPMEC-ST1.6R). Studies have already showed that co-cultures of epithelial with endothelial cells can have a higher sensitive release of IL-8 after exposure of silica NPs (242). The same biological effect was also observed on the co-cultures of A549 with macrophages exposed to the ultrafine particles (412). Alfaro-Moreno *et al.* (2008) demonstrated that IL-8 regulation and secretion is dependent of time of exposure, dose and due to interactions between different cell type (258). In this work, the triple co-culture (A549 + THP-1 + HMC-1), combined or not with endothelial cells, presented an increase of IL-8 comparatively to bi-cultures of A549 + HMC-1 and the endothelial monoculture, after exposure to particulate matter in concentrations between 10-30 μg/cm^2. But for higher concentration (100 μg/cm^2), the levels of IL-8 decreased.

Despite the endothelial cells had released considerable amounts of IL-8, statistical analysis demonstrated that the concentration produced by bi-culture of NCI-H441+ HPMEC-ST1.6R was lower than triple co-culture, independently of LPS treatment (figure A7 from Appendix III). Moreover, bi-cultures of NCI-H441+ dTHP-1 and triple co-culture released the same amount of this cytokine, also independently of LPS treatment, so that in this case, the presence of endothelial cells apparently did not affect the IL-8 release.

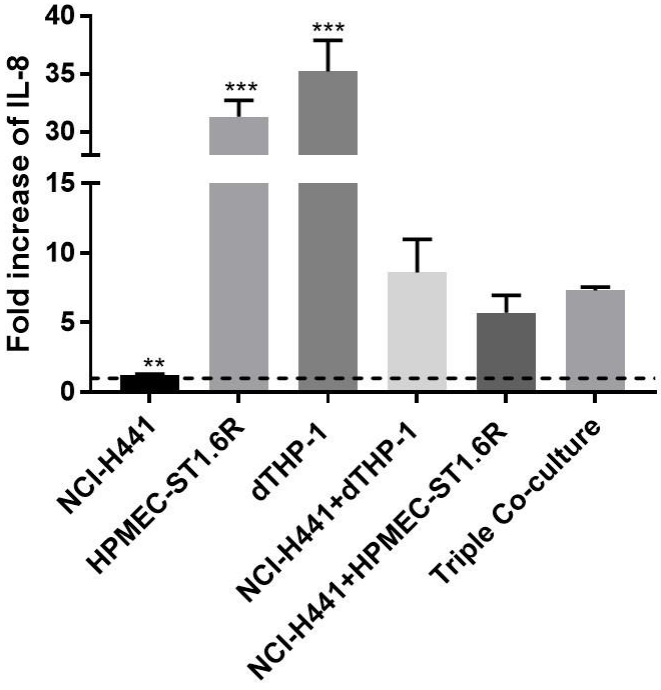

Figure 5.7. Release of IL-8 after 24 hours of LPS incubation (10 µg/mL during 24 hours). Data are expressed as the fold increase after normalization with the amount of IL-8 released by the respective untreated control (cells without LPS incubation); mean ± SD from 3 replicates; Statistical analysis assessed trough One-way ANOVA with Dunnett's multiple comparisons, being the triple co-culture the control group.

3.7. Influence of lipopolysaccharide on Isn permeability

The inflammation is involved on the pathogenesis of acute lung injury. In that situation, microvascular endothelium is injured and the permeability of vascular endothelium increases. Then, the flow of proteins and fluids towards the lung interstitial spaces also

increases, originating the formation of pulmonary edema (400, 413). During the acute lung injury, loss of epithelium integrity occurs mainly due to the recruitment of inflammatory cells, in particular the neutrophils (414, 415). *In vivo* studies also showed that LPS could increase the permeability of alveolar-capillary membrane (416, 417).

In this work, it was evaluated the suitability of the triple co-culture as a tool to assess the permeability of drugs during a proinflammatory state. Therefore, the permeability of free Isn was assessed in different *in vitro* models and compared with the Isn permeability across untreated *in vitro* models after LPS challenge.

For all *in vitro* models tested, the TEER was not influenced by the incubation of LPS (figure 5.8A), showing that the integrity of NCI-H441 monoculture, bi-cultures and triple co-cultures was kept. This outcome was also achieved by Hermanns *et al.* (2010). NCI-H441 cells, either co-cultured with HPMEC or ISO-HAS-1 cells, showed no differences on TEER after apical stimulation with TNF-α (418). This cytokine showed to have implications on the permeability of vascular endothelium (419), and when was incubated on the basolateral compartment, the integrity of co-cultures reduced (418).

Free Isn permeability across the different *in vitro* models is showed on figure 5.8B. Overall, *in vitro* models treated with LPS showed an increase on the Isn permeability comparatively to cells without LPS treatment. But only the bi-culture of NCI-H441+HPMEC-ST1.6R presented a statistically significant difference on the permeability of this drug. *In vivo* experiments indicated that LPS increased the permeability of lung epithelium (420) and endothelium (421, 422). The triple co-culture models used in this work is still a simplistic model regarding the *in vivo* models, so that factors like the presence of neutrophils may contribute for the absence of differences on these studies. The absence of significant differences in this experiment could be also attributed to the short period of incubation (3 hours). Moreover, *in vivo* studies also showed that the permeability of FITC-Dextran increased in a LPS dose-dependent manner, so that the amount of LPS used in this study could not be enough to increase the permeability (417). The higher level of IL-8 released by the triple co-culture is an indicator of proinflammatory state, but some *in vivo* experiments also demonstrated that LPS had no effect on the epithelial permeability (423, 424), despite the increase of IL-8 and the number of neutrophils on the epithelial lining fluid (423).

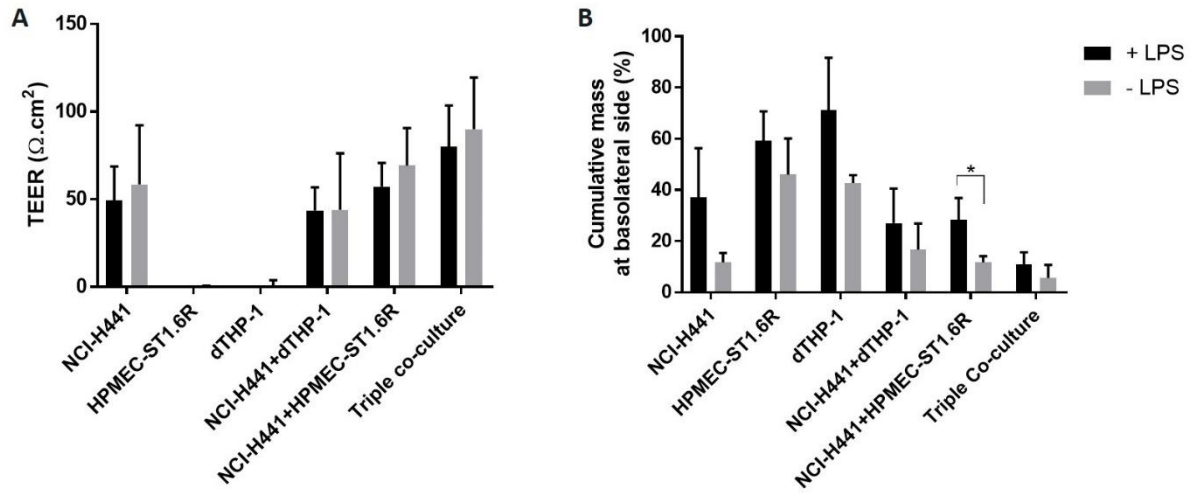

Figure 5.8. Influence of LPS on the TEER (A) and on the permeability of free Isn (B) across the different *in vitro* cell culture models; TEER was evaluated in 6 replicates from 2 independent studies; Permeability of free Isn was assessed in the presence and absence of LPS on 3 replicates; mean ± SD; Statistical analyses assessed through unpaired t-test.

4. Conclusion

In this work, a triple co-culture model of air-blood barrier cultured under ALI conditions was established. Through CLSM, TEM and histology analyses was observed that this *in vitro* model was constituted by epithelial cells, that mainly formed a monolayer at apical side, with macrophage-like cells spread over the epithelial surface. Separated by the Transwell®, endothelial cells were growth on the basolateral side, although they were not homogeneously distributed over its surface.

Different studies were performed to evaluate the functionality of triple co-culture, namely the paracellular transport of small substances as well the translocation of different nanocarriers. The relative low TEER and the high P_{app} of NaFlu suggest that the triple co-culture did not form a selective barrier and may not be suitable to mediate the permeability of small hydrophilic substances.

50 nm-fluorospheres could translocate the triple co-culture, but this *in vitro* model was able to retain large particles, namely 1.0 µm-fluorospheres which were also tested in this work. It was concluded that triple co-culture presented enough integrity to retain 1.0 µm-sized compounds, that may come from inhaled air and deposit at the alveolar

region, where they will remain until being cleared. Triple co-culture was also able to retain Isn-SLN, on the apical compartment, while higher amounts of free drug permeated the same *in vitro* model. The particle size is an important factor for the translocation of nanoparticles, and unlike microparticles that mainly remains on lungs (390, 425), nanoparticles can translocate the alveolar epithelium and be biodistributed by other organs (426-428). Triple co-culture model presented a low TEER and depicted a high permeability of small compounds, but still had enough integrity to mediate differently the translocation of nanosystems and microsystems. Epithelial cells are the main responsible for barrier properties of triple co-culture, and although this model better represents the alveolar airway structure, no differences were observed between NCI-H441 monoculture, and both bi-cultures during these translocation studies.

A proinflammatory cytokine (IL-8) was measured on the supernatant collected from each *in vitro* cell culture model. In these experiments, the triple co-culture could produce IL-8 after LPS stimulation, demonstrating an additional advantage over NCI-H441 monoculture, which showed to be unresponsiveness to the same stimulus. The combination of macrophage-like cells and endothelial cells with epithelial cells also provided a higher sensibility than epithelial monocultures, upon the presence of LPS.

The interaction between epithelium-endothelium-macrophage cells are crucial for the regulation of proinflammatory cytokines release. Based on these results, the presence of endothelium on the IL-8 release is not cleared, and to understand the influence of each cell type on the release of proinflammatory cytokines, it must be considered to analyze the supernatant from the apical and basolateral compartment separately. Other proinflammatory cytokines (namely IL-1β, IL-6 and TNF-α) should be also analyzed to have more information regarding the proinflammatory response provided by this new model.

Regarding the permeability of Isn across LPS-induced *in vitro* models, only the NCI-H441+HPMEC-ST1.6R showed a significative difference regarding the untreated control. More studies would be needed to correlate the inflammatory response of these *in vitro* cell culture models with the increase of permeability. As alternative to LPS, other proinflammatory cytokines could be also used, in particularly TNF-alpha or IFN-γ, alone or in combination (429-432). Moreover, the induction of inflammatory response through the basolateral side could be considered, as the barrier properties, permeability and the release of proinflammatory cytokine showed a different behavior

when the proinflammatory stimulus was incubated on the apical compartment (239, 418).

CHAPTER VI

GENERAL CONCLUSIONS AND FUTURE PERSPECTIVES

GENERAL CONCLUSIONS AND FUTURE PERSPECTIVES

In this innovative work, a new SLN system was developed through a modified solvent emulsification-evaporation method based on a W/O/W double emulsion technique, to encapsulate Isn as a model drug. The nanocarrier was designed to target AMs, where the drug is intended to be delivered. Isn-loaded SLN presented a mean particle size close to 500 nm, a positive zeta potential conferred by the SA, and showed a slow drug release up to 48 hours. The encapsulation of Isn into SLN provided a system with a reduced cytotoxicity when tested against NCI-H441 and dTHP-1 cell lines. FTIR analysis revealed the presence of mannose on the surface of SLN after functionalization, and this outcome was confirmed by biological evidence: M-SLN presented a higher internalization by dTHP-1 over SLN and the internalization was reduced when incubated with mannose, indicating that internalization of M-SLN was based on receptor-mediated endocytosis. Despite the promising results obtained, the *in vitro* effectiveness of Isn-SLN and M-SLN on MTB-infected macrophages should be evaluated. Moreover, *in vivo* studies should be also performed in order to assess the safety/toxicity of these systems.

The SLN were used as a model to evaluate the translocation across a newly developed 3D *in vitro* model of air-blood barrier (a triple co-culture model) cultured at ALI conditions. This model was established by seeding endothelial cells (HPMEC-ST1.6R) on the basolateral side of a Matrigel™-coated Transwell® (that aimed to mimic the BM), followed the seeding of epithelial cells (NCI-H441) on the apical side. Lastly, macrophage-like cells (PMA-dTHP-1) were placed on the surface of epithelium.

The accomplishment of a triple co-culture system with a considerable degree of complexity, such as proposed in this work, relied on an extensive process of optimization of several distinct variables. In this particular case, the time of culture, amount of serum and supplements, like ITS, the number of cells revealed to be crucial for the development of a functional triple-co-culture only constituted by a layer of epithelium and endothelium.

The triple co-culture was established by seeding 1.0×10^5 NCI-H441 cells/Transwell® and 5.0×10^4 HPMEC-ST1.6R cells/Transwell® on the apical and basolateral side of the Transwell, respectively, grown for 5 days: the first 3 days at LLI conditions and at

ALI conditions for the following 2 days; at day 4, 1.0 x 10^5 dTHP-1 cells were added to the apical side of each Transwell® and incubated until day 5, being afterwards used to assess for permeability and translocation studies.

The preparation of the proposed triple co-culture presented some challenges regarding the Matrigel™ coating, that may present different thickness or could not be uniformly distributed over the Transwell® membrane. That fact is probably underlying the non-homogenous distribution of endothelial cells, which is a limitation that can compromise the reproducibility of this model. However, these drawbacks could be overcome through the use of 3D printing technique, an automatized system that allows the formation of thinner and more homogenous cell layers (283).

Despite displaying adequate morphological features, the triple co-culture presented a TEER value much lower than what is found on the primary cultures of hAEpC and showed a high NaFlu permeability. Similar results have been reported for A549 cell models and these outcomes suggest that this model is not the most adequate for evaluating the paracellular transport of small hydrophilic drugs. Further improvements could be done to enhance the barrier properties, namely by using a Transwell® membrane with a smaller pore size (0.4 µm) and by optimizing the culture conditions that favors the expression of tight junction proteins.

Under normal physiological conditions, the alveolar epithelium forms a barrier against inhaled particles, including particles with a size higher than 1.0 µm. Once at the alveoli, these particles do not translocate, being instead entrapped on the surfactant and cleared by the AMs. The translocation of fluorospheres with a size of 50 nm and 1.0 µm was also evaluated, and the absence of translocation related with 1.0 µm-fluorospheres reflects the integrity of this model in retain particles with a size of 1.0 µm, despite the high permeability of NaFlu. The same conclusion was validated after assessing the translocation of Isn-SLN. This nanocarrier with an average size of 500 nm was designed for deposition at the alveolar airways, for a local delivery of anti-TB drugs, thus allowing to increase the drug concentration at the lung tissue and to reduce systemic absorption. Based on the translocation studies performed in this work, it was concluded that the triple co-culture presented the capacity of retaining this nanocarrier, when compared with free drug that permeated in a higher extension. Therefore, this triple co-culture can form an airway model that allows the retention of microparticles, and potentially, other pharmaceutical systems. Further, this model still has the ability to enable the translocation of small nanocarriers, that under an *in vivo* situation can

cross the air-blood barrier and be distributed to other tissues. Nevertheless, no differences on the translocation of different nanocarrier (either fluorospheres and Isn-SLN) were observed between and NCI-H441 monoculture and bi-cultures when compared with triple co-culture.

In order to evaluate the occurrence of size-dependent translocation across the triple co-culture, additional transport studies with differently sized fluorospheres should be performed. It would be also interesting to perform translocation studies with Isn-SLN and M-SLN and to quantify intracellular Isn inside of dTHP-1 from the triple co-culture model, with the aim to achieve differences on the internalization of Isn-SLN and M-SLN. However, to perform this study, the M2-phenotype of dTHP-1 must be first induced to allow the MRs expression; second, a suitable protocol that allows the separation of each cell type that forms the triple co-culture still need to be established. NCI-H441 cells are recognized to express ATI-like receptors, namely p-glycoprotein and OCT, essential for drug absorption at the alveolar space (240). Therefore, experiments to explore the expression and regulation of these receptors on the triple co-culture model, bi-cultures and monocultures could be done. Through the use of transporter inhibitors, the role of transporters on drug absorption could also be explored, in order to achieve a more relevant model that can predict drug bioavailability into bloodstream.

The triple co-culture model also produced high levels of IL-8 upon LPS stimulation, when compared with a single epithelial monoculture, evidencing that this model had a higher sensitivity in promoting a lung inflammatory response upon inflammatory stimuli. The levels of IL-8 release were the same when compared with both bi-cultures. Therefore, assessing the release of other proinflammatory should be done to confirm the responsiveness of the triple co-culture upon an inflammatory inductor. It is known that the interactions between different cell types are important for homeostasis of alveolar airway, either in healthy or proinflammatory conditions, and to understand the cross-talk between these three cell lines, more studies must be done. Independent analysis of supernatant collected from the apical and basolateral content could also help to understand the most relevant cell type responsible for the release of proinflammatory cytokines.

The high release of IL-8 in the triple co-culture after LPS incubation is an indicator of a proinflammatory state, although it does not implicate the presence of a complete inflammatory process. As mentioned before, the inflammatory response provided by

this *in vitro* model still needs to be better studied. The possibility to use the triple co-culture as a tool to evaluate drug permeability under a proinflammatory state was also evaluated. Still, no differences on the Isn permeability were observed when compared with LPS-non-induced triple co-culture. With exception of the bi-culture NCI-H441+HPMEC-ST1.6R, the absence of differences was also observed for the monocultures and bi-culture of NCI-H441+dTHP-1.

Further studies that include the use of another proinflammatory inductors as well as to prolong the time of permeability study, could be done to confirm if the permeability of drugs across triple co-culture culture is changed after induction of a proinflammatory state. Instead of incubating the inflammatory inducer at apical side, the stimulation could be done directly on the basolateral side, also with the aim to evaluate differences on the inflammatory response as well on the permeability.

In conclusion, this 3D *in vitro* model of air blood barrier presents morphological similar features with the alveolar airway tissue, despite not presenting significant differences on the translocation of different nanocarriers when compared to NCI-H441 monoculture and both bi-cultures. Moreover, the triple co-culture showed to be a promising *in vitro* model to assess the release of proinflammatory cytokines. More experiments must be done to confirm the induction of a proinflammatory state, to understand the role of each cell on the release of cytokines and lastly, to assess if the proinflammatory state modifies the permeability/translocation of drug/nanocarriers across this 3D *in vitro* model of air-blood barrier.

CHAPTER VII

REFERENCES

REFERENCES

1. Stocks J, Hislop AA. Structure and function of the respiratory system: Developmental aspects and their relevance to aerosol therapy. In: Bisgaard H, O'Callaghan C, Smaldone GC, editors. Drug delivery to the lung. 162. New York Marcel Dekker, Inc; 2001.47-104.

2. Chang AB. The physiology of cough. Paediatr Respir Rev. 2006;7(1):2-8.

3. Chilvers MA, O'Callaghan C. Local mucociliary defence mechanisms. Paediatr Respir Rev. 2000;1(1):27-34.

4. Sakagami M. *In vivo*, *in vitro* and *ex vivo* models to assess pulmonary absorption and disposition of inhaled therapeutics for systemic delivery. Adv Drug Deliv Rev. 2006;58(9–10):1030-60.

5. Mercer RR, Russell ML, Roggli VL*, et al.* Cell number and distribution in human and rat airways. Am J Respir Cell Mol Biol. 1994;10(6):613-24.

6. White JB, Douville NJ, Moraes C*, et al.* Microfluidic approaches toward pulmonary tissue constructs. In: Bettinger C, Borenstein JT, Tao SL, editors. Microfluidic Cell Culture Systems. Amsterdam: Elsevier Inc; 2013.247–78.

7. Harkema JR, Carey SA, Wagner JG. The nose revisited: a brief review of the comparative structure, function, and toxicologic pathology of the nasal epithelium. Toxicol Pathol. 2006;34(3):252-69.

8. Shaykhiev R, Crystal RG. Innate Immunity and chronic obstructive pulmonary disease: A mini-review. Gerontology. 2013;59(6):481-9.

9. Rock JR, Hogan BL. Epithelial progenitor cells in lung development, maintenance, repair, and disease. Annu Rev Cell Dev Biol. 2011;27:493-512.

10. Gaga M, Vignola AM, Chanez P. Upper and lower airways: Similarities and differences. In: Godard P, Wallert B, Chanez P, editors. The Nose and Lung Diseases (ERS Monograph). 18. Sheffield: European Respiratory Society 2001.1-15.

11. Berkhout MC, van Velzen AJ, Touw DJ*, et al.* Systemic absorption of nasally administered tobramycin and colistin in patients with cystic fibrosis. J Antimicrob Chemother. 2014;69(11):3112-5.

12. Kozlovskaya L, Abou-Kaoud M, Stepensky D. Quantitative analysis of drug delivery to the brain via nasal route. J Control Release. 2014;189c:133-40.

13. Casettari L, Illum L. Chitosan in nasal delivery systems for therapeutic drugs. J Control Release. 2014;190:189-200.

14. Brand-Saberi BEM, Schäfer T. Trachea: anatomy and physiology. Thorac Surg Clin. 2014;24(1):1-5.

15. Roomans GM. Tissue engineering and the use of stem/progenitor cells for airway epithelium repair. Eur Cell Mater. 2010;19:284-99.

16. Crowley C, Birchall M, Seifalian AM. Trachea transplantation: from laboratory to patient. J Tissue Eng Regen Med. 2014;9(4):357-67.

17. Muhlfeld C, Ochs M. Functional aspects of lung structure as related to interaction with particles. In: Gehr P, Mühlfeld C, Rothen-Rutishauser B, Blank F, editors. Particle-lung interactions 2ed. New York: Informa Healthcare; 2009.1-16.

18. Patton JS, Byron PR. Inhaling medicines: delivering drugs to the body through the lungs. Nat Rev Drug Discov. 2007;6(1):67-74.

19. Jackson AD. Airway goblet-cell mucus secretion. Trends Pharmacol Sci. 2001;22(1):39-45.

20. Rogers AV, Dewar A, Corrin B*, et al.* Identification of serous-like cells in the surface epithelium of human bronchioles. Eur Respir J. 1993;6(4):498-504.

21. Boucherat O, Boczkowski J, Jeannotte L*, et al.* Cellular and molecular mechanisms of goblet cell metaplasia in the respiratory airways. Exp Lung Res. 2013;39(4-5):207-16.

22. Evans CM, Koo JS. Airway mucus: The good, the bad, the sticky. Pharmacol Ther. 2009;121(3):332-48.

23. Ballard ST, Spadafora D. Fluid secretion by submucosal glands of the tracheobronchial airways. Respir Physiol Neurobiol. 2007;159(3):271-7.

24. Finkbeiner WE. Physiology and pathology of tracheobronchial glands. Respir Physiol. 1999;118(2–3):77-83.

25. Knight DA, Holgate ST. The airway epithelium: structural and functional properties in health and disease. Respirology. 2003;8(4):432-46.

26. Suarez CJ, Dintzis SM, Frevert CW. Respiratory. In: Dintzis PMTM, editor. Comparative anatomy and histology. San Diego: Academic Press; 2012.121-34.

27. Reynolds SD, Malkinson AM. Clara cell: Progenitor for the bronchiolar epithelium. Int J Biochem Cell Biol. 2010;42(1):1-4.

28. Roth F, Quintar A, Uribe Echevarría E*, et al.* Budesonide effects on Clara cell under normal and allergic inflammatory condition. Histochem Cell Biol. 2007;127(1):55-68.

29. Treacy K, Tunney M, Elborn JS*, et al.* Mucociliary clearance in cystic fibrosis: Physiology and pharmacological treatments. Paediatr Child Health. 2011;21(9):425-30.

30. Shusterman D. Toxicology of nasal irritants. Curr Allergy Asthma Rep. 2003;3(3):258-65.

31. Bennett WD. Effect of β-adrenergic agonists on mucociliary clearance. J Allergy Clin Immunol. 2002;110(6, Supplement):291-7.

32. Tarran R. Regulation of airway surface liquid volume and mucus transport by active Ion transport. Proc Am Thorac Soc. 2004;1(1):42-6.

33. Knowles MR, Boucher RC. Mucus clearance as a primary innate defense mechanism for mammalian airways. J Clin Invest. 2002;109(5):571-7.

34. Roomans GM, Kozlova I, Nilsson H*, et al.* Measurements of airway surface liquid height and mucus transport by fluorescence microscopy, and of ion composition by X-ray microanalysis. J Cyst Fibros. 2004;3, Supplement 2(0):135-9.

35. Hussong J, Lindken R, Faulhammer P*, et al.* Cilia-driven particle and fluid transport over mucus-free mice tracheae. J Biomech. 2013;46(3):593-8.

36. Siebert TA, Rugonyi S. Influence of liquid-layer thickness on pulmonary surfactant spreading and collapse. Biophys J. 2008;95(10):4549-59.

37. Féréol S, Fodil R, Pelle G*, et al.* Cell mechanics of alveolar epithelial cells (AECs) and macrophages (AMs). Respir Physiol Neurobiol. 2008;163(1–3):3-16.

38. Meban C. Thickness of the air-blood barriers in vertebrate lungs. J Anat. 1980;131(Pt 2):299-307.

39. Crowell RE, Heaphy E, Valdez YE*, et al.* Alveolar and interstitial macrophage populations in the murine lung. Exp Lung Res. 1992;18(4):435-46.

40. Archambaud C, Salcedo SP, Lelouard H*, et al.* Contrasting roles of macrophages and dendritic cells in controlling initial pulmonary Brucella infection. Eur J Immunol. 2010;40(12):3458-71.

41. Brain JD, Molina RM, DeCamp MM*, et al.* Pulmonary intravascular macrophages: their contribution to the mononuclear phagocyte system in 13 species. Am J Physiol. 1999;276(1 Pt 1):146-54.

42. Schneberger D, Aharonson-Raz K, Singh B. Pulmonary intravascular macrophages and lung health: What are we missing? Am J Physiol Lung Cell Mol Physiol. 2012;302(6):498-503.

43. Kaczmarek M, Sikora J. Macrophages in malignant pleural effusions – alternatively activated tumor associated macrophages. Contemp Oncol (Pozn). 2012;16(4):279–84.

44. Cailhier JF, Sawatzky DA, Kipari T*, et al.* Resident pleural macrophages are key orchestrators of neutrophil recruitment in pleural inflammation. Am J Respir Crit Care Med. 2006;173(5):540-7.

45. Kaczmarek M, Frydrychowicz M, Nowicka A*, et al.* Influence of pleural macrophages on proliferative activity and apoptosis regulating proteins of malignant cells. J Physiol Pharmacol. 2008;59S:321-30.

46. Gjomarkaj M, Pace E, Melis M*, et al.* Phenotypic and functional characterization of normal rat pleural macrophages in comparison with autologous peritoneal and alveolar macrophages. Am J Respir Cell Mol Biol. 1999;20(1):135-42.

47. Forbes B, O'Lone R, Allen PP*, et al.* Challenges for inhaled drug discovery and development: Induced alveolar macrophage responses. Adv Drug Deliv Rev. 2014;71:15-33.

48. Hashimoto D, Chow A, Noizat C*, et al.* Tissue-resident macrophages self-maintain locally throughout adult life with minimal contribution from circulating monocytes. Immunity. 2013;38(4):792-804.

49. Yona S, Kim K-W, Wolf Y*, et al.* Fate mapping reveals origins and dynamics of monocytes and tissue macrophages under homeostasis. Immunity. 2013;38(1):79-91.

50. Fathi M, Johansson A, Lundborg M*, et al.* Functional and morphological differences between human alveolar and interstitial macrophages. Exp Mol Pathol. 2001;70(2):77-82.

51. Salez L, Singer M, Balloy V*, et al.* Lack of IL-10 synthesis by murine alveolar macrophages upon lipopolysaccharide exposure. Comparison with peritoneal macrophages. J Leukoc Biol. 2000;67(4):545-52.

52. Takabayshi K, Corr M, Hayashi T*, et al.* Induction of a homeostatic circuit in lung tissue by microbial compounds. Immunity. 2008;28(4):475-87.

53. Gordon SB, Read RC. Macrophage defences against respiratory tract infections. Br Med Bull. 2002;61:45-61.

54. van Eeden SF, Tan WC, Suwa T*, et al.* Cytokines involved in the systemic inflammatory response induced by exposure to particulate matter air pollutants (PM10). Am J Respir Crit Care Med. 2001;164(5):826-30.

55. Hiraiwa K, van Eeden SF. Contribution of lung macrophages to the inflammatory responses induced by exposure to air pollutants. Mediators Inflamm. 2013;2013:1-10.

56. Benoit M, Desnues B, Mege J-L. Macrophage polarization in bacterial Infections. J Immunol. 2008;181(6):3733-9.

57. Herold S, Mayer K, Lohmeyer J. Acute lung injury: how macrophages orchestrate resolution of inflammation and tissue repair. Front Immunol. 2011;2(65):1-13.

58. Mosser DM, Edwards JP. Exploring the full spectrum of macrophage activation. Nat Rev Immunol. 2008;8(12):958-69.

59. Palecanda A, Paulauskis J, Al-Mutairi E*, et al.* Role of the scavenger receptor MARCO in alveolar macrophage binding of unopsonized environmental particles. J Exp Med. 1999;189(9):1497-506.

60. Makino K, Yamamoto N, Higuchi K*, et al.* Phagocytic uptake of polystyrene microspheres by alveolar macrophages: Effects of the size and surface properties of the microspheres. Colloids Surf B Biointerfaces. 2003;27(1):33-9.

61. Hasegawa T, Hirota K, Tomoda K*, et al.* Phagocytic activity of alveolar macrophages toward polystyrene latex microspheres and PLGA microspheres loaded with anti-tuberculosis agent. Colloids Surf B Biointerfaces. 2007;60(2):221-8.

62. Champion JA, Walker A, Mitragotri S. Role of particle size in phagocytosis of polymeric microspheres. Pharm Res. 2008;25(8):1815-21.

63. Aderem A, Underhill DM. Mechanisms of phagocytosis in macrophages. Annu Rev Immunol. 1999;17(1):593-623.

64. Hirota K, Terada H. Endocytosis of particle formulations by macrophages and its application to clinical treatment. In: Ceresa B, editor. Molecular Regulation of Endocytosis. London: InTech; 2012.413-28.

65. Lasarte JJ, Sarobe P, Prieto J*, et al. In vivo* cytotoxic T-lymphocyte induction may take place via CD8+ T helper lymphocytes. Res Immunol. 1995;146(1):35-44.

66. Li P, Gregg JL, Wang N*, et al.* Compartmentalization of class II antigen presentation: Contribution of cytoplasmic and endosomal processing. Immunol Rev. 2005;207(1):206-17.

67. Chavez-Santoscoy AV, Roychoudhury R, Pohl NLB*, et al.* Tailoring the immune response by targeting C-type lectin receptors on alveolar macrophages using “pathogen-like” amphiphilic polyanhydride nanoparticles. Biomaterials. 2012;33(18):4762-72.

68. Andrade F, Rafael D, Videira M*, et al.* Nanotechnology and pulmonary delivery to overcome resistance in infectious diseases. Adv Drug Deliv Rev. 2013;65(13-14):1816-27.

69. Thorley AJ, Tetley TD. New perspectives in nanomedicine. Pharmacol Ther. 2013;140(2):176-85.

70. Dhand C, Prabhakaran MP, Beuerman RW*, et al.* Role of size of drug delivery carriers for pulmonary and intravenous administration with emphasis on cancer therapeutics and lung-targeted drug delivery. RSC Adv. 2014;4(62):32673-89.

71. Mehanna MM, Mohyeldin SM, Elgindy NA. Respirable nanocarriers as a promising strategy for antitubercular drug delivery. J Control Release. 2014;187:183-97.

72. Ferron GA. Aerosol properties and lung deposition. Eur Respir J. 1994;7(8):1392-4.

73. Thomas RJ. Particle size and pathogenicity in the respiratory tract. Virulence. 2013;4(8):847-58.

74. Mitchison DA, Fourie PB. The near future: improving the activity of rifamycins and pyrazinamide. Tuberculosis (Edinb). 2010;90(3):177-81.

75. El-Sherbiny IM, El-Baz NM, Yacoub MH. Inhaled nano- and microparticles for drug delivery. Glob Cardiol Sci Pract. 2015;2015(2):1-14.

76. Kreyling WG, Semmler M, Erbe F*, et al.* Translocation of ultrafine insoluble iridium particles from lung epithelium to extrapulmonary organs is size dependent but very low. J Toxicol Environ Health A. 2002;65(20):1513-30.

77. Furuyama A, Kanno S, Kobayashi T*, et al.* Extrapulmonary translocation of intratracheally instilled fine and ultrafine particles via direct and alveolar macrophage-associated routes. Arch Toxicol. 2009;83(5):429-37.

78. Oberdorster G. Safety assessment for nanotechnology and nanomedicine: concepts of nanotoxicology. J Intern Med. 2010;267(1):89-105.

79. Sosnik A, Carcaboso AM, Glisoni RJ*, et al.* New old challenges in tuberculosis: potentially effective nanotechnologies in drug delivery. Adv Drug Deliv Rev. 2010;62(4-5):547-59.

80. World Health Organization. Bending the curve - ending TB: Annual report 2017. India: World Health Organization, Regional Office for South-East Asia. Geneva: World Health Organization; 2017. Available from http://apps.who.int/iris/bitstream/10665/254762/1/978929022584-eng.pdf. Accessed at 8th February of 2018.

81. Keane J, Balcewicz-Sablinska MK, Remold HG, *et al.* Infection by *Mycobacterium tuberculosis* promotes human alveolar macrophage apoptosis. Infect Immun. 1997;65(1):298-304.

82. Sturgill-Koszycki S, Schlesinger PH, Chakraborty P, *et al.* Lack of acidification in Mycobacterium phagosomes produced by exclusion of the vesicular proton-ATPase. Science. 1994;263(5147):678-81.

83. Smith I. *Mycobacterium tuberculosis* pathogenesis and molecular determinants of virulence. Clin Microbiol Rev. 2003;16(3):463-96.

84. Peyron P, Vaubourgeix J, Poquet Y, *et al.* Foamy macrophages from tuberculous patients' granulomas constitute a nutrient-rich reservoir for M. tuberculosis persistence PLoS Pathogens. 2008;4(11):1-14.

85. Ordway D, Henao-Tamayo M, Orme IM, *et al.* Foamy macrophages within lung granulomas of mice infected with *Mycobacterium tuberculosis* express molecules characteristic of dendritic cells and antiapoptotic markers of the TNF receptor-associated factor family. J Immunol. 2005;175(6):3873-81.

86. World Health Organization. Treatment of tuberculosis: guidelines for national programmes – 4th ed. Geneva: World Health Organization; 2010. Available from: http://apps.who.int/iris/bitstream/10665/44165/1/9789241547833_eng.pdf. Accessed at 29th January of 2018.

87. Ahmad S, Mokaddas E. Current status and future trends in the diagnosis and treatment of drug-susceptible and multidrug-resistant tuberculosis. J Infect Public Health. 2014;7(2):75-91.

88. D'Ambrosio L, Centis R, Sotgiu G, *et al.* New anti-tuberculosis drugs and regimens: 2015 update. ERJ Open Research. 2015;1(1):1-15.

89. Gunther G. Multidrug-resistant and extensively drug-resistant tuberculosis: a review of current concepts and future challenges. Clin Med (Lond). 2014;14(3):279-85.

90. European Medicine Agency. Available from: http://www.ema.europa.eu/ema/index.jsp?curl=pages/medicines/human/medicines/0

02552/human_med_001699.jsp&mid=WC0b01ac058001d124. Acessed at 19th January of 2018 [

91. European Medicines Agency. Available from: http://www.ema.europa.eu/ema/index.jsp?curl=pages/medicines/human/medicines/002614/human_med_001730.jsp&mid=WC0b01ac058001d124. Accessed at 19th January of 2018.

92. World Health Organization. The use of delamanid in the treatment of multidrug-resistant tuberculosis in children and adolescents: interim policy guidance. Geneva: World Health Organization; 2016. Available from: https://www.ncbi.nlm.nih.gov/books/NBK396145/. Accessed at 29th January of 2018.

93. Sarkar S, Ganguly A, Sunwoo HH. Current overview of anti-tuberculosis drugs: metabolism and toxicities. Mycobact Dis. 2016;6(2):1-6.

94. Wang P, Pradhan K, Zhong X-b*, et al.* Isoniazid metabolism and hepatotoxicity. Acta Pharm Sin B. 2016;6(5):384-92.

95. Ramachandran G, Swaminathan S. Safety and tolerability profile of second-line anti-tuberculosis medications. Drug Saf. 2015;38(3):253-69.

96. Pham DD, Fattal E, Tsapis N. Pulmonary drug delivery systems for tuberculosis treatment. Int J Pharm. 2015;478(2):517-29.

97. Moghimi SM, Hunter AC, Murray JC. Nanomedicine: Current status and future prospects. FASEB J. 2005;19(3):311-30.

98. Gill S, Löbenberg R, Ku T*, et al.* Nanoparticles: characteristics, mechanisms of action, and toxicity in pulmonary drug delivery—a review. J Biomed Nanotechnol. 2007;3(2):107-19.

99. Gao L, Liu G, Ma J*, et al.* Drug nanocrystals: *In vivo* performances. J Control Release. 2012;160(3):418-30.

100. Ranjita SL, A.S.; Khalil, M. Present status of nanoparticle research for treatment of tuberculosis. J Pharm Pharmaceut Sci. 2011;14(1):100-16.

101. Bangham A. Liposomes: the Babraham connection. Chem Phys Lipids. 1993;64:275–85.

102. Mouritsen OG. Model answers to lipid membrane questions. Cold Spring Harb Perspect Biol. 2011;3(9):1-15.

103. Chimote G, Banerjee R. Effect of antitubercular drugs on dipalmitoylphosphatidylcholine monolayers: Implications for drug loaded surfactants. Respir Physiol Neurobiol. 2005;145(1):65-77.

104. Pinheiro M, Lúcio M, Lima J*, et al.* Liposomes as drug delivery systems for the treatment of TB. Nanomedicine. 2011;6(8):1413–28.

105. Chono S, Kaneko K, Yamamoto E*, et al.* Effect of surface-mannose modification on aerosolized liposomal delivery to alveolar macrophages. Drug Dev Ind Pharm. 2010;36(1):102-7.

106. Chono S, Tanino T, Seki T*, et al.* Uptake characteristics of liposomes by rat alveolar macrophages: Influence of particle size and surface mannose modification. J Pharm Pharmacol. 2007;59(1):75-80.

107. Kong F, Zhou F, Ge L*, et al.* Mannosylated liposomes for targeted gene delivery. Int J Nanomedicine. 2012;7:1079-89.

108. Wijagkanalan W, Kawakami S, Takenaga M*, et al.* Efficient targeting to alveolar macrophages by intratracheal administration of mannosylated liposomes in rats. J Control Release. 2008;125(2):121-30.

109. Justo OR, Moraes AM. Incorporation of antibiotics in liposomes designed for tuberculosis therapy by inhalation. Drug Deliv. 2003;10(3):201-7.

110. Anabousi S, Kleemann E, Bakowsky U*, et al.* Effect of pegylation on the stability of liposomes during nebulisation and in lung surfactant. J Nanosc Nanotechnol. 2006;6(9):3010-6.

111. Chattopadhyay S, Ehrman SH, Bellare J*, et al.* Morphology and bilayer integrity of small liposomes during aerosol generation by air-jet nebulisation. J Nanopart Res. 2012;14(4):1-15.

112. Gaur PK, Mishra S, Gupta VB*, et al.* Targeted drug delivery of rifampicin to the lungs: formulation, characterization, and stability studies of preformed aerosolized liposome and *in situ* formed aerosolized liposome. Drug Dev Ind Pharm. 2010;36(6):638-46.

113. Chimote G, Banerjee R. Evaluation of antitubercular drug-loaded surfactants as inhalable drug-delivery systems for pulmonary tuberculosis. J Biomed Mater Res A. 2009;89(2):281-92.

114. Patil JS, Devi VK, Devi K*, et al.* A novel approach for lung delivery of rifampicin-loaded liposomes in dry powder form for the treatment of tuberculosis. Lung India. 2015;32(4):331-8.

115. Patil-Gadhe A, Pokharkar V. Single step spray drying method to develop proliposomes for inhalation: a systematic study based on quality by design approach. Pulm Pharmacol Ther. 2014;27(2):197-207.

116. Videira MA, Botelho MF, Santos AC*, et al.* Lymphatic uptake of pulmonary delivered radiolabelled solid lipid nanoparticles. J Drug Target. 2002;10(8):607-13.

117. Pandey R, Khuller GK. Solid lipid particle-based inhalable sustained drug delivery system against experimental tuberculosis. Tuberculosis (Edinb). 2005;85(4):227-34.

118. Jain D, Banerjee R. Comparison of ciprofloxacin hydrochloride-loaded protein, lipid, and chitosan nanoparticles for drug delivery. J Biomed Mater Res B Appl Biomater. 2008;86(1):105-12.

119. Chuan J, Li Y, Yang L*, et al.* Enhanced rifampicin delivery to alveolar macrophages by solid lipid nanoparticles. J Nanopart Res. 2013;15(5):1-9.

120. Naseri N, Valizadeh H, Zakeri-Milani P. Solid lipid Nanoparticles and nanostructured lipid carriers: structure, preparation and application. Adv Pharm Bull. 2015;5(3):305-13.

121. Song X, Lin Q, Guo L*, et al.* Rifampicin loaded mannosylated cationic nanostructured lipid carriers for alveolar macrophage-specific delivery. Pharm Res. 2015;32(5):1741-51.

122. Pinheiro M, Ribeiro R, Vieira A*, et al.* Design of a nanostructured lipid carrier intended to improve the treatment of tuberculosis. Drug Des Devel Ther. 2016;10:2467-75.

123. Pandey R, Ahmad Z. Nanomedicine and experimental tuberculosis: facts, flaws, and future. Nanomedicine. 2011;7(3):259-72.

124. Beck-Broichsitter M, Merkel OM, Kissel T. Controlled pulmonary drug and gene delivery using polymeric nano-carriers. J Control Release. 2012;161(2):214-24.

125. Ahmad Z, Sharma S, Khuller GK. Inhalable alginate nanoparticles as antitubercular drug carriers against experimental tuberculosis. Int J Antimicrob Agents. 2005;26(4):298-303.

126. Abdulla JM, Tan YT, Darwis Y. Rehydrated lyophilized rifampicin-loaded mPEG-DSPE formulations for nebulization. AAPS PharmSciTech. 2010;11(2):663-71.

127. Grenha A, Seijo B, Remunan-Lopez C. Microencapsulated chitosan nanoparticles for lung protein delivery. Eur J Pharm Sci. 2005;25(4-5):427-37.

128. Sharma K, Somavarapu S, Colombani A*, et al.* Crosslinked chitosan nanoparticle formulations for delivery from pressurized metered dose inhalers. Eur J Pharm Biopharm. 2012;81(1):74-81.

129. Pourshahab PS, Gilani K, Moazeni E*, et al.* Preparation and characterization of spray dried inhalable powders containing chitosan nanoparticles for pulmonary delivery of isoniazid. J Microencapsul. 2011;28(7):605-13.

130. Garg T, Rath G, Goyal AK. Inhalable chitosan nanoparticles as antitubercular drug carriers for an effective treatment of tuberculosis. Artif Cells Nanomed Biotechnol. 2015;44(3):997-1001.

131. Sung JC, Padilla DJ, Garcia-Contreras L*, et al.* Formulation and pharmacokinetics of self-assembled rifampicin nanoparticle systems for pulmonary delivery. Pharm Res. 2009;26(8):1847-55.

132. Jain SKG, Y.; Ramalingam, L.; Jain, A.; Jain, A.; Khare, P.; Bansal, D. Lactose-conjugated PLGA nanoparticles for enhanced delivery of rifampicin to the lung for effective treatment of pulmonary tuberculosis. J Pharm Sci Technol. 2010;64:278-87.

133. Cheow WS, Hadinoto K. Enhancing encapsulation efficiency of highly water-soluble antibiotic in poly(lactic-co-glycolic acid) nanoparticles: Modifications of standard nanoparticle preparation methods. Colloids Surf A Physicochem Eng Asp. 2010;370(1-3):79-86.

134. Cheow WS, Hadinoto K. Factors affecting drug encapsulation and stability of lipid-polymer hybrid nanoparticles. Colloids Surf B Biointerfaces. 2011;85(2):214-20.

135. Taylor PR, Gordon S, Martinez-Pomares L. The mannose receptor: Linking homeostasis and immunity through sugar recognition. Trends Immunol. 2005;26(2):104-10.

136. Singodia D, Verma A, Verma RK*, et al.* Investigations into an alternate approach to target mannose receptors on macrophages using 4-sulfated N-acetyl galactosamine more efficiently in comparison with mannose-decorated liposomes: an application in drug delivery. Nanomedicine. 2012;8(4):468-77.

137. East L, Isacke CM. The mannose receptor family. Biochim Biophys Acta. 2002;1572(2–3):364-86.

138. Christine Leteux, Wengang Chai, R. Wendy Loveless*, et al.* The cysteine-rich domain of the macrophage mannose receptor is a multispecific lectin that recognizes chondroitin sulfates A and B and sulfated oligosaccharides of blood group lewisa and lewisx types in addition to the sulfated N-glycans of lutropin. J Exp Med. 2000;191(7):1117-26

139. Nimje N, Agarwal A, Saraogi GK*, et al.* Mannosylated nanoparticulate carriers of rifabutin for alveolar targeting. J Drug Target. 2009;17(10):777-87.

140. Ajit V, Takashi A. Siglecs - the major subfamily of I-type lectins. Glycobiology. 2006;16(1):1-27.

141. Crocker PR. Siglecs in innate immunity. Curr Opin Pharmacol. 2005;5(4):431-7.

142. Delputte PL, Nauwynck HJ. Porcine arterivirus infection of alveolar macrophages is mediated by sialic acid on the virus. J Virol. 2004;78(15):8094-101.

143. Vanderheijden N, Delputte PL, Favoreel HW*, et al.* Involvement of sialoadhesin in entry of porcine reproductive and respiratory syndrome virus into porcine alveolar macrophages. J Virol. 2003;77(15):8207-15.

144. Crocker PR, Gordon S. Mouse macrophage hemagglutinin (sheep erythrocyte receptor) with specificity for sialylated glycoconjugates characterized by a monoclonal antibody. J Exp Med. 1989;169(4):1333–46.

145. Hartnell A, Steel J, Turley H*, et al.* Characterization of human sialoadhesin, a sialic acid binding receptor expressed by resident and inflammatory macrophage populations. Blood. 2001;97(1):288-96.

146. Takeda K, Akira S. Toll-like receptors in innate immunity. Int Immunol. 2005;17(1):1-14.

147. Cario E, Podolsky D. Differential alteration in intestinal epithelial cell expression of toll-like receptor 3 (TLR3) and TLR4 in inflammatory bowel disease. Infect Immun. 2000;68:7010-7.

148. Zarember K, Godowski P. Tissue expression of human toll-like receptors and differential regulation of toll-like receptor mRNAs in leukocytes in response to microbes, their products, and cytokines. J Immunol. 2002;168:554-61.

149. Yu L, Wang L, Chen S. Endogenous toll-like receptor ligands and their biological significance. J Cell Mol Med. 2010;14(11):2592-603.

150. Juarez E, Nunez C, Sada E*, et al.* Differential expression of Toll-like receptors on human alveolar macrophages and autologous peripheral monocytes. Respir Res. 2010;11(1):1-13.

151. Blander JM. Coupling toll-like receptor signaling with phagocytosis: potentiation of antigen presentation. Trends Immunol. 2007;28(1):19-25.

152. Takeda K, Kaisho T, Akira S. Toll-like receptors. Annu Rev Immunol. 2003;21:335-76.

153. Xu S, Olenyuk BZ, Okamoto CT*, et al.* Targeting receptor-mediated endocytotic pathways with nanoparticles: Rationale and advances. Adv Drug Deliv Rev. 2013;65(1):121-38.

154. Tarone G, Hirsch E, Brancaccio M*, et al.* Integrin function and regulation in development. Int J Dev Biol. 2000;44(6):725-31.

155. Peiser L, Gordon S. The function of scavenger receptorsexpressed by macrophages and their rolein the regulation of inflammation. Microbes Infect. 2001;3(2):149-59.

156. Postlethwait EM. Scavenger receptors clear the air. J Clin Invest. 2007;117(3):601-4.

157. Zhang Y, Zhou Y, Yang Q*, et al.* Ligation of Fc gamma receptor IIB enhances levels of antiviral cytokine in response to PRRSV infection *in vitro*. Vet Microbiol. 2012;160(3–4):473-80.

158. García-García E, Rosales C. Signal transduction during Fc receptor-mediated phagocytosis. J Leukoc Biol. 2002;72(6):1092-108.

159. Oh N, Park JH. Endocytosis and exocytosis of nanoparticles in mammalian cells. Int J Nanomedicine. 2014;9 51-63.

160. Kumar PV, Asthana A, Dutta T*, et al.* Intracellular macrophage uptake of rifampicin loaded mannosylated dendrimers. J Drug Target. 2006;14(8):546-56.

161. Jain A, Agarwal A, Majumder S*, et al.* Mannosylated solid lipid nanoparticles as vectors for site-specific delivery of an anti-cancer drug. J Control Release. 2010;148(3):359-67.

162. Jain K, Kesharwani P, Gupta U*, et al.* A review of glycosylated carriers for drug delivery. Biomaterials. 2012;33(16):4166-86.

163. Yeeprae W, Kawakami S, Yamashita F*, et al.* Effect of mannose density on mannose receptor-mediated cellular uptake of mannosylated O/W emulsions by macrophages. J Control Release. 2006;114(2):193-201.

164. Cui Z, Hsu CH, Mumper RJ. Physical characterization and macrophage cell uptake of mannan-coated nanoparticles. Drug Dev Ind Pharm. 2003;29(6):689-700.

165. Smola M, Vandamme T, Sokolowski A. Nanocarriers as pulmonary drug delivery systems to treat and to diagnose respiratory and non respiratory diseases. Int J Nanomedicine. 2008;3(1):1-19.

166. Drulis-Kawa Z, Dorotkiewicz-Jach A. Liposomes as delivery systems for antibiotics. Int J Pharm. 2010;387(1–2):187-98.

167. Vyas SP, Katare YK, Mishra V*, et al.* Ligand directed macrophage targeting of amphotericin B loaded liposomes. Int J Pharm. 2000;210(1–2):1-14.

168. Vyas SP, Quraishi S, Gupta S*, et al.* Aerosolized liposome-based delivery of amphotericin B to alveolar macrophages. Int J Pharm. 2005;296(1–2):12-25.

169. Vyas SP, Kannan ME, Jain S*, et al.* Design of liposomal aerosols for improved delivery of rifampicin to alveolar macrophages. Int J Pharm. 2004;269(1):37-49.

170. Mukhopadhyay A, Chaudhuri G, Arora S*, et al.* Receptor-mediated drug delivery to macrophages in chemotherapy of leishmaniasis. Science. 1989;244(4905):705-7.

171. Pardeike J, Hommoss A, Müller RH. Lipid nanoparticles (SLN, NLC) in cosmetic and pharmaceutical dermal products. Int J Pharm. 2009;366(1–2):170-84.

172. Sarmento B, Martins S, Ferreira D*, et al.* Oral insulin delivery by means of solid lipid nanoparticles. Int J Nanomedicine. 2007;2(4):743-9.

173. Sahu PK, Mishra DK, Jain N*, et al.* Mannosylated solid lipid nanoparticles for lung-targeted delivery of Paclitaxel. Drug Dev Ind Pharm. 2015;41(4):1-10.

174. Yu W, Liu C, Liu Y*, et al.* Mannan-modified solid lipid nanoparticles for targeted gene delivery to alveolar macrophages. Pharm Res. 2010;27(8):1584-96.

175. Hoppe CA, Lee YC. Stimulation of mannose-binding activity in the rabbit alveolar macrophage by simple sugars. J Biol Chem. 1982;257(21):12831-4.

176. Song E-H, Manganiello MJ, Chow Y-H*, et al. In vivo* targeting of alveolar macrophages via RAFT-based glycopolymers. Biomaterials. 2012;33(28):6889-97.

177. Baldrick P. The safety of chitosan as a pharmaceutical excipient. Regul Toxicol Pharmacol. 2010;56(3):290-9.

178. Park J-H, Jin H-E, Kim D-D*, et al.* Chitosan microspheres as an alveolar macrophage delivery system of ofloxacin via pulmonary inhalation. Int J Pharm. 2013;441(1–2):562-9.

179. Sarmento B, Mazzaglia D, Bonferoni MC*, et al.* Effect of chitosan coating in overcoming the phagocytosis of insulin loaded solid lipid nanoparticles by mononuclear phagocyte system. Carbohydr Polym. 2011;84(3):919-25.

180. Kim TH, Jin H, Kim HW*, et al.* Mannosylated chitosan nanoparticle–based cytokine gene therapy suppressed cancer growth in BALB/c mice bearing CT-26 carcinoma cells. Mol Cancer Ther. 2006;5(7):1723-32.

181. Jiang H-L, Kim Y-K, Arote R*, et al.* Mannosylated chitosan-graft-polyethylenimine as a gene carrier for Raw 264.7 cell targeting. Int J Pharm. 2009;375(1–2):133-9.

182. Jiang H-L, Kang ML, Quan J-S*, et al.* The potential of mannosylated chitosan microspheres to target macrophage mannose receptors in an adjuvant-delivery system for intranasal immunization. Biomaterials. 2008;29(12):1931-9.

183. Chaubey P, Mishra B. Mannose-conjugated chitosan nanoparticles loaded with rifampicin for the treatment of visceral leishmaniasis. Carbohydr Polym. 2014;101(0):1101-8.

184. Moretton MA, Chiappetta DA, Andrade F*, et al.* Hydrolyzed galactomannan-modified nanoparticles and flower-like polymeric micelles for the active targeting of rifampicin to macrophages. J Biomed Nanotechnol. 2013;9(6):1076-87.

185. Bot A, Smith D, Bot S*, et al.* Receptor-mediated targeting of spray-dried lipid particles coformulated with immunoglobulin and loaded with a prototype vaccine. Pharm Res. 2001;18(7):971-9.

186. Pritchard K, Lansley AB, Martin GP*, et al.* Evaluation of the bioadhesive properties of hyaluronan derivatives: detachment weight and mucociliary transport rate studies. Int J Pharm. 1996;129(1–2):137-45.

187. Hwang SM, Kim DD, Chung SJ*, et al.* Delivery of ofloxacin to the lung and alveolar macrophages via hyaluronan microspheres for the treatment of tuberculosis. J Control Release. 2008;129(2):100-6.

188. Zhou A, Guo L, Tang L. Effect of an intrathoracic injection of sodium hyaluronic acid on the prevention of pleural thickening in excess fluid of tuberculous thoracic cavity. Clin Exp Pharmacol Physiol. 2003;30(3):203-5.

189. Makino K, Nakajima T, Shikamura M*, et al.* Efficient intracellular delivery of rifampicin to alveolar macrophages using rifampicin-loaded PLGA microspheres: Effects of molecular weight and composition of PLGA on release of rifampicin. Colloids Surf B Biointerfaces. 2004;36(1):35-42.

190. Hirota K, Hasegawa T, Hinata H*, et al.* Optimum conditions for efficient phagocytosis of rifampicin-loaded PLGA microspheres by alveolar macrophages. J Control Release. 2007;119(1):69-76.

191. Ohashi K, Kabasawa T, Ozeki T*, et al.* One-step preparation of rifampicin/poly(lactic-co-glycolic acid) nanoparticle-containing mannitol microspheres using a four-fluid nozzle spray drier for inhalation therapy of tuberculosis. J Control Release. 2009;135(1):19-24.

192. Mohamed F, van der Walle CF. Engineering biodegradable polyester particles with specific drug targeting and drug release properties. J Pharm Sci. 2008;97(1):71-87.

193. Gajbhiye V, Ganesh N, Barve J*, et al.* Synthesis, characterization and targeting potential of zidovudine loaded sialic acid conjugated-mannosylated poly(propyleneimine) dendrimers. Eur J Pharm Sci. 2013;48(4–5):668-79.

194. Chono S, Tanino T, Seki T*, et al.* Efficient drug targeting to rat alveolar macrophages by pulmonary administration of ciprofloxacin incorporated into mannosylated liposomes for treatment of respiratory intracellular parasitic infections. J Control Release. 2008;127(1):50-8.

195. Jain SK, Gupta Y, Jain A*, et al.* Mannosylated gelatin nanoparticles bearing an anti-HIV drug didanosine for site-specific delivery. Nanomedicine. 2008;4(1):41-8.

196. Saraogi GK, Sharma B, Joshi B*, et al.* Mannosylated gelatin nanoparticles bearing isoniazid for effective management of tuberculosis. J Drug Target. 2011;19(3):219-27.

197. Harsha S, R C, Rani S. Ofloxacin targeting to lungs by way of microspheres. Int J Pharm. 2009;380(1–2):127-32.

198. Ruge CA, Hillaireau H, Grabowski N*, et al.* Pulmonary surfactant protein A-mediated enrichment of surface-decorated polymeric nanoparticles in alveolar macrophages. Mol Pharm. 2016;13(12):4168-78.

199. Wu M, Zhao H, Li M*, et al.* Intranasal vaccination with mannosylated chitosan formulated DNA vaccine enables robust IgA and cellular response Induction in the lungs of mice and improves protection against pulmonary mycobacterial challenge. Front Cell Infect Microbiol. 2017;7:1-12.

200. Roberts SA. High-throughput screening approaches for investigating drug metabolism and pharmacokinetics. Xenobiotica. 2001;31(8-9):557-89.

201. Araujo F, Sarmento B. Towards the characterization of an *in vitro* triple co-culture intestine cell model for permeability studies. Int J Pharm. 2013;458(1):128-34.

202. Franke H, Galla H-J, Beuckmann CT. An improved low-permeability *in vitro*-model of the blood–brain barrier: Transport studies on retinoids, sucrose, haloperidol, caffeine and mannitol. Brain Res. 1999;818(1):65-71.

203. Mathia NR, Timoszyk J, Stetsko PI*, et al.* Permeability characteristics of Calu-3 human bronchial epithelial cells: *in vitro-in vivo* correlation to predict lung absorption in rats. J Drug Target. 2002;10(1):31-40.

204. Costa A, Sarmento B, Seabra V. An evaluation of the latest *in vitro* tools for drug metabolism studies. Expert Opin Drug Metab Toxicol. 2014;10(1):103-19.

205. Buckley ST, Kim K-J, Ehrhardt C. *In vitro* cell culture models for evaluating controlled release pulmonary drug delivery. In: Smyth HDC, Hickey AJ, editors. Controlled Pulmonary Drug Delivery. New York: Springer New York; 2011.417-42.

206. Kaur G, Dufour JM. Cell lines: valuable tools or useless artifacts. Spermatogenesis. 2012;2(1):1-5.

207. Maqsood MI, Matin MM, Bahrami AR*, et al.* Immortality of cell lines: Challenges and advantages of establishment. Cell Biol Int. 2013;37(10):1038-45.

208. Denayer T, Stöhr T, Van Roy M. Animal models in translational medicine: Validation and prediction. New Horiz Transl Med. 2014;2(1):5-11.

209. Martić-Kehl MI, Schibli R, Schubiger PA. Can animal data predict human outcome? Problems and pitfalls of translational animal research. Eur J Nucl Med Mol Imaging. 2012;39(9):1492-6.

210. Cabrera-Pérez MÁ, Sanz MB, Sanjuan VM*, et al.* Importance and applications of cell- and tissue-based *in vitro* models for drug permeability screening in early stages of drug development. In: Sarmento B, editor. Concepts and Models for Drug Permeability Studies. Cambridge: Woodhead Publishing; 2016.3-29.

211. Labiris NR, Dolovich MB. Pulmonary drug delivery. Part I: Physiological factors affecting therapeutic effectiveness of aerosolized medications. Br J Clin Pharmacol. 2003;56(6):588-99.

212. Ehrhardt C, Forbes B, Kim K-J. *In vitro* models of the tracheo-bronchial epithelium. In: Ehrhardt C, Kim K-J, editors. Drug absorption studies: *In situ, in vitro* and *in silico* models. Boston: Springer US; 2008.235-57.

213. Tscheik C, Blasig IE, Winkler L. Trends in drug delivery through tissue barriers containing tight junctions. Tissue Barriers. 2013;1(2):1-8.

214. Pezron I, Mitra R, Pal D*, et al.* Insulin aggregation and asymmetric transport across human bronchial epithelial cell monolayers (Calu-3). J Pharm Sci.91(4):1135-46.

215. Andrade F, Albuquerque J, Nascimento A. Cell-based *in vitro* models for pulmonary permeability studies. In: Sarmento B, editor. Concepts and Models for Drug Permeability Studies. Cambridge: Woodhead Publishing; 2016.101-13.

216. Olsson B, Bondesson E, Borgström L*, et al.* Pulmonary drug metabolism, clearance, and absorption. In: Smyth HDC, Hickey AJ, editors. Controlled Pulmonary Drug Delivery. New York: Springer New York; 2011.21-50.

217. Wittekindt OH. Tight junctions in pulmonary epithelia during lung inflammation. Pflugers Archiv. 2017;469(1):135-47.

218. Patton JS, Fishburn CS, Weers JG. The lungs as a portal of entry for systemic drug delivery. Proc Am Thorac Soc. 2004;1(4):338-44.

219. Kim KJ, Malik AB. Protein transport across the lung epithelial barrier. Am J Physiol Lung Cell Mol Physiol. 2003;284(2):247-59.

220. Tuma P, Hubbard AL. Transcytosis: crossing cellular barriers. Physiol Rev. 2003;83(3):871-932.

221. Bur M, Huwer H, Lehr C-M*, et al.* Assessment of transport rates of proteins and peptides across primary human alveolar epithelial cell monolayers. Eur J Pharm Sci. 2006;28(3):196-203.

222. Roth M, Obaidat A, Hagenbuch B. OATPs, OATs and OCTs: the organic anion and cation transporters of the SLCO and SLC22A gene superfamilies. Br J Pharmacol. 2012;165(5):1260-87.

223. Nakanishi T, Tamai I. Solute carrier transporters as targets for drug delivery and pharmacological intervention for chemotherapy. J Pharm Sci. 2011;100(9):3731-50.

224. van der Deen M, de Vries EGE, Timens W*, et al.* ATP-binding cassette (ABC) transporters in normal and pathological lung. Respir Res. 2005;6(1):1-16.

225. Arvelo F, Poupon MF, Bichat F*, et al.* Adding a reverser (verapamil) to combined chemotherapy overrides resistance in small cell lung cancer xenografts. Eur J Cancer. 1995;31a(11):1862-8.

226. Endter S, Francombe D, Ehrhardt C*, et al.* RT-PCR analysis of ABC, SLC and SLCO drug transporters in human lung epithelial cell models. J Pharm Pharmacol. 2009;61(5):583-91.

227. de Souza Carvalho C, Daum N, Lehr C-M. Carrier interactions with the biological barriers of the lung: Advanced *in vitro* models and challenges for pulmonary drug delivery. Adv Drug Deliv Rev. 2014;75:129-40.

228. Wan H, Winton HL, Soeller C*, et al.* Tight junction properties of the immortalized human bronchial epithelial cell lines Calu-3 and 16HBE14o. Eur Respir J. 2000;15(6):1058-68.

229. Grainger CI, Greenwell LL, Lockley DJ*, et al.* Culture of Calu-3 cells at the air interface provides a representative model of the airway epithelial barrier. Pharm Res. 2006;23(7):1482-90.

230. Fiegel J, Ehrhardt C, Schaefer UF*, et al.* Large porous particle impingement on lung epithelial cell monolayers-toward improved particle characterization in the lung. Pharm Res. 2003;20(5):788-96.

231. Mukherjee M, Pritchard DI, Bosquillon C. Evaluation of air-interfaced Calu-3 cell layers for investigation of inhaled drug interactions with organic cation transporters *in vitro*. Int J Pharm. 2012;426(1):7-14.

232. Stentebjerg-Andersen A, Notlevsen IV, Brodin B*, et al.* Calu-3 cells grown under AIC and LCC conditions: Implications for dipeptide uptake and transepithelial transport of substances. Eur J Pharm Biopharm. 2011;78(1):19-26.

233. Ehrhardt C, Kneuer C, Fiegel J*, et al.* Influence of apical fluid volume on the development of functional intercellular junctions in the human epithelial cell line 16HBE14o-: Implications for the use of this cell line as an *in vitro* model for bronchial drug absorption studies. Cell Tissue Res. 2002;308(3):391-400.

234. Hittinger M, Juntke J, Kletting S*, et al.* Preclinical safety and efficacy models for pulmonary drug delivery of antimicrobials with focus on *in vitro* models. Adv Drug Deliv Rev. 2015;85:44-56.

235. Davis AS, Chertow DS, Moyer JE*, et al.* Validation of normal human bronchial epithelial cells as a model for influenza A infections in human distal trachea. J Histochem Cytochem. 2015;63(5):312-28.

236. Zhang C, Elkahloun AG, Dennis PA. Changes in gene expression that accompany the immortalization or transformation of human bronchial epithelial cells. Cancer Res. 2004;64(7).

237. Perkins TN, Shukla A, Peeters PM*, et al.* Differences in gene expression and cytokine production by crystalline vs. amorphous silica in human lung epithelial cells. Part Fibre Toxicol. 2012;9(1):1-18.

238. Stewart CE, Torr EE, Mohd Jamili NH*, et al.* Evaluation of differentiated human bronchial epithelial cell culture systems for asthma research. J Allergy (Cairo). 2012;2012:1-11.

239. Hermanns MI, Unger RE, Kehe K*, et al.* Lung epithelial cell lines in coculture with human pulmonary microvascular endothelial cells: development of an alveolo-capillary barrier *in vitro*. Lab Invest. 2004;84(6):736-52.

240. Salomon JJ, Muchitsch VE, Gausterer JC*, et al.* The cell line NCI-H441 is a useful *in vitro* model for transport studies of human distal lung epithelial barrier. Mol Pharm. 2014;11(3):995-1006.

241. Haghi M, Hittinger M, Zeng Q*, et al.* Mono- and cocultures of bronchial and alveolar epithelial cells respond differently to proinflammatory stimuli and their modulation by salbutamol and budesonide. Mol Pharm. 2015;12(8):2625-32.

242. Kasper J, Hermanns MI, Bantz C*, et al.* Inflammatory and cytotoxic responses of an alveolar-capillary coculture model to silica nanoparticles: Comparison with conventional monocultures. Part Fibre Toxicol. 2011;8(1):1-16.

243. Korpi-Steiner NL, Valkenaar SM, Bates ME*, et al.* Human monocytic cells direct the robust release of CXCL10 by bronchial epithelial cells during rhinovirus infection. Clin Exp Allergy. 2010;40(8):1203-13.

244. Blom RAM, Erni ST, Krempaská K*, et al.* A triple co-culture model of the human respiratory tract to study immune-modulatory effects of liposomes and virosomes. PloS one. 2016;11(9):1-25.

245. Pohl C, Hermanns MI, Uboldi C*, et al.* Barrier functions and paracellular integrity in human cell culture models of the proximal respiratory unit. Eur J Pharm Biopharm. 2009;72(2):339-49.

246. Skibinski G, Elborn JS, Ennis M. Bronchial epithelial cell growth regulation in fibroblast cocultures: the role of hepatocyte growth factor. Am J Physiol Lung Cell Mol Physiol. 2007;293(1):69-76.

247. Baxter A, Thain S, Banerjee A*, et al.* Targeted omics analyses, and metabolic enzyme activity assays demonstrate maintenance of key mucociliary characteristics in long term cultures of reconstituted human airway epithelia. Toxicol In Vitro. 2015;29(5):864-75.

248. MatTek Coorporation. Available from: https://www.mattek.com/products/epiairway/. Accessed at 23rd January of 2018.

249. Epithelix. Available from: http://www.epithelix.com/products/mucilair. Accessed at 23rd January of 2018.

250. Fuchs S, Hollins A, Laue M*, et al.* Differentiation of human alveolar epithelial cells in primary culture: morphological characterization and synthesis of caveolin-1 and surfactant protein-C. Cell Tissue Res. 2003;311(1):31-45.

251. Hittinger M, Janke J, Huwer H*, et al.* Autologous co-culture of primary human alveolar macrophages and epithelial cells for investigating aerosol medicines. Part I: model characterisation. Altern Lab Anim. 2016;44(4):337-47.

252. Lehmann AD, Daum N, Bur M*, et al.* An *in vitro* triple cell co-culture model with primary cells mimicking the human alveolar epithelial barrier. Eur J Pharm Biopharm. 2011;77(3):398-406.

253. Foster KA, Oster CG, Mayer MM*, et al.* Characterization of the A549 cell line as a type II pulmonary epithelial cell model for drug metabolism. Exp Cell Res. 1998;243(2):359-66.

254. Forbes B, Ehrhardt C. Human respiratory epithelial cell culture for drug delivery applications. Eur J Pharm Biopharm. 2005;60(2):193-205.

255. Kobayashi S, Kondo S, Juni K. Permeability of peptides and proteins in human cultured alveolar A549 cell monolayer. Pharm Res. 1995;12(8):1115-9.

256. Rothen-Rutishauser BM, Kiama SG, Gehr P. A three-dimensional cellular model of the human respiratory tract to study the interaction with particles. Am J Respir Cell Mol Biol. 2005;32(4):281-9.

257. Rothen-Rutishauser B, Mühlfeld C, Blank F*, et al.* Translocation of particles and inflammatory responses after exposure to fine particles and nanoparticles in an epithelial airway model. Part Fibre Toxicol. 2007;4:1-9.

258. Alfaro-Moreno E, Nawrot TS, Vanaudenaerde BM*, et al.* Co-cultures of multiple cell types mimic pulmonary cell communication in response to urban PM10. Eur Respir J. 2008;32(5):1184-94.

259. Kasper JY, Hermanns MI, Unger RE*, et al.* A responsive human triple-culture model of the air-blood barrier: incorporation of different macrophage phenotypes. J Tissue Eng Regen Med. 2017;11(4):1285-97.

260. Kuehn A, Kletting S, de Souza Carvalho-Wodarz C*, et al.* Human alveolar epithelial cells expressing tight junctions to model the air-blood barrier. ALTEX. 2016;33(3):251-60.

261. Kletting S, Barthold S, Repnik U*, et al.* Co-culture of human alveolar epithelial (hAELVi) and macrophage (THP-1) cell lines. ALTEX. 2017;34(4):1-11.

262. Bhise NS, Ribas J, Manoharan V*, et al.* Organ-on-a-chip platforms for studying drug delivery systems. J Control Release. 2014;190:82-93.

263. Hassell BA, Goyal G, Lee E*, et al.* Human organ chip models recapitulate orthotopic lung cancer growth, therapeutic responses, and tumor dormancy *in vitro*. Cell Rep. 2017;21(2):508-16.

264. Shamir ER, Ewald AJ. Three-dimensional organotypic culture: experimental models of mammalian biology and disease. Nat Rev Mol Cell Biol. 2014;15(10):647-64.

265. Huh D, Hamilton GA, Ingber DE. From three-dimensional cell culture to organs-on-chips. Trends Cell Biol. 2011;21(12):745-54.

266. Halldorsson S, Lucumi E, Gómez-Sjöberg R*, et al.* Advantages and challenges of microfluidic cell culture in polydimethylsiloxane devices. Biosen Bioelectron. 2015;63:218-31.

267. Waheed S, Cabot JM, Macdonald NP*, et al.* Enhanced physicochemical properties of polydimethylsiloxane based microfluidic devices and thin films by incorporating synthetic micro-diamond. Sci Rep. 2017;7(1):1-10.

268. Wang JD, Douville NJ, Takayama S*, et al.* Quantitative analysis of molecular absorption into PDMS microfluidic channels. Ann Biomed Eng. 2012;40(9):1862-73.

269. Kimura H, Yamamoto T, Sakai H*, et al.* An integrated microfluidic system for long-term perfusion culture and on-line monitoring of intestinal tissue models. Lab Chip. 2008;8(5):741-6.

270. Huh D, Fujioka H, Tung YC*, et al.* Acoustically detectable cellular-level lung injury induced by fluid mechanical stresses in microfluidic airway systems. Proc Natl Acad Sci U S A. 2007;104(48):18886-91.

271. van der Helm MW, van der Meer AD, Eijkel JCT*, et al.* Microfluidic organ-on-chip technology for blood-brain barrier research. Tissue Barriers. 2016;4(1):1-13.

272. Wagner I, Materne EM, Brincker S*, et al.* A dynamic multi-organ-chip for long-term cultivation and substance testing proven by 3D human liver and skin tissue co-culture. Lab Chip. 2013;13(18):3538-47.

273. Huh D, Matthews BD, Mammoto A*, et al.* Reconstituting organ-level lung functions on a chip. Science. 2010;328(5986):1662-8.

274. Douville NJ, Zamankhan P, Tung YC*, et al.* Combination of fluid and solid mechanical stresses contribute to cell death and detachment in a microfluidic alveolar model. Lab Chip. 2011;11(4):609-19.

275. van Midwoud PM, Merema MT, Verpoorte E*, et al.* A microfluidic approach for *in vitro* assessment of interorgan interactions in drug metabolism using intestinal and liver slices. Lab Chip. 2010;10(20):2778-86.

276. Yi H-G, Lee H, Cho D-W. 3D printing of organs-on-chips. Bioengineering. 2017;4(1):1-22.

277. Wu Z, Su X, Xu Y*, et al.* Bioprinting three-dimensional cell-laden tissue constructs with controllable degradation. Sci Rep. 2016;6:1-10.

278. Lee H, Cho D-W. One-step fabrication of an organ-on-a-chip with spatial heterogeneity using a 3D bioprinting technology. Lab Chip. 2016;16(14):2618-25.

279. Chang R, Emami K, Wu H*, et al.* Biofabrication of a three-dimensional liver micro-organ as an *in vitro* drug metabolism model. Biofabrication. 2010;2(4).

280. Bhise NS, Manoharan V, Massa S*, et al.* A liver-on-a-chip platform with bioprinted hepatic spheroids. Biofabrication. 2016;8(1).

281. Lee V, Singh G, Trasatti JP*, et al.* Design and fabrication of human skin by three-dimensional bioprinting. Tissue Eng Part C Methods. 2014;20(6):473-84.

282. Homan KA, Kolesky DB, Skylar-Scott MA*, et al.* Bioprinting of 3D convoluted renal proximal tubules on perfusable chips. Sci Rep. 2016;6:1-13.

283. Horváth L, Umehara Y, Jud C*, et al.* Engineering an *in vitro* air-blood barrier by 3D bioprinting. Sci Rep. 2015;5:1-8.

284. Chuquimia OD, Petursdottir DH, Periolo N*, et al.* Alveolar epithelial cells are critical in protection of the respiratory tract by secretion of factors able to nodulate the activity of pulmonary macrophages and directly control bacterial growth. Infect Immun. 2013;81(1):381-9.

285. Miyata R, van Eeden SF. The innate and adaptive immune response induced by alveolar macrophages exposed to ambient particulate matter. Toxicol Appl Pharmacol. 2011;257(2):209-26.

286. Chanteux H, Guisset AC, Pilette C*, et al.* LPS induces IL-10 production by human alveolar macrophages via MAPKinases- and Sp1-dependent mechanisms. Respir Res. 2007;8(1):1-10.

287. Amoozgar Z, Yeo Y. Recent advances in stealth coating of nanoparticle drug delivery systems. Wiley Interdiscip Rev Nanomed Nanobiotechnol. 2012;4(2):219-33.

288. Rodriguez PL, Harada T, Christian DA*, et al.* Minimal "self" peptides that inhibit phagocytic clearance and enhance delivery of nanoparticles. Science. 2013;339(6122):971-5.

289. Trapani A, Di Gioia S, Ditaranto N*, et al.* Systemic heparin delivery by the pulmonary route using chitosan and glycol chitosan nanoparticles. Int J Pharm. 2013;447(1):115-23.

290. Gupta A, Kaul A, Tsolaki AG*, et al. Mycobacterium tuberculosis*: Immune evasion, latency and reactivation. Immunobiology. 2012;217(3):363-74.

291. Clemens DL, Lee BY, Xue M*, et al.* Targeted intracellular delivery of antituberculosis drugs to *Mycobacterium tuberculosis*-infected macrophages via functionalized mesoporous silica nanoparticles. Antimicrob Agents Chemother. 2012;56(5):2535-45.

292. Maretti E, Rossi T, Bondi M*, et al.* Inhaled solid lipid microparticles to target alveolar macrophages for tuberculosis. Int J Pharm. 2014;462(1):74-82.

293. Gaspar DP, Faria V, Gonçalves LMD*, et al.* Rifabutin-loaded solid lipid nanoparticles for inhaled antitubercular therapy: Physicochemical and *in vitro* studies. Int J Pharm. 2016;497(1):199-209.

294. Costa A, Sarmento B, Seabra V. Targeted drug delivery systems for lung macrophages. Curr Drug Targets. 2015;16(14):1565-81.

295. Garcia-Vallejo JJ, van Kooyk Y. Endogenous ligands for C-type lectin receptors: The true regulators of immune homeostasis. Immunol Rev. 2009;230(1):22-37.

296. Staines K, Hunt LG, Young JR*, et al.* Evolution of an expanded mannose receptor gene family. PloS one. 2014;9(11):1-10.

297. Vigerust DJ, Vick S, Shepherd VL. Characterization of functional mannose receptor in a continuous hybridoma cell line. BMC Immunol. 2012;13:1-13.

298. Irache JM, Salman HH, Gamazo C*, et al.* Mannose-targeted systems for the delivery of therapeutics. Expert Opin Drug Deliv. 2008;5(6):703-24.

299. Kang PB, Azad AK, Torrelles JB*, et al.* The human macrophage mannose receptor directs *Mycobacterium tuberculosis* lipoarabinomannan-mediated phagosome biogenesis. J Exp Med. 2005;202(7):987-99.

300. Weber S, Zimmer A, Pardeike J. Solid lipid nanoparticles (SLN) and nanostructured lipid carriers (NLC) for pulmonary application: A review of the state of the art. Eur J Pharm Biopharm. 2014;86(1):7-22.

301. Soares S, Fonte P, Costa A*, et al.* Effect of freeze-drying, cryoprotectants and storage conditions on the stability of secondary structure of insulin-loaded solid lipid nanoparticles. Int J Pharm. 2013;456(2):370-81.

302. Geisow MJ, D'Arcy Hart P, Young MR. Temporal changes of lysosome and phagosome pH during phagolysosome formation in macrophages: studies by fluorescence spectroscopy. J Cell Biol. 1981;89(3):645-52.

303. Liu J, Lu W, Reigada D*, et al.* Restoration of Lysosomal pH in RPE Cells from Cultured Human and ABCA4(−/−) Mice: Pharmacologic Approaches and Functional Recovery. Invest Ophthalmol Vis Sci. 2008;49(2):772-80.

304. Moura CC, Segundo MA, Neves Jd*, et al.* Co-association of methotrexate and SPIONs into anti-CD64 antibody-conjugated PLGA nanoparticles for theranostic application. Int J Nanomedicine. 2014;9:4911-22.

305. Littlefield M, Teboul I, Voloshyna I*, et al.* Polarization of human THP-1 macrophages: link between Adenosine receptors, inflammation and lipid accumulation. Int J Immunol Immunother. 2014;1(1):1-8.

306. Chanput W, Mes JJ, Savelkoul HF*, et al.* Characterization of polarized THP-1 macrophages and polarizing ability of LPS and food compounds. Food & function. 2013;4(2):266-76.

307. Daigneault M, Preston JA, Marriott HM*, et al.* The identification of markers of macrophage differentiation in PMA-stimulated THP-1 cells and monocyte-serived macrophages. PloS one. 2010;5(1):1-10.

308. Sorvillo N, Pos W, van den Berg LM*, et al.* The macrophage mannose receptor promotes uptake of ADAMTS13 by dendritic cells. Blood. 2012;119(16):3828-35.

309. Staitieh BS, Egea EE, Fan X*, et al.* Activation of alveolar macrophages with interferon-γ promotes antioxidant defenses via the Nrf2-ARE Pathway. J Clin Cell Immunol. 2015;6(5):1-17.

310. Vranic S, Boggetto N, Contremoulins V*, et al.* Deciphering the mechanisms of cellular uptake of engineered nanoparticles by accurate evaluation of internalization using imaging flow cytometry. Part Fibre Toxicol. 2013;10:1-16.

311. Shah M, Agrawal YK, Garala K*, et al.* Solid lipid nanoparticles of a water soluble drug, ciprofloxacin hydrochloride. Indian J Pharm Sci. 2012;74(5):434-42.

312. Aburahma MH, Badr-Eldin SM. Compritol 888 ATO: A multifunctional lipid excipient in drug delivery systems and nanopharmaceuticals. Expert Opin Drug Deliv. 2014;11(12):1865-83.

313. Wang JJ, Liu KS, Sung KC*, et al.* Lipid nanoparticles with different oil/fatty ester ratios as carriers of buprenorphine and its prodrugs for injection. Eur J Pharm Sci. 2009;38(2):138-46.

314. Zhang C, Peng F, Liu W*, et al.* Nanostructured lipid carriers as a novel oral delivery system for triptolide: Induced changes in pharmacokinetics profile associated with reduced toxicity in male rats. Int J Nanomedicine. 2014;9:1049-63.

315. Yang R, Gao R, Li F*, et al.* The influence of lipid characteristics on the formation, *in vitro* release, and *in vivo* absorption of protein-loaded SLN prepared by the double emulsion process. Drug Dev Ind Pharm. 2011;37(2):139-48.

316. Souto EB, Mehnert W, Muller RH. Polymorphic behaviour of Compritol888 ATO as bulk lipid and as SLN and NLC. J Microencapsul. 2006;23(4):417-33.

317. zur Mühlen A, Schwarz C, Mehnert W. Solid lipid nanoparticles (SLN) for controlled drug delivery – Drug release and release mechanism. Eur J Pharm Biopharm. 1998;45(2):149-55.

318. Sood S, Jawahar N, Jain K*, et al.* Olanzapine loaded cationic solid lipid nanoparticles for improved oral bioavailability. Curr Nanosci. 2013;9(1):26-34.

319. Weyenberg W, Filev P, Van den Plas D*, et al.* Cytotoxicity of submicron emulsions and solid lipid nanoparticles for dermal application. Int J Pharm. 2007;337(1–2):291-8.

320. Kerrigan AM, Brown GD. C-type lectins and phagocytosis. Immunobiology. 2009;214(7):562-75.

321. Song KC, Lee HS, Choung IY*, et al.* The effect of type of organic phase solvents on the particle size of poly(d,l-lactide-co-glycolide) nanoparticles. Colloids Surf A Physicochem Eng Asp. 2006;276(1–3):162-7.

322. Rejman J, Oberle V, Zuhorn IS*, et al.* Size-dependent internalization of particles via the pathways of clathrin- and caveolae-mediated endocytosis. Biochem J. 2004;377(Pt 1):159-69.

323. Conner SD, Schmid SL. Regulated portals of entry into the cell. Nature. 2003;422(6927):37-44.

324. Vieira AC, Chaves LL, Pinheiro M*, et al.* Design and statistical modeling of mannose-decorated dapsone-containing nanoparticles as a strategy of targeting intestinal M-cells. Int J Nanomedicine. 2016;11:2601-17.

325. Pandey R, Sharma S, Khuller GK. Oral solid lipid nanoparticle-based antitubercular chemotherapy. Tuberculosis (Edinb). 2005;85(5-6):415-20.

326. Huang ZR, Hua SC, Yang YL*, et al.* Development and evaluation of lipid nanoparticles for camptothecin delivery: a comparison of solid lipid nanoparticles,

nanostructured lipid carriers, and lipid emulsion. Acta Pharmacol Sin. 2008;29(9):1094-102.

327. Attama AA, Umeyor CE. The use of solid lipid nanoparticles for sustained drug release. Ther Deliv. 2015;6(6):669-84.

328. Xavier A, Srividhya N. Synthesis and study of Schiff base Ligands. IOSR-JAC. 2014;7(11):6-15.

329. Coates J. Interpretation of Infrared Spectra, A Practical Approach. Meyers RA, editor. Chichester: John Wiley & Sons Ltd; 2000. 10815–37 p.

330. Carneiro G, Silva EL, Pacheco LA*, et al.* Formation of ion pairing as an alternative to improve encapsulation and anticancer activity of all-trans retinoic acid loaded in solid lipid nanoparticles. Int J Nanomedicine. 2012;7:6011-20.

331. Arisaka M, Nakamura T, Yamada A*, et al.* Involvement of protein kinase C delta in induction of apoptosis by cationic liposomes in macrophage-like RAW264.7 cells. FEBS letters. 2010;584(5):1016-20.

332. Dekali S, Gamez C, Kortulewski T*, et al.* Assessment of an *in vitro* model of pulmonary barrier to study the translocation of nanoparticles. Toxicol Rep. 2014;1(0):157-71.

333. Ehrhardt C, Laue M, Kim K-J. *In vitro* models of the alveolar epithelial barrier. In: Ehrhardt C, Kim K-J, editors. Drug absorption studies: *In situ, in vitro* and *in silico* models. Boston: Springer; 2008.258-82.

334. Andrade F, Videira M, Ferreira D*, et al.* Nanocarriers for pulmonary administration of peptides and therapeutic proteins. Nanomedicine. 2010;6(1):123-41.

335. Kreft ME, Jerman UD, Lasič E*, et al.* The characterization of the human nasal epithelial cell line RPMI 2650 under different culture conditions and their optimization for an appropriate *in vitro* nasal model. Pharm Res. 2015;32(2):665-79.

336. Dvorak A, Tilley AE, Shaykhiev R*, et al.* Do airway epithelium air–liquid cultures represent the *in vivo* airway epithelium transcriptome? Am J Respir Cell Mol Biol. 2011;44(4):465-73.

337. Lenz AG, Karg E, Lentner B*, et al.* A dose-controlled system for air-liquid interface cell exposure and application to zinc oxide nanoparticles. Part Fibre Toxicol. 2009;6:1-17.

338. Limbach LK, Li YC, Grass RN*, et al.* Oxide nanoparticle uptake in human lung fibroblasts: Effects of particle size, agglomeration, and diffusion at low concentrations. Environ Sci Technol. 2005;39:9370-6.

339. Teeguarden JG, Hinderliter PM, Orr G*, et al.* Particokinetics *in vitro*: Dosimetry considerations for *in vitro* nanoparticle toxicity assessments. Toxicol Sci. 2007;95(2):300-12.

340. Krump-Konvalinkova V, Bittinger F, Unger RE*, et al.* Generation of human pulmonary microvascular endothelial cell lines. Lab Invest. 2001;81(12):1717-27.

341. Konkle BA, Ginsburg D. The addition of endothelial cell growth factor and heparin to human umbilical vein endothelial cell cultures decreases plasminogen activator inhibitor-1 expression. J Clin Invest. 1988;82(2):579-85.

342. Srinivasan B, Kolli AR, Esch MB*, et al.* TEER measurement techniques for *in vitro* barrier model systems. J Lab Autom. 2015;20(2):107-26.

343. Ward PD, Tippin TK, Thakker DR. Enhancing paracellular permeability by modulating epithelial tight junctions. Pharm Sci Technolo Today. 2000;3(10):346-58.

344. Bartels H. The air-blood barrier in the human lung. A freeze-fracture study. Cell Tissue Res. 1979;198(2):269-85.

345. Sowa G. Caveolae, caveolins, cavins, and endothelial cell function: New insights. Front Physiol. 2011;2:1-13.

346. Sun Y, Minshall RD, Hu G. Role of caveolin-1 in the regulation of pulmonary endothelial permeability. Methods Mol Biol. 2011;763:303-17.

347. Neuhaus W, Samwer F, Kunzmann S*, et al.* Lung endothelial cells strengthen, but brain endothelial cells weaken barrier properties of a human alveolar epithelium cell culture model. Differentiation. 2012;84(4):294-304.

348. Klein SG, Serchi T, Hoffmann L*, et al.* An improved 3D tetraculture system mimicking the cellular organisation at the alveolar barrier to study the potential toxic effects of particles on the lung. Part Fibre Toxicol. 2013;10(1).

349. Moynagh PN. Toll-like receptor signalling pathways as key targets for mediating the anti-inflammatory and immunosuppressive effects of glucocorticoids. J Endocrinol. 2003;179(2):139-44.

350. Bhattacharyya S, Brown DE, Brewer JA*, et al.* Macrophage glucocorticoid receptors regulate Toll-like receptor 4–mediated inflammatory responses by selective inhibition of p38 MAP kinase. Blood. 2007;109(10):4313-9.

351. Nalayanda DD, Puleo C, Fulton WB*, et al.* An open-access microfluidic model for lung-specific functional studies at an air-liquid interface. Biomed Microdevices. 2009;11(5):1081-9.

352. Tavana H, Zamankhan P, Christensen PJ*, et al.* Epithelium damage and protection during reopening of occluded airways in a physiologic microfluidic pulmonary airway model. Biomed Microdevices. 2011;13(4):731-42.

353. Chiu C-C, Shi Y-F, Yang J-J*, et al.* Effects of human parvovirus B19 and bocavirus VP1 unique region on tight junction of human airway epithelial A549 cells. PloS one. 2014;9(9):1-6.

354. Ren H, Suresh V. A cell culture model for alveolar epithelial transport. PeerJ Prepr. 2014;2014:1-29.

355. Geys J, Coenegrachts L, Vercammen J*, et al. In vitro* study of the pulmonary translocation of nanoparticles: a preliminary study. Toxicology letters. 2006;160(3):218-26.

356. Ren H, Birch NP, Suresh V. An optimised human cell culture model for alveolar epithelial transport. PloS one. 2016;11(10):1-22.

357. Stone KC, Mercer RR, Gehr P*, et al.* Allometric relationships of cell numbers and size in the mammalian lung. Am J Respir Cell Mol Biol. 1992;6(2):235-43.

358. Clift MJ, Fytianos K, Vanhecke D*, et al.* A novel technique to determine the cell type specific response within an *in vitro* co-culture model via multi-colour flow cytometry. Sci Rep. 2017;7(1):1-15.

359. Georas SN, Rezaee F. Epithelial barrier function: at the frontline of asthma immunology and allergic airway inflammation. J Allergy Clin Immunol. 2014;134(3):509-20.

360. Niessen CM. Tight junctions/adherens junctions: basic structure and function. J Invest Dermatol. 2007;127(11):2525-1532.

361. Vogelmann R, Nelson WJ. Fractionation of the epithelial apical junctional complex: Reassessment of protein distributions in different substructures. Mol Biol Cell. 2005;16(2):701-16.

362. Miyoshi J, Takai Y. Structural and functional associations of apical junctions with cytoskeleton. BBA - Mol Cel Res. 2008;1778(3):670-91.

363. Chen S, Einspanier R, Schoen J. Transepithelial electrical resistance (TEER): a functional parameter to monitor the quality of oviduct epithelial cells cultured on filter supports. Histochem Cell Biol. 2015;144(5):509-15.

364. Meyle J, Gultig K, Rascher G*, et al.* Transepithelial electrical resistance and tight junctions of human gingival keratinocytes. J Periodontal Res. 1999;34(4):214-22.

365. Madgula VL, Avula B, Reddy VLN*, et al.* Transport of decursin and decursinol angelate across Caco-2 and MDR-MDCK cell monolayers: *in vitro* models for intestinal and blood-brain barrier permeability. Planta medica. 2007;73(4):330-5.

366. Gazdar AF, Linnoila RI, Kurita Y*, et al.* Peripheral Airway Cell Differentiation in Human Lung Cancer Cell Lines. Cancer Res. 1990;50(17):5481-7.

367. Wong PS, Vogel CF, Kokosinski K*, et al.* Arylhydrocarbon receptor activation in NCI-H441 Cells and C57BL/6 Mice: Possible mechanisms for lung dysfunction. Am J Respir Cell Mol Biol. 2010;42(2):210-7.

368. Blume C, Reale R, Held M*, et al.* Cellular crosstalk between airway epithelial and endothelial cells regulates barrier functions during exposure to double-stranded RNA. Immun Inflamm Dis. 2017;5(1):45-56.

369. Chowdhury F, Howat WJ, Phillips GJ*, et al.* Interactions between endothelial cells and epithelial cells in a combined cell model of airway mucosa: Effects on tight junction permeability. Exp Lung Res. 2010;36(1):1-11.

370. Ehsan SM, Welch-Reardon KM, Waterman ML*, et al.* A three-dimensional *in vitro* model of tumor cell intravasation. Integr Biol (Camb). 2014;6(6):603-10.

371. Carterson AJ, Höner zu Bentrup K, Ott CM*, et al.* A549 lung epithelial cells grown as three-dimensional aggregates: Alternative tissue culture model for *Pseudomonas aeruginosa* pathogenesis. Infect Immun. 2005;73(2):1129-40.

372. Susewind J, de Souza Carvalho-Wodarz C, Repnik U*, et al.* A 3D co-culture of three human cell lines to model the inflamed intestinal mucosa for safety testing of nanomaterials. Nanotoxicology. 2016;10(1):53-62.

373. Lin H, Li H, Cho HJ*, et al.* Air-liquid interface (ALI) culture of human bronchial epithelial cell monolayers as an *in vitro* model for airway drug transport studies. J Pharm Sci. 2007;96(2):341-50.

374. Foster KA, Avery ML, Yazdanian M*, et al.* Characterization of the Calu-3 cell line as a tool to screen pulmonary drug delivery. Int J Pharm. 2000;208(1–2):1-11.

375. Forbes B, Shah A, Martin GP*, et al.* The human bronchial epithelial cell line 16HBE14o− as a model system of the airways for studying drug transport. Int J Pharm. 2003;257(1–2):161-7.

376. Astashkina A, Mann B, Grainger DW. A critical evaluation of *in vitro* cell culture models for high-throughput drug screening and toxicity. Pharmacol Ther. 2012;134(1):82-106.

377. Vuong H, Patterson T, Adiseshaiah P*, et al.* JNK1 and AP-1 regulate PMA-inducible squamous differentiation marker expression in Clara-like H441 cells. Am J Physiol Lung Cell Mol Physiol. 2002;282(2):215-25.

378. Costa A, Sarmento B, Seabra V. Mannose-functionalized solid lipid nanoparticles are effective in targeting alveolar macrophages. Eur J Pharm Sci. 2018;114:103-13.

379. Ma TY, Tran D, Hoa N*, et al.* Mechanism of extracellular calcium regulation of intestinal epithelial tight junction permeability: role of cytoskeletal involvement. Microsc Res Tech. 2000;51(2):156-68.

380. Citi S. Protein kinase inhibitors prevent junction dissociation induced by low extracellular calcium in MDCK epithelial cells. J Cell Biol. 1992;117(1):169-78.

381. Rigo LA, Carvalho-Wodarz CS, Pohlmann AR*, et al.* Nanoencapsulation of a glucocorticoid improves barrier function and anti-inflammatory effect on monolayers of pulmonary epithelial cell lines. Eur J Pharm Biopharm. 2017;119(Supplement C):1-10.

382. Andrade F, Neves Jd, Gener P*, et al.* Biological assessment of self-assembled polymeric micelles for pulmonary administration of insulin. Nanomedicine. 2015;11(7):1621-31.

383. Endter S, Becker U, Daum N*, et al.* P-glycoprotein (MDR1) functional activity in human alveolar epithelial cell monolayers. Cell Tissue Res. 2007;328(1):77-84.

384. Goodwin AM. *In vitro* assays of angiogenesis for assessment of angiogenic and anti-angiogenic agents. Microvasc Res. 2007;74(2-3):172-83.

385. Fleetwood AJ, Achuthan A, Schultz H*, et al.* Urokinase plasminogen activator is a central regulator of macrophage three-dimensional invasion, matrix degradation, and adhesion. J Immunol. 2014;192(8):3540-7.

386. Cougoule C, Le Cabec V, Poincloux R*, et al.* Three-dimensional migration of macrophages requires Hck for podosome organization and extracellular matrix proteolysis. Blood. 2010;115(7):1444-52.

387. Nemmar A, Vanbilloen H, Hoylaerts MF*, et al.* Passage of intratracheally instilled ultrafine particles from the lung into the systemic circulation in hamster. Am J Respir Crit Care Med. 2001;164(9):1665-8.

388. Thorley AJ, Ruenraroengsak P, Potter TE*, et al.* Critical determinants of uptake and translocation of nanoparticles by the human pulmonary alveolar epithelium. ACS Nano. 2014;8(11):11778-89.

389. Brandenberger C, Rothen-Rutishauser B, Mühlfeld C*, et al.* Effects and uptake of gold nanoparticles deposited at the air-liquid interface of a human epithelial airway model. Toxicol Appl Pharmacol. 2010;242:56-65.

390. Sarlo K, Blackburn KL, Clark ED*, et al.* Tissue distribution of 20 nm, 100 nm and 1000 nm fluorescent polystyrene latex nanospheres following acute systemic or acute and repeat airway exposure in the rat. Toxicology. 2009;263(2-3):117-26.

391. Avital A, Shapiro E, Doviner V*, et al.* Polystyrene microspheres as a specific marker for the diagnosis of aspiration in hamsters. Am J Respir Cell Mol Biol. 2002;27(4):511-4.

392. Snipes MB, Chavez GT, Muggenburg BA. Disposition of 3-, 7-, and 13-microns microspheres instilled into lungs of dogs. Environ Res. 1984;33(2):333-42.

393. George I, Vranic S, Boland S*, et al.* Development of an *in vitro* model of human bronchial epithelial barrier to study nanoparticle translocation. Toxicol In Vitro. 2015;29(1):51-8.

394. Manford F, Tronde A, Jeppsson A-B*, et al.* Drug permeability in 16HBE14o- airway cell layers correlates with absorption from the isolated perfused rat lung. Eur J Pharm Sci. 2005;26(5):414-20.

395. Raemy DO, Limbach LK, Rothen-Rutishauser B*, et al.* Cerium oxide nanoparticle uptake kinetics from the gas-phase into lung cells *in vitro* is transport limited. Eur J Pharm Biopharm. 2011;77(3):368-75.

396. Santos T, Varela J, Lynch I*, et al.* Effects of transport inhibitors on the cellular uptake of carboxylated polystyrene nanoparticles in different cell lines. PloS one. 2011;6(9):1-10.

397. Parr A, Hidalgo IJ, Bode C*, et al.* The effect of excipients on the permeability of BCS Class III compounds and implications for biowaivers. Pharm Res. 2016;33(1):167-76.

398. Becker C, Dressman JB, Amidon GL*, et al.* Biowaiver monographs for immediate release solid oral dosage forms: isoniazid. J Pharm Sci. 2007;96(3):522-31.

399. Moldoveanu B, Otmishi P, Jani P*, et al.* Inflammatory mechanisms in the lung. J Inflamm Res. 2009;2:1-11.

400. Johnson ER, Matthay MA. Acute lung injury: Epidemiology, pathogenesis, and treatment. J Aerosol Med Pulm Drug Deliv. 2010;23(4):243-52.

401. Xavier AM, Isowa N, Cai L*, et al.* Tumor necrosis factor-alpha mediates lipopolysaccharide-induced macrophage inflammatory protein-2 release from alveolar

epithelial cells. Autoregulation in host defense. Am J Respir Cell Mol Biol. 1999;21(4):510-20.

402. Chuquimia OD, Petursdottir DH, Rahman MJ*, et al.* The role of alveolar epithelial cells in initiating and shaping pulmonary immune responses: communication between innate and adaptive immune systems. PloS one. 2012;7(2):1-10.

403. Harada A, Sekido N, Akahoshi T*, et al.* Essential involvement of interleukin-8 (IL-8) in acute inflammation. J Leukoc Biol. 1994;56(5):559-64.

404. Turner MD, Nedjai B, Hurst T*, et al.* Cytokines and chemokines: At the crossroads of cell signalling and inflammatory disease. BBA - Mol Cel Res. 2014;1843(11):2563-82.

405. Iwaki M, Ito S, Morioka M*, et al.* Mechanical stretch enhances IL-8 production in pulmonary microvascular endothelial cells. Biochem Biophys Res Commun. 2009;389(3):531-6.

406. Driscoll KE, Carter JM, Hassenbein DG*, et al.* Cytokines and particle-induced inflammatory cell recruitment. Environ Health Perspect. 1997;105(Suppl 5):1159-64.

407. Park BS, Lee J-O. Recognition of lipopolysaccharide pattern by TLR4 complexes. Exp Mol Med. 2013;45(12):1-9.

408. Mako V, Czucz J, Weiszhar Z*, et al.* Proinflammatory activation pattern of human umbilical vein endothelial cells induced by IL-1beta, TNF-alpha, and LPS. Cytometry A. 2010;77(10):962-70.

409. Azizan A, Sweat J, Espino C*, et al.* Differential proinflammatory and angiogenesis-specific cytokine production in human pulmonary endothelial cells, HPMEC-ST1.6R infected with dengue-2 and dengue-3 virus. J Virol Methods. 2006;138(1-2):211-7.

410. Schutte RJ, Parisi-Amon A, Reichert WM. Cytokine profiling using monocytes/macrophages cultured on common biomaterials with a range of surface chemistries. J Biomed Mater Res A. 2009;88(1):128-39.

411. Klezovitch O, Edelstein C, Scanu AM. Stimulation of interleukin-8 production in human THP-1 macrophages by apolipoprotein(a). Evidence for a critical involvement of elements in its C-terminal domain. J Biol Chem. 2001;276(50):46864-9.

412. Wottrich R, Diabaté S, Krug HF. Biological effects of ultrafine model particles in human macrophages and epithelial cells in mono- and co-culture. Int J Hyg Environ Health. 2004;207(4):353-61.

413. Ware LB. Pathophysiology of acute lung injury and the acute respiratory distress syndrome. Seminars in respiratory and critical care medicine. 2006;27(4):337-49.

414. Chignard M, Balloy V. Neutrophil recruitment and increased permeability during acute lung injury induced by lipopolysaccharide. Am J Physiol Lung Cell Mol Physiol. 2000;279(6):1083-90.

415. Kantrow SP, Shen Z, Jagneaux T*, et al.* Neutrophil-mediated lung permeability and host defense proteins. Am J Physiol Lung Cell Mol Physiol. 2009;297(4):738-45.

416. Murakami K, Okajima K, Uchiba M. The prevention of lipopolysaccharide-induced pulmonary vascular injury by pretreatment with cepharanthine in rats. Am J Respir Crit Care Med. 2000;161(1):57-63.

417. Chen H, Wu S, Lu R*, et al.* Pulmonary permeability assessed by fluorescent-labeled dextran instilled intranasally into mice with LPS-induced acute lung injury. PloS one. 2014;9(7):1-7.

418. Hermanns MI, Kasper J, Dubruel P*, et al.* An impaired alveolar-capillary barrier *in vitro*: effect of proinflammatory cytokines and consequences on nanocarrier interaction. J Royal Soc Interface. 2010;7(Suppl 1):41-54.

419. Angelini DJ, Hyun SW, Grigoryev DN*, et al.* TNF-alpha increases tyrosine phosphorylation of vascular endothelial cadherin and opens the paracellular pathway through fyn activation in human lung endothelia. Am J Physiol Lung Cell Mol Physiol. 2006;291(6):1232-45.

420. Eutamene H, Theodorou V, Schmidlin F*, et al.* LPS-induced lung inflammation is linked to increased epithelial permeability: role of MLCK. Eur Respir J. 2005;25(5):789-96.

421. Zhang H, Sun G-Y. LPS induces permeability injury in lung microvascular endothelium via AT1 receptor. Arch Biochem Biophys. 2005;441(1):75-83.

422. Tian J, Lin X, Guan R*, et al.* The effects of hydroxyethyl starch on lung capillary permeability in endotoxic rats and possible mechanisms. Anesth Analg. 2004;98(3):768-74.

423. Azghani AO, Miller EJ, Peterson BT. Virulence factors from *Pseudomonas aeruginosa* increase lung epithelial permeability. Lung. 2000;178(5):261-9.

424. Wiener-Kronish JP, Albertine KH, Matthay MA. Differential responses of the endothelial and epithelial barriers of the lung in sheep to *Escherichia coli* endotoxin. J Clin Investig. 1991;88(3):864-75.

425. Lehnert BE, Valdez YE, Tietjen GL. Alveolar macrophage-particle relationships during lung clearance. Am J Respir Cell Mol Biol. 1989;1(2):145-54.

426. Kreyling WG, Semmler-Behnke M, Seitz J*, et al.* Size dependence of the translocation of inhaled iridium and carbon nanoparticle aggregates from the lung of rats to the blood and secondary target organs. Inhal Toxicol. 2009;21(sup1):55-60.

427. Choi HS, Ashitate Y, Lee JH*, et al.* Rapid translocation of nanoparticles from the lung airspaces to the body. Nat Biotechnol. 2010;28(12):1300-3.

428. Mohammad AK, Amayreh LK, Mazzara JM*, et al.* Rapid lymph accumulation of polystyrene nanoparticles following pulmonary administration. Pharm Res. 2013;30(2):424-34.

429. Wang F, Vallen Graham W, Wang Y*, et al.* Interferon-γ and tumor necrosis factor-α synergize to induce intestinal epithelial barrier dysfunction by up-regulating myosin light chain kinase expression. Am J Pathol. 2005;166(2):409-19.

430. Wang L, Taneja R, Wang W*, et al.* Human alveolar epithelial cells attenuate pulmonary microvascular endothelial cell permeability under septic conditions. PloS one. 2013;8(2):1-11.

431. Lucas R, Verin AD, Black SM*, et al.* Regulators of endothelial and epithelial barrier integrity and function in acute lung injury. Biochem Pharmacol. 2009;77(12):1763-72.

432. Dewi BE, Takasaki T, Kurane I. *In vitro* assessment of human endothelial cell permeability: Effects of inflammatory cytokines and dengue virus infection. J Virol Methods. 2004;121(2):171-80.

APPENDICES

APPENDIX I

Supplementary information for supporting the Chapter III

Physical-chemical characterization of coumarin-6-loaded SLN

Samples were diluted in Milli-Q® water. Z-average, PdI and zeta potential was characterized through a Malvern Zetasizer Nano ZS instrument (Malvern Instruments Ltd, Malvern, UK) in triplicate.

For quantify the association efficiency of coumarin-6, the fluorescent SLN were purified through ultracentrifugation, using a Beckman Coulter Optimal-XP (Brea, USA), at 30000 rpm (rotor 70.1Ti) during 1.5 hours, at 4°C. The supernatant was discharged and after resuspension of the pellet in Milli-Q® water, 1 mL of formulation was placed in a tube with 5 mL of ACN and left under magnetic stirring during 5 hours to allow the complete destruction of lipid matrix of SLN. The mixture was centrifuge at 3200 *g* during 30 minutes (Eppendorf® Centrifuge) to remove the lipids in suspension, and the supernatant was collected; the association efficiency of coumarin-6 was quantified by measuring the fluorescence through a microplate reader Synergy Mx (BioTek, Winooski, USA) using an excitation/emission wavelength of 460/540 nm.

Table A1. Physical-chemical properties of coumarin-6-loaded SLN.

Z- Average (nm)	PdI	Zeta potential (mV)	Association efficiency (%)
584.9 ± 27.5	0.48 ± 0.07	35.7 ± 0.7	52.9 ± 8.2

Results expressed as mean ± SD from 3 independent experiments

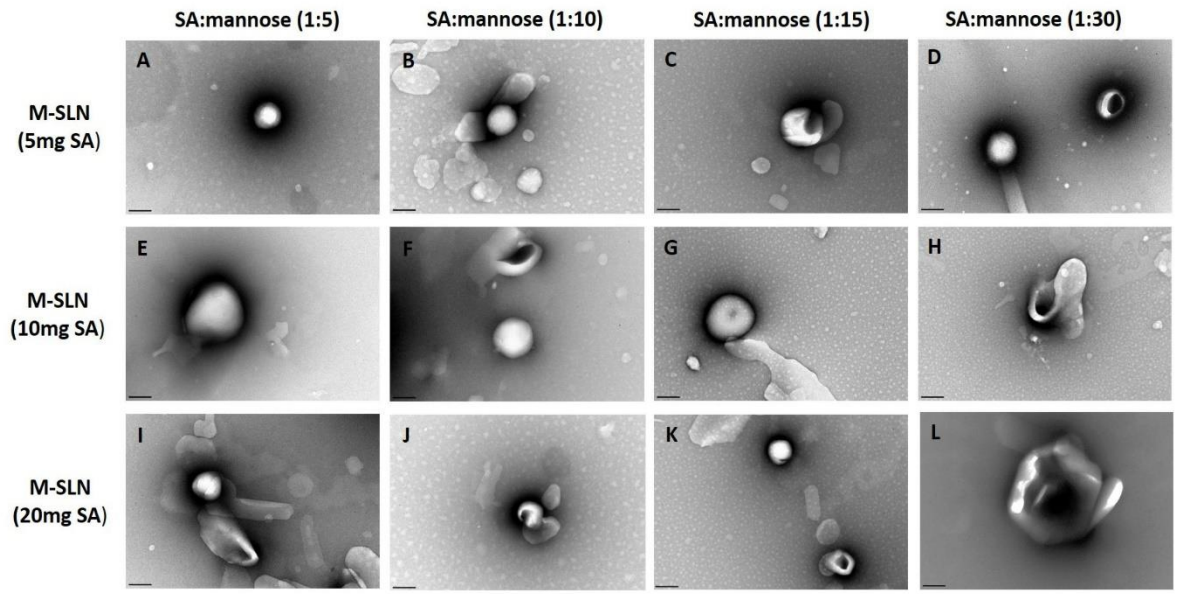

Figure A1. TEM microphotographs of M-SLN with 5 mg of SA (A-D), 10 mg of SA (E-H), and 20 mg of SA (I-L) and with different molar ration of SA:mannose. Scale bar: 200 nm.

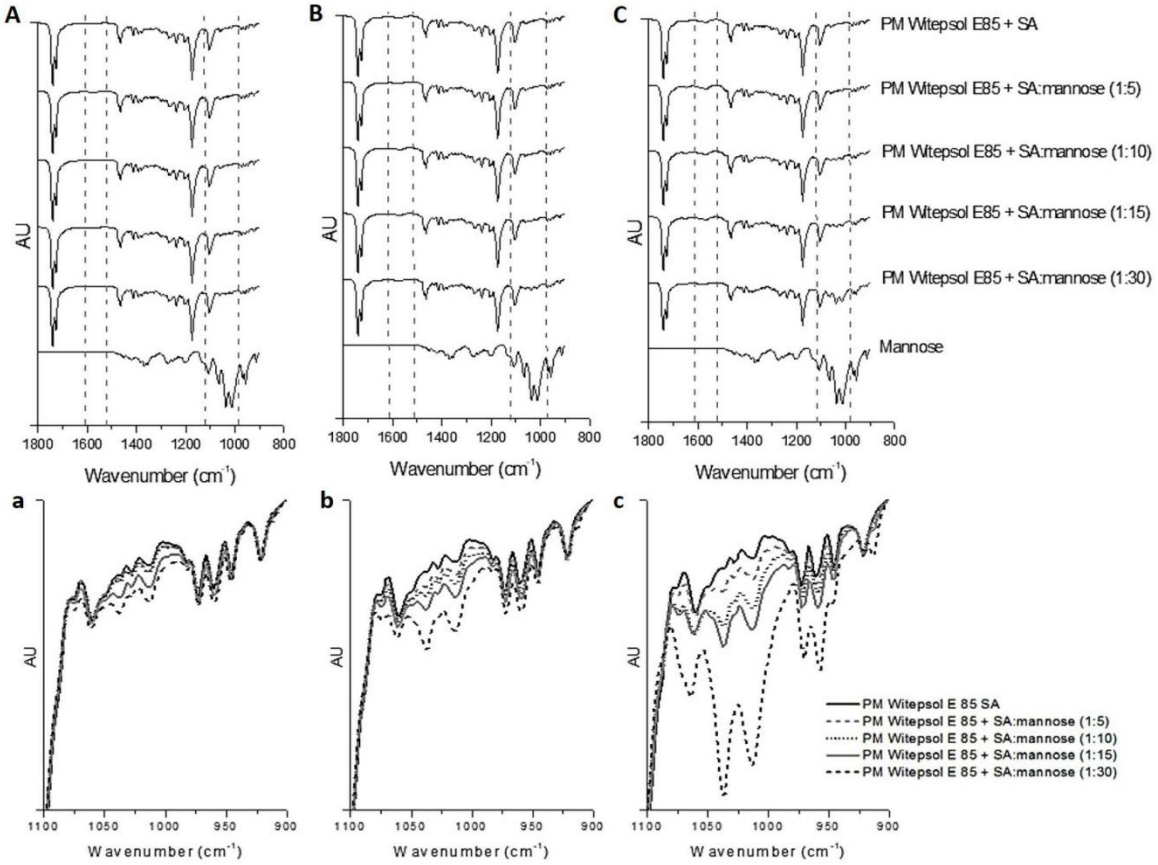

Figure A2. Normalized-FTIR spectra of PM of Witepsol® E85 either with 5 mg (A), 10 mg (B) or 20 mg (C) of SA, in the presence or absence of mannose. a, b and c) represents magnification of spectra A, B and C, respectively, between 1100-900 cm^{-1}.

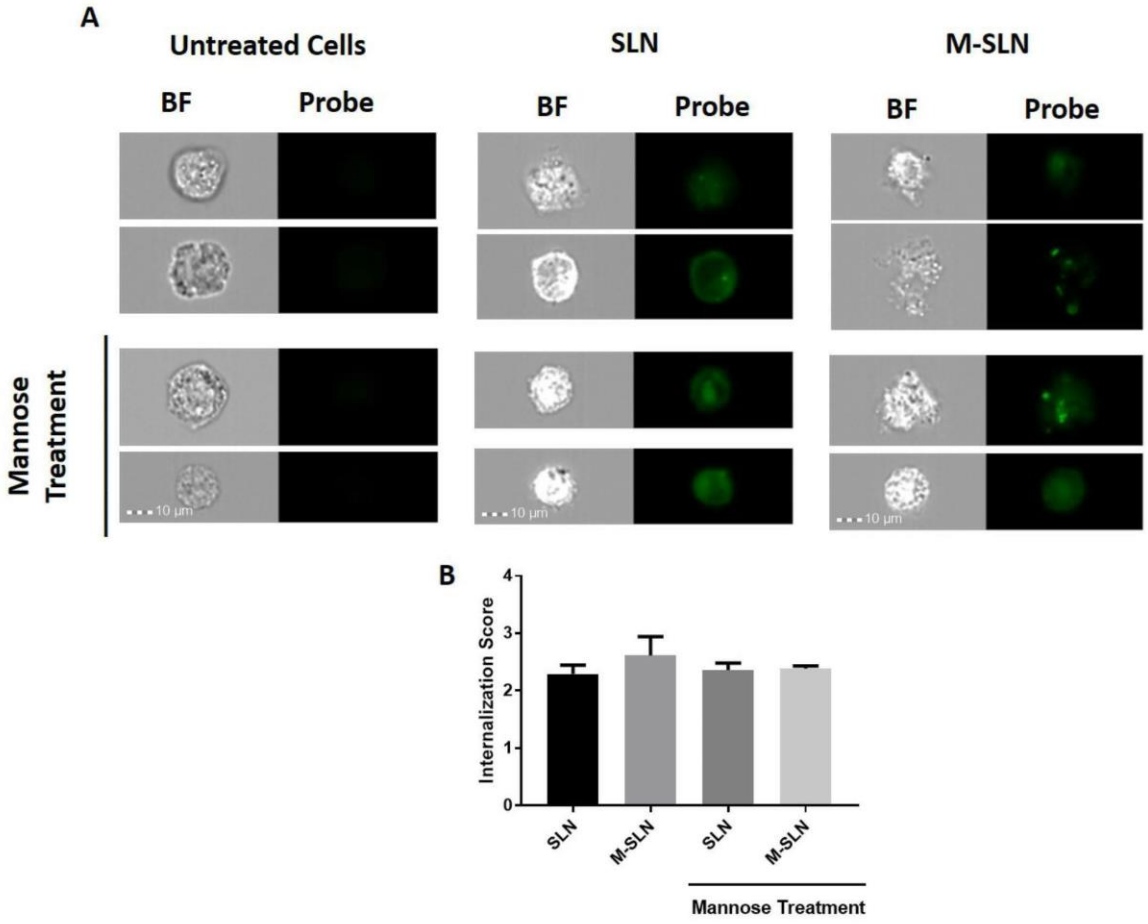

Figure A3. Representative images acquired by ImageStream®^{X} imaging flow cytometer related with *in vitro* uptake studies in dTHP-1 cells (A). Scale barr: 10 µm; B) Internalization score of SLN and M-SLN on dTHP-1 cell line; mean ± SD, from 3 independent experiments.

APPENDIX II

Supplementary information for supporting the Chapter IV

Table A1. Growth rate and doubling time of NCI-H441 and HPMEC-ST1.6R grown on Medium A

	Growth Rate		Doubling time (hours)	
	NCI-H441	**HPMEC-ST1.6R**	**NCI-H441**	**HPMEC-ST1.6R**
Day 0-4	0,015 ± 0,001	0.027 ± 0,002	48 ± 5	26 ± 2
Day 4-8	0.017 ± 0,002	0.016 ± 0,003	40 ± 5	44 ± 10
Day 8-12	0.013 ± 0,001	0.007 ± 0,001	53 ± 6	89 ± 5

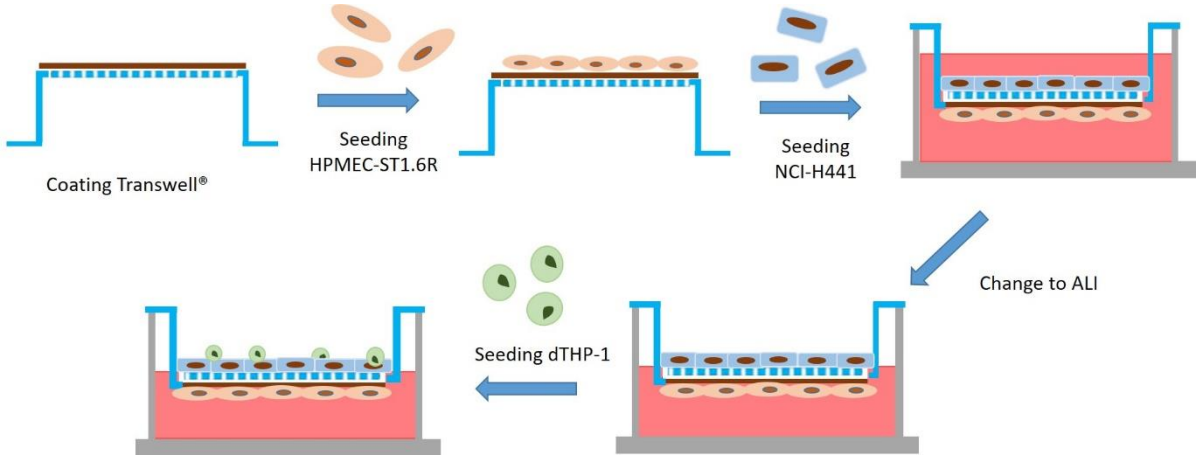

Scheme A1. Set-up used to perform the *in vitro* triple co-culture model of air-blood barrier.

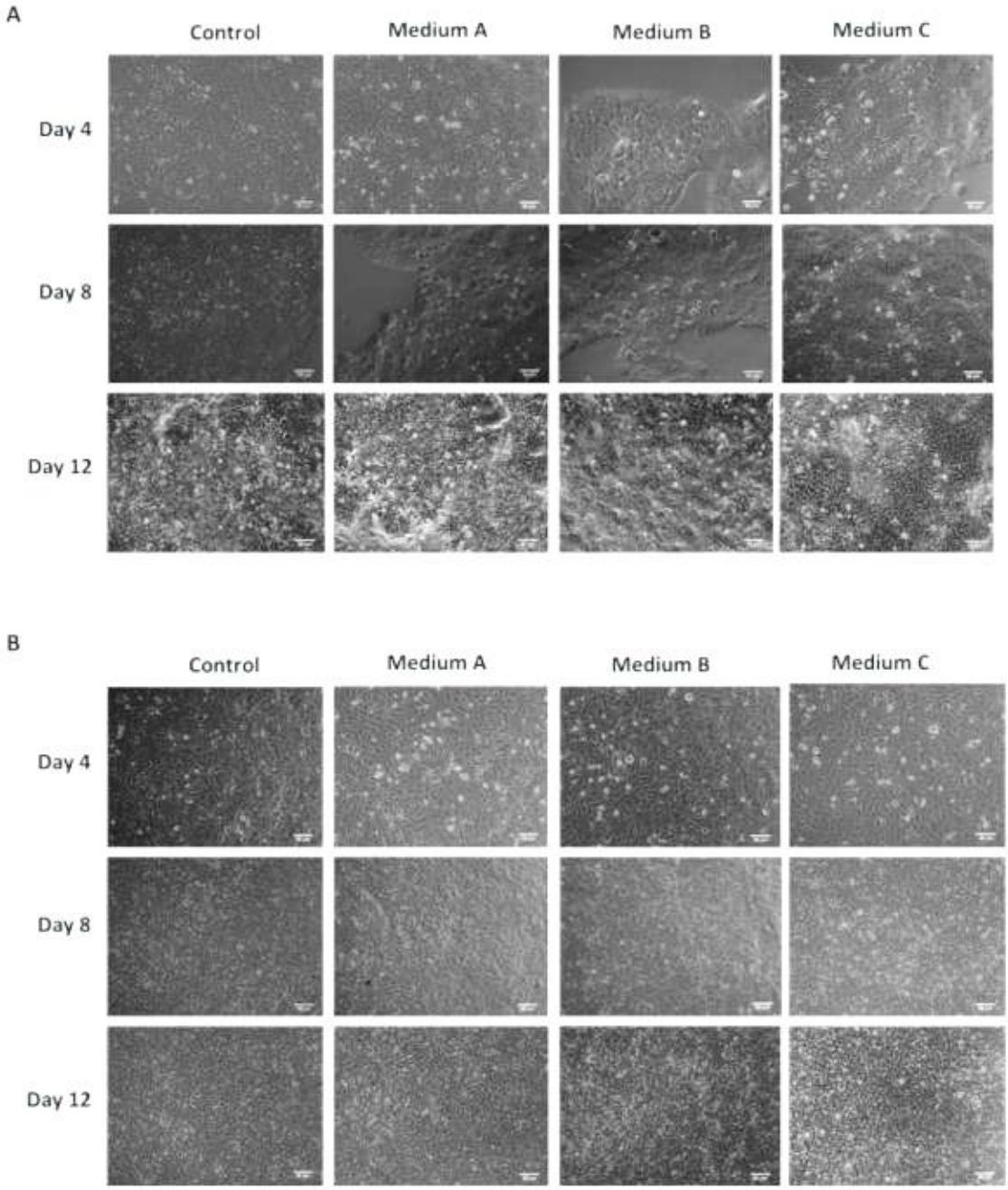

Figure A1. Images from light microscope of NCI-H441 (A) and HPMEC-ST1.6R (B) monocultures at different time points after seeding on a 24-well plate (2.0 x 10^4 cells/cm^2 and 2.5 x 10^4 cells/cm^2, respectively); cells were cultured with different cell culture medium; Scale bar: 10 µm.

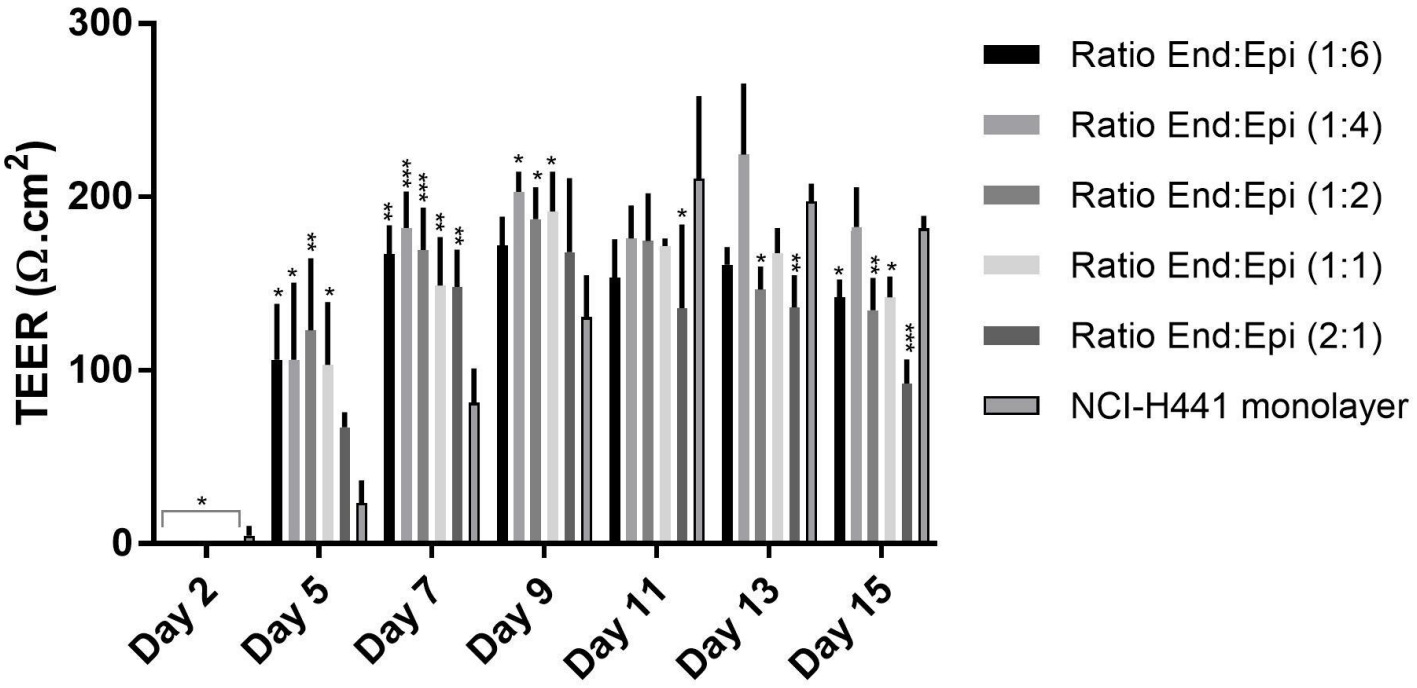

Figure A2 Bi-culture of NCI-H441+HPMEC-ST1.6R: NCI-H441 cells ($2.5x10^5$ cells/ Transwell®) were seeded with different ratios of HPMEC-ST1.6R cells. *In vitro* models were cultured at ALI after 2 days of seeding with 200 nM of Dex to induce the polarization of epithelium; Statistical analysis performed through One-way ANOVA with Dunnett's multiple comparison test; * represent the significant differences when compared with the respective control (NCI-H441 monoculture); mean ± SD, n=3 from 1 independent experiment. Differences were considered to be significant at a level of $p < 0.05$ (*), very significant at level of $p < 0.01$ (**) and highly significant at a level of $P < 0.001$ (***).

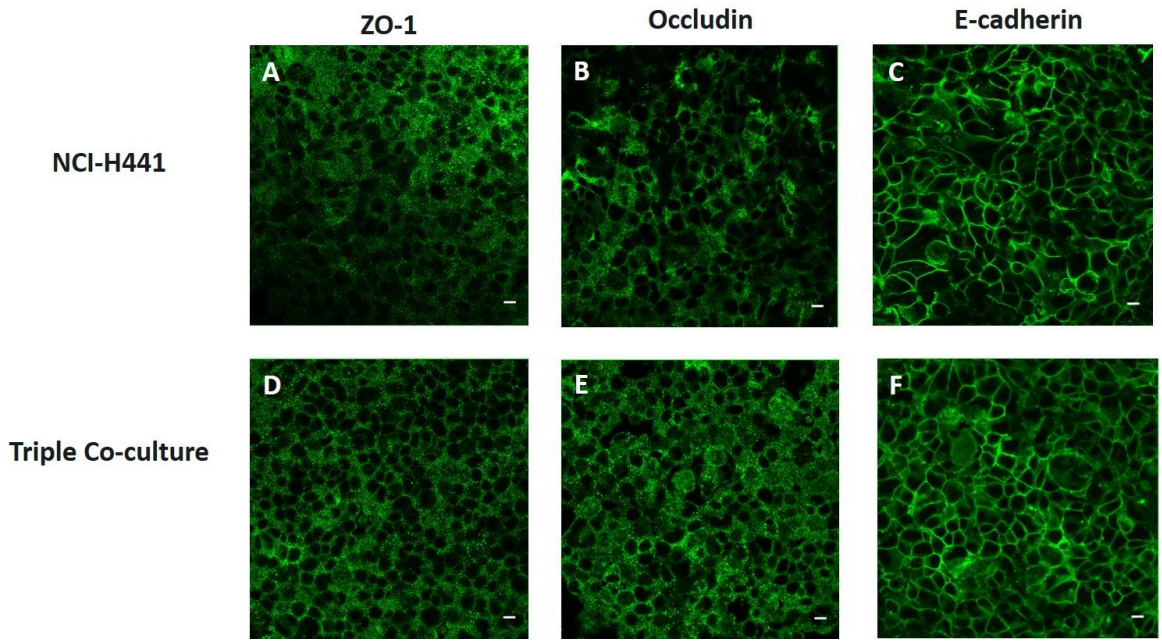

Figure A3 ICC of ZO-1, occludin and E-cadherin on NCI-H441 monoculture and triple co-culture at day 8 of culture; Scale bar: 10 µm; Number of cells/Transwell®: 2.5 x 10^5 NCI-H441 cells, 1.25 x 10^5 HPMEC-ST1.6R cells and 1.0 x 10^5 dTHP-1 cells.

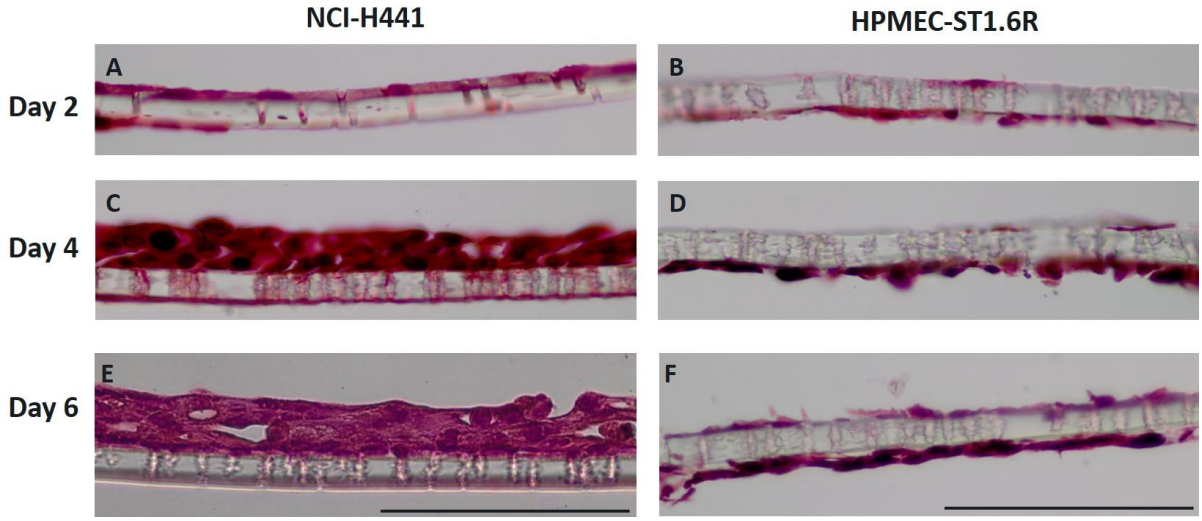

Figure A4. Histologic section of NCI-H441 monoculture (A, C and E) and HPMEC-ST1.6R monoculture (B, D and F) seeded on 12-well Transwell® with different days of culture; Scale bar: 100 µm; Number of cells/Transwell®: 2.5 x 10^5 NCI-H441 cells and 1.25 x 10^5 HPMEC-ST1.6R cells.

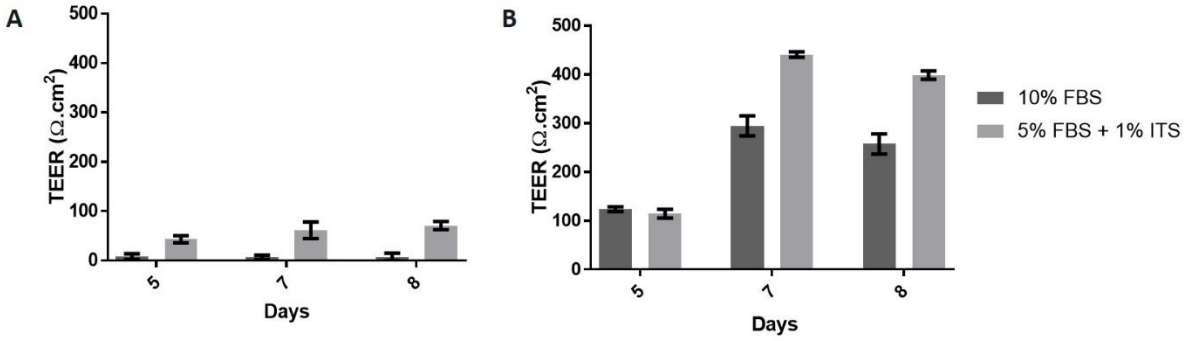

Figure A5. TEER of NCI-H441 monoculture grown on a 12-well Transwell® with pore size of 3.0 µm (A) and 0.4 µm (B) at day 5, 7 and 8 days of culture. The influence of 10% (v/v) FBS and 5% (v/v) FBS + 1% (v/v) ITS was assessed; Data were expressed as mean ± SD from 1 to 3 replicates of 1 study (preliminary study).

APPENDIX III

Supplementary information for supporting the Chapter V

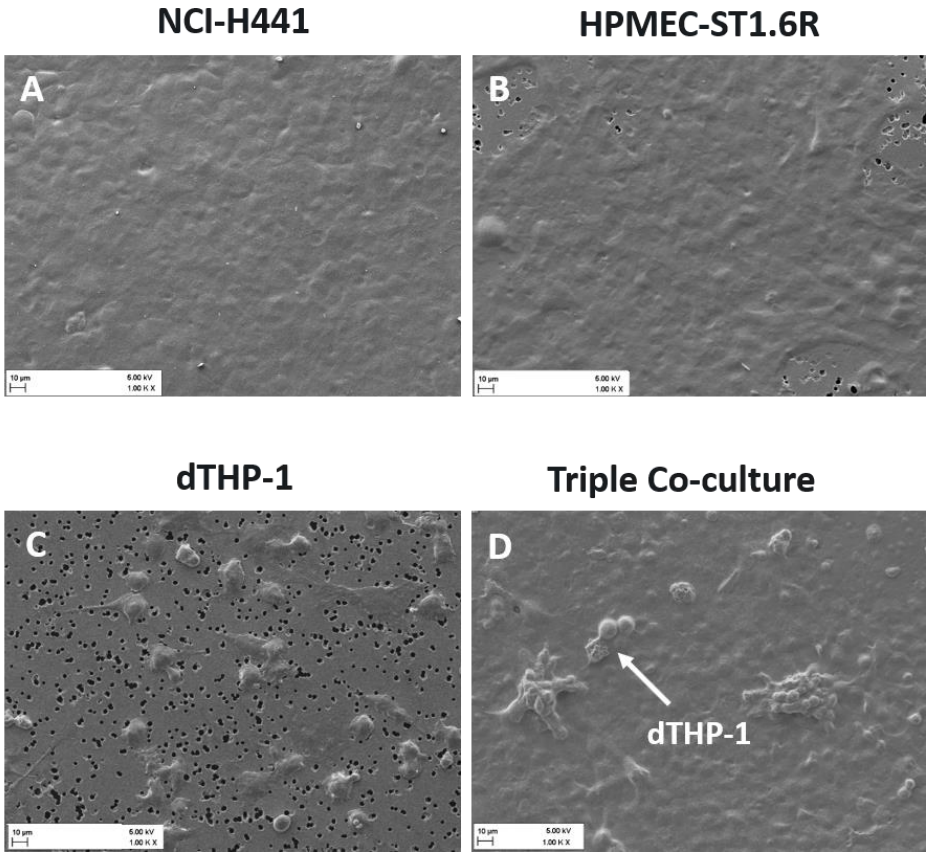

Figure A1. SEM images of NCI-H411 monoculture (A), HPMEC-ST1.6R monoculture (B), dTHP-1 monoculture (C) and *in vitro* triple co-culture at apical side (D) after 5 days of culture; Scale bar: 10 µm.

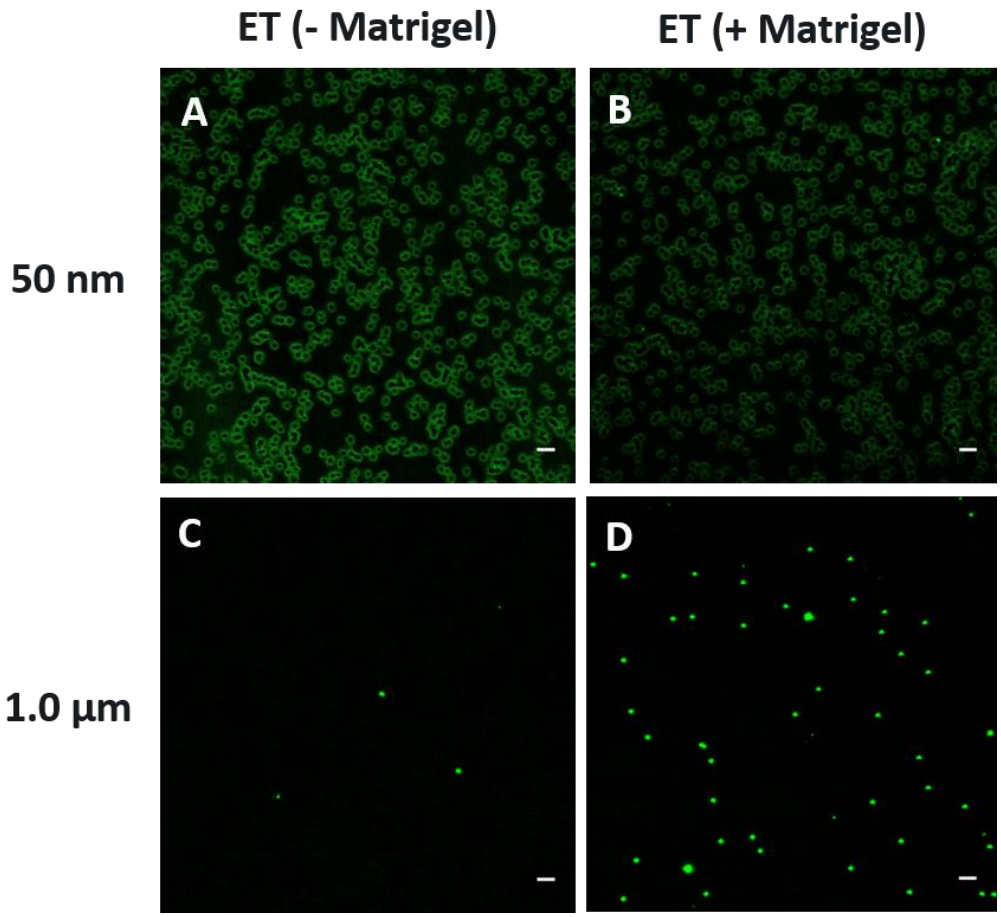

Figure A2. ET with and without Matrigel™ after translocation of fluorospheres with a size of 50 nm (A and B) and 1.0 µm (C and D); Scale bar: 10 µm.

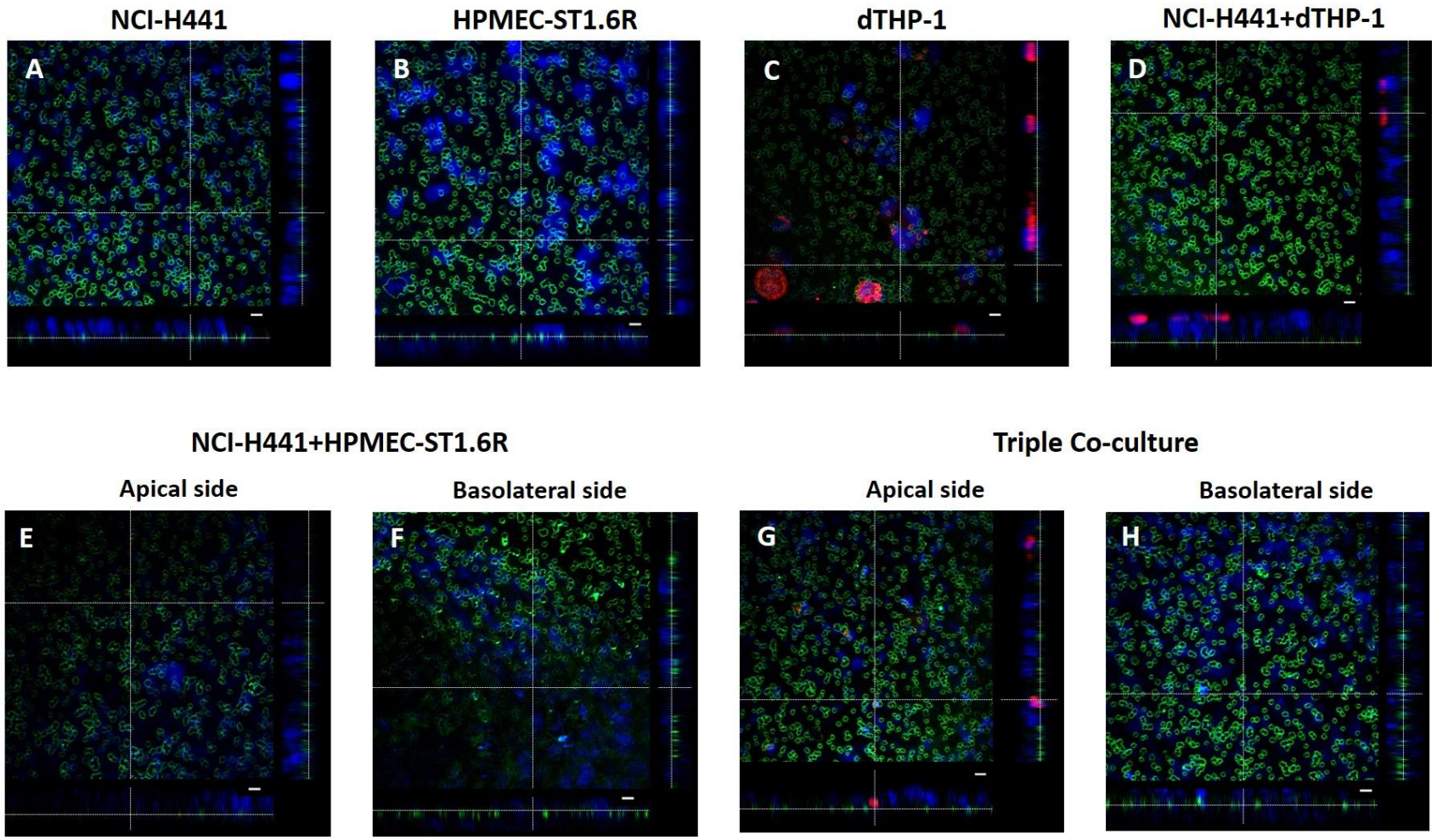

Figure A3. CLSM images of each monocultures, bi-cultures and triple co-culture after translocation studies of 50 nm-fluorospheres. Cell nuclei and dTHP-1 cells were stained with blue and red, respectively, while fluorospheres presented a green color; Scale bar: 10 µm.

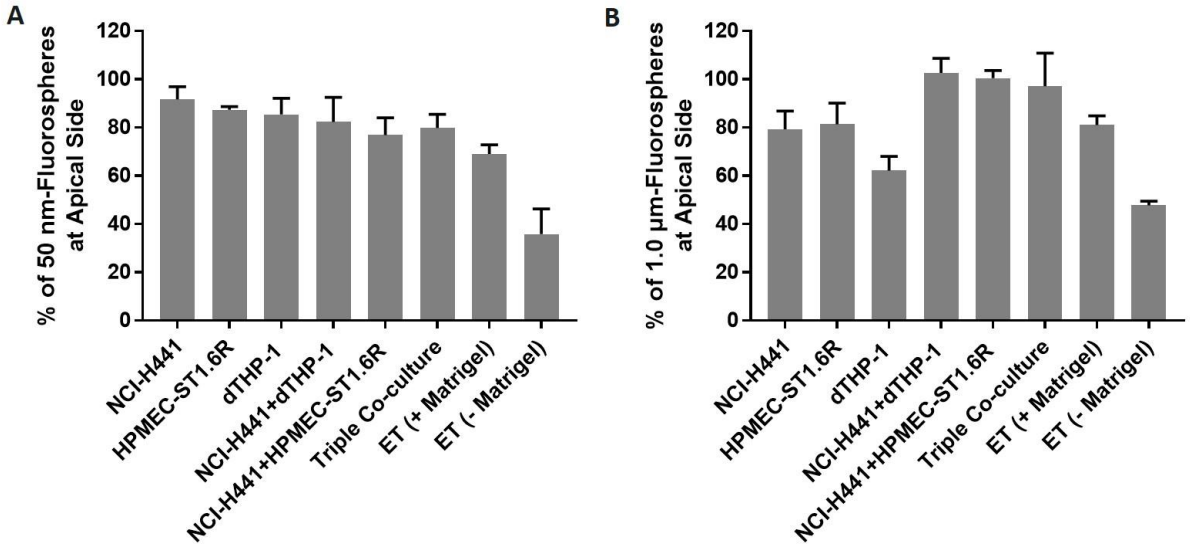

Figure A4. Percentage of fluorospheres with a size of 50 nm (A) and 1.0 µm (B) that remained at apical side after performing translocation studies across different *in vitro* models (monocultures, bi-cultures and triple co-cultures) and through ET.

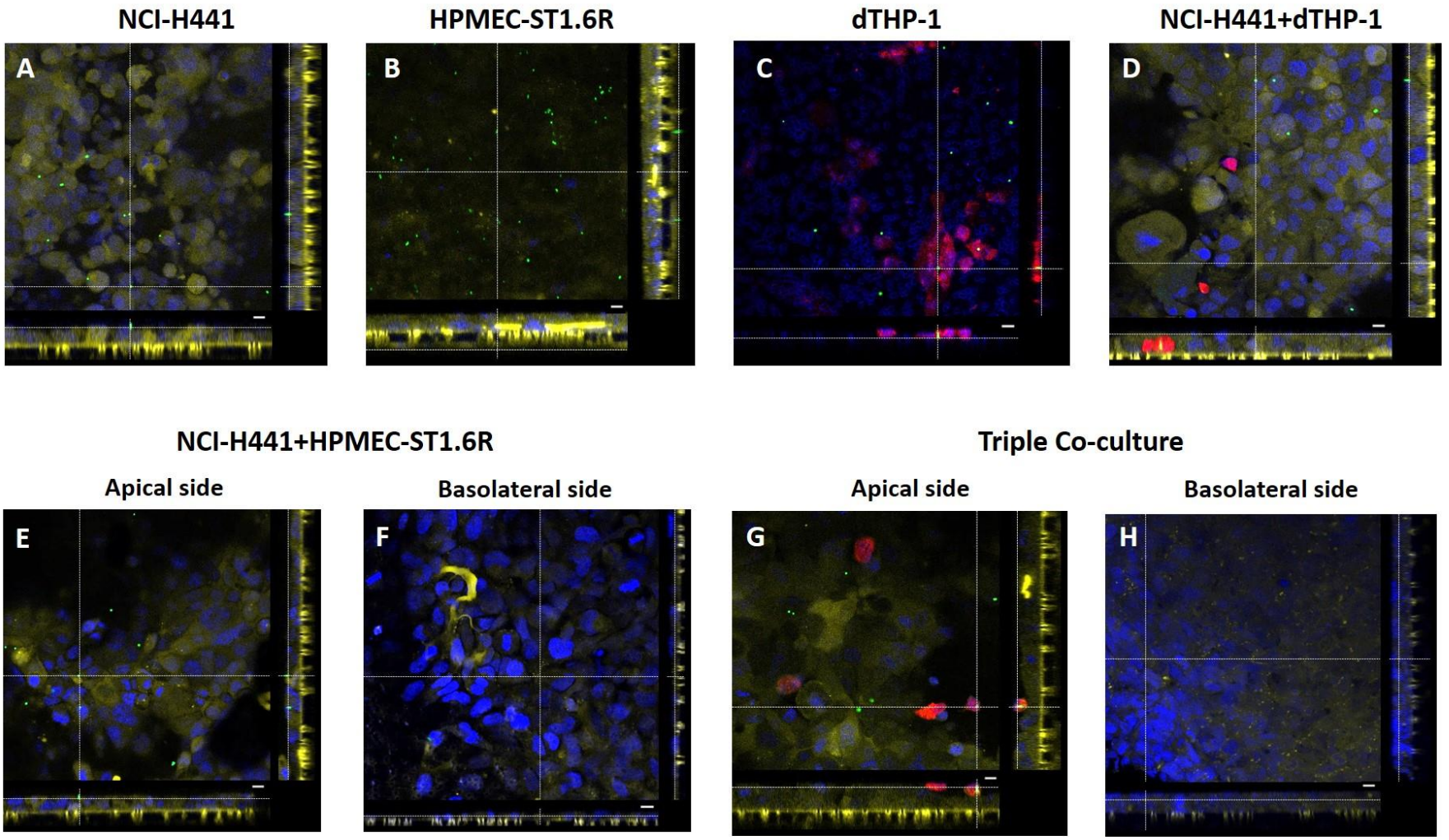

Figure A5. CLSM images of each monocultures, bi-cultures and triple co-culture after translocation studies of 1.0 µm -fluorospheres. Cell nuclei and dTHP-1 cells were stained with blue and red, respectively, epithelial and endothelial cells were stained with a yellow color, and fluorospheres presented a green color; Scale bar: 10 µm.

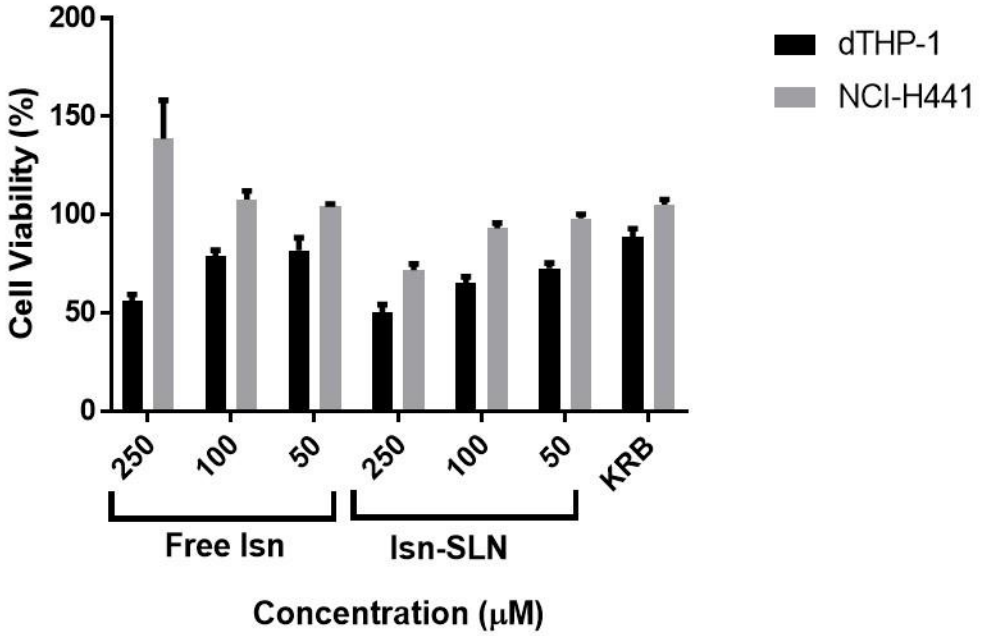

Figure A6. Metabolic activity of dTHP-1 and NCI-H441 cell line after incubation of free Isn and Isn-SLN, both dispersed in KRB with 0.1% (m/v) Pluronic® F-127, for 4 hours. Experiment was performed in 5 replicates and results were expressed as mean ± SD.

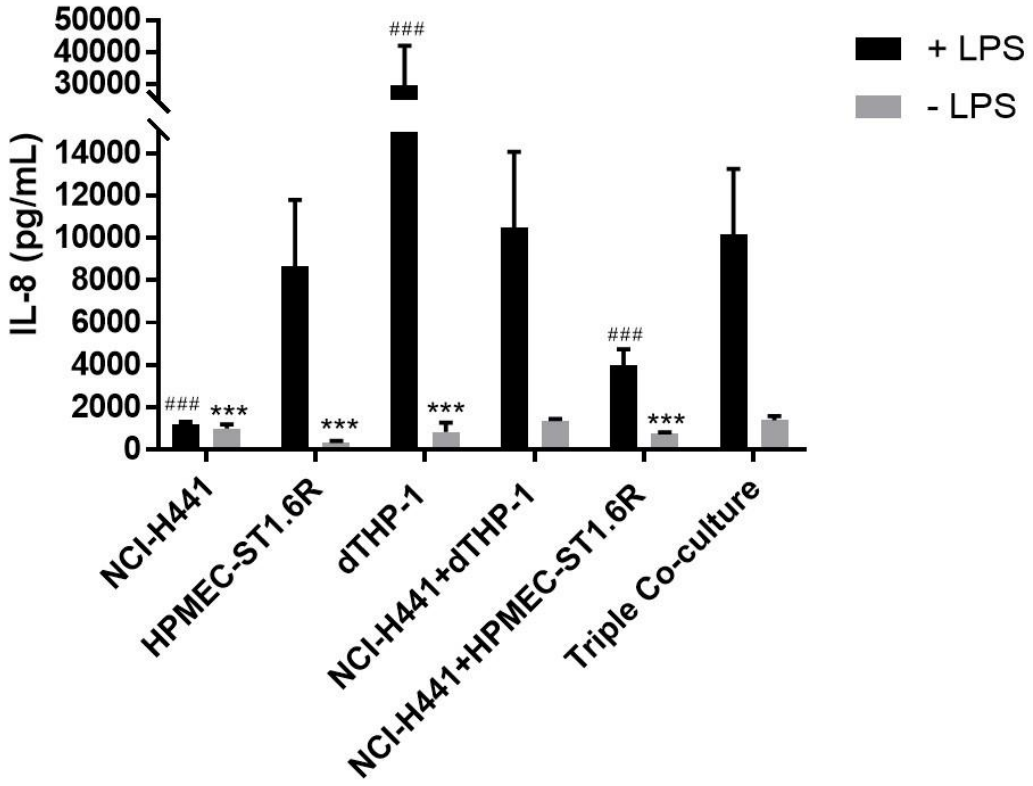

Figure A7. Release of IL-8 by different *in vitro* cell culture models, treated with PBS (untreated controls, designed as - LPS) or incubated with LPS (designed as + LPS); Results are expressed as mean ± SD from 3 replicates. Statistical analysis assessed trough One-way ANOVA with Dunnett's multiple comparisons, being the triple co-culture the control group. Statistical differences between cells from each *in vitro* cell culture models treated with LPS were marked with a #, while differences on the cells without LPS treatment were marked with a *. Differences were considered to be significant at a level of $p < 0.05$ (* or $^{\#}$), very significant at level of $p < 0.01$ (** or $^{\#\#}$) and highly significant at a level of $P < 0.001$ (*** or $^{\#\#\#}$).